Chassis Dynamometer Software,

Inertia Determination and Recalibration

A thesis

submitted in partial fulfilment

of the requirements for the Degree

of

Master of Engineering

in the

University of Canterbury

by

Christopher Dean Bennetts

Department of Mechanical Engineering
University of Canterbury
2002

Abstract

The University of Canterbury chassis dynamometer exists to enable specific and repeatable motor vehicle testing to be carried out in the University's Department of Mechanical Engineering. Dynamometer testing is invaluable in the development of new vehicle technologies, such as electric and hybrid configurations, and the assessment of existing vehicles' performance. This thesis includes a description of the dynamometer, and of the recalibration and software work that has been carried out to enable computer-controlled vehicle testing of a flexible and reliable nature.

In order to exert a known force at the wheels of a vehicle on the chassis dynamometer, the appropriate equations of motion must be applied to the known inertial mass and frictional characteristics of the dynamometer system. These equations of motion are discussed in terms of the chassis dynamometer and their application in the simulation of realistic on-road vehicle forces. Several techniques have been proposed to determine the system friction and inertia, and the most appropriate method was chosen on the basis of repeatability and equipment limitations.

Dynamometer control and data acquisition software has been written in the C++ programming language, which includes automated routines for the calibration of the chassis dynamometer as well as several vehicle testing regimes. Analysis software has been created to enable graphical display of test data and the calculation of useful parameters such as energy consumption and efficiency.

Several tests were conducted on a motor vehicle owned by the University of Canterbury, with a view to determining the effectiveness of the testing procedures, and the accuracy of the dynamometer instrumentation. In light of these test results and observations made during the dynamometer development, a number of potential improvements to the system have been proposed.

Acknowledgements

I would like to express my appreciation to all the people whose support and encouragement made this project possible.

Firstly, to my supervisor Professor John Raine, whose knowledge and enthusiasm for the subject have provided impetus throughout. Thanks also to Philip Hindin for his admirable patience and memory when consulted on the details.

The Mechanical Engineering staff at the University of Canterbury have been of immense help in many ways. I would like to recognise the expertise of Julian Murphy and Julian Phillips in all things electrical, Eric Cox in all things automotive, and Dr Andrew Cree in almost anything I cared to ask him.

Thanks also for the conversation and condolences from my fellow postgraduates, particularly my office-mates in Room 304, David and Michael. Many a refreshing lunch-hour was spent consulting the Oxford Reference Dictionary, or calculating how many helium balloons it takes to lift a child.

Full credit to my family and friends, who always tried to look interested. Thank you Angela for being there for me, and giving me the space do things in my own time. And finally, my love and gratitude go to my parents, for putting a roof over my head, and letting me stay under it for so long.

Contents

List of Appendices

List of Figures

List of Plates

List of Tables

Nomenclature

A	vehicle frontal area (m^2)
C_D	vehicle aerodynamic drag coefficient
C_{R1}	constant vehicle rolling resistance coefficient
C_{R2}	speed-dependent vehicle rolling resistance coefficient
f_{0d}, f_{1d}, f_{2d}	chassis dynamometer friction coefficients
f_{0dr}, f_{1dr}, f_{2dr}	roller drum friction coefficients
F_{drfric}	total roller drum friction force (N)
f_{0V}, f_{1V}, f_{2V}	combined vehicle on-road friction coefficients
f_{0Vd}, f_{1Vd}, f_{2Vd}	combined vehicle friction coefficients on chassis dynamometer
F_{corr}	tractive effort load cell force corrected for drum characteristics (N)
F_{de}	eddy-current dynamometer electromagnetic force (N)
F_{df}	eddy-current dynamometer internal friction (N)
F_{dt}	eddy-current dynamometer trunnion bearing friction (N)
F_{dra}	aerodynamic friction on drum surface (N)
F_{drf}	friction from differential and drum axle (N)
F_{drt}	friction from drum assembly trunnion bearings (N)
F_{dyno}	net force from dynamometer, as measured by load cell (N)
F_{ff}	flywheel friction force (N)
F_{fric}	total chassis dynamometer friction force (N)
$F_{loadcell}$	raw force indicated by tractive effort load cell (N)
F_{me}	electric motor electromagnetic force (N)
F_{mf}	electric motor internal friction force (N)
F_{motor}	net force from electric motor, as measured by load cell (N)
F_{mt}	electric motor trunnion bearing friction force (N)
F_{net}	combined demand force from dynamometer and motor (N)

F_{sf}	chassis dynamometer shaft and bearing friction (N)
F_V	vehicle tractive force (N)
F_{Vf}	vehicle rolling and transmission friction when on dynamometer (N)
g	acceleration due to gravity (m/s^2)
m_{cd}	combined equivalent mass of all chassis dynamometer components (kg)
m_V	vehicle mass (kg)
m_{Veq}	equivalent vehicle mass, including rotational inertias (kg)
ρ	density (kg/m^3)

CHAPTER 1:

Introduction

With increasing market pressure from oil companies and the continuing need to investigate alternative fuels and vehicle propulsion methods, it is important that the University of Canterbury has a facility to allow research in this area. The maturation of electric and hybrid vehicle technologies demands meaningful and repeatable testing of not just engines but complete drivetrains, often including features such as regenerative braking. The efficacy of after-market products and fuel additives is also of interest, and these too are best investigated in a laboratory environment.

1.1 University of Canterbury Chassis Dynamometer History

In 1978, the University of Canterbury Mechanical Engineering Department began redesigning their existing chassis dynamometer with funding from the Liquid Fuels Trust Board (LFTB). Several alterations were required to achieve the testing aims mentioned above, including the addition of an electronic data acquisition system and new power absorbing equipment [Raine, 1981]. This system was commissioned in 1980 by Philip Hindin, and was—until 1992—in frequent use, including an extensive fleet trial for the LFTB between 1983 and 1985. However, subsequent extensions to the building required that entire system be relocated to maintain the external access needed to bring vehicles in and out of the laboratory. The new chassis dynamometer laboratory was designed by Dr John Raine during 1992 and 1993 and the installation was completed in 1994. The original software was written in Fortran and assembly language to be run on a Digital PDP-11/03 computer as part of a MINC-11 data processing system. A simple, menu-driven program allowed the user some control over the system, and data was stored and transferred using a series of floppy disks. At the time of the new installation, it was decided that the visual display and data handling capabilities should be upgraded. To this end, Mr Hindin oversaw the

installation of the data cables, analogue-to-digital conversion cards and general system wiring that are currently in use. The chassis dynamometer was not used under computer control between 1994 and 2000, during which time an incomplete attempt was made by Neil Glasson to adapt the latest engine dynamometer software for use with the chassis dynamometer.

1.2 Chassis Dynamometer Testing

Dynamometers enable a wide range of performance tests to be undertaken, which can determine the power output of a vehicle as well as recording information such as exhaust emissions and fuel economy data. One type of test, known as a vehicle mapping test, is used to measure parameters of interest over a matrix of loads and speeds, so that maximal and minimal points can be determined for data such as thermal efficiency. Accurate measurement of speed and vehicle power are required, as well as stability in terms of the load applied by the dynamometer. Another testing regime best carried out on a chassis dynamometer is the driving cycle test. During such tests, the vehicle is driven over a predefined sequence of accelerations and speeds to simulate on-road driving in a repeatable way. Realistic estimates can then be made of fuel and energy consumption. The speed sequence to be followed by the vehicle is best stored on file in a computer and displayed during the test. Any dynamometer system must be flexible in its application so that it can accommodate a variety of specific test schedules and vehicles. In all cases, rapid and accurate dynamometer control is particularly important.

1.3 Thesis Overview

To ensure that any experimental data would be as repeatable and usable as possible, re-evaluation of several calibration techniques and the measurement accuracy of the system were needed. Chapter 4 includes details of the load cell calibrations, and determination of dynamometer velocity and acceleration. To measure the forces exerted by a vehicle under test, and to apply a known load, one must first calculate the internal frictional and inertial forces present in the dynamometer system. Calculation of the dynamometer inertia, and a means of using this to find system and vehicle friction constants are dealt with in Chapter 5. This discussion also includes the limitations of the equipment that lead to the selection of this method.

The majority of effort on this project was devoted to the presentation of an efficient and simple computer user interface. To ensure its continued use, it was important that this program should appear and operate in a familiar way. During any test, a large number of options are available to the user, from dynamometer and vehicle settings to the test configuration and duration. As well as presenting the user with these initial options, the dynamometer control program must also handle the physical running of the tests, including hardware switching and outputs, A/D data sampling, and on-screen feedback of test parameters and progress. Chapter 6 contains specifics of the programming tasks undertaken and the resulting software system.

The repeatability of tests carried out on a chassis dynamometer enables a comparison between two or more different vehicles undergoing the same test, or a single vehicle with its configuration altered. For example, the performance of after-market fuel additives can be determined in a series of trials with and without the product. Analysis of test data is best made in graphical form, and a versatile results display program was desired for use with the chassis dynamometer. Ideally, test results should be able to be plotted quickly and easily, with the capacity to display one or more test runs on the same axis for the purpose of comparison. The calculation and prediction of vehicle energy consumption—particularly during a driving cycle run—is also of interest, and may be used to determine the relative effect of variable cycle parameters such as the vehicle friction coefficients. Energy consumption modelling and data graphing software are detailed in Chapter 7. Graphical outputs have been used to display the results of a series of proving tests that were carried out as part of the system recommissioning. The response and repeatability of the system as a whole have been documented in Chapter 8 so that potential improvements can be identified and to put experimental results in perspective with regards to accuracy and precision.

The purpose of this project was to prepare the University of Canterbury chassis dynamometer and its accompanying software for use by students of the University as well as outside parties for the purpose of vehicle testing. Several improvements have been identified in Chapter 9 that would increase the usefulness of the system as a whole, and these may form the basis of future student projects at Canterbury.

CHAPTER 2:

The University of Canterbury Chassis Dynamometer

2.1 Common System Configurations

All chassis dynamometers have several key features in common. Most importantly, a means of absorbing the power output from the test vehicle's engine is needed to allow different loads to be applied for a variety of testing procedures. Energy is transmitted to this power absorber via a direct connection to the vehicle's wheel hubs, or through a set of rollers, which are rotated by the wheels of the test vehicle. Flywheels and/or a motoring capability may also be included if vehicle inertia is to be simulated. Descriptions of inertia simulation and the modelling of various vehicle forces are included in Chapter 3. Systems that incorporate a set of large rollers (one roller for each driven wheel) are more common in applications requiring long term running of the vehicle, in which tyre overheating can occur. Hub dynamometers are best suited to engine tuning applications which demand rapid response and minimal set-up time between tests. A common and versatile dynamometer layout consists of a single DC or AC machine mounted outside the rollers and on the same axis, as shown in Figure 2.1.

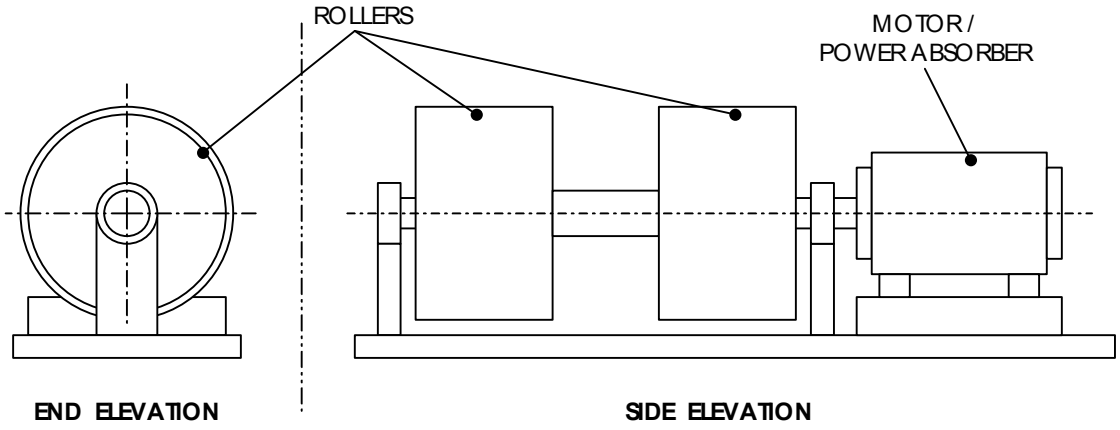

Figure 2.1 Typical arrangement of a roller-type chassis dynamometer

Output power is most commonly absorbed by hydraulic or electric machines—also known as dynamometers—which dissipate power either as heat or electrical energy. A single unit that can perform both motoring (power output) and generating (power absorption) functions is a common feature in commercially available chassis dynamometers.

All but the simplest of garage tuning dynamometers include the capacity to measure the equivalent road speed and tractive force applied at the vehicle's wheels. Chassis dynamometers for in-depth driving cycle and vehicle mapping tests customarily incorporate many different measuring devices, which are sampled and recorded by a computer-controlled data acquisition system. Common features of interest during a dynamometer test include the exhaust emissions (such as CO, CO_2, NO_X and unburnt hydrocarbons), vehicle cooling water and oil temperatures, and of course tractive force and power output. Fuel consumption and air inlet flowrates may also be recorded for combustion powered vehicles, and these often require adjustment to the standard engine intake equipment. Where the system is controlled by a computer, processing power and user interfaces vary greatly. The simplest forms may consist only of a data logging function which saves information for later viewing, while more sophisticated systems incorporate digital control of the dynamometer, prompts and feedback to the operator, as well as the recording and graphical display of data. Rates of screen update, data sampling, and control signal output are dependent mostly upon the processing speed of the control computer and its associated electronics.

2.2 System Configuration at the University of Canterbury

As mentioned in Chapter 1, the entire chassis dynamometer was transplanted into a new laboratory in 1994. The new layout of the laboratory and the desire to reuse the present equipment dictated that the power absorbing shaft be mounted at right angles to the roller drums. The overall dynamometer system is shown in Figure 2.2 and Plate 2.1. The roller drums are carried on a trunnion-mounted Ford 15C truck axle, with its differential locked and a ratio of 43:7 (6.14:1). The axle assembly is located laterally by a Watt linkage lying in a horizontal plane beneath the axle, as shown in Figure 2.3.

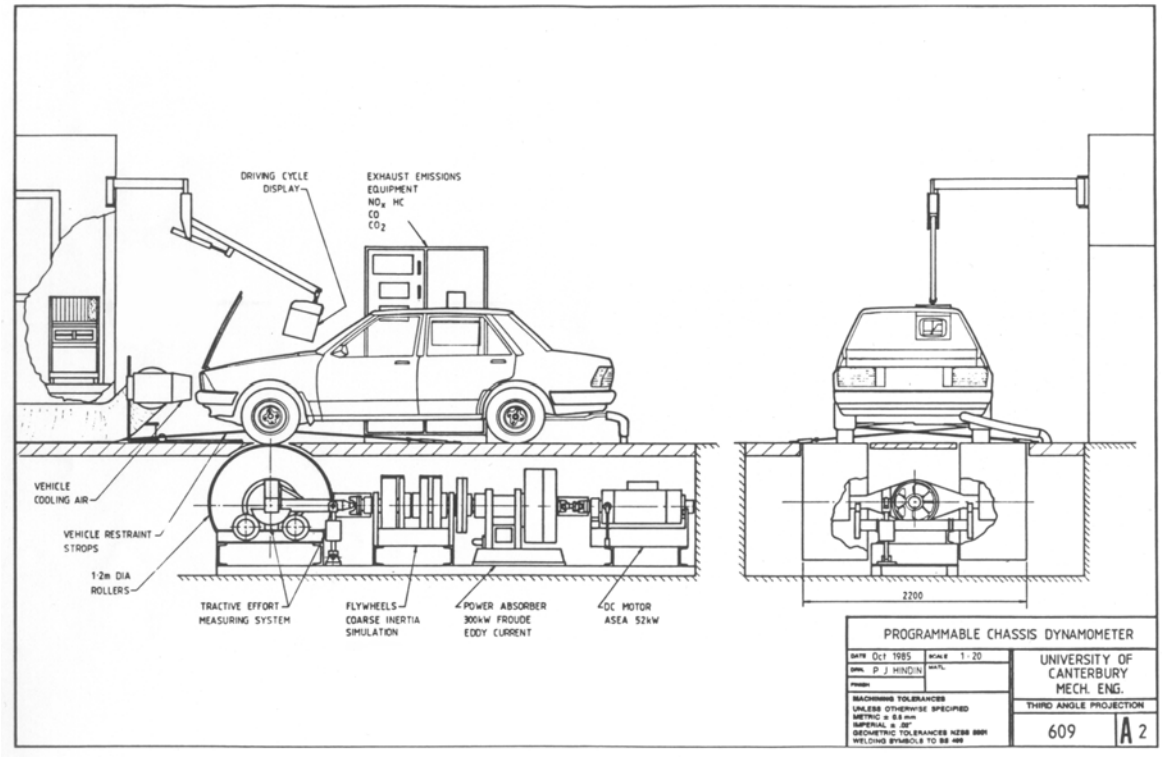

Figure 2.2 University of Canterbury chassis dynamometer schematic diagram

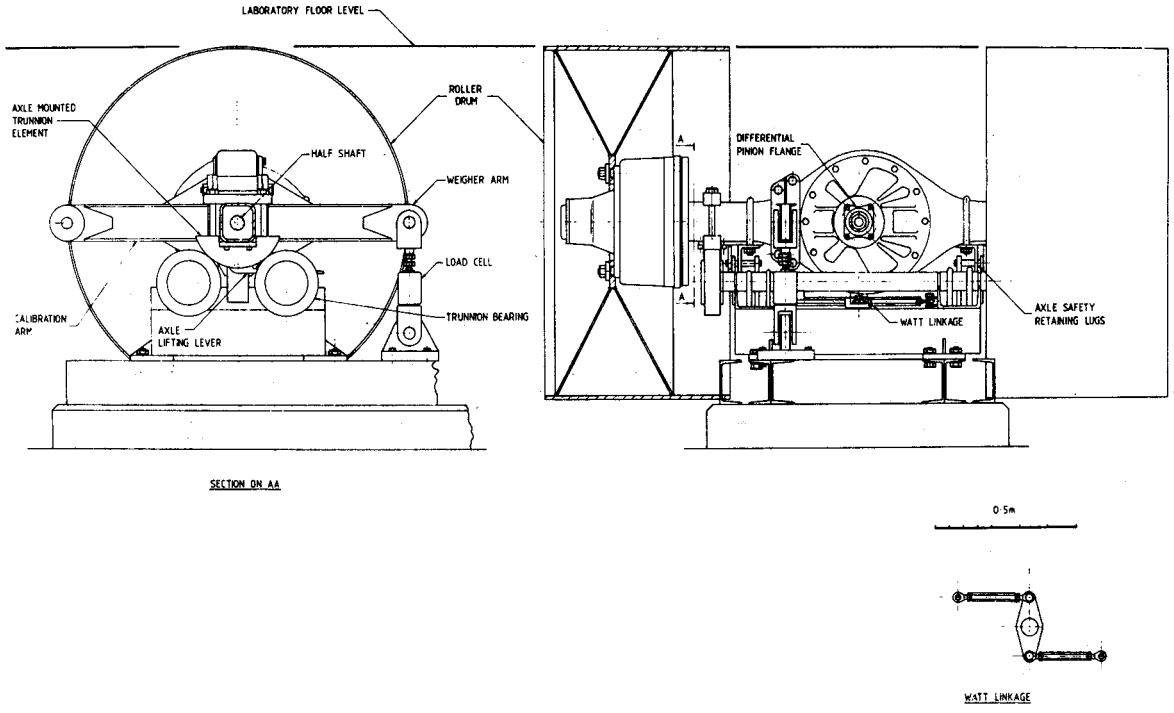

Figure 2.3 Chassis dynamometer drum axle configuration

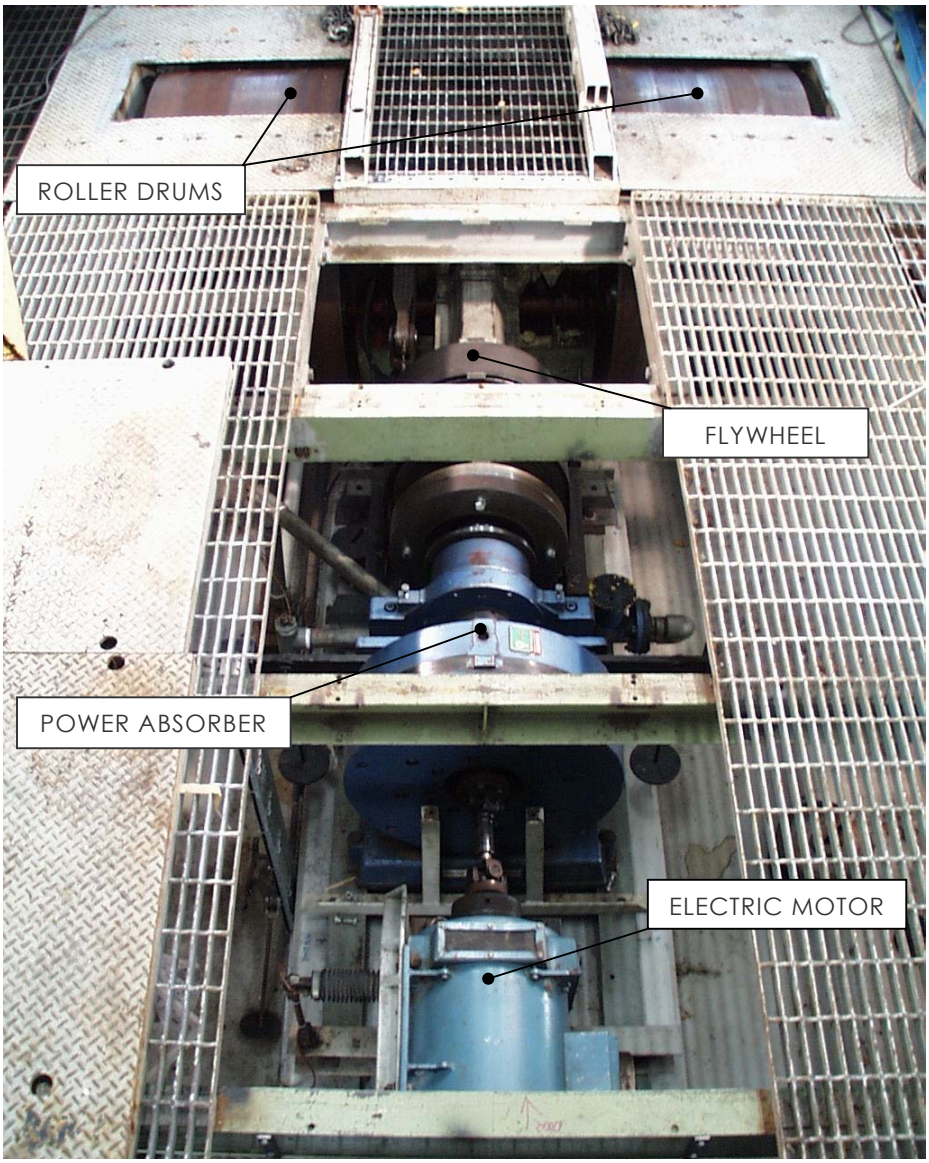

Plate 2.1 University of Canterbury chassis dynamometer main shaft (from above)

The use of trunnion bearings means that forces applied at the surface of the drums can be detected by a strain-gauge load cell recording the reaction force of the assembly on the rigid support stand. To determine the actual force at the drum surface, the friction and inertia of the drum axle assembly must be taken in to account. This tractive effort correction is detailed in Section 5.5.

Power is absorbed by a Froude EC50TA Eddy-Current Dynamometer. The supplied torque and speed measuring equipment of this instrument are used for control purposes. Originally, the design included a 166 kW D.C. motor-generator set which

could motor and absorb in both directions. However, this compact regenerative system was not practical due to a lack of sufficient A.C. mains current capacity. The water-cooled, disc-type dynamometer was chosen in preference to a hydrokinetic absorber on the grounds of a superior low-speed torque capacity and a lesser requirement on the water supply for a given maximum torque rating. The gearing incorporated in the axle assembly means that the dynamometer operates at a higher speed and lower torque than if it were connected in a direct fashion to the roller drums.

A set of flywheels is mounted between the axle and dynamometer to allow inertia simulation of vehicle masses between 664 kg and 1794 kg. Running through the centre of the flywheel set is a hollow shaft, which can be rigidly coupled to the main shaft, or allowed to rotate independently on bearings. Each of the four flywheels sits on bearings on the outside of the hollow shaft. Flywheels may be engaged to spin with this shaft—and therefore, with the main shaft—by bolting on the respective flanges. The discrete inertia intervals that can be achieved by including or omitting individual flywheels are listed in Appendix A and provide steps of not more than 120 kg over the entire range. While the inertial loads present during acceleration and deceleration of the roller drums may be accommodated by the eddy-current dynamometer, the inclusion of flywheels lessens the overall power absorption requirement. Figure 2.4 shows a schematic of the flywheel assembly.

During calibration and warming up of the system, it is useful to be able to motor the dynamometer and rollers without the presence of a vehicle. A 26 kW ASEA LAK 180LA D.C. motor has been installed, which is controlled by a 3 phase thyristor converter with polarity reversing switch gear to enable motoring in both directions. It was intended that this machine perform additional inertia simulation—particularly during deceleration—in the original configuration. However, it was found that the response time and control accuracy were insufficient for this task (see Section 5.2.3) and that the power absorber and flywheels offered superior inertia approximation without the use of the electric motor. As shown in Figure 2.2, the components of the system are connected via universal shafts to accommodate any misalignment.

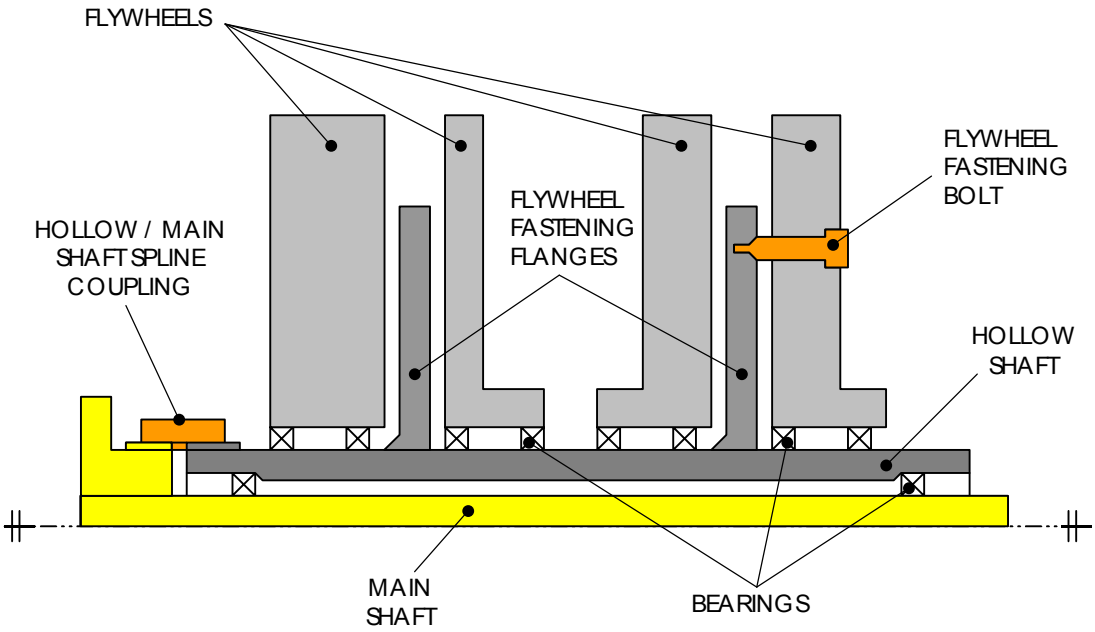

Figure 2.4 Flywheel set half-section schematic, showing hollow shaft, bearings and coupling flanges

2.3 Original Equipment and Testing

The design of the University of Canterbury chassis dynamometer as commissioned in 1980 is detailed by Raine [1981]. The addition of new power absorbing equipment, as well as computer control and data recording facilities were necessary to increase both the accuracy and flexibility of the dynamometer system. The Liquid Fuels Trust Board provided funding for this project with a view to conducting extensive trials of individual and fleet vehicles running on alternative fuels. Vehicle mapping tests as well as driving cycles measuring an array of performance parameters were conducted for more than 30 vehicles between 1983 and 1985. In addition, a dynamometer test was specifically designed to investigate vehicle drivability, including cold starting and acceleration characteristics [Hindin, 1986]. In this earlier configuration a Digital Equipment DECLAB-11 MINC computer was used to record and manipulate test data. However, it was severely limited in terms of memory capacity and a series of floppy disks were required to store data and test parameter information.

Computer processing speed was also a problem in 1980, and a large proportion of the control software was written in machine code for maximum efficiency. A monitor linked to the control computer was added in the test cell to assist the operator.

Extended inertia simulation was achieved by means of the flywheel set discussed in Section 2.2, which was added in 1985.

When extensions to the building required that the chassis dynamometer be relocated, it was decided that a further computer upgrade would be beneficial. The Froude dynamometer, ASEA electric motor, flywheel set, and drum/axle assembly have remained largely the same, with the most important changes being in the control of the machines and the acquisition of test data. Although the system was not used for any significant testing between 1994 and 2000, the existing sensors and wiring remain essentially as they were set up during 1994. The notable exceptions being the addition of several thermocouples, new electronic filtering circuitry, and the inclusion of air flowrate, fuel flowrate, and NO_X emission meters to the A/D data sampling capability. The inherent capability of the current hardware has also been enhanced by the introduction of the current computer program, particularly in regards to repeatable driving cycle, mapping, and maximum power testing.

2.4 Peripheral System Elements

The current facility at the University of Canterbury includes several features that aid successful testing, but are not intrinsic parts of the chassis dynamometer system. Stationary testing of any kind places a high demand on cooling systems for both the vehicle under test and the dynamometer itself. The Mechanical Engineering chassis dynamometer laboratory is equipped with a portable fan for cooling of the test vehicle, while a constant air temperature is maintained by large extractor fans with associated ducting. This extraction system was designed to remove all the waste heat from a vehicle supplying a constant wheel power of 200 kW, with a 10ºC rise in ventilation air temperature. An exhaust extraction fan and duct is also supplied to remove unwanted contaminants from the laboratory environment. The dynamometer drum axle and power absorber are both water cooled, and have temperature sensors which can be monitored in the control room. To anchor the test vehicle, a set of steel cables and chains are secured to the laboratory floor on purpose-built fastenings. To assist the driver of the test vehicle, 13-inch repeater monitor linked to the control-room computer provides visual feedback and allows the operator to set parameters and view results without leaving the test cell. The monitor and keyboard are mounted

on an adjustable pendant arm, which also services the electrical wiring for several sensors including the tachometer and vehicle temperature thermocouples.

2.5 Computer and Electronics Specifications

The control computer consists of an AMD-K6/200 processor, 64 Mb RAM, and 4.01 Gb hard drive running Microsoft® Windows 95[1] on the Mechanical Engineering network. As mentioned in Section 2.4, a repeater monitor and keyboard are provided in the test cell and control of the CPU can be switched between this and the control room equipment. The user interface and test control program was designed to be run in a DOS environment, and was written using Borland C++ Version 3.1[2]. The overall appearance is an outcome of the decision to use the Turbo Vision®[3] application framework, which implements a Windows-like appearance and method of navigation. Additional software has been written using MATLAB® version 5.3.0.10183 (R11)[4] for the viewing and presentation of test data. This software is menu-driven, and has been used to produce the graphs presented in Chapters 7 and 8. All output files generated by the main program are also suitable for importing into Microsoft Excel®[5] for producing tables or further data manipulation.

Up to 16 A/D channels of data input are handled through a PC-LabCard PCL-812PG data acquisition card with a PCLD-889 daughter board providing an additional 16 multiplexed channels, which are used mainly for thermocouple temperature sensors. The computer is also programmed to send digital switching commands and variable voltage D/A signals via the PCL-812PG. Switching commands include the dynamometer and electric motor operation modes (via a PCLD-785 digital output board), as well as gain and channel bit-codes for the PCLD-889 multiplexer. The two D/A channels may be used to control the motor output power under speed or torque control, and the power absorber by means of speed, torque, or a power law control. A

---

[1] Copyright Microsoft Corporation

[2] Copyright 1990, 1992 Borland International

[3] Copyright 1991, Borland International

[4] Copyright 1984–1999 The Mathworks, Inc

[5] Copyright Microsoft Corporation

differential-input low-pass filter circuit board designed and constructed at the University of Canterbury is used to decrease the signal noise before voltages are received by the A/D card. Various equipment modes, as well the state of the air and water supplies, are also monitored by the PCL-812PG via a PCLD-782 opto-isolated digital input board. The software timing is interrupt-based and controlled by a Universal Pulse Processor (UPP) card, based on the Hitachi HD63140 UPP chip. In addition, this card handles the pulsed signals from the spark plug pickup and dynamometer speed encoder, which are converted from raw pulses to digital signals by purpose-built comparator and opto-coupling circuitry. Figure 2.5 illustrates the relationships between various elements of the chassis dynamometer data acquisition system.

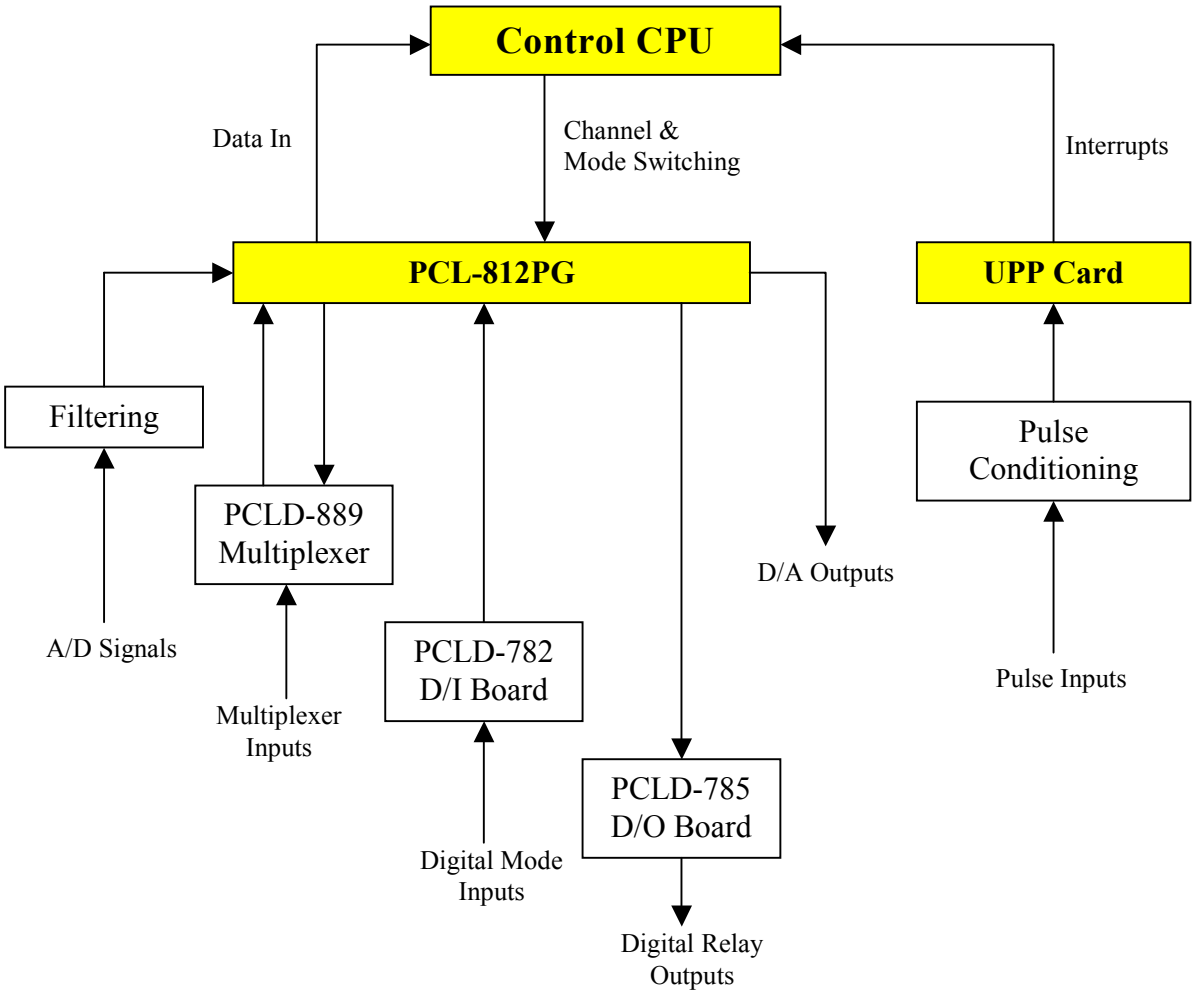

Figure 2.5 Data acquisition system block diagram

The Plate 2.2 shows the arrangement of the various circuit boards located in the automotive control room. Note that the UPP card and PCL-812PG are mounted in ISA slots inside the PC and so are not visible.

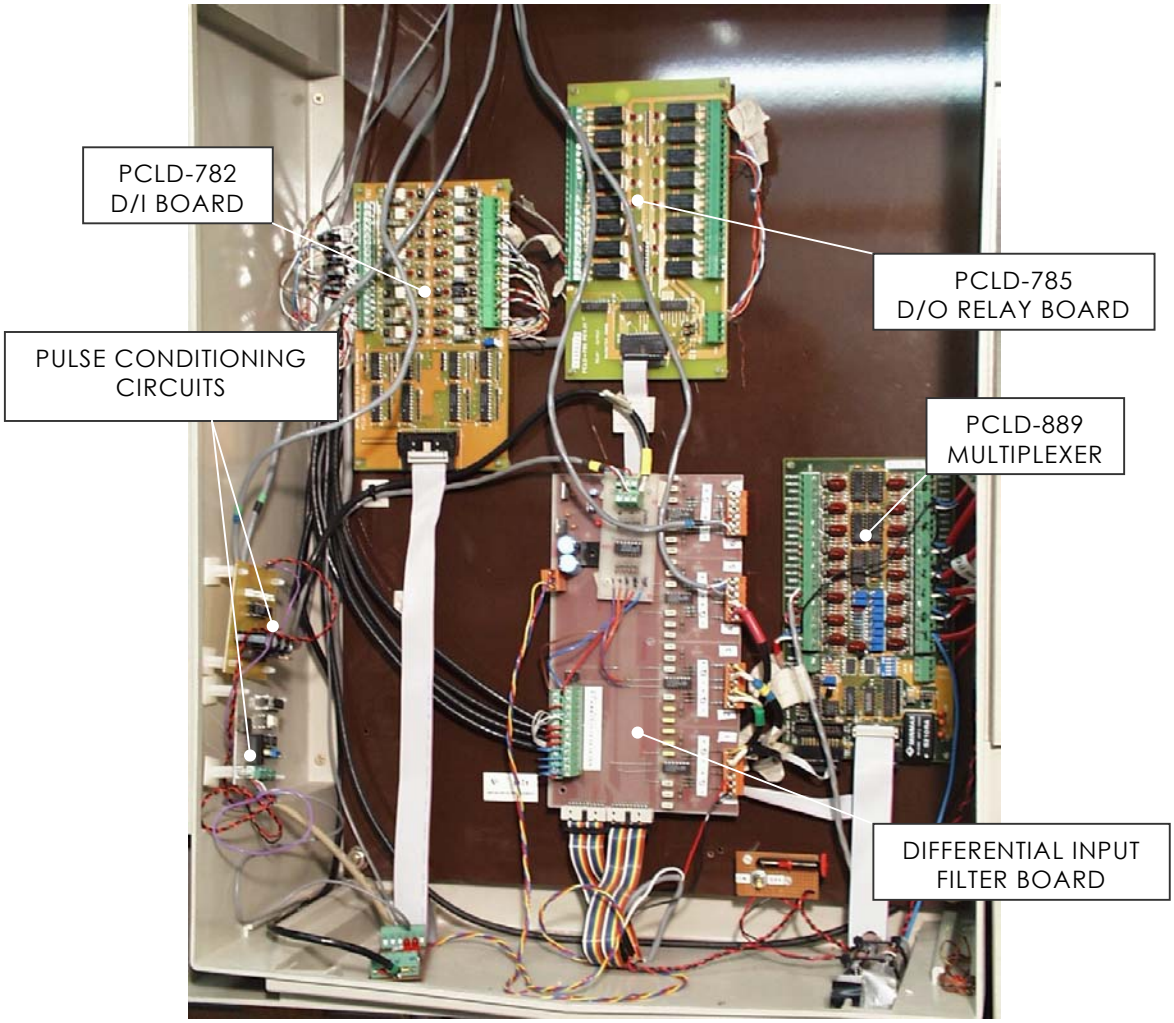

Plate 2.2 Control room electronics cabinet

2.5.1 Measured Parameters

In the main data acquisition program, inputs are recognised in several ways, including: voltages converted directly by the PCL-812PG A/D card, voltages received by the PCL-812PG via the PCLD-889 multiplexer, and external inputs that do not fall into either of these two categories. The multiplexer has 16 available channels in addition to a cold junction compensation (CJC) signal. Of these, six are currently in use. On the PCL-812PG, one channel is used to access the multiplexing channels and another the CJC channel. Of the remaining 14 channels, seven are

currently in use (including a spare channel kept free for miscellaneous voltage testing). There is no express limit on the number of external inputs, but at this point velocity and engine speed are the only inputs not read through the PCL-812PG. Table 2.1 summarises the measured parameters.

Channel	Parameter	Units	Signal
External Inputs: UPP card			
	Speed	kph	0–5500Hz
	RPM	RPM	0–350Hz
PCL-812PG			
0	Test Channel	V	±10V
1	PA Torque	Nm	0–10V
2	Tractive Effort	N	±5V
3	Motor Torque	Nm	±2.5V
4	Fuel Flowrate	gm/s	0–5V
5	Air Flowrate	gm/s	4–20mA
6	NO_X Concentration	ppm	0–5V
8	CJC (thermocouple compensation)	V	±1.25V
9	Multiplexer	V	from PCLD-889
PCLD-889 Daughter Board			
0	Ambient Air Temp.	°C	±2.5mV
1	Drum Axle Oil Temp.	°C	±5mV
2	Vehicle Water Temp.	°C	±10mV
3	Vehicle Oil Temp.	°C	±10mV
4	Spare Thermocouple	°C	±10mV
10	Ambient Air Pressure	mb	0–1999mV

Table 2.1 Channel assignment table

During a chassis dynamometer driving cycle or mapping test, demand signals from the computer are sent to the Froude dynamometer at the rate of 10 Hz . D/A output signals may be used to control the machine in any of its three modes of operation; constant speed, constant torque, or ‘power law’. However, the power law mode—in which torque varies with speed—was not used for any of the testing detailed in Chapter 8, and is not discussed any further in this thesis. Constant speed mode was used to maintain the set points during mapping tests, while driving cycle and

maximum power runs were best controlled with constant torque. While a consistent demand may be sent from the computer, the 3-term analogue controller built in to the dynamometer is continuously updating the actual electric field that defines the absorbed torque. During a driving cycle test, which requires a continuously varying load on the vehicle, the demand torque may be varying rapidly. From the software point of view, this demand sequence consists of a series of open-loop commands, with each new command being acted on by the closed-loop analogue controller. The same may be said of the motor control. Although it is not commonly used during quantitative tests, the ASEA electric motor has its own controller, which may be provided with a series of constant demands by the computer program.

2.6 Overview of Software Functionality

A brief outline of the capability and scope of the main C++ computer program is included here. A more detailed description, including the specific programming challenges and complete functionality, can be found in Chapter 6.

2.6.1 Preliminary Details

The main program can be operated either using a mouse and keyboard, or keystrokes only. A series of pull-down menus present the various options for calibration, file handling, and testing routines. Numerical inputs can be selected and typed in, and the results confirmed in a familiar way by the use of ‘OK’ or ‘Cancel’ buttons. Each vehicle to be tested has its own data file, which contains the make and model as well as data such as mass and on-road frictional resistance. Vehicle mass is important in determining which of the selectable flywheels are to be included to most closely match the on-road inertia. Once a vehicle and configuration file have been chosen, several testing options may be selected.

Before meaningful measurements can be made, it is important to ensure that all the measurement devices are correctly calibrated against known values. The program includes a simple, general-purpose routine that prompts the user for an independently measured value, then records and compares the A/D input from the appropriate pre-selected channel. A mathematical curve-fit is generated for each set of data, which can then be used to calculate the physical value, given the A/D voltage input during

testing. These calibration coefficients (often taking the linear form of a gradient and an offset) can be entered by the user into a configuration file for future use. The calibration data capture procedure and on-screen display is discussed further in Section 6.5.4.

Routines are also included to account for day-to-day variations in system friction and the zero value of the load cells, with step-by-step instructions given on screen. Section 4.3 discusses the limitations of these load cells, and the rationale behind the inclusion of a re-zeroing procedure. Friction calibration is accomplished using a series of dynamometer *coastdowns,* which are introduced in Chapter 5.

2.6.2 Routines for Running a Vehicle

Several modes of operation were incorporated to allow a wide variety of flexible testing programs to be carried out on the University of Canterbury chassis dynamometer. Each routine requires that a known force be applied by the dynamometer to the wheels of the test vehicle. By analysing the equations of motion of the system (see Chapter 3) the power absorber demand required to achieve a given tractive force—particularly under *road load* simulation—may be calculated. In this so-called road load simulation mode, the driver can accelerate and decelerate at will while the computer sends a load demand to the eddy-current dynamometer such that the forces experienced at the wheels of the vehicle are equal to those on a vehicle undergoing similar speeds and accelerations on the road. The specific routines mentioned below, and the underlying program structure, are discussed in more detail in Chapter 6.

The ‘Warm Up’ routine is available to prepare the chassis dynamometer and vehicle for testing by running at constant speed, or under an approximate road load until the lubricating oil and all bearing surfaces have stabilised in terms of temperature and frictional attributes.

The ‘Road Load Driving’ option allows running of a vehicle under road load conditions, while all the measured parameters are shown on the screen—updated at the rate of 5 Hz—and can be saved to a pre-selected file at the touch of a button.

'Manual Control' mode is similar in appearance to 'Road Load Driving', but allows the operator to select constant speed and torque demands for both the motor and the dynamometer. This mode is useful for performing maximum power tests in which full throttle is applied and the vehicle is allowed to accelerate over a set speed range, while measuring—in particular—the power output by the vehicle. Such tests are invaluable in tuning work where small changes in settings on the engine are not easily discerned except by comparison of the resulting torque curves.

The entire performance envelope of a vehicle may be investigated by carrying out a 'Mapping Test'. By running at a series of predetermined speeds and dynamometer loads, a map of each measured parameter can be built up which shows not only the peak numerical value, but also the optimal running conditions in terms of speed and load. Common parameters of interest in this type of test include fuel consumption, brake thermal efficiency, and the proportions of CO, CO_2, HC and NO_X in a vehicle's exhaust. Coloured contour plots of each parameter can be produced using the MATLAB routines detailed in Chapter 7.

Another common method of comparing vehicle performance is the 'Driving Cycle' test. Many different cycles have been created which attempt to reproduce common driving patterns either in an urban environment or on the open road. The speed and duration of these simulated trips depend on the driving habits and traffic conditions in the area of interest. On the chassis dynamometer, a driving cycle file contains the desired speed at each one-second interval for the entire test. This speed is reproduced graphically in the form of a scrolling line, which the driver of the vehicle under test attempts to follow by accelerating and changing gears as one would on the road. The power absorber is sent updating demands at 10 Hz to simulate the road load forces as closely as possible. Again, all the parameters of interest are recorded and saved to a file, which can be used to find the maximum point, the average, or to produce a plot for comparisons. Accidental deviations from the desired speed are inevitable when a human driver controls the test vehicle. However, a record is kept of the total number of discrepancies and the test may be aborted if the schedule is not maintained within the allowable limits. A MATLAB routine (see Section 7.2) has also been designed to compare the total energy consumed in terms of power output at each instant with that

calculated by fuel energy consumption and the hypothetical case of the vehicle exactly following the demand speed throughout. Driving cycle tests are most commonly used to compare the fuel consumption and exhaust emissions of vehicles under local on-road conditions in a repeatable and quantifiable way.

2.7 Comparative Performance of the University of Canterbury Chassis Dynamometer

In terms of power absorbing capacity and maximum speed, the University of Canterbury dynamometer compares favourably to commercially available chassis dynamometers at the time of writing. Several commercial dynamometers have been investigated and a summary of various performance specifications has been included in Appendix B. Comparable roller-type chassis dynamometers produced by Schneck and Froude Consine have similar drum diameters, but are designed to measure a lower tractive effort range than the University of Canterbury facility. However, due to the considerable age of the machinery detailed in this thesis, load response and stability are below industry standard. A faster data sampling rate (which could be facilitated by greater computer processing power) may also be desirable to improve the quality of results using the chassis dynamometer. The testing facility and its associated equipment such as exhaust and cooling fans provide an excellent laboratory environment and capacity exists for significant extension of the sampled data channels.

CHAPTER 3:

Equations of Motion

In order to apply a known dynamometer load, the characteristics of the system and how these relate to the vehicle under test must be determined. The vehicle power output is measured as a force and speed at the road surface. This force is known as the tractive effort and is commonly measured on a roller-type dynamometer by a load cell indirectly connected to the rollers. For steady state testing, it is sufficient to know the frictional losses of the system so that the power absorber can combine with the friction to apply a given load at a given speed. However, if measurements are to be made during speed transients—as in a driving cycle test—it is necessary to include inertial effects.

3.1 Vehicle Tractive Effort

A vehicle in motion is subject to various gravitational, frictional, and inertial loads. The tractive effort to overcome these resistances, F_V applied at the surface of the road wheels is given by:

$$F_V = \underbrace{m_V g\left(C_{R1} + C_{R2} v^n\right)}_{\text{ROLLING RESISTANCE}} + \underbrace{m_V g \sin\theta + m_{Veq}\left(\frac{dv}{dt}\right)}_{\text{GRAVITATIONAL + INERTIAL RESISTANCE}} + \underbrace{\frac{1}{2}\rho C_D A v^2}_{\text{AIR RESISTANCE}} \qquad (3\text{-}1)$$

See following page for notation.

Where: v = linear vehicle velocity (m/s)

$\frac{dv}{dt}$ = linear vehicle acceleration (m/s^2)

θ = road gradient

ρ = air density

n = index dependent on design of tyre and running gear

m_{Veq} = total equivalent mass (kg) = m_V + equivalent mass of rotational components

Other notation as per Nomenclature section.

Rolling resistance depends largely on tyre design and inflation pressure, as well as the condition of the road surface. C_R values vary significantly in the early stages of a journey as the tyres and running gear warm up [Burke et al., 1957]. C_{R1} may range between 0.01 and about 0.04 [Wheeler, 1963], while the $C_{R2}v^n$ term is dependent upon tyre design and temperature, and becomes significant at higher speeds (above 90 kph)[Elliot et al., 1971]. These values are quoted for a warmed up vehicle on a straight road, and frictional constants under cornering are not usually included in the tractive effort model. Note that these coefficients are based on somewhat dated references. Any new chassis dynamometer research should utilise more recent literature to incorporate the latest tyre designs and resulting frictional performance. The aerodynamic drag coefficient C_D depends primarily upon the body shape of the vehicle, as well as the air flow through the radiator and over the external fittings. Typical C_D values for road-going passenger cars at the time of writing were 0.25–0.35 in still air.

In cases where the frictional characteristics of a vehicle are determined experimentally, the individual magnitudes of these constants are not necessarily distinguishable and the tractive effort equation is simplified to:

$$F_V = m_{Veq}\frac{dv}{dt} + f_{0V} + f_{1V}v + f_{2V}v^2 \tag{3-2}$$

Where: f_{0V}, f_{1V}, f_{2V} = combined vehicle friction constants

The gravitational forces brought about by an incline in the road surface may be modelled on the dynamometer, and although capability exists for such a simulation, road gradient effects were not generally incorporated in dynamometer tests conducted at the University of Canterbury. Also, the vehicle mass must include the inertial influence of its rotational parts such as the engine flywheel and road wheels, which act to increase the magnitude of the tractive force required for changes in speed. This rotational component is added to the actual vehicle mass (for $m_{Veq}\ dv/dt$ calculations) and can be either measured experimentally or approximated. A common approximation is:

$$m_{Veq} = m_V \times 1.035 \tag{3-3}$$

This approximation may not hold for a wide variety of vehicle types. Equation 3-3 is used throughout this thesis, although more recent research may indicate a different factor or rotational inertia correction.

3.2 Chassis Dynamometer Equations of Motion

The free-body diagram Figure 3.1 shows all the external forces acting on the chassis dynamometer during motion. It is helpful to express each torque acting on the shaft in terms of the equivalent force at the drum surface. This conversion can be made with the use of the axle differential ratio (43:7) and the roller drum radius (0.6 m). An example is provided for the case of the eddy-current dynamometer electromagnetic force.

$$F_{de} = T_{de} \times \left(\frac{diff\ ratio}{drum\ radius} \right) \tag{3-4}$$

Where: T_{de} = Electromagnetic torque at eddy-current dynamometer

Note that the electric motor always applies a force in the direction of motion, while the dynamometer force and frictional forces are in the opposite direction to the drum velocity.

The rotational inertia of each component is also expressed in terms of the roller drums. The equivalent mass if the inertia was concentrated at the drum surface is found as follows:

$$m_{eq} = \frac{I}{(drum\ radius)^2} \tag{3-5}$$

Where: I = rotational inertia of component

Rotation of the chassis dynamometer in a *positive* direction is arbitrarily defined as being in the direction shown in Figure 3.1. Velocity and acceleration are as indicated at the rollers, and the main shaft rotates in such a way that the top of the flywheels move into the page. Under a *positive* force from the test vehicle, the tractive effort load cell is in compression, indicating a positive tractive force. The power absorber applies an opposing force, and the electric motor exerts a force in the same direction as the shaft rotation, both of which read positive on their respective load cells.

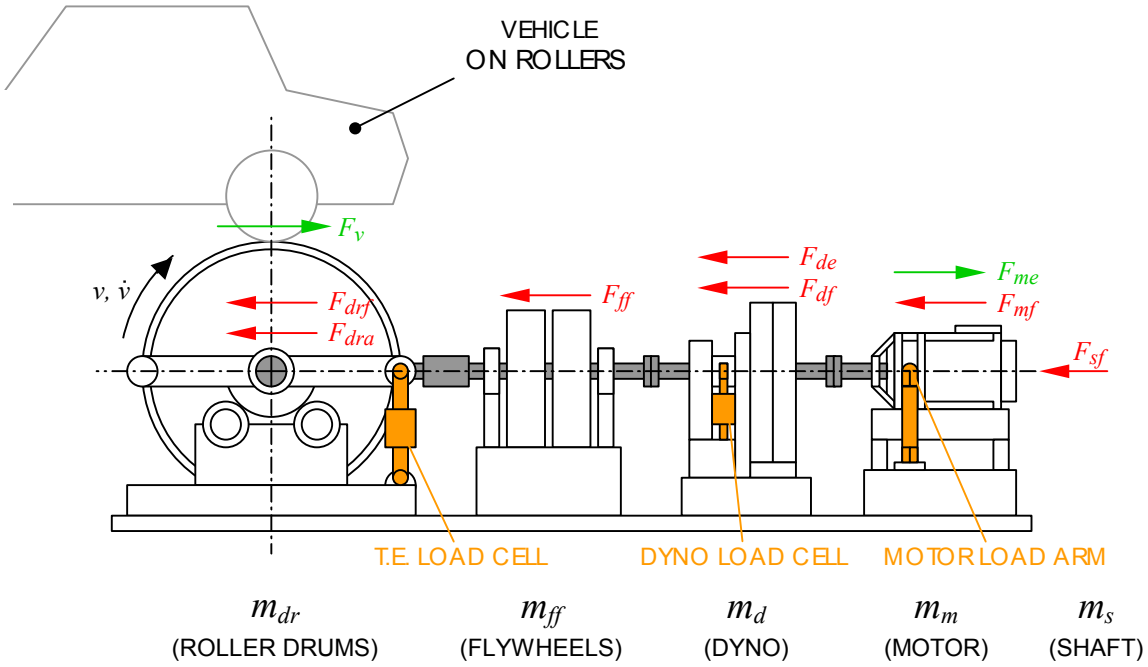

Figure 3.1 Chassis dynamometer free-body diagram

Where: v = velocity at drum surface (m/s)

$\dot{v}$ = acceleration at drum surface (m/s^2)

F_v = vehicle tractive force (N)

Other notation as per Nomenclature section

The overall equation can be stated as per Equation 3-6:

$$\left(F_v + F_{me}\right) - \left(F_{drf} + F_{dra}\right) - \left(F_{ff}\right) - \left(F_{de} + F_{df}\right) - \left(F_{mf}\right) - \left(F_{sf}\right) = \left(m_{dr} + m_{ff} + m_d + m_m + m_s\right)\dot{v} \quad (3\text{-}6)$$

Or, grouping the mass terms together and approximating the total friction force as a quadratic in relation to speed:

$$F_v + F_{me} - F_{de} - \left(f_{0d} + f_{1d}v + f_{2d}v^2\right) = m_{cd}\dot{v} \quad (3\text{-}7)$$

Where: m_{cd} = combined chassis dynamometer equivalent mass (kg)

This equation may be stated in terms of the tractive force from the vehicle, which is equal to the reaction force from the chassis dynamometer as a whole:

$$F_v = m_{cd}\dot{v} + F_{de} - F_{me} + \left(f_{0d} + f_{1d}v + f_{2d}v^2\right) \quad (3\text{-}8)$$

The torque reading given by each of the three load cells includes a friction and inertia component, depending on the individual configurations. Each of these load cell configurations is subject to friction in the trunnion bearings on which they are supported. This friction acts in opposition to the measured force, but is not experienced by the load cell, and therefore cannot be measured or included in the equations of motion. Section 4.3 contains a further description of the load cell dynamics and calibration techniques.

3.3 Combined Tractive Effort

To simulate the appropriate vehicle road load at any given speed and acceleration, the characteristics of both the chassis dynamometer and the vehicle under test must be known and combined. The forces experienced by a vehicle on the road (as per Equation 3-2) are matched by the forces experienced by the same vehicle on the dynamometer. While mounted on the chassis dynamometer, the vehicle is no longer subject to the air resistance component of Equation 3-1 or the rotational inertia of the non-driven wheels. This lesser inertia is generally ignored or included in the approximation of m_{Veq}. To accommodate the differing friction values, a test may be

carried out to determine the frictional characteristics of the dynamometer and test vehicle combined, which are then included in the tractive forces applied by the dynamometer for the purposes of Equation 3-8.

$$m_{Veq}\frac{dv}{dt}+\left(f_{0V}+f_{1V}v+f_{2V}v^2\right) = m_{cd}\frac{dv}{dt}+\left(f_{0Vd}+f_{1Vd}v+f_{2Vd}v^2\right)+F_{de}-F_{me} \quad (3\text{-}9)$$

FORCES ACTING ON VEHICLE ON ROAD = FORCES ACTING ON VEHICLE ON DYNAMOMETER

Where $f_{0Vd}, f_{1Vd}, f_{2Vd}$ = frictional coefficients of vehicle on the dynamometer

In general, the only parameters that can be continuously varied during a test cycle are the power absorber force and the motoring force. We require a formulation that can be solved for these variable parameters. The net output of each device is the combination of electromagnetic force and internal friction, which is set by the respective controllers and measured by the load cells (see Section 5.1). Thus, we modify the coefficients f_{0Vd} etc. to exclude the friction from within the powered devices. During chassis dynamometer operation the modified Equation 3-9 is constantly solved to determine the necessary combined net demand force (F_{net}).

$$F_{net} = \left(m_{Veq}-m_{cd}\right)\frac{dv}{dt}+\left(f_{0V}-f'_{0Vd}\right)+\left(f_{1V}-f'_{1Vd}\right)v+\left(f_{2V}-f'_{2Vd}\right)v^2 \quad (3\text{-}10)$$

Where: $F_{net} = F_{dyno} - F_{motor}$

F_{dyno} = power absorber control demand (N)

F_{motor} = electric motor control demand (N)

$f'_{0Vd}, f'_{1Vd}, f'_{2Vd}$ = combined friction coefficients of chassis dynamometer and vehicle, less the internal friction of the electromagnetic devices

In reality, the magnitudes of these altered f_{Vd} coefficients are determined by whether or not the power absorber or electric motor were operating during the friction calibration (see Section 5.1). The inertial force applied by the chassis dynamometer to account for the mass difference ($m_{Veq} - m_d$) is minimised by the use of the flywheel set, as detailed in Section 2.2. The various flywheel combinations ensure that for

vehicle masses between 604 kg and 1854 kg the absolute value of the mass difference need not be greater than 60 kg (see Appendix A).

For vehicle tests other than driving cycles, a constant tractive effort is often desired, as opposed to a continuously varying road load. Applying a set tractive force at the drum surface does not require knowledge of the vehicle characteristics, and Equation 3-8 is solved for the net demand force F_{net}. Constant load tests (for example, vehicle mapping) are almost always carried out at a series of constant speeds ($dv/dt = 0$), further simplifying the load equation to:

$$F_{net} = F_V - \left(f'_{0d} + f'_{1d} v + f'_{2d} v^2\right) \tag{3-11}$$

Again: $f'_{0d}, f'_{1d}, f'_{2d}$ refer to friction coefficients of the chassis dynamometer not including the contribution from the powered device

CHAPTER 4:

Details of Selected Instrumentation

In order to carry out the inertia calibration and vehicle testing detailed in Chapters 5 and 8 respectively, accurate and repeatable data acquisition procedures were required. The chassis dynamometer currently measures up to 14 different A/D channels, which are recorded via a PCL-812PG A/D card as voltages. The capacity is available to extend the number of channels to 31. Two speed inputs are also read via a UPP card. Each sensor has been calibrated as accurately as possible, and the methods and graphical results are included as appendices (Appendix C and D). Table 4.1 below shows each of the calibrated data parameters, and the appendix section in which the calibration notes and results are included.

Appendix	Instrument	Notes on content
C.1 / C.2	Eddy-current Dynamometer	D/A demand calibration, A/D load cell calibration
C.3 / C.4	Electric Motor	D/A demand calibration, A/D load cell calibration
C.5	Tractive Effort	A/D calibration
C.6	Fuel Flowmeter	A/D calibration, total fuel integration, fuel flow path
C.7	Annubar Air Flowmeter	A/D calibration
C.8	Barometer	A/D calibration
C.9	Thermocouples (various)	A/D calibration
D	Engine Spark Plug Pickup	Photograph, equation

Table 4.1 Instrumentation appendices

Two measurement tasks in particular posed significant difficulty and required detailed investigation into the available methods and their resulting accuracies. It is important that the measurement of vehicle speed and acceleration are as accurate and free from noise as possible. This is dealt with Sections 4.1 and 4.2 below. Most useful dynamometer tests involve recording speed as one of the key variables, and driving cycle tests are especially dependent on the instantaneous velocity and

acceleration of the test vehicle. In the absence of a dedicated accelerometer, it is necessary to calculate acceleration as the change in velocity with time—that is, to differentiate. Section 4.3 details the calibration and software techniques used to ensure accurate load cell measurements, given the existing hardware and geometry. In the case of the power absorber and drum axle load cells, calibration techniques were formulated to accommodate the hysteresis and temperature-dependence of these devices.

4.1 Measurement of Velocity

As mentioned above, the measured velocity is a valuable test parameter, and is also used to calculate the instantaneous acceleration. As with most digitally recorded data, electrical noise and instrument inaccuracies are exacerbated when the signal is differentiated, as small, rapid fluctuations translate to large variations. For this reason, it was necessary to first find the most accurate and noise-free method of measuring the raw vehicle velocity, then to apply the filtering and acceleration calculations most appropriate for the chassis dynamometer system as a whole (see Section 4.2).

4.1.1 Frequency-to-Voltage Conversion

A previous chassis dynamometer configuration at the University of Canterbury recorded the roller rotational speed (and hence, test vehicle velocity) indirectly using a magnetic encoder included in the eddy-current dynamometer. The dynamometer includes a toothed wheel, which rotates with the main shaft, setting up a magnetic field of varying intensity as the teeth pass between a pair of magnets. These pulses are converted to electrical pulses, which in turn are converted to a voltage by the dynamometer circuitry. The output of this frequency-to-voltage conversion is used by the dynamometer when in speed-control mode, and can also be measured by the computer. The advantage of this system was that the voltage signal could be easily recorded using the existing A/D board. The major difficulty in using the voltage from the dynamometer was that the signal was subject to the significant noise experienced by the system, especially within the power absorber circuitry. Plots of the frequency-to-voltage signal under normal operating conditions are in Figure 4.1. A constant speed of approximately 10 kph was maintained by the electric motor while under a

constant loading of 100 Nm from the eddy-current dynamometer. This arrangement was chosen to roughly approximate conditions during testing, while minimising additional vibrations that may have arisen at higher speeds.

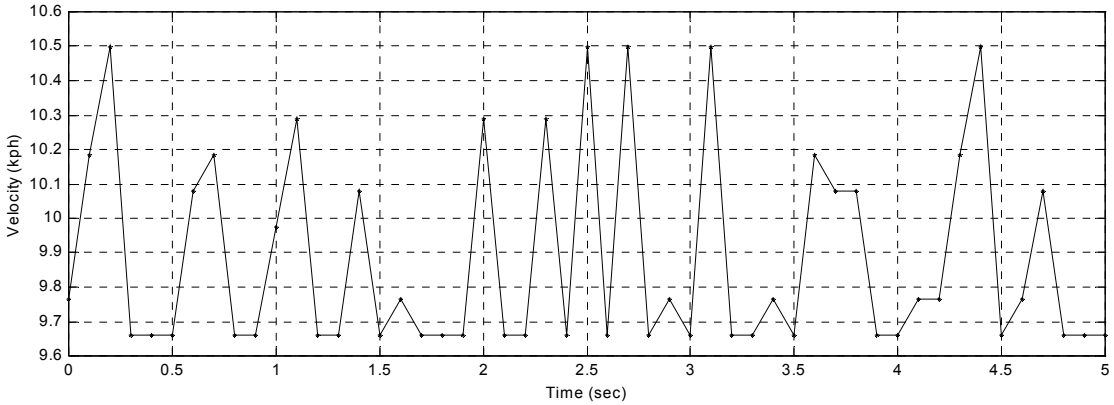

Figure 4.1 Velocity signal generated by dynamometer frequency-to-voltage converter

It can be seen the noise present in the voltage output is of the order of ±0.4 kph, which was considered significant, especially in regards to its eventual conversion to acceleration. By measuring an encoder output more directly, it was hoped that a large portion of this electrical noise could be avoided.

4.1.2 Rotary Encoders

Two rotary shaft encoders were available to measure the chassis dynamometer speed: the built-in magnetic encoder used by the eddy-current dynamometer, and an optical device mounted on the drum axle. Both signals were recorded using a UPP card constructed by University of Canterbury technicians, which performs digital switching on voltage pulses. Both encoders also required additional signal conditioning circuitry for use with the UPP card. All interrupt handling software was written and modified for use with the chassis dynamometer by Dr Andrew Cree.

4.1.2.1 Drum Axle Encoder

Given that the system is torsionally flexible to some degree, a velocity reading taken at the drum axle (which is effectively at the road surface) is more accurate in relation to a vehicle under test. However, if this drum speed were used to determine the dynamometer loading, significant inertia—and corresponding rotational lag—between the speed reading and the power-absorber could potentially lead to a degree

of instability. However, preliminary testing did not indicate that measuring velocity at the drum axle would have a significant effect on torsional stability.

An encoder system was built for the drum axle in 1981 for the purpose of measuring road speed. Two optical switches are activated by a rotating disc with 256 teeth, which periodically blocks light from LEDs to the receptors. The use of two offset opto-switches means that the direction of rotation can be calculated, as well the speed. As shown below (Figure 4.2a), the switches are set such that the pulses are generated half a pulse width apart, thus, an ON signal from switch one always precedes the ON signal from switch two when rotation is in a certain direction. Rotation in the opposite direction results in the pulse from switch one being read *after* switch two's signal. This method of reading pulses is known as quadrature. During testing of this device, it was found that velocity readings were erratic, particularly at high speeds. It was discovered that the teeth on the disc were not cut accurately enough to ensure that the pulses were read in the correct order for a given direction. Figure 4.2b shows an uneven pulse train resulting in a speed error. Subsequent investigation of the drum encoder was carried out by reading the output of a single opto-switch.

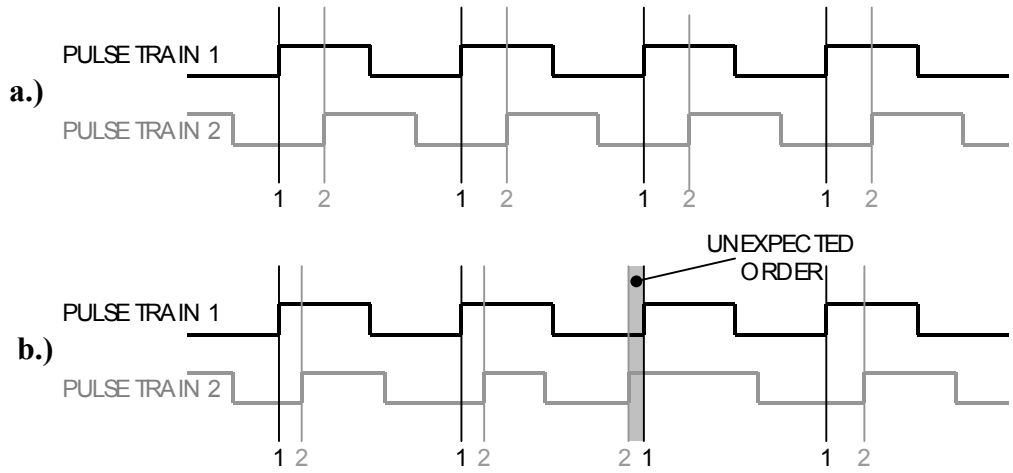

Figure 4.2 Quadrature pulse trains a.) Normal operation b.) Result of uneven teeth

In the case of a single encoder input, the calculation of velocity is relatively simple and can be carried out in one of two different ways. The opto-switches produce a voltage for the period that they are not obscured by the teeth of the disc. This pulsed voltage signal is amplified and compared to a reference voltage, and a software

interrupt is generated when the reference voltage is exceeded. The spacing between the teeth is fixed and represents a certain angle of rotation of the shaft, so the calculation of rotational velocity is a matter of measuring the rotation (in terms of interrupts) and the elapsed time (using the UPP card timer). Either the number of interrupts registered in a given time period is counted, or the duration between successive interrupts is timed. The former method is referred to here as *counting* (Equation 4-1), and the latter as *timing* (Equation 4-2).

$$\dot{\theta} = \frac{d\theta}{dt} = \frac{n_p \theta_p}{T_f} = \frac{(Number\ of\ pulses)(Angle\ per\ pulse)}{(Fixed\ time\ interval)} \tag{4-1}$$

$$\dot{\theta} = \frac{d\theta}{dt} = \frac{\theta_p}{n_c T_c} = \frac{(Angle\ per\ pulse)}{(Number\ of\ clock\ cycles)(Time\ per\ clock\ cycle)} \tag{4-2}$$

Included below is a plot of the speed signal under a constant dynamometer torque as is shown in Figure 4.1. Velocity has been calculated by the counting the pulses in each 0.1s interval. Note the difference in vertical-axis scale between Figures 4.1 and 4.3.

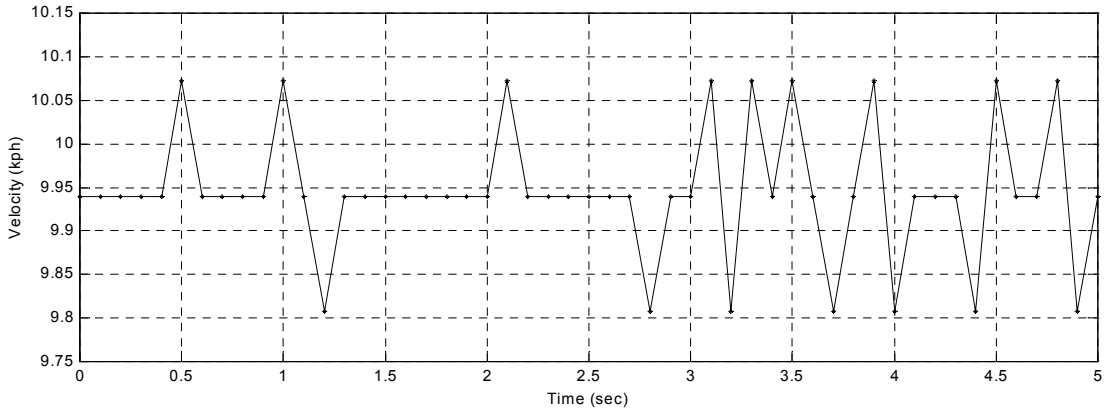

Figure 4.3 Velocity signal generated by counting drum encoder pulses at 10 Hz

The errors due to unevenness of the encoder teeth have an effect on the velocity whether one is counting pulses or timing them. The magnitude of this error depends on the rotational speed, and of course the physical difference in the width of adjacent teeth. The relative errors as a result of speed and method of calculation are addressed in Section 4.1.3. Ordinarily during velocity measurement by timing, one might record

several time intervals and average them to arrive at the rotational speed. However, by recording the time interval between every pulse, the relative angular widths of the teeth can be found (θ = average rotational speed × time between pulses). Figure 4.4 represents each width (i.e. the tooth width plus the width of the gap before the next tooth) on the radial axis and its position around the wheel's perimeter in the circumferential direction. Two consecutive plots are overlaid (one light and one dark line), showing excellent repeatability and proving that each spike can be traced to a specific encoder tooth. The unit on the radial axis is *percentage* with zero being the average tooth angle and those angles which are either greater or lesser shown in proportion.

$$Average\ tooth\ angle \quad = \quad \frac{Total\ angle\ around\ circumference}{Number\ of\ teeth} \quad = \quad \frac{360^{\circ}}{256} \qquad (4\text{-}3)$$

Thus, the large value shown as +5% at 255º represents a tooth width (including the adjacent gap) of approximately (360/256)×1.05 = 1.48º. While these figures are not intended to be highly accurate, they provide a useful relative measure of the encoder wheel *in situ*.

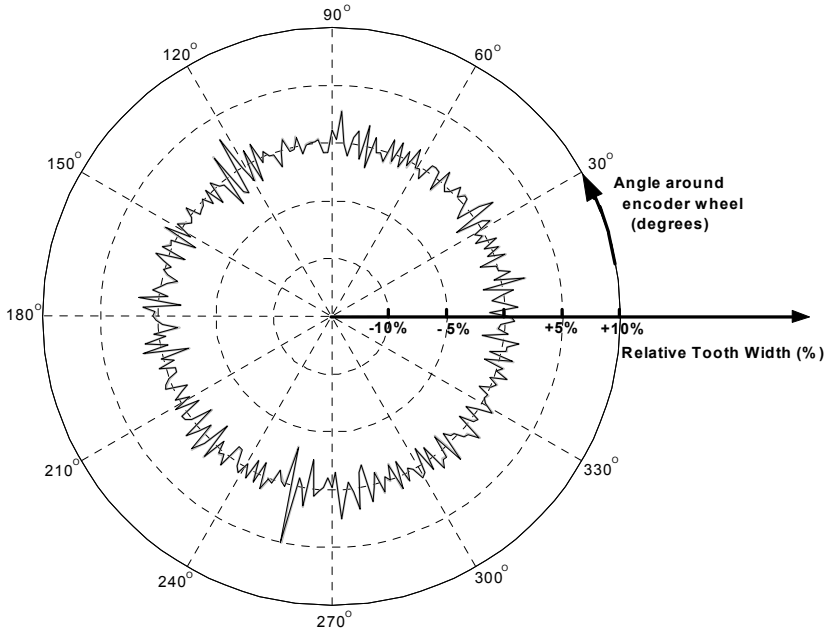

Figure 4.4 Drum axle encoder tooth widths

A maximum departure from the ideal of 5%, as shown above, impacted heavily on the velocity output calculated. This error was also not easily predictable during running of the dynamometer (when each individual tooth was not necessarily being measured) and so a more uniform disc was sought. Investigations were made into the purchase or construction of another disc, as well as possible use of the pulse output from the eddy-current dynamometer encoder.

4.1.2.2 Froude Dynamometer Encoder

As mentioned earlier, the eddy-current dynamometer unit includes a magnetic pulse encoder for feedback purposes in speed control mode. Although the frequency-to-voltage conversion circuit did not provide an adequate velocity signal, direct capture of the encoder pulses was attempted with the use of the UPP card and similar circuitry to that used for the drum encoder signal. The wheel on the dynamometer speed pickup has only 60 teeth, compared to the 256 of the drum encoder. However, because the dynamometer spins at 6.14 times the speed of the drum axle, the dynamometer unit provides approximately 368 pulses per revolution of the roller drums. This provides greater resolution when counting pulses, however it does decrease the accuracy of results when timing (particularly at high speeds), by allowing fewer clock ticks per tooth.

Figure 4.5 shows the velocity signal generated by counting pulses directly from the dynamometer encoder. It can be seen that the random noise is less than that present in the velocities generated by both the frequency-to-voltage converter and the drum encoder.

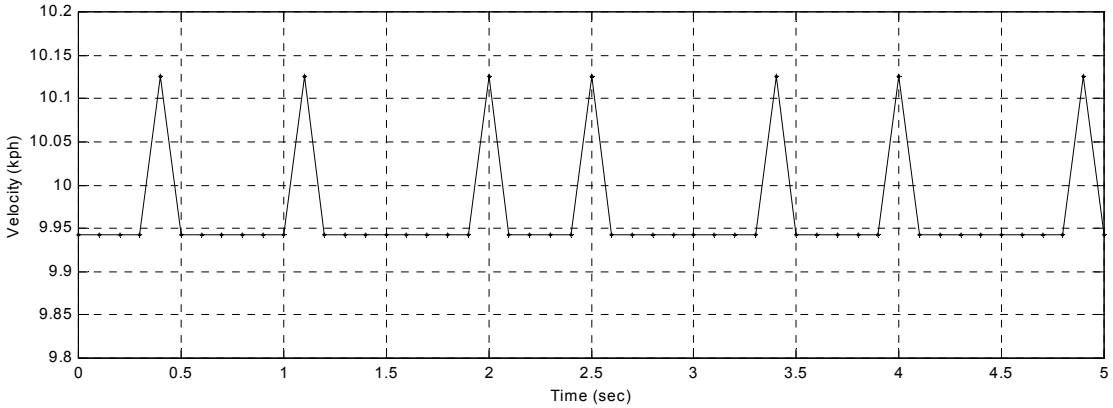

Figure 4.5 Velocity signal generated by counting dynamometer encoder pulses at 10 Hz

The reason for this superior performance is most likely an increase in the number of teeth (resolution) and the more even spacing of these teeth. A similar process to that used for the drum axle encoder was repeated to determine the percentage variation in the width of the teeth, and therefore the duration of the pulses. Again, the radial disturbances represent a variation of tooth angle (width) from the mean. Two consecutive rotations of the wheel have again been included, and use of the same scale as Figure 4.4 allows quantitative comparison.

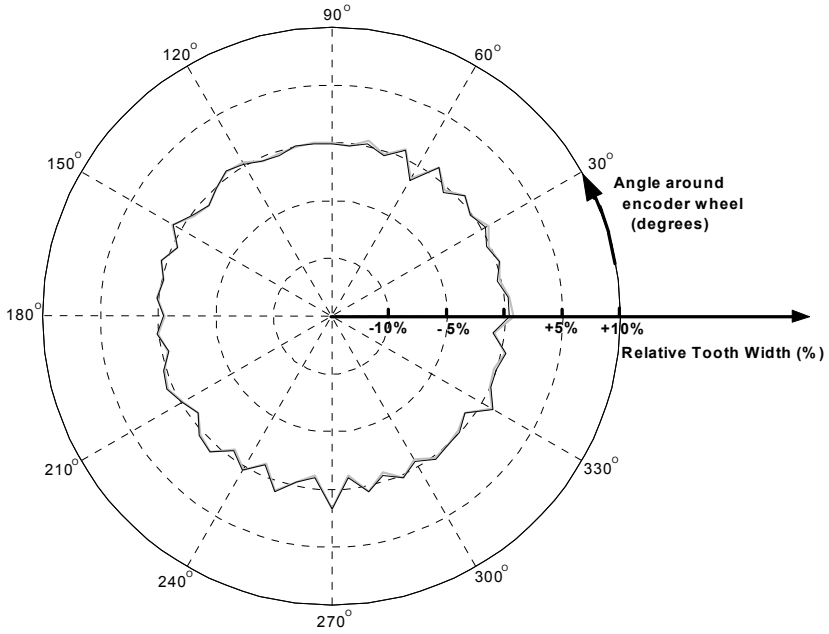

Figure 4.6 Eddy-current dynamometer encoder tooth widths

The factory-produced Froude dynamometer encoder wheel can be seen to be significantly more uniform than the wheel produced at the University of Canterbury. The maximum width error is approximately 2%, meaning a physical angle of 6.12º on the circular disc, compared to the mean width of 6.00º. In light of its greater uniformity and apparently smoother velocity output, it was decided to use only the pulse output from the eddy-current dynamometer in future work. It should be noted that the encoder on the dynamometer shaft has only one pulse-pickup and therefore has no capacity for a quadrature reading. Thus, the direction of motion cannot be detected from the speed readings and the user must ensure that the desired rotation is selected via the motor control panel.

4.1.3 Counting Pulses vs. Timing Pulses for Calculating Velocity

The average velocity during any time interval can be thought of as the displacement divided by the length of the time interval. In the case of the dynamometer shaft encoder, this displacement is a rotational one, whereas vehicle motion is most commonly represented in terms of linear displacement and velocity. Therefore, given the angle of rotation in any given time interval, the road-speed (that is, the surface velocity of the roller drums) can be calculated as below. This conversion was used to produce Figures 4.3 and 4.5 in terms of kilometres per hour.

$$Rotational\ velocity \quad = \quad \dot{\theta}_{dyno} \quad = \quad \frac{\theta}{t} \tag{4-4}$$

Where:

$$\dot{\theta}_{drum} \quad = \quad \frac{\dot{\theta}_{dyno}}{(diff\ ratio)} \tag{4-5}$$

Therefore:

$$Linear\ velocity \quad = \quad v_{drum} \quad = \quad r\dot{\theta}_{drum} \quad = \quad \frac{r\theta_{dyno}}{(diff\ ratio)t} \tag{4-6}$$

To find the velocity by counting pulses, all the pulses within a given time period are added to a computer register via a series of interrupts generated at the UPP card. Time intervals are defined in terms of counts on the UPP card internal clock. A separate interrupt is produced each time the pre-defined number of clock counts is reached. At the end of each time period, the register total is read (and then zeroed) by the software and the corresponding angle used to calculate the average velocity over that time interval (Equation 4-1).If desired, the UPP card can be set to produce an interrupt on both the rise and fall of each pulse signal, effectively doubling the number of pulses. In the case of an ideal encoder wheel, on which the teeth were identical, the uncertainty over any given time period would be ±1 pulse, seeing as whole pulses only can be counted and that the time interval may start at any point between two pulses (as shown in Figure 4.7). This equates to ±3º (360/(60×2)), or ±0.051 m/s for a sampling rate of 10 Hz regardless of the rotational velocity. This type of error will naturally be greater in the non-ideal case of slightly uneven pulse widths, and an investigation into the quality of the actual velocity data is included below, with a comparison to the timing method.

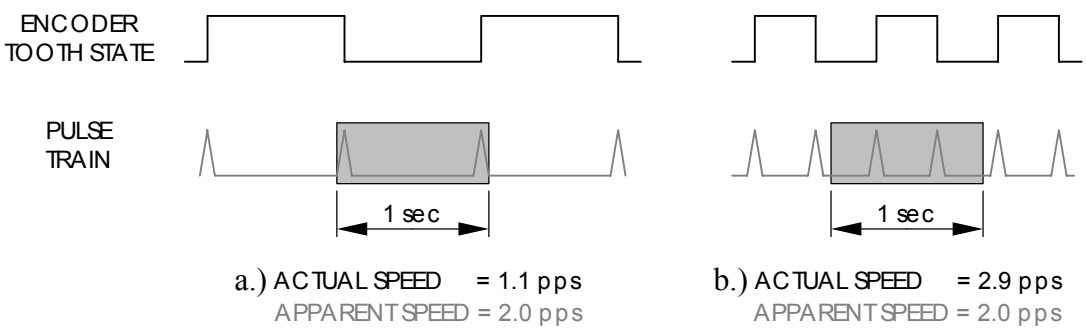

Figure 4.7 Pulse counting error over a single 1 second interval a.) Overestimation b.) Underestimation

The advantages of pulse counting are that this ideal uncertainty remains the same at any velocity, and that it does not require a particularly fast sampling rate. In fact, if the rate is slowed more pulses will be counted per sample, meaning a lower percentage uncertainty and a lessening of the proportional effect of individual uneven tooth widths. One possible downfall of the counting method is at high speeds, when a greater number of pulses introduces the risk of overflow in the counting register if there are insufficient bits to represent the total. This problem can be overcome by sampling at a higher rate or including an overflow procedure in the software. As an example, with a sampling rate of 5 Hz the dynamometer encoder produces approximately 1600 counts at 150 kph. This can be comfortably handled by a 16-bit register, which is capable of storing integers up to 65535.

When using an encoder to calculate the velocity by timing, the UPP card clock is used to determine the time interval between consecutive pulses. The UPP card continuously increments a register at the rate determined by its clock-speed (2.25 μs for this experiment), while waiting for an interrupt from the encoder pulse-train. Each time the UPP card receives a pulse, the total number of clock counts is transferred to a separate register, which can be read at any time by the software. Then the clock total is reset to zero and begins to count again. The velocity is calculated from this time interval as shown in Equation 4-2. The uncertainty is dependent on the encoder tooth widths, and the ratio of UPP card clock speed to input pulse rate. If we assume again that the pulses are of uniform width and duration at a given velocity, the uncertainty is effectively ±1 clock tick. Because we must divide by time to calculate speed, the velocity (and hence, its uncertainty) varies with the inverse of

time. For example, in the ideal-encoder case at say, 10 kph, the UPP card clock will have time to produce 1637±1 increments between each input pulse (rise only, which is preferable when timing) from the dynamometer encoder wheel, which is rotating at 28.4 rad/s. At 150 kph, the dynamometer shaft rotates at 426.4 rad/s, resulting in only 109±1 clock counts. Thus at low speed, the velocity error is approximately ±0.002 m/s and at high speeds is almost ±0.4 m/s. To make the best use of this method, the clock total should be read often and the results averaged, particularly when the encoder wheel is not entirely uniform. This procedure consumes slightly more computer processing time than the counting method and also adds an extra degree of complexity to the software structure. The timing method is most effective in measuring a pulse frequency that is slow in comparison to the counter clock speed. The major disadvantages include the loss in precision at high speeds and the requirement for overflow protection for the counting register at slow speeds, or when the shaft is stationary.

To compare the practical performance of the counting and timing methods, a series of constant velocity runs was made under power from the electric motor and with a dynamometer load present, as for Figures 4.1, 4.3 and 4.5. An analysis of the resulting random fluctuations (mostly due to the resolution and non-uniformity of the encoder wheel) is shown in Table 4.2.

Calculation method	**Timing**	**Counting**	**Timing**	**Counting**
Average velocity (m/s)	2.758	2.756	24.989	24.967
Maximum measured velocity (m/s)	2.781	2.814	25.081	25.019
Minimum measured velocity (m/s)	2.731	2.711	24.839	24.917
Standard deviation (m/s)	**0.0083**	**0.0167**	**0.0639**	**0.0139**

Table 4.2 Comparison of uncertainty in velocity calculated by counting, and timing pulses

Note that this data was collected during four separate runs, so the average speeds in each pair are not identical. As expected, the variation when calculating velocity by timing pulses was less at the lower speed (≈10 kph) and greater at the higher speed (≈90 kph). A more consistent figure was achieved by counting, with a range of approximately 0.05 m/s. In light of a superior performance at high speed, and the ease with which it could be incorporated into the data acquisition software, the

counting method was chosen, and has been used for all subsequent velocity data presented in this thesis.

4.2 Calculation of Acceleration

Once the pulse counting method of calculating velocity had been decided upon, it was necessary to investigate the most appropriate technique to arrive at the instantaneous acceleration. Acceleration of the vehicle under test is particularly useful during driving cycle tests, in which the power absorber may be used to apply any additional inertial resistance not provided by the flywheels. This additional force is equal to the difference in equivalent mass between the vehicle and the dynamometer system, multiplied by the current acceleration.

$$Extra\ inertial\ force\left(N\right) \quad = \quad \left(m_{Veq} - m_{cd}\right)\frac{dv}{dt} \tag{4-7}$$

Instantaneous acceleration was to be calculated from a discrete series of velocity measurements, provided by the pulse-counting scheme detailed above. In this section, a sampling frequency of 10 Hz was used. This is the current sampling rate during driving cycle tests, although some modes of operation sample at 5 Hz and calculate acceleration in a similar way.

4.2.1 Instantaneous Gradient

The most obvious way to differentiate the velocity is to use the rate of change over the last two data points. That is, by computing the difference between two consecutive speed measurements and dividing by the time interval. This gives an average value of the acceleration during that time step (i.e. with no lag). However, in the presence of noise and uncertainty—where the given velocity is not necessarily the actual, exact velocity—the method is extremely sensitive and returns an acceleration signal with exaggerated errors, which is not practical for road load calculations. The resulting acceleration over time is plotted in Figure 4.8 along with a normalised velocity, so that only departures from the median velocity are shown as non-zero.

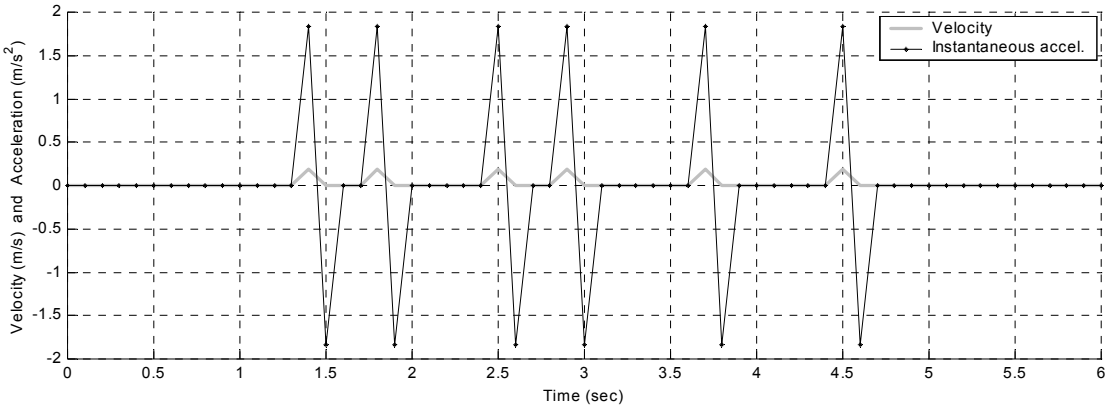

Figure 4.8 Instantaneous gradient method of acceleration at constant average speed

It was apparent that some form of filtering was required to smooth the speed signal out before attempting to calculate the acceleration. This filtering out of the high frequency components cannot be achieved without a degree of lag being introduced. That is, the resulting acceleration will not include as much of the false 'noise acceleration', but also will not be able to represent true accelerations without a time delay. The various methods detailed in the remainder of this section are merely different ways of making this trade-off with a bias towards either rapid response or damping of noise. For the case of road load modelling, it is particularly important to eliminate the noise component so that the dynamometer load can be applied in a stable and predictable manner.

4.2.2 Moving Average

The moving average method generates a sequence of velocity points that are the averages of the preceding values. As each new point is added to the sum, the effect of its variation from the average speed of the previous terms is in proportion to the number of terms. A greater number of terms results in a smoother speed signal, but a greater lag. A simple equation to calculate the latest velocity average for a four-term average is given in Equation 4-8:

$$v_{n+3(avg)} = \frac{v_n + v_{n+1} + v_{n+2} + v_{n+3}}{4} \tag{4-8}$$

Where: v_{n+3} = raw velocity at present time

v_{n+2} = raw velocity one time interval ago (etc)

Once the latest velocity had been calculated, the previous calculated term can be subtracted from it and the instantaneous acceleration determined as per Section 4.2.1. The number of terms is selected on the basis of the required response. A five-term average was selected by experimentation as having a noise attenuation characteristic appropriate for this application, and is plotted below in a similar way to Figure 4.8. Note the delayed negative acceleration that appears when the average returns to zero after five terms. Plots showing the calculated response to a step acceleration input are included in Appendix E.

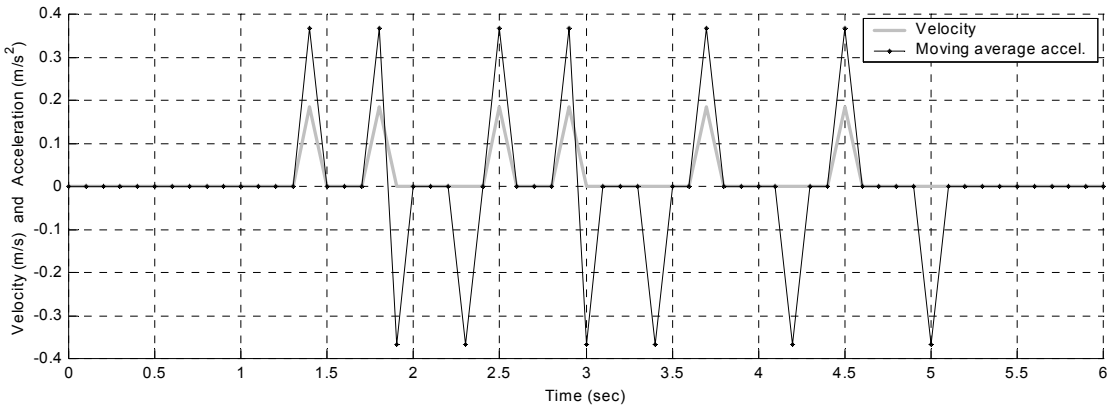

Figure 4.9 Five-term moving average acceleration at constant average speed

4.2.3 Least Squares Differentiator

A sequence of data points can be approximated by fitting a polynomial curve between them. In this case, a given number of velocity points are approximated by the least squares method. Once this velocity polynomial has been calculated, the acceleration is found by analytic differentiation of the curve. The number of data points and the order of the polynomial may be varied, but in order to provide a unique solution which will include some smoothing of the velocity, the order of the least squares polynomial was chosen to be less than the number of data points included. Quadratic approximation to a four-term series is shown in Appendix F to demonstrate the form of the least squares solution

The most rapid response to changes in speed was achieved by substituting the end (latest) time step into the acceleration equation (Equation F-5 in Appendix F). However, the gradient of the approximated velocity varied steeply when used on noisy data, particularly with higher-order approximations. By delaying in time by one

step, smoother acceleration output was produced, at the expense of a greater lag. By experimentation, a 2nd-order, 12-term least squares formulation was chosen as the most appropriate for this application, and the resulting response to velocity fluctuations is shown in Figure 4.10. The response of this filter to a non-zero average acceleration is also included in Appendix E.

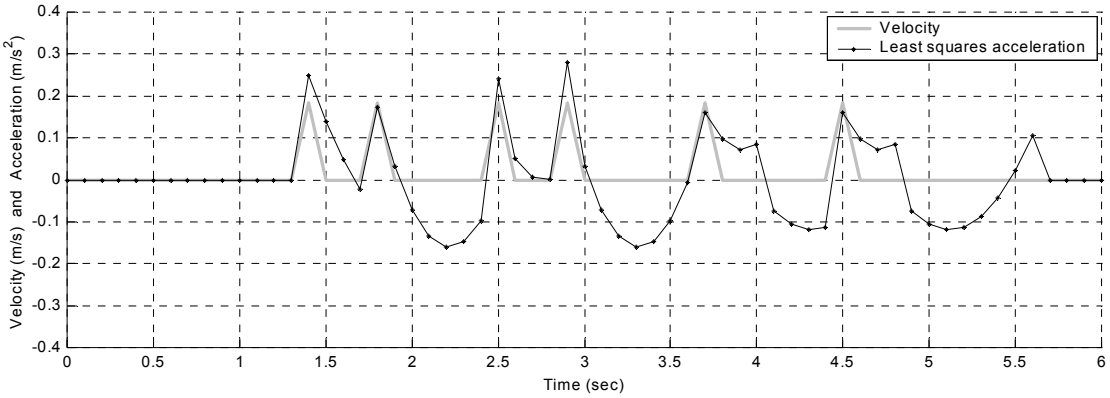

Figure 4.10 Least squares acceleration at constant average speed

The inclusion of matrix manipulations at each calculation of acceleration requires a significant amount of computer processing power. However, this was not found to be a major obstacle during the testing of this method's suitability. Backward Least Squares approximation is the name given to the use of historical data points for this type of curve fitting. For on-the-fly calculations during vehicle testing, this is the only option, as the velocity points forward in time are not yet available. However, once an entire data sequence has been logged, the velocity and acceleration at any point in time may be approximated with no lag. In particular, for the *coastdown* testing described in Chapter 5, a single quadratic least squares formulation may be used for the entire sequence (least squares terms = total number of recorded points), enabling very smooth approximations of velocity and acceleration.

4.2.4 Butterworth Differentiating Filter

A large variety of digital techniques are available to filter out random fluctuations in discrete data series. Digital filtering employs past and present input data to produce an approximation of the original signal by using difference equations. As with the methods detailed earlier, a compromise must be reached between response time and attenuation of noise. MATLAB was used to select an appropriate filter type and parameters by experimenting on real velocity data and an ideal acceleration step

input of the type included in Appendix E. A low-pass Butterworth filter was chosen, which provides an extremely flat passband and acceptable lower order (fewer historical terms) performance. Filter design was carried out using the MATLAB `butter`[6] function, which takes the order of the filter and the desired cut-off frequency as parameters and returns the discrete filter coefficients.

Using the so-called *z-domain* form, and transforming it to the continuous *s-domain*, a differentiation operation can be added to the filter. A full description of the z-domain, Laplace Transforms, and discrete-continuous filtering can be found in Franklin et al. [1994]. Multiplication in the s-domain corresponds directly to a differentiation in the time-domain. So by multiplying the s-domain representation, then transferring back to the discrete formulation, the digital filter can output filtered acceleration given a discrete series of velocities. The following equation shows the filter coefficients calculated in this way, for velocity sampling at 10 Hz.

$$\dot{v}_n = \frac{\left(a_0 v_n + a_1 v_{n-1} + a_2 v_{n-2}\right) - \left(b_1 \dot{v}_{n-1} + b_2 \dot{v}_{n-2}\right)}{b_0} \tag{4-9}$$

Where: $a_0 = 1.024$, $a_1 = 0$, $a_2 = -1.024$

$b_0 = 1$, $b_1 = -1.266$, $b_2 = 0.4706$

v_n indicates the velocity at the current point

v_{n-1} indicates the velocity one time interval previous, and so on.

The response of this differentiating filter can be represented on a Bode plot, which is included in Appendix G and is illustrated on an instantaneous acceleration step in Figure 4.12. In a discrete sequence, an ‘instantaneous’ increase in acceleration is one which occurs in the time between two recorded time steps.

---

[6] `Courier` font denotes software-specific syntax (e.g. entered at MATLAB command prompt)

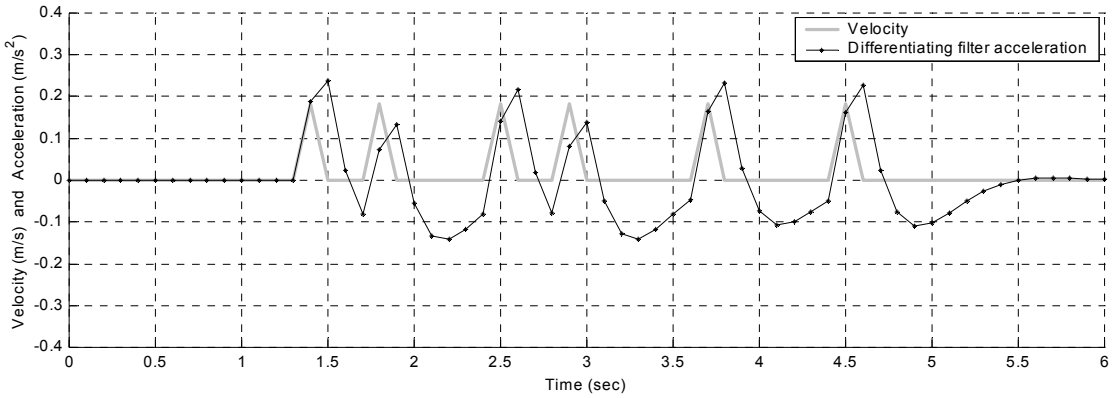

Figure 4.11 Butterworth differentiating filter acceleration at constant average speed

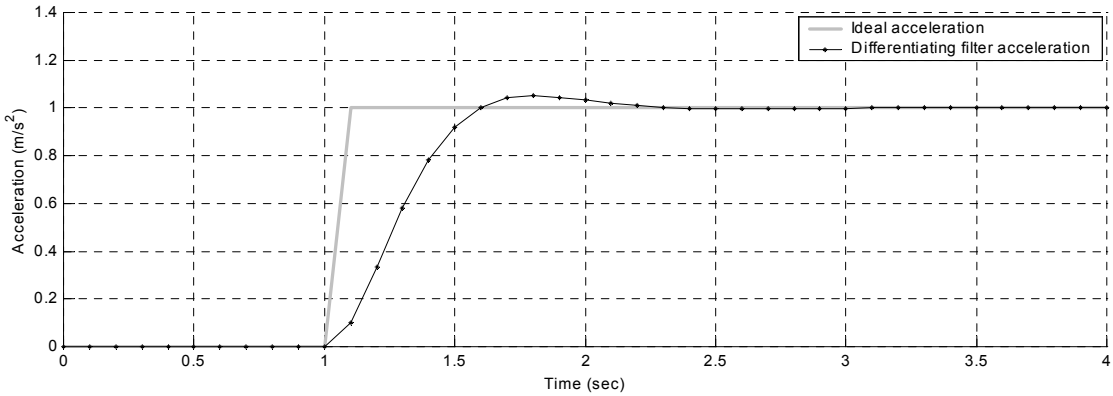

Figure 4.12 Butterworth differentiating filter acceleration response to a step increase in acceleration

It should be noted that the coefficients chosen for a Butterworth filter are frequency dependent and must be altered if the sampling frequency is to be changed. A separate filter of the same form was designed by experiment for use with routines operating at 5 Hz.

$$\dot{v}_n = \left(0.851v_n - 0.851v_{n-2}\right) - \left(-1.022\dot{v}_{n-1} + 0.363\dot{v}_{n-2}\right) \tag{4-10}$$

The response of this formulation to 5 Hz data comparable to the previous acceleration step is also included in Appendix E.

4.2.5 Filter Selection Summary

The response of the first technique (referred to previously as the Instantaneous Gradient method) to random fluctuations at constant average velocity immediately ruled it out, and initiated the search for alternate ways to calculate acceleration. The Moving Average technique also exhibited unsatisfactory noise attenuation and time

lag. The performance of the Least Squares and Butterworth formulations were similar and superior to the two previous filtering methods. However, the Butterworth differentiating filter exhibited a smaller overshoot in response to the acceleration step plotted in Appendix E. In light of its attenuation and lag characteristics, and the minimal computation required for implementation in the data acquisition program, it was decided that Butterworth filtering would be used for chassis dynamometer acceleration calculations. Acceleration for use in road load modelling may be applied either in 'Driving Cycle', or 'Road Load Driving' mode. However, for the data included in Chapter 8, the ideal driving cycle acceleration was substituted to standardise results and further stabilise the power absorber demand. Software adjustments to the road load are discussed in more depth in Section 6.5.12.2.

4.3 Load Cell Calibrations

The University of Canterbury chassis dynamometer includes three load measurement devices, used to determine shaft torque via the force on each of three load arms. The electric motor employs a strain gauge arrangement in which the motor torque is resisted (and measured) by a bending moment in the torque arm. The arm is fixed at one end to the motor body (mounted on trunnion bearings), and at the other to a rigid vertical member via a low-friction pin-joint. The eddy-current dynamometer and drum axle load arm configurations incorporate commercial load cells, which undergo tension or compression via the torque arm arrangements shown diagrammatically in Figures 4.13 to 4.15 (not to scale).

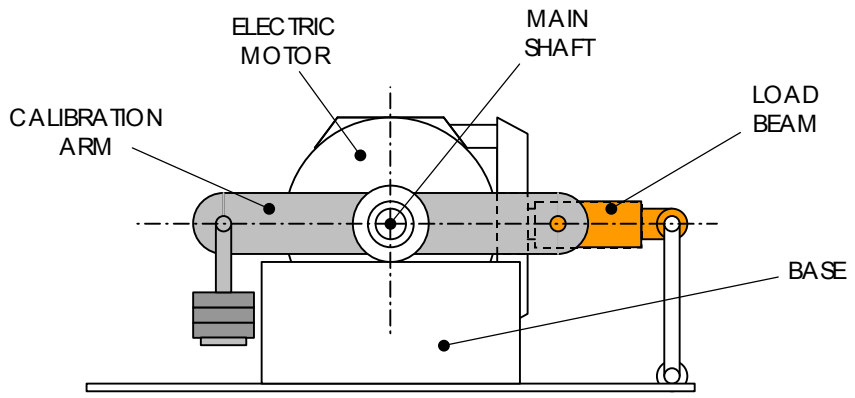

Figure 4.13 Electric motor torque arm arrangement

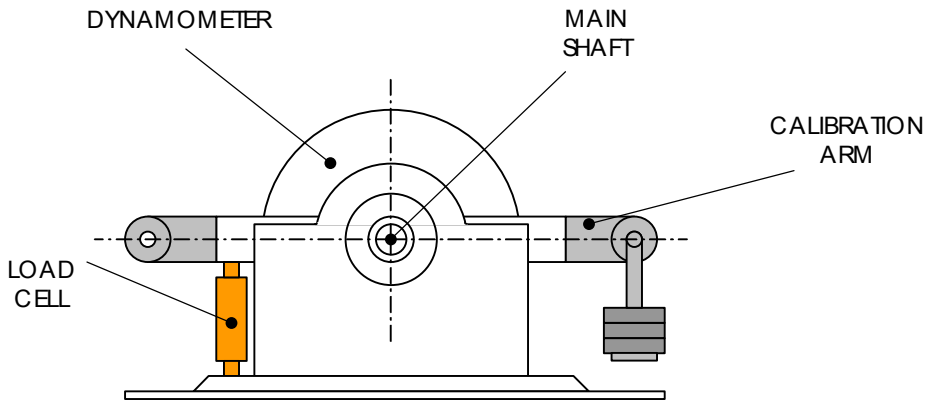

Figure 4.14 Eddy-current dynamometer torque arm arrangement

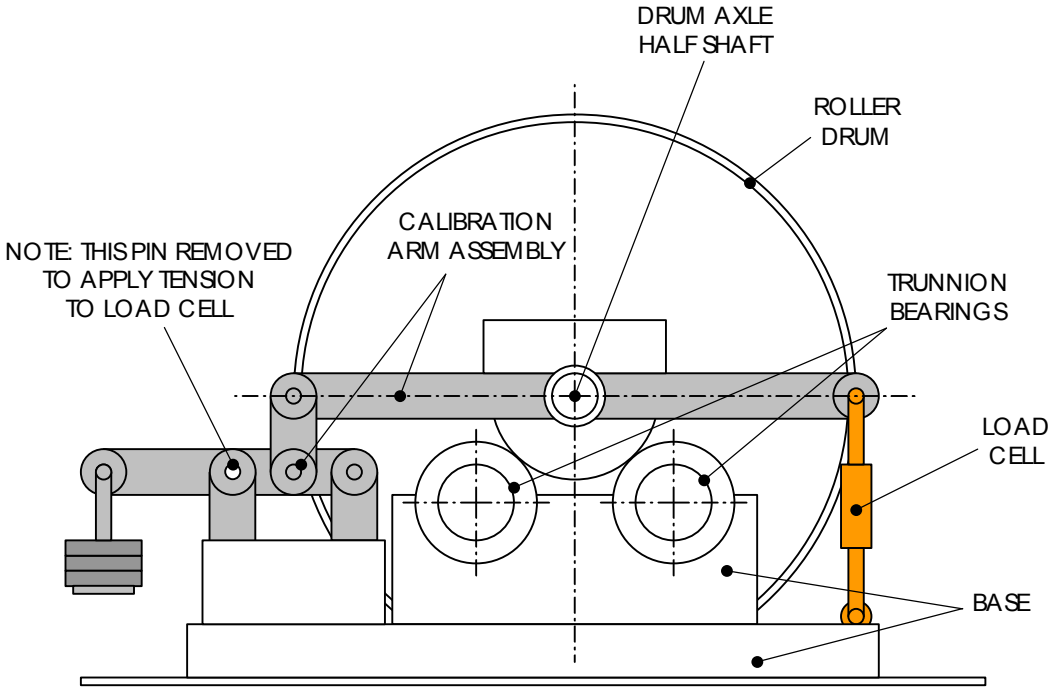

Figure 4.15 Drum axle torque arm arrangement (section view, showing load arm, which lies between the rollers)

The axle assembly, power absorber and electric motor are each supported on trunnion bearings such that their centre of rotation coincides with the axis of rotation of the shaft, or—in the case of the axle—the axis of the roller drums. Each load cell force is opposed by friction in these trunnion bearings, which cannot be measured and

generates a small error in the load cell reading. The forces at the electric motor, and dynamometer load cells are shown in Equations 4-11 and 4-12 with notation and directions as shown in Figure 3.1.

Electric motor load cell reads:

$$F_{motor} = F_{me} - F_{mf} - F_{mt} \tag{4-11}$$

Where: F_{mt} = electric motor trunnion bearing friction

Dynamometer load cells reads:

$$F_{dyno} = F_{de} + F_{df} - F_{dt} \tag{4-12}$$

The tractive effort BLH U3G1 load cell attempts to measure the tangential force at the drum surface, which introduces additional complexity to the equation of motion. Because the roller drums have a significant inertia and frictional effect, the tractive effort reading delivered by the load cell is not equivalent to the force at the drum surface, as applied by the vehicle tyres. As well as the load arm reaction force, the tractive effort input is also opposed by the windage friction on the drum surface and the inertial mass of the rollers themselves.

TE load cell reads:

$$F_{te} = F_{v} - F_{drt} - \left(F_{dra} + m_{dr}\dot{v}\right) \tag{4-13}$$

The tractive effort load cell does not measure the inertial or aerodynamic forces on the drum assembly, since they do not act on the drum axle housing. These forces may be measured independently and used to correct the load cell reading (see Section 5.5).

Each of Figures 4.13–4.15 indicate the location of a calibration arm, upon which known weights were hung in order to calibrate the device. With knowledge of the mass added and its effective distance from the centre of the shaft, the output of each device was calibrated by a combination of signal amplification adjustment and software coefficients. The power absorber and drum axle load cells presented particular difficulties related to their susceptibility to temperature and the inherent hysteresis in the mechanical systems.

4.3.1 Temperature Effect

After an initial calibration of the dynamometer load cell, it was discovered that the results—particularly the readings when no load was applied—were not consistent. An investigation was made into the effects of ambient temperature on the zero reading of the dynamometer load cell. Regular readings of temperature were taken using a thermocouple-type digital thermometer while slowly heating the air in the chassis dynamometer laboratory. At each temperature reading, a small load was applied to each side of the load arm in turn to remove possible hysteresis. Also, a load cell measurement was made with 68 kg (equating to approximately 340 Nm) on the weigher arm in a positive direction (i.e. compression of the load cell, as explained in Section 3.2). The results of this trial are shown in Figure 4.16 below with air temperature on the *x*-axis and zero-load reading on the *y*-axis.

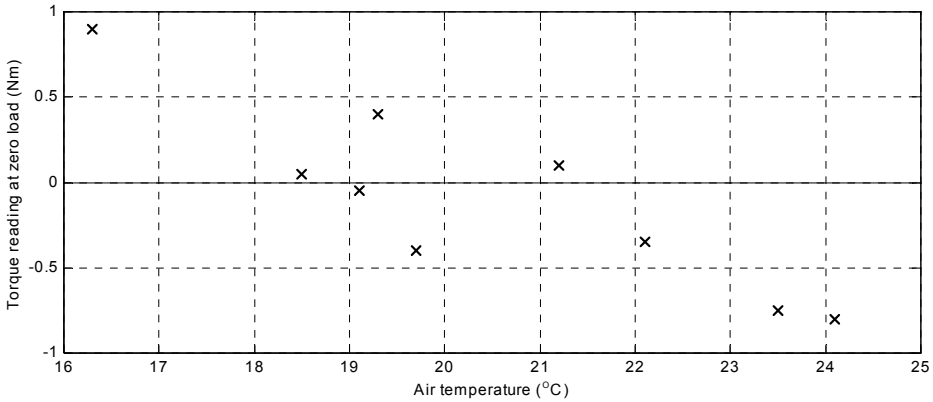

Figure 4.16 Temperature effect on eddy-current dynamometer zero reading

It can be seen that there was a significant decrease in the zero readings with an increase in air temperature. This offset was also noted in the 68 kg measurements, as the torque measured on the load cell tended to decrease with an increase in temperature. Figure 4.17 below shows the difference between the average zero readings as shown above, and the 68 kg readings recorded during the same temperature run. It is interesting to note that the *difference* does not appear to follow the same trend as the zero readings.

This indicates that the temperature effect manifests itself as a pure offset as opposed to a change in the span of the device, which would give an increasingly greater error

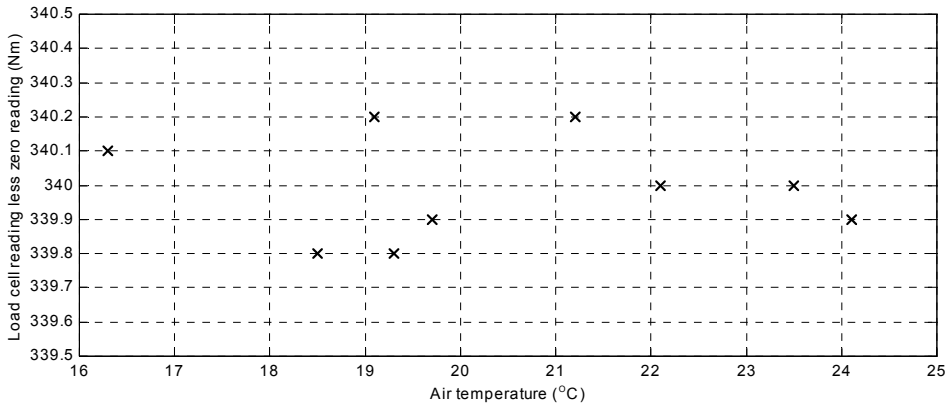

Figure 4.17 Temperature effect on the eddy-current dynamometer reading with 68kg on the load arm

magnitude with greater temperature. It should be noted that the load cell devices used do include some form of temperature compensation to allow for the changes that result when the electronics heat up. However, it would appear that this compensation circuitry on both the dynamometer and the drum axle load cells may be damaged or have aged and can no longer provide a predictable output. Replacement of these faulty load cells is suggested. However, to obtain useful results with the existing equipment, some form of software compensation was desired. Measuring the air temperature and adjusting the torque readings accordingly may have been possible, but without a knowledge of the exact relationship between the temperature of the ambient air and the state of the internal load cell electronics, such a technique would be difficult to put into practice. Instead, it was decided that the load cell should be manually zeroed (by removing hysteresis and taking a zero reading) at the beginning of each testing session. The constant flow of air from the external cooling fans in the laboratory should ensure a constant temperature during testing. The A/D voltage during this zeroing process is stored by the computer for future tests. A constant calibration span is maintained, but an offset is added so that zero torque is recorded whenever this offset voltage is encountered. The software routine to handle this zeroing is further described in Section 6.5.6.

4.3.2 Tractive Effort Hysteresis

The load cell arrangements on the electric motor, eddy-current dynamometer and the drum axle all exhibited some degree of hysteresis. That is, the friction of the load arm arrangement, and/or the electronic characteristics of the load cells caused the

load reading to have a 'memory' of sorts. For example, after a high loading, hysteresis in the load cell system resulted in an error in the direction of this load, even after the load was removed. However, in the case of the motor and dynamometer, a small load applied on each side of the load arm in turn was sufficient to remove this error during calibration. The drum axle load cell, which measures the tractive effort applied by a vehicle under test, was found to generate greater errors due to a change in load direction.

Hysteresis in the tractive effort load cell was most likely due to a combination of the greater complexity in the load arm mechanism (meaning greater friction) and the age of the load cell. The problem was compounded by the large torque loads experienced by this shaft. The magnitudes of loading and the arrangement of the load arm meant that maximal calibration loads in the positive direction (load cell in compression, using the calibration linkage shown in Figure 4.15) tended to lift the axle off its bearings, obviously affecting the loading angles and load cell readings. One way to overcome this lifting was to clamp the axle (at the drum surface) thus preventing vertical motion while allowing freedom of rotation. However, the increased compressive force on the static axle bearings contributed further towards hysteresis.

By rotating the system at a constant speed during calibration, a large proportion of this static friction hysteresis could be eliminated. The electric motor was used to turn the drum shaft over slowly, while a vehicle was placed on the rollers to serve a clamping role. This rotation introduced its own set of errors related to the frictional resistance to motion and any misalignment of the vehicle on the drums. In particular, whenever the drums are rotated by the electric motor, a finite torque must be applied to the axle to overcome the bearing friction. This torque, which is applied at the differential, is measured by the tractive effort load cell, which effectively records the forces between the drum shaft and the main shaft. To overcome this difficulty, the zero load cell reading was first taken in the absence of any motion or the clamping load. Then the vehicle was placed on the rollers, the motor was started, and the calibration arm engaged. The offset at this point was balanced by the addition of masses in a trial and error fashion onto the calibration arm, to return the tractive effort reading to its previous zeroed value. The calibration masses were then added in

a sequential manner, and the measured loads recorded while the system was in motion. The offset balancing masses mentioned above ensure that a calibration curve acquired in this way will be applicable during testing, when the calibration arm and motor do not play a part. The electric motor was not generally used during chassis dynamometer testing for reasons detailed in Section 5.2.3.

Hysteresis during calibration was also minimised by decreasing the maximum load to be applied. The lesser the total loading, the more likely the load cell reading was to return to its original value when the load was removed. The maximum tractive force generated by the test vehicle (as described in Chapter 8) was less than 2500 N, which is approximately quarter of the load cell's rated maximum load. To reduce hysteresis during calibration, and to increase the A/D resolution, the tractive effort load cell was only calibrated to a maximum of 5560 N, as shown in Figure 4.18.

Figure 4.18 shows the comparison between a calibration performed with a stationary clamp at the drum surface, and one performed with a vehicle on the rollers and powered by the electric motor. After a calibration run, the masses (and hence the actual applied load) were compared with the load cell signal recorded via the PCL812-PG A/D card and a linear approximation was determined. Figure 4.18 shows the difference (error) between this approximation and the actual force, which gives an indication of the accuracy of the device and the magnitude of the hysteresis. Note that the clamped calibration also includes a greater maximum load, further increasing the hysteresis.

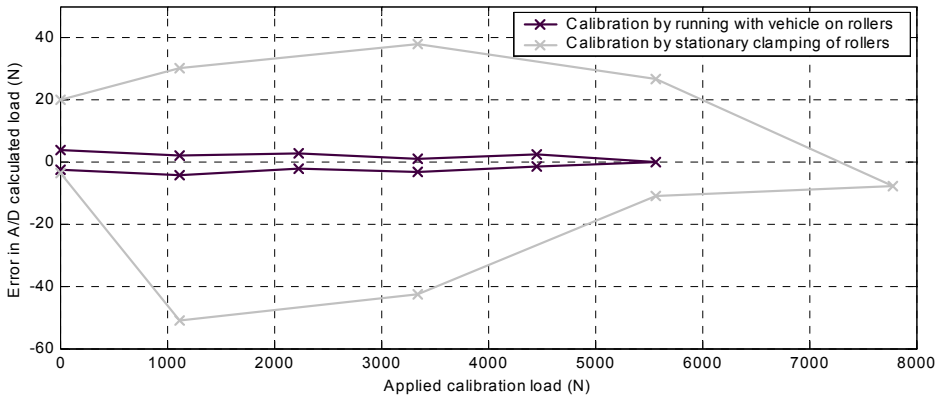

Figure 4.18 Tractive effort load cell calibration error under different clamping conditions

Note that Figure 4.18 contains only positive loading for each calibration technique. It was found that the load cell outputs of the dynamometer torque and tractive effort transducers were dependent on the direction of loading. That is, the voltage for a given load cell tension was different to the voltage output under a compressive load of the same magnitude. For this reason, both the eddy-current dynamometer and tractive effort load cell calibrations have separate calibration curves for each rotational direction. Refer to Appendix C for full details of these load cell calibration functions and equations.

Results from the rolling calibration runs lead to an estimated measurement uncertainty of ±9 N. Additional uncertainty was introduced by the temperature effects discussed in Section 4.3.1, and the requirement for correction of the tractive effort load cell reading for the inertia and windage friction of the roller drum assembly (see Section 5.5.3). The overall tractive effort uncertainty was expected to be ±50 N during moderate changes in velocity (e.g. driving cycle testing) and ±10 N under constant speed conditions (e.g. vehicle mapping tests).

CHAPTER 5:

Inertia and Friction Determination

5.1 Inertia Overview

Testing on the chassis dynamometer involves the application of a known force at the surface of the vehicle tyres. This force is represented by Equation 3-8, where F_{de} and F_{me} are the inputs from the power absorber (Froude eddy-current dynamometer) and motor (ASEA D.C. motor) respectively. A free-body diagram of all the forces acting on the chassis dynamometer is shown in Figure 3.1.

With knowledge of the materials and components as well as the relevant shaft sizes, a calculation of the equivalent mass of each component could be made, as was carried out by Raine [1981]. However, experimental confirmation of this calculation was sought, and is detailed in Sections 5.2 and 5.3.

The combined equivalent mass of the motor, dynamometer, drums, and shafts was determined by experimentation (see Section 5.3). Calculation of the flywheel inertias based on their thickness and diameter was thought to be sufficiently accurate, as no major simplifications were needed. Similarly, the combined frictional coefficients were found by experiment, and require ongoing recalibration to account for wear-related changes in friction. The individual mass and frictional characteristics of the drum axle assembly were also determined in order to generate useful tractive effort measurements from the roller drum load cell.

It should be noted that the particular method used to find these inertial and frictional constants determined which of these were to be included in subsequent testing procedures. For example, for calibrations under power from the electric motor, the friction, F_{mf} and the actual motoring force F_{me} are measured as a single torque at the motor load cell (see Equation 4-11). The motor controller adjusts to give a certain output torque, meaning that the internal friction—whatever it may be—is motored

out, rendering the friction and motoring forces indistinguishable, unless independent measurements were available. If the chassis dynamometer were subsequently run without a motoring force from the electric motor, only the unknown friction would act on the shaft, leaving an undefined variable in the motion equations. In a similar way, the dynamometer load cell only detects the combined forces F_{df} and F_{de} at the power absorber. Sections 5.2 and 5.3 include several different calibration techniques and their associated difficulties. The interrelationship between friction and inertia forces, as well as the specific forces which are not included (e.g. those that are motored out) are explained in detail below.

As suggested by Equation 3-8, inertial forces ($m_{cd}\, dv/dt$) are only encountered during changes in velocity of the dynamometer shaft. Therefore, any experimentation to determine the inertia of a physical system must involve either acceleration or deceleration. The most common method of calibrating for inertia is by *coastdown* of the system. In the case of a chassis dynamometer, the system is brought up to a certain speed (either by external means, or a motor if one is present) then allowed to decelerate under the influence of friction while measurements of time and velocity are made. In some cases, a known power-absorber and/or motoring torque is also applied to generate different rates of deceleration. The presence of motoring or power-absorbing forces means that the system cannot strictly be thought of as 'coasting' down. However, for the purposes of this discussion any deceleration under constant dynamometer or motor load will be referred to as a coastdown. For inertia calibration, the dynamics of the University of Canterbury chassis dynamometer are similar to those of Figure 3.1, but without the complication of a vehicle on the rollers. This means that the tractive force at the roller drum surface (F_V) is zero, with the exception of windage friction on the rollers, which can be included in the overall friction force.

$$m_{cd}\frac{dv}{dt} = F_{motor} - F_{dyno} - F_{fric} \tag{5-1}$$

Where: F_{fric} = combined chassis dynamometer friction forces (excluding contribution from motor and dynamometer)

Note: $\frac{dv}{dt}$ is negative during deceleration

It can be seen from this equation that the determination of inertia using the coastdown technique demands recording of the motoring/power-absorbing forces as well as a prior knowledge of the frictional characteristics of the system as a whole. These frictional forces can be determined in a separate experiment or accounted for by setting up parallel tests in which all friction terms can be mathematically cancelled.

5.2 Inertia Determination Using the Motor

To calculate the system inertia, two different techniques were attempted involving power input from the electric motor. The first is a common method wherein the frictional characteristics of the system are determined in a separate calibration, then used to calculate the inertia during a coastdown run. The second method eliminates the need to determine the friction by running an acceleration and a deceleration run in which the friction forces can be cancelled during calculation. These motor-driven methods were subject to the limitations of the chassis dynamometer configuration, and this difficulty is discussed in Section 5.2.3.

5.2.1 Calculating Friction from Constant Speed Trials

By assuming that the friction of the various system components is dependent only upon the rotational velocity, the frictional coefficients can be determined in a series of constant velocity tests. Under constant speed and with a known (possibly zero) dynamometer torque Equation 5-1 may be reduced to:

$$F_{motor} = F_{dyno} + F_{fric} \tag{5-2}$$

Where:

$$F_{fric} = f_{0d} + f_{1d} v + f_{2d} v^2 \tag{5-3}$$

In the case of the University of Canterbury chassis dynamometer, the load cells indicate either the internal friction of the motoring/absorbing devices (if no control demand is made) or the total force applied by them. Thus, the total friction sought in Equation 5-2 does not include any power-absorber or electric motor friction

component. In order to achieve a stable force from the dynamometer, constant load demands were implemented in torque mode on the power absorber. Constant speed was maintained by the ASEA motor controller at several predefined set-points, and the torque (converted to force) at each load cell was recorded, along with the speed. Thus the total friction force at each velocity could be calculated. A minimum of three speed points was required to solve for f_{0d}, f_{1d}, f_{2d}, simultaneously, but a greater number were generally recorded and the resulting data used to calculate a quadratic equation for F_{fric} as a function of velocity on a least squares basis. General use of the least squares velocity-time approximation is included in Appendix F, and this technique may be extended to other data sets such as the friction-velocity relationship. An example of several constant velocity friction data sets is included in Appendix H with the accompanying calculated friction coefficients. To obtain a single final value, the total frictions from each run were combined to arrive at an average least squares approximation, from which the average coefficients were taken (see also Appendix H). Over the range of motor and dynamometer torques available, there appeared to be a large variation at each velocity of ±20 N in the total friction recorded. In addition, negative constant and squared term coefficients (f_0, f_2) were calculated for the runs employing 100 Nm power absorber torque. Since this would lead to the impossible case of a negative total friction force at low speeds, doubt was cast on the suitability of using the motor and power absorber in this way to determine the system friction.

Using the average system friction coefficients as calculated above (f_{0d} = 13.28, f_{1d} = 6.86, f_{2d} = -0.031) the equivalent mass of the chassis dynamometer could be found by carrying out a coastdown and applying Equation 5-1. By measuring each of the other components—including acceleration differentiated from a least squares approximation of the velocity signal—the equivalent mass could be found at each instant during the deceleration. Coastdown data such as velocity and dynamometer torque were recorded at 0.1 second intervals using a purpose-designed C++ program. To minimise experimental error, a series of tests were performed at different dynamometer loads and the resulting inertias were averaged during each coastdown. An idealised sample of a single inertia calculation is illustrated in Figure 5.1, while the complete coastdown results are tabulated in Appendix I.

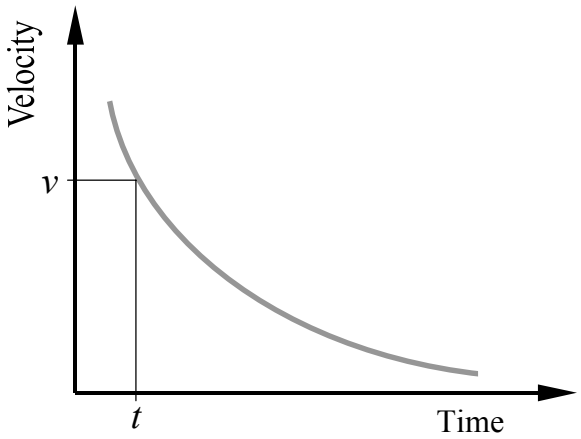

F_{motor} = 100 N
F_{dyno} = 400 N
F_{fric} = 50 N
v = 20 m/s
$\frac{dv}{dt}$ = –0.5 m/s^2

Figure 5.1 Example of inertia coastdown

From Equation 5-1:

$$m_{cd} = \frac{F_m - F_d - F_{fric}}{\left(\frac{dv}{dt}\right)} = \frac{100 - 400 - 50}{-0.5} = \mathbf{700\ kg}$$

The average m_{cd} was found to be 716.6 kg, with experimental variations of ±14 kg (std. dev. = 9.2%) assuming the friction forces during each run were as calculated earlier. That is, the inertia of a vehicle with an equivalent mass of 716.6 kg could be simulated by the chassis dynamometer with no additional motoring or power-absorbing torque.

During the friction calibrations, constant speed trials conducted at higher dynamometer torques tended to yield a lower total friction (see Appendix H). That is, the apparent difference between the motor and power absorber torques (Equation 5-2) was less at any given velocity, when it should have remained the same if the equipment was performing as expected. Therefore, during coastdowns with high power absorber loads (e.g. 100 Nm), the averaged friction from Appendix H may be higher than the apparent friction calculated at that particular dynamometer torque. When this average friction is applied to Equation 5-1, the resulting inertia is lower for the runs employing high power absorber torque, and higher for those with less power absorber load (see Appendix I). Since the averaging of these frictional constants provided a somewhat arbitrary result, another method was sought to calculate the equivalent mass of the system.

5.2.2 Cancelling Friction Using Matched Acceleration and Deceleration Runs

To avoid the uncertainties brought about by using the previously calculated frictional characteristics, a method was sought that would not require prior knowledge of the system friction. If we still assume the total friction is dependent only upon velocity, then the work done by friction during an acceleration between speed A and speed B will be the same as the work done during a deceleration from speed B to speed A, if the time taken is identical. This principle is demonstrated below, beginning with a restatement of Equation 5-1:

$$m_{cd}\frac{dv}{dt} = F_{motor} - F_{dyno} - F_{fric}$$

$$\int m_{cd}\,dv = \int \left(F_{motor} - F_{dyno} - F_{fric}\right)dt$$

$$m_{cd}\left(v_2 - v_1\right) = \underbrace{\int F_{motor}.dt}_{\text{CONSTANT}} - \underbrace{\int F_{dyno}.dt}_{\text{CONSTANT}} - \underbrace{\int F_{fric}.dt}_{\text{VARIES}}$$

F_{fric} is a function of velocity

Acceleration (dyno and motor subscript α):

$$m_{cd}\left(v_B - v_A\right) = F_{motor\alpha}\left(t_2 - t_1\right) - F_{dyno\alpha}\left(t_2 - t_1\right) - \int_{t_1}^{t_2} F_{fric}.dt$$

Where: $v_A < v_B$

MATCHES

If we undergo **deceleration** (subscript β), such that:

$$m_{cd}\left(v_A - v_B\right) = F_{motor\beta}\left(t_2 - t_1\right) - F_{dyno\beta}\left(t_2 - t_1\right) - \int_{t_1}^{t_2} F_{fric}.dt$$

Acceleration – deceleration (friction term cancels):

$$2m_{cd}\left(v_B - v_A\right) = \left(F_{motor\alpha} - F_{motor\beta}\right)\Delta t - \left(F_{dyno\alpha} - F_{dyno\beta}\right)\Delta t$$

$$m_{cd} = \frac{\left(F_{motor\alpha} - F_{motor\beta}\right)\Delta t - \left(F_{dyno\alpha} - F_{dyno\beta}\right)\Delta t}{2\left(v_B - v_A\right)} \qquad (5\text{-}4)$$

By deciding on a certain sample run length, then adjusting the motor and dynamometer torque on a trial and error basis, one can produce the mirror

acceleration for any prior deceleration (assuming the maximum motor power is sufficient). Thus, with all the elements of Equation 5-4 known, the equivalent mass of the chassis dynamometer could be calculated. This approach was implemented in a series of acceleration and deceleration pairs to determine the repeatability for a given time span and speed interval, and the variation between runs of differing speeds or acceleration/deceleration rates. The motor torque was varied manually on the instrument panel or by entering a fixed D/A demand, and all data was again captured by a C++ program, which read the A/D values and UPP card velocity at each 0.1 second interval. Several sets of acceleration/deceleration runs are included in Appendix J, and the averaged results for each set are shown in Table 5.1 below.

Results Set		**Velocity** v_A **(m/s)**	**Velocity** v_B **(m/s)**	F_{motor} **(N)**	F_{dyno} **(N)**	Δt **(s)**	**Mass** m_{cd} **(kg)**
A	Deceleration	16.68	22.16	257.66	517.02	9.90	
	Acceleration	16.63	22.16	723.83	208.17	9.90	696.2
B	Deceleration	12.65	20.76	278.82	719.39	9.90	
	Acceleration	12.68	20.77	901.81	210.90	9.90	691.2
C	Deceleration	19.54	24.94	165.41	405.97	9.90	
	Acceleration	19.49	24.90	948.18	398.67	9.90	723.1
D	Deceleration	14.40	19.43	151.46	381.89	9.90	
	Acceleration	14.39	19.47	898.56	396.25	9.90	717.5
E	Deceleration	9.08	13.86	144.31	373.88	9.90	
	Acceleration	9.10	13.86	864.88	401.79	9.90	719.0
Average							**709.4**

Table 5.1 Summary of acceleration/deceleration inertia determination trials

Within each set of data shown in Table 5.1 (and included in Appendix J) the velocity differences, and the average motor and dynamometer force readings, each typically varied by less than 0.5%. However, the range of masses calculated in this way was approximately 32 kg, which was similar (in terms of variation) to the results obtained from the previous method using coastdowns with assumed friction values. The calculated equivalent mass of the chassis dynamometer (without flywheels) was noticeably lower (709.4 vs. 716.6 kg).

5.2.3 Limitations of the Electric Motor

As mentioned in Chapter 2, the ideal chassis dynamometer operation involves both a power absorber and a motoring capacity, both of which can be rapidly set depending on the load and inertia simulation requirements. For example, in the case where a vehicle's inertia is greater than that of the dynamometer flywheels, a motoring torque is required during deceleration, and a resisting torque is required during acceleration (see Equation 4-7).

During the inertia calibrations in Sections 5.2.1 and 5.2.2 in which the eddy-current dynamometer was operating at high load, the electric motor torque reading became more noisy, and also increased in magnitude slightly. Investigation revealed that the most likely cause was that the high-current, high-frequency eddy-current demand was coupling with the low-current motor load-cell (and hence, control feedback) signal. In addition, the response time of the motor and dynamometer to their respective command signals was a factor. Particularly in the case of the electric motor, it was necessary to set the load demand several seconds before the initial coastdown speed point was reached, in order that the system should have time to settle down. Rapid application of large loads resulted in torsional vibrations, which also lasted a few seconds, but these were not as significant as the electric motor settling period. This lag in motor output torque was especially evident at low speeds, or when starting the system from stationary.

One possible solution to the difficulty of slow motor response is to apply a constant motoring torque, which is balanced by a varying power absorber torque as required. Equation 3-10 contains a term F_{net}, which determines the net effect of the motor and power absorber ($F_{dyno} - F_{motor}$). The constant motor torque must be at least equal to the greatest negative F_{net} that will be encountered. When lesser motoring loads are required, the dynamometer—with its superior response characteristics—is programmed to overcome the unwanted proportion (or the entirety) of the motor torque. In the course of most driving cycle testing, the vehicle is required to stop for length of time, which also creates problems for the chassis dynamometer. The power absorber requires a rotational movement within its electric field to create a force, and thus it cannot produce any motion-resisting torque at zero velocity. In addition, the

electric motor is at its least stable at zero velocity, and so applying the vehicle brakes is not a full solution. The instability of the electric motor is demonstrated in Figure 5.2, which shows the response to a step command while the system is held stationary under braking. While step commands would not be required under a constant motoring-load scheme, the experiment shows that the motor controller was generally susceptible to disturbances while stationary.

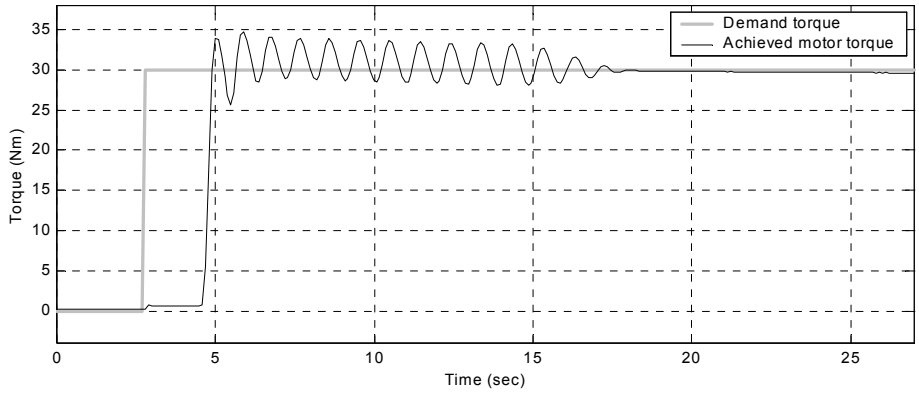

Figure 5.2 Response of electric motor controller at zero velocity

Oscillations with a period of approximately 1 second can be seen, which take a significant amount of time to dissipate. An attempt to improve performance was made by implementing a software controller in series with the existing analogue hardware. With additional control, it was also expected that the demand following characteristics could also be improved. Note that while the relationships between D/A demand voltage and output torque were largely linear (see Appendix C for calibration) small non-linear inaccuracies were observed.

Proportional-Integral gain, and simple Integral-only controllers were tested, but were found to further exacerbate the present oscillations due to the feedback lag. That is, the time delay between the software acquiring the latest motor torque, and the sending of another constant torque demand to the analogue controller—which also exhibits a finite delay. The results for an Integrator controller at zero velocity are included in Appendix K.

In light of this unsatisfactory response, it was decided that the electric motor would be used only for warming the system up, or bringing the rollers up to speed for

coastdown testing and the like. With the motoring force reduced to zero, F_{net} in Equations 3-10 and 3-11 becomes equal to the power absorber force, F_{dyno}. It is evident that under some road load conditions, the required force, F_{net} will become negative. This can be the case if the relative frictional coefficients of the dynamometer system are larger than those of the vehicle, or more significantly, under changes in velocity. For example, the inertial component $(m_{Veq} - m_{cd})dv/dt$ will become negative during acceleration if the equivalent mass of the vehicle being modelled is exceeded by the chassis dynamometer mass. In such cases a dynamometer motoring capability is desired. Where none is available, errors arise as the motion of the vehicle is resisted to a greater degree than it would be under the same conditions on the road. However, making use of the flywheel set, $(m_{Veq} - m_{cd})$ should never exceed 60 kg, which was thought to be acceptable in light of the apparent inaccuracies brought about by the use of the electric motor. Also, in testing situations where the energy absorbed by the vehicle during braking is not important, the dynamometer equivalent mass may be set lower, so that less braking will be needed during deceleration, with the shortfall in rotational inertia being supplemented with an additional positive power absorber load for acceleration phases.

Excluding the motoring force creates an additional problem in that the previous methods used to calculate the inertia and friction do not include the frictional characteristics of the motor when it is not applying a load. The friction of the unemployed motor was previously included in the F_{motor} value and is not easily separated, as described in Section 5.1. The chassis dynamometer as a whole should be used for testing in the same mode of operation as it was calibrated. Thus, a method of finding the system inertia and friction was desired that would not require direct use of the electric motor.

5.3 Inertia Determination Without the Motor

By default, the only dynamometer situation with no vehicle present and no input from the motor is a coastdown (or no motion at all), be it under torque from the power absorber, or friction only. Equation 5-5 below is a restatement of the coastdown

Equation 5-1, without the presence of a motoring force, and with the friction terms (including the unpowered electric motor friction) grouped together as a single value.

$$m_{cd} = \frac{-F_{dyno} - F_{fric}}{\left(\frac{dv}{dt}\right)} \tag{5-5}$$

Measuring F_{dyno}, and calculating dv/dt, we have two unknowns at each instant: the equivalent mass, m_{cd}, which remains constant throughout, and F_{fric} which is assumed to be dependent upon instantaneous velocity. Therefore, if we have recorded data from two coastdowns under different dynamometer loads—and hence, rates of deceleration—the total friction term can be cancelled at any one velocity, leaving only one unknown value. For example, if two generic coastdowns are performed under F_{dynoA} and F_{dynoB}, the velocity vs. time relationships take the form shown in Figure 5.3.

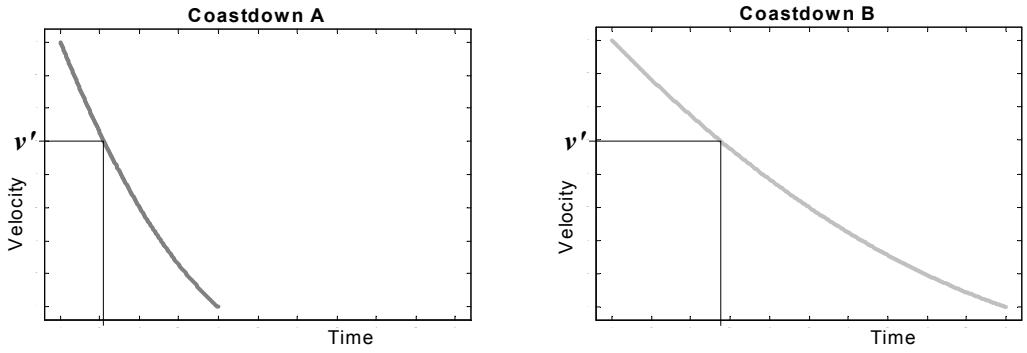

$$m_{cd}\left(\frac{dv'}{dt}\right)_A = -F_{fricA} - F_{dynoA} \qquad m_{cd}\left(\frac{dv'}{dt}\right)_B = -F_{fricB} - F_{dynoB}$$

Figure 5.3 General form of two different coastdowns under dynamometer torque

At the desired speed point (v') marked on the diagram, the friction terms F_{fricA} and F_{fricB} are identical, so by subtracting the second coastdown equation from the first, we arrive at Equation 5-6.

$$m_{cd}\left(\dot{v}_A - \dot{v}_B\right) = -F_{dynoA} - F_{dynoB} \tag{5-6}$$

Where: $\dot{v} = \frac{dv}{dt}$

From which the equivalent mass, m_{cd} can be calculated. It should be noted that m_{cd} is constant for any choice of velocity, so that the two coastdowns can be matched in any number of ways, provided *dv/dt* and F_{dyno} are also measured. Figure 5.4 shows various combinations of the same coastdown pair.

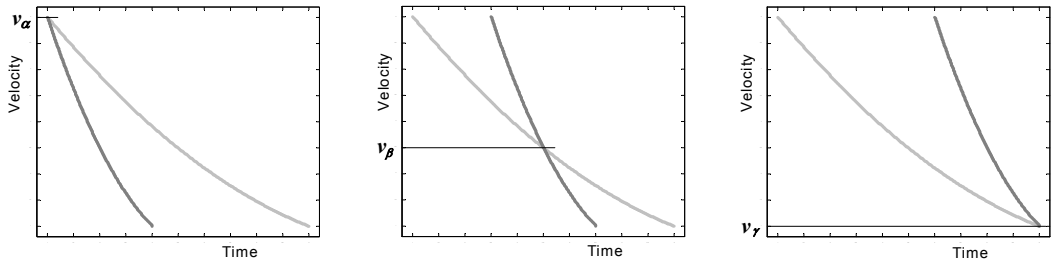

Figure 5.4 Two coastdowns combined at several different velocities

In practice, the electric motor was used to bring the system up to approximately 20 kph above the maximum recorded velocity (to ensure a stable state before the desired speed range was reached). At this point, the motor was switched off, so that no residual or random current could be introduced during the coastdown. A known dynamometer load was then applied via a D/A signal from the computer, and the velocity and torque were recorded from when the upper speed was reached until the minimum recorded velocity was registered. Eddy-current dynamometer control and data acquisition were accomplished in a simple purpose-written C++ program, while the analysis of coastdown data and simultaneous solving for the inertia were carried out in a MATLAB function (see program `solve_inertia` on CD). It was found that the dynamometer equivalent masses calculated according to Equation 5-6 exhibited a small speed-dependent variation. For this reason, it was decided that several coastdown runs should be carried out at several different dynamometer torques, and the results averaged. This variation in inertia with the velocity at which it was calculated is shown in Figure 5.5, where a set of three coastdown runs have been combined in each of the three possible ways. That is, if data exists for coastdowns under nominal loads of 60 Nm, 80 Nm, and 100 Nm respectively, the simultaneous solution may be calculated at any velocity by combining the 60 Nm and 80 Nm, the 60 Nm and 100 Nm, or the 80 Nm and 100 Nm data sets.

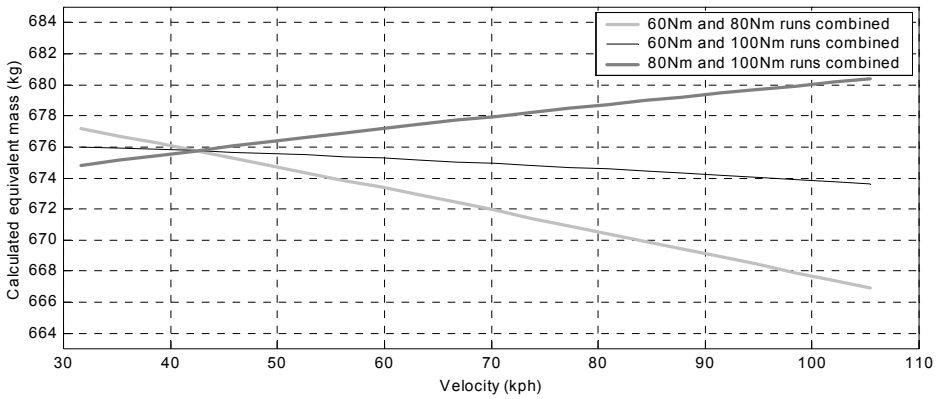

Figure 5.5 Variation in calculated equivalent mass with differing velocity and dynamometer loads

The variation over this range of speeds and loads (similar to those encountered during vehicle testing) was found to be of the order of 2% in this case. To obtain a single dynamometer inertia value, the calculations were averaged over the whole speed range during post-processing, and the coastdown data at each power-absorber torque was itself the average of eight individual runs under such conditions. Satisfactory repeatability was observed with these averaged sets of data. A series of 32 individual coastdowns with nominal dynamometer torques of 40, 60, 80, and 100 Nm identified the base inertia (no additional flywheels) as 673.8 kg. Averaging the eight files at each power-absorber torque, and combining these torque sets in different ways produced equivalent masses with a standard deviation of 2.3 kg (0.3%). Full results of these repeatability tests are included in Appendix L. Determination of the system inertia by coasting down without torque from the electric motor was identified as the most appropriate method in light of the difficulties with the motor control and the repeatability of the various techniques employed in Section 5.2.

5.3.1 Base Inertia Correction

Further coastdown tests were conducted in a similar way with the addition of flywheels to increase the total equivalent mass. In terms of repeatability, the results obtained in these trials were comparable to those detailed in Section 5.3 and Appendix L. The mass added by the inclusion of these flywheels was relatively easy to calculate since each is a simple steel disc. The flywheel set was originally constructed with this in mind, to give round numbers for the equivalent mass. A

description of the chassis dynamometer flywheel set is included in Section 2.2. The moment of inertia (in kg.m^2) of each flywheel is equal to the moment of inertia of a solid disc of the same size, less the removed portion that the shaft passes through.

$$I_{disc} = \frac{\rho \pi r^4 t}{2} \tag{5-7}$$

Where: ρ = material density (kg/m^3)
r = disc radius (m)
t = disc thickness (m)

Moments of inertia at the fast (flywheel) end of the shaft can be converted into equivalent mass at the roller drums by first converting to moment of inertia at the slow (drum) end:

$$I_{slow} = (diff\ ratio) I_{slow} \tag{5-8}$$

Note: *diff ratio* = 43/7

Then calculating the equivalent mass at the drum surface:

$$m = \frac{I}{r_{dr}^{\ 2}} \tag{5-9}$$

Where: r_{dr} = drum radius = 0.6 m

If these equivalent masses are known, the only unknown inertia is that of the system with no flywheels attached, as was previously calculated. However, tests involving some or all of these flywheels revealed that the coastdown method did not exactly predict the equivalent mass steps that had been calculated using Equations 5-7 to 5-9. Table 5.2 shows the experimental equivalent mass of several flywheel combinations against the nominal values calculated from their size. The inertia of the flywheels alone is represented by subtracting the equivalent mass of 674 kg calculated in Section 5.3. Figure 5.6 shows the error between the experimental and the nominal flywheel mass values.

Nominal mass (kg)	0	450	450	460	680	680	1130	1130
Experimental mass (kg)	0	456	458	466	692	693	1146	1146

Table 5.2 Nominal, geometrically calculated flywheels masses and experimentally measured masses

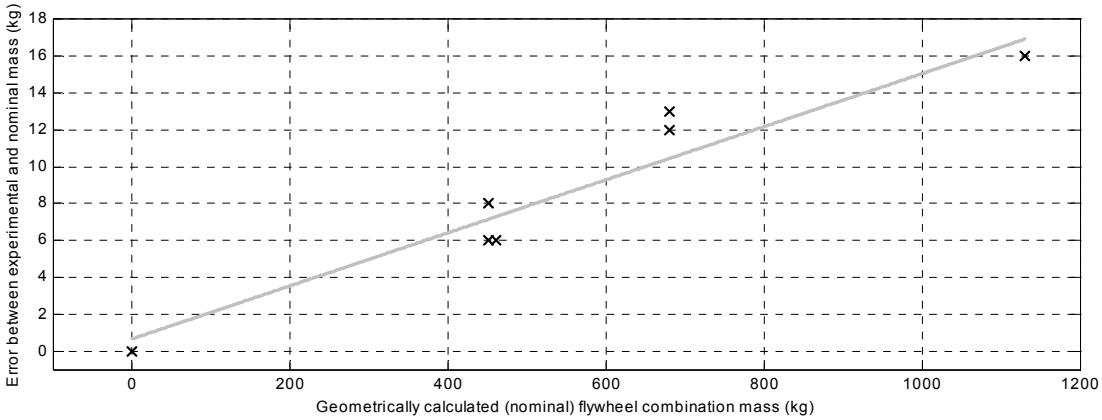

Figure 5.6 Nominal flywheel equivalent mass vs. error between experimental and nominal equivalent mass

The form of the equivalent mass error in Figure 5.6 indicates a systematic error in the coastdown method that may have been brought about by timing or measurement inaccuracies. The gradient of this increasing error was found to be 0.0144 kg/kg, that is, 1.44%. Using the available data, a base inertia (equivalent mass without flywheels) was sought that would not include this error. Two assumptions were made in this case. Firstly, the assumption that this error trend would continue in cases where the total inertia was approaching zero, which seems likely given the linear trend shown in Figure 5.6. Secondly, if we assume that there is no offset in this error, that is, that the coastdown technique would return zero in a hypothetical case where no inertia were present. Therefore, at the calculated base inertia of 674 kg, we assume that the inherent error has caused this value to be 1.44% too high. Thus, the corrected base inertia may be calculated as per Equation 5-10:

$$Base\ Inertia \quad = \quad 674 \times \left(1 - 0.0144\right) \quad = \quad 664.3 kg \tag{5-10}$$

It should be noted that this 1.44% adjustment is based on observed trends rather than a known error mechanism, and the result should be treated with some caution. The base inertia of the chassis dynamometer remains constant, and the value calculated above has been used during all subsequent calibrations and testing. A table of the

total equivalent masses resulting from the various flywheel combinations that can be acheived on the dynamometer is included in Appendix A.

5.4 Friction Determination from Coastdown Data

Having arrived at an appropriate equivalent mass, and assuming that the motoring force is zero, Equation 5-5 now has only one unknown quantity at any given velocity and acceleration; that of the system friction, F_{fric}. The chassis dynamometer is subject to frictional forces from the bearings, differential losses, and air resistance on the flywheels and drum. Each of these forces acts in a direction opposite to the direction of motion, and may vary according to the rotational velocity. It was assumed for simplicity that the combination of frictional forces would be represented as a single quadratic equation depending only upon speed, as represented in Equation 5-3. Thus, whereas Equation 5-5 was solved simultaneously using two sampled coastdowns (Equation 5-6), the three frictional coefficients require solving of data from three or more points, which can be from the same coastdown. Note that the term coastdown here indicates a deceleration under torque from the eddy-current dynamometer, as mentioned in Section 5.1.

With a knowledge of velocities and dynamometer loads over the course of a coastdown run, Equation 5-5 can be rearranged to solve for the total frictional force at a given speed. Equivalent mass (constant) and F_{dyno} are known at each point, while the friction is dependent upon velocity.

$$F_{fric} = m_{cd}\frac{dv}{dt} - F_{dyno} \tag{5-11}$$

Data was collected in the same way as the inertia calculations of Section 5.3 with several coastdown runs being performed at each of four different dynamometer loads. As a repeatability trial, the total friction was calculated at shaft speeds equivalent to 35 kph and 105 kph at the roller drums for 32 separate coastdowns under various dynamometer torques. At 35 kph the average frictional force was 73.4 N (referenced to the drum surface) with a standard deviation of 1.5 N (2.0%). At 105 kph the average friction was found to be 136.5 N with a standard deviation of 1.1 N (0.8%). These variations were in the range of uncertainty of the load cell readings, and

therefore the method was deemed sufficiently repeatable. A complete table of results is included in Appendix M. It should be noted that frictional coefficients calculated in a similar way to the equivalent inertias of Section 5.3 may be subject to the same systematic error in magnitude mentioned in Section 5.3.1. However, a 1.4% error in the total friction would also be less than the smallest measurable torque, and thus any such error was ignored.

For each coastdown, the velocity series was approximated by a least squares quadratic equation, as detailed in Appendix F. From this equation, the approximate acceleration (*dv/dt* in Equation 5-11) at any point can be calculated by differentiation. In order to solve for each of the frictional coefficients (f_{0d}, f_{1d}, f_{2d}) the total friction was calculated from Equation 5-11 at each of three speeds (e.g. 35, 70 and 105 kph) and averaged over the various dynamometer load runs. This provided three known friction totals at three known velocities:

$$F_{fricA} = f_{0d} + f_{1d} v_A + f_{2d} v_A^2 \quad (5\text{-}12a)$$

$$F_{fricB} = f_{0d} + f_{1d} v_B + f_{2d} v_B^2 \quad (5\text{-}12b)$$

$$F_{fricC} = f_{0d} + f_{1d} v_C + f_{2d} v_C^2 \quad (5\text{-}12c)$$

These three equations could then be solved simultaneously to arrive at unique values of f_{0d}, f_{1d}, and f_{2d}. For example, the data summarised in Appendix M was collected during coastdowns with flywheels adding to an equivalent mass of 1114kg, and yielded friction coefficients thus:

$$F_{fric} = 40.0 + 3.47v - 0.006v^2 \quad (5\text{-}13)$$

Where v = velocity in m/s

The friction mechanisms at work in this situation dictate that each of these coefficients should be greater then zero. However, a small negative value was calculated for the velocity-squared term, which may have been result of experimental errors. The magnitude of this term also justifies the use of a three-term approximation for friction, as opposed to higher orders. That is, no significant

increase in accuracy would be expected if the relationship between friction and velocity were modelled as a cubic, for example.

It was evident that the frictional characteristics of the system change depending on the number of flywheels rotating with the shaft (introducing air resistance) and the number that are stationary on the shaft (friction between the moving inner and stationary outer race of each bearing). Also, the friction may vary throughout the life of the chassis dynamometer as various components age and wear. Thus, it was necessary to include the friction calibration procedure in the main dynamometer program. Details of this implementation are included in Section 6.5.5. Given the repeatability of the calculated frictional forces shown in Appendix M, it was thought that the averaging of three or four coastdowns (under different torques) would provide satisfactory friction coefficients. It is recommended that the coefficients for each flywheel combination be recalculated at least every two months during use and that the dynamometer be thoroughly warmed up before any testing session. Warming up of the system generally entails running under power from the electric motor or a test vehicle to ensure all the rotating components have reached a state of thermal and frictional stability. Details of the warm up routine can be found in Section 6.5.8.

5.5 Tractive Effort Load Cell Correction

As mentioned in Chapter 4, the characteristics of the roller drum assembly need to be known before useful measurements can be made using the tractive effort load cell. Equation 4-13 shows that the output force from a vehicle on the rollers is balanced by the inertial forces of the drums, the aerodynamic frictional forces on the rollers, and the other combined resistances from the flywheels and power absorber that are measured by the load cell. In order to record the actual force at the surface of the vehicle tyres, the equivalent mass and frictional characteristics of the roller drums must be known, along with the instantaneous velocity and acceleration.

5.5.1 Roller Drum Inertia

Calculation of the drum assembly inertia was performed in almost exactly the same way as for the total system inertia, except that the measurement of torque at the eddy-current dynamometer was replaced by the roller drum load cell reading. The tractive

effort load cell is set up to read the tangential force as at the surface of the drums by means of the load arm and computer calibration coefficients. A simplified free-body diagram represents the relationship between the trunnion-mounted axle assembly and the fixed support (measured by the load cell).

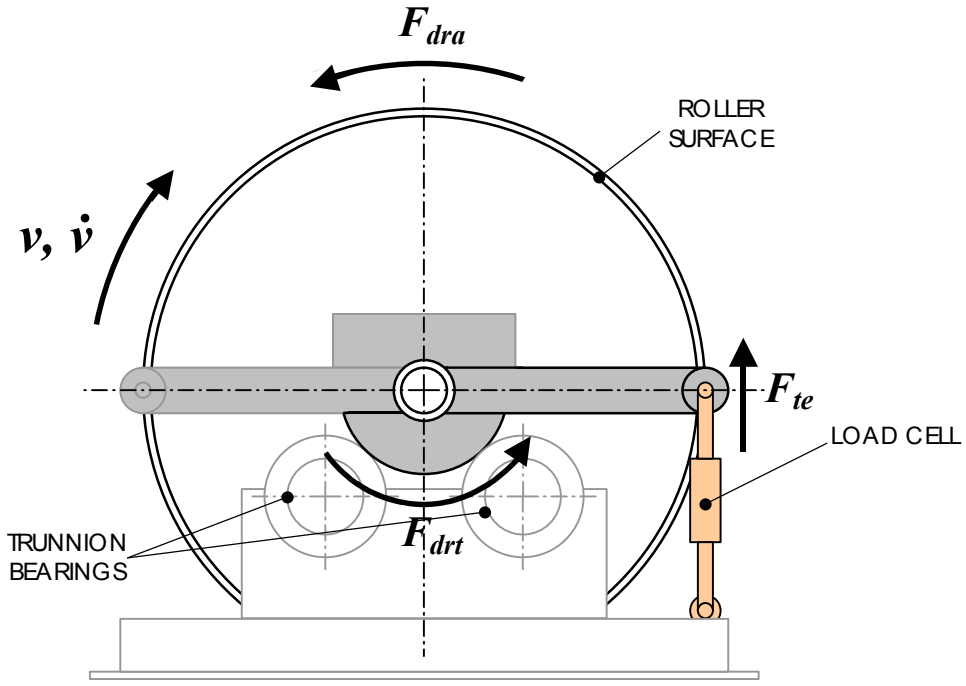

Figure 5.7 Free body diagram of forces on the drum axle assembly during coastdown

Where: v = velocity at drum surface (m/s)

$\dot{v}$ = acceleration at drum surface (m/s^2, negative during coastdown)

F_{te} = reaction force measured at load cell (N)

F_{drt} = drum axle trunnion bearing friction (N)

F_{dra} = aerodynamic friction on drum surface (N)

During a coastdown, each of these forces opposes the direction of motion, and the acceleration, $\dot{v}$ is negative. Referencing the forces to the drum surface, gives an equation of motion as shown in Equation 5-14.

$$m_{dr}\dot{v} = -F_{te} - F_{drt} - F_{dra} \tag{5-14}$$

F_{drt} represents the Coulomb friction at the trunnion bearings, which introduces hysteresis when the direction of loading is changed. Because the direction of this

force is related to the tractive force direction (not the direction of motion), it cannot be included in velocity-dependent friction equations, and must be neglected. This omission introduces an error, which is not particularly significant in the determination of the drum inertia since the direction of the tractive force does not change in the course of a coastdown run.

Since F_{te} is known, and $\dot{v}$ can be calculated at any point during a coastdown, the drum friction, F_{dra} can be cancelled between two different runs to allow a solution for m_{dr} as per Equation 5-6. Again, averaging over several different dynamometer loads (which varies F_{te} and the rate of deceleration) a single value for the equivalent mass was arrived at. Recording data from a total of 32 separate coastdowns with four different dynamometer loads, the average equivalent mass (as at drum surface) was found to be 599.3 kg with a standard deviation of 3.6 kg (0.6%). In the absence of accurate empirical calculations (like those used in Section 5.3.1), it was decided not to subtract the 1.4% error that was present in the whole system calibration, since the error may have been due to the dynamometer load cell, which was not used during the drum assembly calculations. Appendix N contains a full table of sampled results leading to the calculation of the roller drums' equivalent mass. Raine [1981] lists geometrically calculated inertias for each element of the dynamometer system. In these calculations, the roller drums and axle assembly account for 89.8% of the total system inertia, with no flywheels present. The equivalent mass of 599 kg shown above represents 90.3% of the 664 kg base inertia. This provides a measure of vindication for both the experimental and geometric calculation approaches.

5.5.2 Roller Drum Friction

Once the inertia of the roller drum assembly had been determined, a similar method to that detailed in Section 5.4 could be used to find the windage friction force, F_{dra}. As in the case of the whole system, the resistance to motion was modelled as having a second-order relationship to the rotational velocity. However, the aerodynamic friction on the drum surfaces is present only while the drums are rotating, and thus $f_{0dr} = 0$. A series of coastdowns was again used to determine the repeatability of the method. At 35 kph the total friction force was found to be 4.6 N with a standard deviation of 1.6 N (35%), while the total friction at 105 kph was 22.6 N with a

standard deviation of 1.7 N (8%). A complete set of drum friction results is included in Appendix O. The level of repeatability (in absolute terms) was comparable to the calculations of friction for the chassis dynamometer as a whole (see Section 5.4), although the percentage error was significantly greater in the case of the drum friction. Provision is also made in the main computer program for the regular updating of these frictional coefficients. Whenever new friction coefficients are generated for the system as a whole, the option is given for the user to also record the tractive effort data to calculate the roller drum friction as well. Again, a description of this routine is included in Chapter 6.

5.5.3 Effectiveness of the Load Cell Correction

In order to determine the actual force applied by a vehicle to the rollers, the equivalent mass of the drum assembly and its frictional coefficients are determined beforehand using the methods above. During operation, the instantaneous velocity and acceleration, and the load cell force are continuously changing with time. It was necessary to determine whether the response of these updated parameters was sufficient to accommodate the rapid changes that occur during driving cycle testing. While an instantaneous response would be ideal, it was realised that some delay would be inevitable due to the requirement for acceleration filtering (introducing a time lag) as detailed in Section 4.2. The load cell signal also includes a degree of damping, and it was important that the measured tractive effort and the calculated velocity and acceleration were all appropriate when solving Equation 4-13 for F_V at each point in time. A series of experiments were carried out recording the acceleration, raw load cell signal, velocity-dependent friction and the final, corrected tractive effort. By accelerating and decelerating the chassis dynamometer under power from the electric motor and power absorber respectively, there is no tractive force (as from a vehicle) on the rollers. Therefore, the corrected tractive force should remain zero through any increase or decrease in velocity. The constituents represented in Figure 5.8 are shown in Equation 5-15:

$$F_{corr} = F_{loadcell} + m_{drum}\frac{dv}{dt} + F_{drfric} \qquad (5\text{-}15)$$

CORRECTED TRACTIVE EFFORT = RAW TRACTIVE EFFORT + CORRECTION COMPONENT

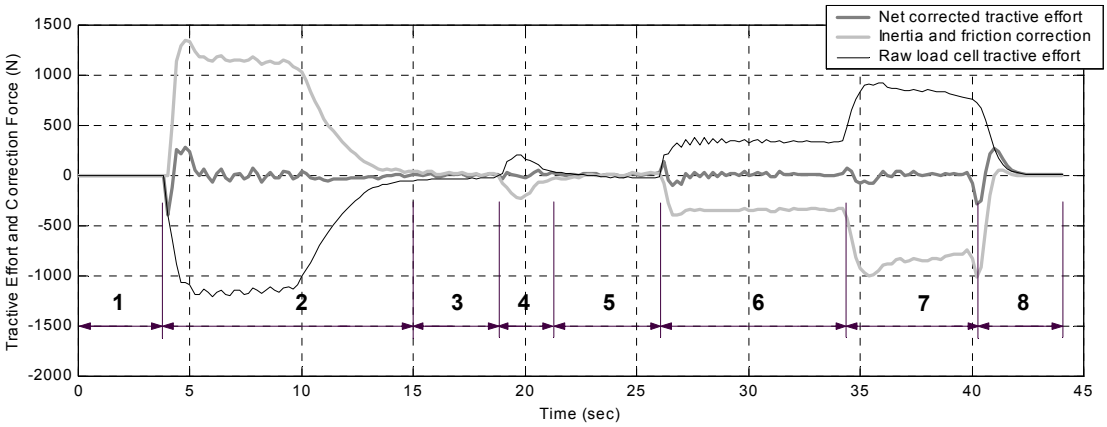

Figure 5.8 Tractive effort correction response under motor and dynamometer power

Phase	Activity
1	Zero load from motor and dyno. Speed = 0 m/s
2	Motor brings system up to speed. Maximum acceleration = 2.2 m/s^2
3	Constant speed control from motor. Speed = 14.5 m/s
4	Dyno load 50 Nm added. Small deceleration.
5	Motor restores constant speed. Dyno load = 50 Nm. Speed = 14.5 m/s
6	Motor load removed. Dyno load = 50 Nm. Average deceleration = 0.6 m/s^2
7	Dyno load increased to 150 Nm. Average deceleration = 1.2 m/s^2
8	System comes to rest. Speed = 0 m/s

Table 5.3 Tractive effort correction response test phases (see Figure 5.8)

It can be seen in Figure 5.8 that the average corrected tractive effort remains at zero, as it should when no force is applied at the roller surface. However, there are several small excursions from this zero point at the changes in acceleration. This indicates that the time lag in the acceleration calculation exceeds any lag in the load cell signal. For example, under a rapid increase in speed (e.g. at the beginning of Phase 2), the correction component does not immediately include the energy that is being expended in accelerating the drums, and therefore the corrected tractive effort momentarily reads too low. This method of correcting the tractive effort load cell signal was applied throughout the testing described in Chapter 8, often making use of an approximated or 'ideal' acceleration (see Section 6.5.12.2).

CHAPTER 6:

Control and Data Acquisition Software

This chapter contains both a general description of the chassis dynamometer software program and specific details of its functionality and implementation in the C++ programming language. Significant decisions regarding the overall form and data sharing with other applications are highlighted, as well as the constraints that have lead to some of these decisions. Each mode of operation requires a different on-screen appearance and data-handling capabilities, and these are discussed in Sections 6.5.4–6.5.12. Computer program files are shown in upper case, while the names of specific software functions and syntax are printed in `courier` font.

6.1 Program Layout

The chassis dynamometer control software consists of an executable program written and compiled using Borland C++ version 3.1. The layout and menu options may be viewed by running this executable, which is included—along with each of the source code files—on the CD accompanying this thesis. However, without the necessary A/D electronics and file structure, several warnings are triggered and most of the functionality is disabled. Upon running, the user is greeted by the screen display shown in Figure 6.1. The majority of the coloured screen displays included in this section are printed in black and white, with arrowed notes included for the readers' benefit. The colour of the background, and indeed all colours throughout the program can be adjusted by setting numerical constants in the C++ source files.

The Turbo Vision set of object-oriented classes and libraries allows a Windows-like interface wherein the user can navigate using a mouse or key strokes through a series of pull-down menus and display windows. Selections are made with the usual 'buttons', which can be activated by the mouse button, or the Space or Enter keys.

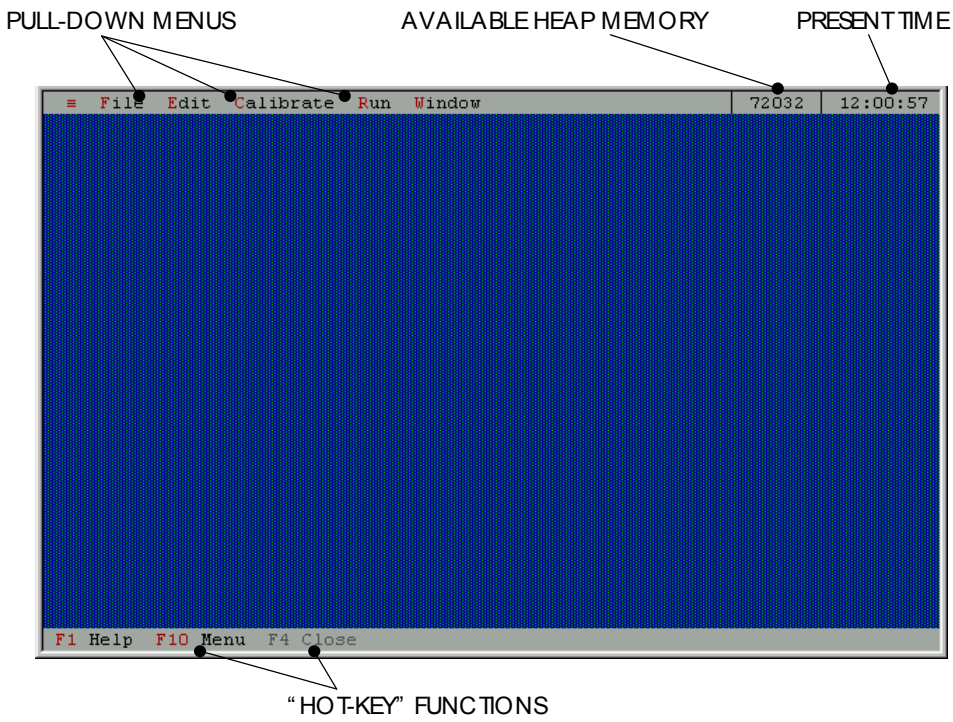

Figure 6.1 Initial display screen showing available pull-down menus

Standard Turbo Vision menu and window classes were used to produce screen displays like those shown in Figure 6.2.

Within this structure, the various testing and calibration functions can be accessed, each having their own set of user preferences, which are stored in separate text files. These preference files are saved at each edit so that the latest settings are still usable if the program is shut down and restarted. Appendix P lists every available menu option in the main program. It should be noted that some operations—such as the 'Flywheel Setup' function—are required before every test and as such can be accessed from more than one place in the program.

The principal function of the program is to facilitate chassis dynamometer testing. During a test, data must be sent to the computer, received, and saved, while also providing user feedback to the monitor. A program loop is used that performs each of these operations, then waits for a timed interrupt before repeating the process. This allows the program to record and send data at regular intervals in time and is further discussed in Section 6.5.3.

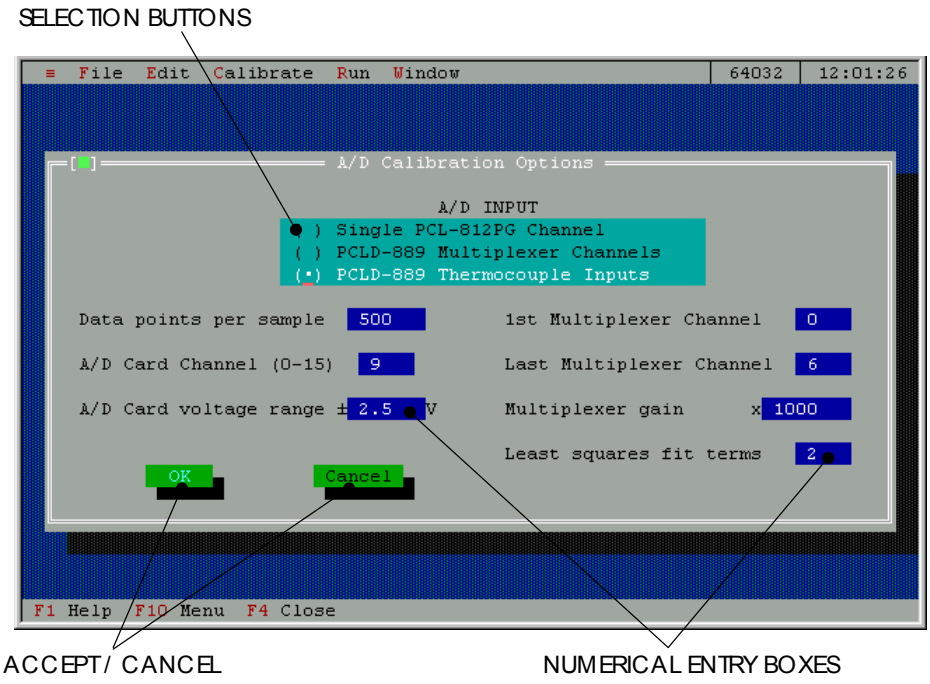

Figure 6.2 Example of a window showing the available user options

6.2 Programming Constraints

Early on in the project, it was decided that the final control program should be a DOS application, using the Turbo Vision classes and libraries to achieve a graphical user interface. There were several reasons that this format was chosen over a Windows-based application, including the programming work already carried out, and difficulties with program running speed and interrupt timing under Windows.

In 1994 a former student, Neil Glasson, had written a C++ program to control the operations of the University of Canterbury's engine dynamometer. The overall concept and form of this software was similar to what would be required for the chassis dynamometer, and a small number of routines could be renamed and used in their existing form. Although crossover from the engine dynamometer program was minimal in the long run, the layout and programming style provided a useful springboard for the writing of the chassis dynamometer software. In addition, Neil Glasson had written software for the visual driving cycle display. This scrolling graphic was implemented in the final program with minor additions, and is detailed in Section 6.5.12.1.

All programs running under Windows (particularly earlier versions) are subject to the timing and task-allocation procedures of this software. The Windows operating system tends to disable interrupts for long periods of time, which could result in timing errors or program crashes in certain cases. Since all the data-recording processes were to be controlled by interrupts from a UPP card, an application running under the Windows operating system was thought to be unsatisfactory.

The implementation of a DOS application—in particular, one using Turbo Vision—also created a number of problems. The Turbo Vision application framework is relatively old, having been marketed in 1991. It was thus designed with less powerful computers in mind, meaning that its capabilities were limited with respect to the amount of *data memory* that could be made available by the compiler. The enforced use of short data pointers (16-bit) restricted the data memory (storage of global data array variables) to one 64K 'page'. These constraints demanded that certain blocks of memory within the main program be dynamically allocated (especially during the creation of large numerical arrays) so as to access areas of memory not limited by the compiler settings. In addition, the size of any DOS executable file cannot exceed 1Mb because the hardware addresses are limited to 20-bits. These difficulties did not seriously limit the program capabilities, although the future addition of large in-program help files may be troublesome.

6.3 Data Handling

Once numerical data has been read by the A/D card and other calculating routines, it is necessary to display the information on screen, as well as save it in a file that can be accessed later. Consistent and coherent screen display and file storage is achieved by the use of a configuration file, which stores all the necessary information for data handling.

6.3.1 The Configuration File

The configuration file contains—in text form—all the information required for the reading of A/D data, converting it the appropriate useful units, checking the maximal limits of the data, and outputting the information to the screen or a file. As well as data inputs, the configuration file also includes the digital-analogue output settings,

such as multiplication factors and upper and lower limits. By storing all these details in a single file, standardised settings can be used by different testing routines, and changes to the C++ code will not affect the specifics of A/D or D/A operations.

Prior to any operation involving the PCL-812PG card, the configuration file is opened and the important information stored in arrays that can be accessed during data collection operations. This routine can be found in the source code in file CH_CMDS.CPP, routine `read_AtoD_config`. The parameters in the configuration text file (given a file extension *.cfg) may be edited by the user from within the control program, or using any text editor, such as MS Notepad[7]. A printout of a sample configuration file is included in Appendix Q, with a description of the each parameter.

6.3.2 File Input/Output

All testing routines (as well as the calibration operations) involve the saving of captured data in a file for later use either by the control program, or to be viewed by the user. Before any of the testing routines begin saving data, a header is written in the user-defined save-file which includes time and date information, as well as the type of test, the last measured frictional coefficients of the system, and the details of all the data to be collected (e.g. 'Roller Speed (kph)'). Typically, during each of the timed loops mentioned in Section 6.1, all the required data is read from the PCL-812PG and PCLD-889 cards according to the settings in the configuration file, and temporarily stored in one or more numerical arrays. At the end of each loop, a single file-writing operation transfers this array data to the file in a prescribed order and form.

The form of the save-file was intended to be comprehensible as text only, while also maintaining portability for other applications like MATLAB and Excel. In particular, delimiting commas have been included to aid its opening in Excel, and the post-processing MATLAB programs discussed in Chapter 7 include routines that transfer the file data into matrices from which the information can be edited or plotted. An

---

[7] Copyright Microsoft Corporation

example of a saved data file is included in Appendix R with a description of each of the text components. Example data files can also be found on the CD accompanying this thesis, in the directory Sample Output Files.

6.4 Mathematics Functions

Solving sets of simultaneous equations using a computer program is most easily achieved with matrix algebra. The methods discussed in this section are included as part of the chassis dynamometer control software for the calculation of least squares approximations, and the simultaneous solving from coastdown data to determine the system friction (Section 4.4).

The elementary array structures of C++ do not immediately lend themselves to calculations involving matrices of more than one dimension. This is due to the sequential storage and recall of data in numerical arrays. To work with two-dimensional arrays, it was necessary to set up a structure for each matrix that included row and column data to access the sequential block of memory in which the numbers were stored.

For example, a 3×4 matrix would be stored with the following information: Number of rows = 3, number of columns = 4, as well as pointer to the memory location of the first element. Element (2,3) for example, could then be accessed in a fictional 3×4 matrix as shown in Figure 6.3.

Matrix Data:

$$\begin{bmatrix} 9 & 10 & 11 & 12 \\ 1 & 2 & 3 & 4 \\ 8 & 7 & 6 & 5 \end{bmatrix}$$

C++ Memory Storage: (name = `array`, rows = 3, cols = 4)

INDEX	0	1	2	3	4	5	6	7	8	9	10	11	12
DATA	9	10	11	12	1	2	3	4	8	7	6	5	

Element (**2**,**3**) accessed by C++ command: `array[cols×(2-1) + 3 - 1]`

`= array[6]`

Figure 6.3 Example of matrix storage and indexing

Having allocated the memory and defined the row width and column height of each matrix, separate routines were generated to complete various simple matrix manipulations. Matrix transposition, inversion (using the Gauss-Jordan method) and multiplication and are included in MATH.CPP. Least squares coefficients are calculated using the following equation as shown in Appendix F.

$$\boldsymbol{\alpha} = \left(X^T X\right)^{-1} X^T y \tag{6-1}$$

Solving for frictional coefficients also requires multiplying and inverting matrices as shown below:

At each speed point: $$\begin{pmatrix}1 & v & v^2\end{pmatrix}\begin{pmatrix}f_0\\ f_1\\ f_2\end{pmatrix} = F_{fric} = \textit{total friction}$$

Combining data from three points:

$$\begin{pmatrix}1 & v_a & v_a^2\\ 1 & v_b & v_b^2\\ 1 & v_c & v_c^2\end{pmatrix}\begin{pmatrix}f_0\\ f_1\\ f_2\end{pmatrix} = \begin{pmatrix}F_a\\ F_b\\ F_c\end{pmatrix}$$

$$X\,\boldsymbol{f} = F$$

And solving for coefficients: $$\boldsymbol{f} = \left(X^{-1}\right)F \tag{6-2}$$

6.5 Control Program Functionality

This section details each of the most important tasks carried out by the chassis dynamometer control software. Where possible, the sequence of events has been represented in the form of a flow diagram, while C++ programming specifics and syntax has been minimised. However, the names of several classes and functions have been included so that reference can be made to the source code (supplied on CD) if desired.

6.5.1 Turbo Vision `idle` Function

Most Turbo Vision applications include the same background operations that keep the program running and wait for what are known as *events*. An event is essentially a piece of information that requires an action. For example, keyboard inputs, mouse button presses, and messages sent from one part of the program to another are all

events. The chassis dynamometer control program includes a loop that continuously retrieves any new events (Turbo Vision's `getEvent`) and acts on these events (`handleEvent`). The `getEvent` function checks for keyboard and mouse inputs, then calls the `idle` function. These operations can be simplified in flow diagram form (Figure 6.4).

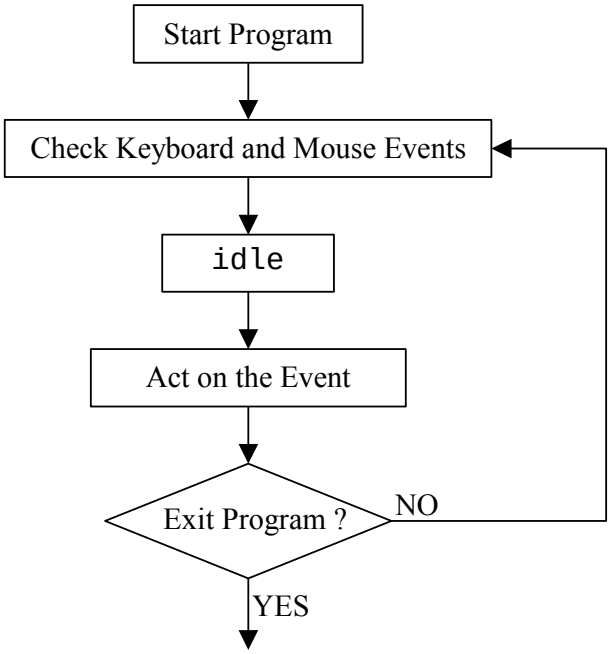

Figure 6.4 Flow diagram of continuous background loop of main program

Within the `idle` function, there are several commands that update the state of the program. For example, the on-screen clock is checked against the computer clock and updated, the heap-memory indicator displays the latest size of available memory, and the digital inputs (e.g. equipment off/on and mode switches) are read via the PCL-812PG card. Most importantly, this `idle` function—so called because it is executed when only when there are no other tasks awaiting action—creates an event which instructs the program to run the function designated by `cmUpdate`. Each mode of dynamometer operation has its own implementation of the `cmUpdate` function, which usually involves all the other ongoing tasks such as reading the A/D signals, sending out D/A demands, and writing data to a file. The generic form of this updating routine is discussed in Section 6.5.3.

6.5.2 Setting Test Parameters

Each task performed on the chassis dynamometer has various parameters that alter the mode of operation, or the nature of the results. Instead of entering new values for these parameters each time a certain function is carried out, the details are stored in a series of files which are read by the program before commencing a particular operation. These user-defined settings include: vehicle details such as mass and frictional coefficients, the current flywheel combination, which A/D configuration file to use, and the test duration. If any particular option is not changed by the user before running the dynamometer, the most recently entered value is read from the appropriate file.

In most cases, the necessary parameters are chosen by selecting button-type options, or through a keyboard input such as typing in the desired numerical value. Dedicated windows show which options are available to be edited, and automatic checks are made to ensure the entered data is within the pre-defined allowable limits (limits are maintained in the C++ header files e.g. TESTING.H). The vehicle details window is shown as an example (Figure 6.5), with appropriate labelling.

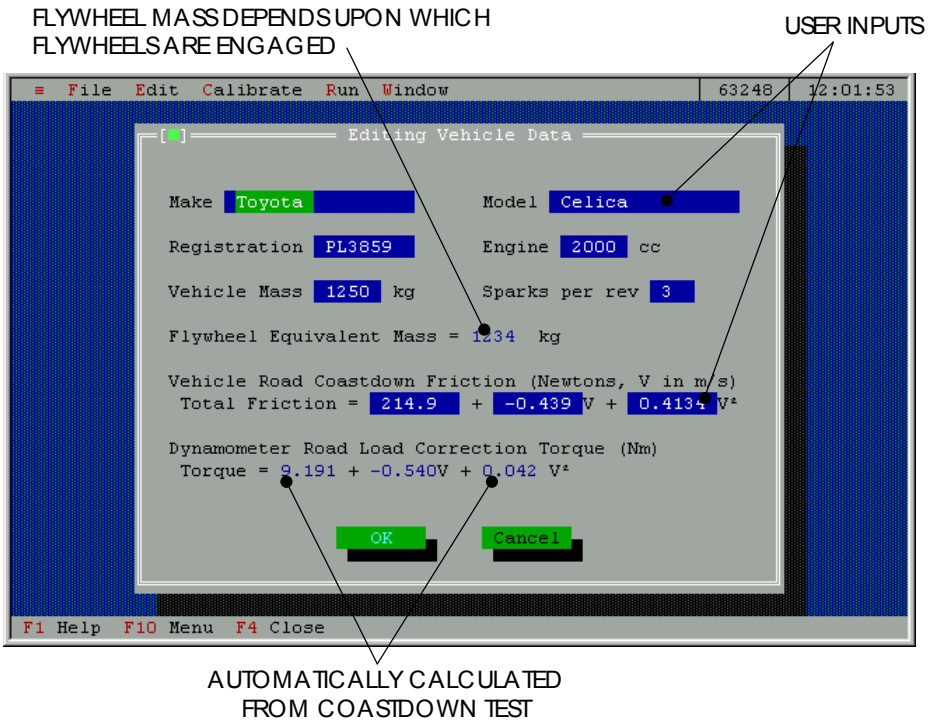

Figure 6.5 Vehicle options selection window

The flywheel selection window is a special case in the setting of test parameters. Most friction calibrations and testing routines require a knowledge of the chassis dynamometer equivalent mass for inertia calculations. However, the actual mass of the system is changed by physically transferring the various components of the flywheel set. Therefore, it is important that the flywheel combination selected in the options window is representative of the actual situation on the test rig. A graphical diagram is provided, from which the attached flywheels can be selected. A calculation is made to show the total equivalent mass, which is then stored in a file for use during running of the dynamometer.

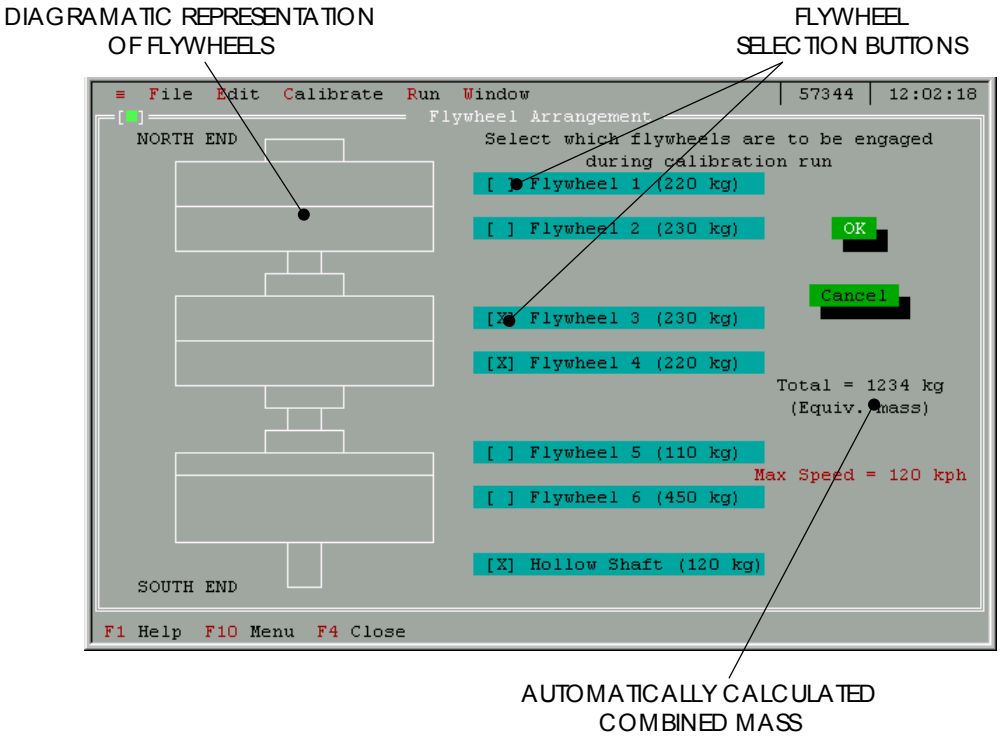

Figure 6.6 Flywheel selection window

6.5.3 Basic Data Acquisition Sequence

During calibration, warm up, and testing routines the same basic operations are performed by the control program on a continuous basis. This set of actions is instigated by the `idle` function and involves timing of the operations, input and output of data, as well as file writing and screen display functions, if required. A generic loop is shown in flow diagram form in Figure 6.7 with all the major tasks summarised. Note that not all these functions are required for all modes of operation.

Specific exclusions or additional items of interest are included in Sections 6.5.4–6.5.12.

Before any operations involving running of the chassis dynamometer, several equipment checks are made to ensure that the correct modes are engaged, and that the water and compressed air pressures are sufficient. These checks make use of sensors, which are wired to the PCLD-782 digital-input daughter board and depend on what type of dynamometer running is required. The user may be prompted to correctly set any of the following parameters before the program will continue: Main panel on/off, ASEA motor mode, Froude dynamometer panel on/off, dynamometer mode, dynamometer over-speed, dynamometer water valve, axle brake air valve, axle oil heater, or exhaust fan on/off. This checking routine is included as `ModeCheck` in the file UTILITY.CPP.

6.5.3.1 Timing

As mentioned in Section 6.5.1, the updating data acquisition routine is called as a result of the `idle` function, which only functions if there are no other program tasks awaiting processor time. Thus, the time taken outside the routines shown in Figure 6.7 may vary depending—for instance—on whether there were any keyboard events to handle since the last time the data acquisition sequence was called. To enable the accurate timing of data capture and D/A demands, the UPP card is used to generate an interrupt every 4.75 μs, which is counted by the software and used to set a flag at 0.1s or 0.2s intervals (4.75μs×421×50 = 0.099999 sec). Regardless of the time taken outside the update routine, once the timing loop is entered, the program is delayed until the next time interval is reached (indicated by the state of the software flag).

An exception occurs if the time taken by the update loop added to the time taken by the external processes exceeds the prescribed time interval. In this case, a time error record is generated, and no significant time is spent in the waiting loop. To avoid such instances, a record of the wait-time is generated each time through, and displayed on screen as well as being saved to the file (if needed). This delay function records the time at which the wait loop was entered and when it was exited, thus giving the total amount of time that was spent waiting. This figure is presented as a

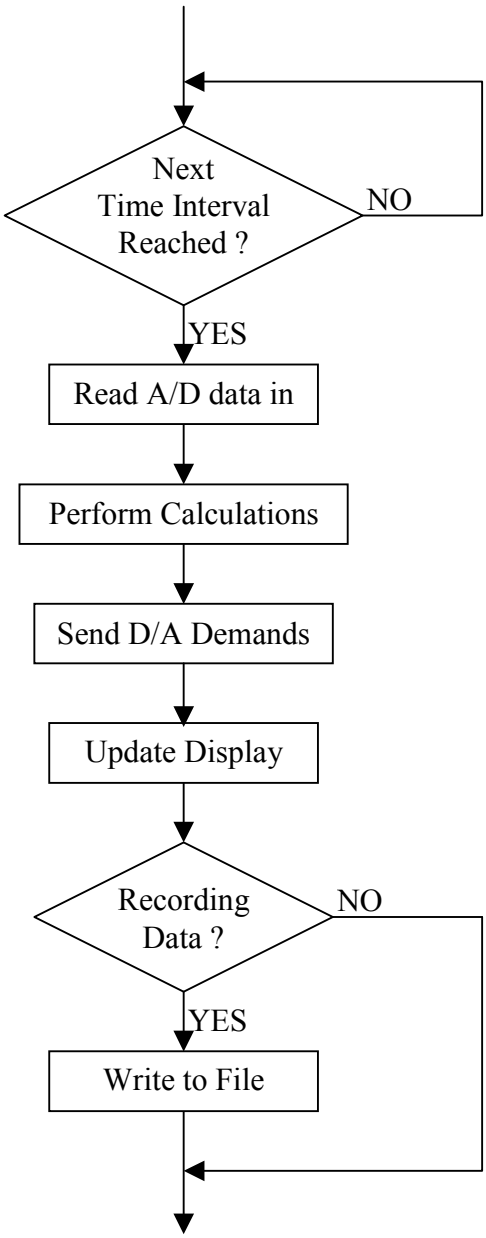

Figure 6.7 Flow diagram of basic data acquisition routine

percentage of the total available time interval (0.1s or 0.2s) and was most useful during creation of each routine and debugging to determine the ideal time interval to set, and which tasks were consuming the most processor time.

6.5.3.2 Data Inputs

Each of the A/D channels in use on the PCL-812PG card has a corresponding group of settings in the configuration file, as described in Section 6.3.1. All the PCL-812PG

channels are read in a single step, using the appropriate gains from this configuration file. Several channels, such as the thermocouple inputs to the PCLD-889 daughter-board and the Annubar pressure transducers require more than a simple linear relationship to relate the voltage signal to the correct units for the data (see calibration Appendix C). All calculations are performed on the raw data immediately after being read, and the results are displayed and stored in the correct units only, as opposed to the original digital bits or their corresponding voltages.

Two important data inputs are derived from sources other than the PCL-812PG and PCLD-889 cards. The rotational velocity (and hence drum surface speed) as well as the engine speed (rpm) are both found using pulse counting and timing routines with the UPP card, as detailed in Section 4.1. As soon as the timing delay loop is exited, the number of shaft encoder and engine spark pulses counted since last time are read in. With knowledge of the time and number of pulses, the speeds can be calculated using the pulse counting method of Equation 4-1. Note that the vehicle data file must include the number of sparks generated per engine revolution so the spark speed can be converted to engine revolutions-per-minute.

In the case where the allotted loop time is exceeded (see Section 6.5.3.1) the time taken before the number of pulses are read is greater than expected. This gives the appearance of a rapid jump in speed, followed by a rapid decrease, as the next time through the loop is slightly shorter (meaning less pulses are counted). Errors can also arise from the inductive loop that records spark plug pulses (see Appendix D). Occasionally, an extra spark pulse is detected from one of the nearby leads, or a single pulse is not detected by the circuitry. These pulse inaccuracies are brought about by slight inconsistencies in the intensity of the spark plug current, and result in significant fluctuations in the measured speed. Apparent jumps in roller and spark speed are corrected for in the software by checking new speed values against the previously recorded values. If a timing error is known to have occurred, or if an implausible increase or decrease in speed is measured (e.g. >2000 rpm in 0.1s) the new data is skipped and the previous data substituted in its place so that the speed appears constant. Although this constant approximation may not be entirely accurate, is it superior to including large errant speed values.

Specific routines for reading A/D values, calculating thermocouple temperatures, and determining speed from pulses can be found in the source code in file DATA_AQ.CPP.

6.5.3.3 Power Calculation and Atmospheric Correction

Vehicle output power is an important test parameter that cannot be directly measured, and may be calculated in one of several different ways. Power is defined as the product of force and velocity. In this case, the force at the roller surface can either be measured using the tractive effort load cell, or assumed, given the sum of the resisting forces.

$$Power = F_{corr} v \tag{6-3}$$

Where: F_{corr} = Raw tractive effort + Correction (as per Equation 5-14)

$$Power = \left(m_{cd} \frac{dv}{dt} + F_{dyno} + F_{fric} \right) v \tag{6-4}$$

Experiments were carried out on both methods, and it was decided that using the tractive effort load cell was more appropriate, particularly when acceleration was a factor. Although the dynamometer load cell tended to exhibit greater accuracy and less hysteresis, Equation 6-4 requires that the acceleration be multiplied by the total equivalent mass, as opposed to the mass of the drum assembly only in Equation 6-3. This means any error in the determination of acceleration (see Section 5.2) would induce a greater error in the final calculated power when using Equation 6-4.

Once the force and velocity at the drum surface have been measured, it is necessary to standardise these measurements to account for atmospheric conditions. Changes in air temperature and pressure can have a significant effect on vehicle performance, particularly in relation to the density of the air entering the engine. Equation 6-5 shows the standard power correction, which is carried out each time through the data acquisition loop. If desired, on-road fuel consumption figures may also be corrected to account for atmospheric conditions [SAE J1082, 1995].

$$P_{corr} = P_m\left(\frac{p_{std}}{p_m}\right)\sqrt{\frac{T_m}{T_{std}}} \quad (6\text{-}5)$$

Where: P_m = power calculated from force and velocity (W)

p_m = measured air pressure (kPa)

T_m = measured absolute air temperature (K)

p_{std} = standard atmospheric pressure (1013kPa)

T_{std} = standard atmospheric absolute temperature (293K)

Also of interest is the power output of the vehicle referenced to the engine flywheel. This can be loosely approximated as the power output at the road wheels less the rolling and transmission frictions, which is measured during a coastdown on the dynamometer (Section 5.4). An engine power approximation of this sort is offered as an option in the MATLAB post-processing software discussed in Chapter 7.

6.5.3.4 Data Outputs

Depending of the mode of operation of the chassis dynamometer, the power absorber may be controlled in speed or torque mode. 'Power law' control is available, but is not generally used in chassis dynamometer applications. The electric motor can also be switched between speed and torque control using the digital output capability of the PCL-812PG. The required demand is calculated in terms of useful units (kph for velocity, and Nm for torque), which must be converted to a 12-bit integer for use by the A/D card. The PCL-812PG receives this number and applies a proportional voltage output. The linear equations to convert from useful units to the appropriate 12-bit integer are included in the configuration file (see Section 6.3.1), as are appropriate upper and lower limits for the demand output. Each output voltage is applied to the motor or dynamometer as a constant demand requirement, which is acted upon by the built-in analogue control circuitry (see Section 2.5.1). D/A demand calibration details are included in Appendix C.

6.5.3.5 Text Display

Text is displayed on screen and updated each time through the loop so the user can track the progress of warm up or testing procedures. Before a test can begin, the screen display is initially set up with all the necessary buttons as well the data labels

and units that do not change throughout the operation. Data labels, such as 'Roller Speed' are again stored in—and retrieved from—the configuration file. Once the routine is running, data is read (as per Section 6.5.3.2) and displayed on screen in a similar way to how it is written in the file. A special text class was created to enable the efficient updating of this data, without flickering or delays in the display. Each mode of operation has a similar on-screen appearance, with some variation in the amount of data and button options that are available. The major exception is the 'Driving Cycle' mode, which dispenses with the Turbo Vision format to enable an efficient and highly visible scrolling display (see Section 6.5.12.1). Refreshing the Turbo Vision screen display is a relatively time-consuming process and in some cases this dictates the updating rate (set by the time interval as per Section 6.5.3.1). The slower timing rate of 0.2s is used for 'Road Load Driving', 'Manual Control' and 'Warming Up' where on-screen user feedback of all measured parameters is more important than the rate at which data is saved.

6.5.3.6 File Saving

As discussed in Section 6.3.2, test data may be saved to a file specified in advance by the user. A complete set of data is written to the save file each time the updating routine is executed, provided that the program is in a recording phase. Data may be saved continually when under 'Manual' or 'Road Load' control, and is always saved in 'Driving Cycle' mode. Averaged data values are stored in the file only at specific points during mapping tests. All the A/D data and external inputs such as roller and engine speeds are temporarily stored in a numerical array as they are received, then the entire array is written to the predefined file at the end of each updating sequence. In addition, several other pieces of information, such as the latest calculated acceleration and power, and the power absorber demand, are transferred from separate arrays into the file each time through the loop.

The computing time required for file transfer operations can—in some cases—become restrictive, since the correct location on the hard drive must be accessed each time by the scanning head. If additional operations were added to the data acquisition loop, different ways of saving the input data may need to be implemented. One such technique is to write the data from an array into the computer's random-access

memory instead of into a file on the hard disk. Further information on this option is included in Section 9.2.

6.5.4 A/D and D/A Calibration Function

The chassis dynamometer control program includes a simple, multi-purpose routine designed for calibration of the various PCL-812PG inputs and outputs. The calibration program displays a text-only (DOS format) screen with the necessary prompts, and reads the desired channels applying user-defined settings. Instead of reading the A/D settings from a configuration file, the user is prompted for all the important information such as which channel to use, the gain to set, and how many samples to average each time.

During A/D calibration, a known magnitude is applied to the appropriate device (e.g. a known force on a load cell) and the user enters this value on the keyboard. Acceptance of this entry initiates sampling of the desired channel, and the voltage and 12-bit integer (0–4095) representation are both stored in a file. After several different points have been recorded, the user exits and the mathematics routines as described in Section 6.4 are used to calculate a linear or quadratic relationship between the known entries and the A/D reading. This equation is then displayed and saved to a file, from which the coefficients can be copied into the configuration file for future use during testing.

Digital to analogue calibrations operate in much the same way, but rather than a known quantity being supplied, the user enters a series of 12-bit numbers as inputs to the PCL-812PG. Depending on the mode of operation selected by the user, this 12-bit integer entry sets the voltage for the speed or torque controller on either the electric motor or the power absorber. Once a steady state is reached on the control output, the user presses a key, which stores the combinations of raw entry and final output. Again, a least squares approximation is performed so that when in use, the required value (e.g. torque in Nm) can be related to the 12-bit D/A input that will set the correct controller voltage.

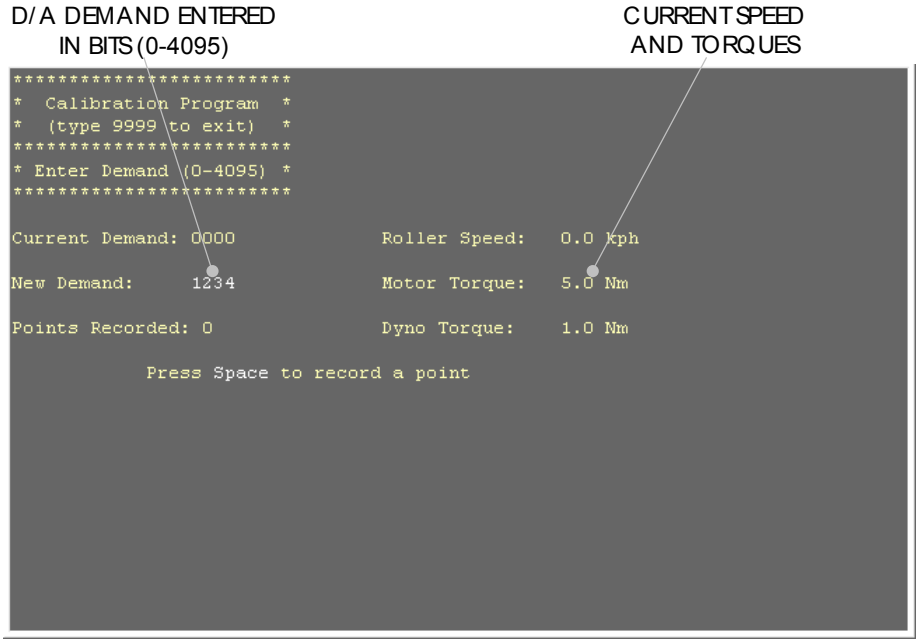

Figure 6.8 Screenshot of D/A calibration display

6.5.5 Friction Calibration Function

As mentioned in Section 5.4, the frictional characteristics of the chassis dynamometer system are likely to change over time. For this reason it was necessary to have a simple procedure to follow that would measure the friction forces and calculate the current coefficients of the system as whole, and the drum assembly in isolation. Friction calibrations should be carried out both with a vehicle in place, and with the chassis dynamometer alone, so the appropriate forces can be used in road load calculations as well as correction of the raw tractive effort load cell signal, as per Equation 5-16.

Best results are obtained by running a series of coastdowns, and averaging the solution of Equations 5-13. Various options can be set to ensure accurate and repeatable data. Choices include: maximum and minimum speed of coastdown, how many runs to perform, and the desired dynamometer torque for each. On-screen display during the coastdown process includes velocity, dynamometer torque, tractive effort, and timer, as well as ‘Start’, ‘Accept’, ‘Redo Run’, and ‘Exit’ buttons. Each coastdown starts with the electric motor accelerating the chassis dynamometer (with vehicle in neutral, if present) to a point approximately 15 kph above the maximum recorded coastdown velocity. At this point, the motor load is removed and the

dynamometer torque applied to decelerate the rig. The speed overshoot is to ensure that all forces are stabilised by the time the data is recorded. Once the speed of the rollers drops below the predefined maximum speed, data is saved at each 0.1s interval to a temporary file. The basic data acquisition loop as detailed in Section 6.5.3 is used, with the exclusion of any on-the-fly calculations or updating D/A demands. Signals from the dynamometer and drum axle load cells are recorded, as well as the current roller speed, until the minimum speed is reached. At this point the user is prompted as to whether they wish to accept the latest coastdown, or repeat the same run, overwriting previous data. If the run is rejected (user activates the 'Redo Run' button), the dynamometer load stays the same; otherwise a new load is defined for the next coastdown. After the required number of coastdowns has been satisfactorily completed, the dynamometer is stopped and the various calculations are carried out automatically.

As was discussed in Section 5.2.3, the electric motor and dynamometer control signals tend to interfere with each other. In practice, to avoid these complications the motor is physically switched off when the desired overshoot speed is reached. A constant voltage demand from the A/D card throughout the acceleration and coastdown processes means that the dynamometer load is stable (no on/off transients), but significantly slows down the acceleration phase. The dynamometer mode can also be switched manually so that the resistance to motion is only applied in the latter stages of the acceleration, when the target speed has almost been reached. The user can achieve a good balance between initial stability and acceleration delays by trial and error. The coastdown procedure is illustrated in flow diagram form in Figure 6.9 on the following page.

Overall dynamometer system friction and roller drum friction coefficients can be found by performing friction coastdowns with no vehicle present. The addition of a vehicle enables the combined friction forces of the dynamometer and the vehicle to be measured and stored in the vehicle's data file. By carrying out coastdowns on the road, the frictional characteristics of the vehicle are known and may be used with the combined friction forces of the vehicle on the dynamometer to calculate the required

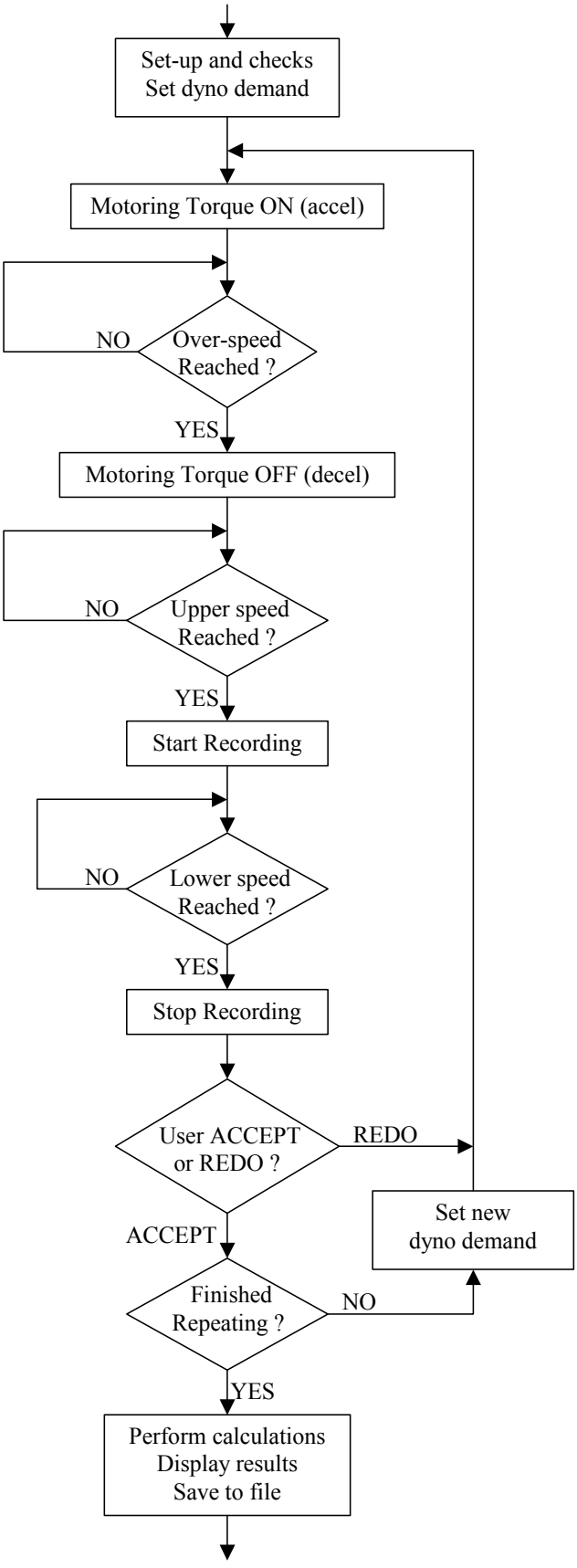

Figure 6.9 Friction coastdown flow chart

road load power absorber torque as per Equation 3-10. Roller drum friction is used to correct the tractive effort load cell reading as detailed in Section 5.5, while the frictional resistance of the dynamometer alone may be used to approximate the vehicle power output at the engine flywheel as follows. The transmission and rolling friction of a vehicle on the dynamometer is calculated as the friction of the vehicle and the dynamometer combined, less the friction of the dynamometer alone.

$$F_{Vf} = \left(f_{0Vd} - f_{0d}\right) + \left(f_{1Vd} - f_{1d}\right)v + \left(f_{2Vd} - f_{2d}\right)v^2 \tag{6-6}$$

Where: F_{Vf} = transmission and rolling friction of vehicle on dynamometer
Other notation as per Nomenclature section

Therefore, the power generated at the engine flywheel is approximated as the power output at the road wheels (measured by the tractive effort load cell) plus the frictional power absorbed by the vehicle transmission, driveshaft and tyres.

$$P_{eng} = \left(F_V + F_{Vf}\right)v \tag{6-7}$$

Where: P_{eng} = engine power referenced to the flywheel (W) which may then be corrected for atmospheric conditions (see Equation 6-5)
F_V = tractive force at roller surface (N)

The actual determination of each set of frictional coefficients is carried out immediately after exiting the coastdown routine, and the specific calculations depend on whether a vehicle was present on the rollers or not. All the necessary data is saved to a file, from which arrays are generated for use by the mathematics functions mentioned in Section 6.4. Measured data is replaced by least squares approximations, which are then used to generate systems of equations for the simultaneous solving of Equation 5-12. These coefficients are in turn stored in the appropriate file. Dynamometer system and drum friction characteristics are automatically saved in a file whose name includes a numerical representation of the particular dynamometer flywheel combination in use at the time. This is because the system friction as a whole changes depending on which flywheels are engaged, and which are spinning on their shaft bearings (see Section 5.4). The combined vehicle and dynamometer

friction is saved in the data file of the vehicle indicated by the user, so that the appropriate frictional forces will be loaded next time the same vehicle is used. When calibrating dynamometer and vehicle friction, it is important to engage the flywheel combination most appropriate to the vehicle so that the calculated coefficients can be used for tests that involve road load simulation with these flywheels.

Friction coastdown theory and examples of the repeatability of the system friction and drum friction methods are included in Sections 5.4 and 5.5.2 respectively. Graphs of velocity, acceleration, dynamometer torque, and tractive effort during a friction coastdown run are included as an example in Appendix S.

6.5.6 Re-zeroing Load Cells

As described in Section 4.3.1, the dynamometer and tractive effort load cells were affected by temperature and required regular re-zeroing. Simple routines were devised to find the appropriate offsets for the tractive force and power absorber torque readings before each batch of testing.

For the dynamometer load cell, the user is prompted to push down briefly on the appropriate load arm (depending on the desired direction of rotation) to remove the hysteresis, then by hitting the ‘Accept’ button the A/D 12-bit reading is recorded at this zero load. Because the power absorber always applies a force which opposes the direction of motion, the hysteresis is best accounted for by applying the initial loading in the load direction only. This 12-bit integer is stored as a global variable, as well as in a file, and is reloaded before any testing is carried out. During testing, the offset obtained during re-zeroing is subtracted from the raw A/D value read from the load cell, and then the predefined linear multiplier (from the configuration file) is applied.

In the case of the tractive effort load cell, loading can occur in both directions, so the user is prompted to apply a small load (≈50 N) to the load arm, first in the positive direction and then in the negative direction. The zero point is taken as the average of these two small readings and again is stored as a global variable and in a file for use during testing.

6.5.7 NO_X Meter Setup

The University of Canterbury Mechanical Engineering Department possesses a suite of exhaust emissions measuring equipment for the purpose of engine and vehicle testing. Separate Beckman devices to measure CO, CO_2, NO_X and unburnt hydrocarbons are all available. However, due to time constraints in the present project, only one of these was reinstalled for use with the chassis dynamometer. The Beckman NO_X meter (Model 951A), detects oxides of nitrogen (NO and NO_2) in a given sample and outputs the concentration via an analogue needle gauge on the equipment and a 0–5 V output that can be read by the PCL-812PG. Setting up of the NO_X equipment involves first passing a 'zero gas' through the meter to ascertain the zero concentration reading, then passing a 'span gas' of known concentration through to check that the near maximum reading is correct. Trim knobs are used to obtain the desired reading with zero and span inputs.

The software routine to assist this initial calibration consists of a single display window, which shows the current voltage output, the previous zero and span voltages, and buttons to accept zero and span gas readings. The user is also able to enter the span gas concentration and the range to be used during the span reading, as well the range to be used during subsequent testing. In terms of the basic data acquisition loop (Figure 6.7), the major differences are that there are no D/A demands and that the data recording is only performed as a one-off upon use of the 'Zero Accept 'or 'Span Accept' buttons.

While the zero gas is passed through the device, the most sensitive range setting is chosen and the trim should be adjusted to provide a zero volt output to the A/D card. A suitable range should then be chosen and indicated on-screen to most closely approximate the particular span gas concentration in parts per million (ppm). For example, the 0–2500 ppm range (the actual figures are only a guide) could be used with 3000 ppm span gas, with a full 5 V then representing 3000 ppm. The span gas concentration entered by the user is utilised during subsequent testing to calculate concentrations depending upon the range setting indicated in this window. For example, if a 3000 ppm span gas was used on the 2500 ppm range setting, and testing

was to be carried out using the 10000 ppm range setting, the following factors would be calculated and applied to the sample voltage during testing.

$$TEST\ CONC = \frac{TEST\ VOLTAGE}{SPAN\ VOLTAGE} \times \frac{TEST\ RANGE}{SPAN\ RANGE} \times SPAN\ CONC \quad (6\text{-}8)$$

For example, during testing:

SPAN RANGE = 2500 ppm *TEST RANGE* = 10000 ppm

SPAN VOLTAGE = 5 V *TEST VOLTAGE* = 2.5 V

SPAN GAS CONC = 3000 ppm

$$TEST\ CONC = \frac{2.5}{5} \times \frac{10000}{2500} \times 3000 = 6000\,ppm$$

The combination of span range, test range, span voltage, and span gas concentration is stored as a single variable which can be applied to each A/D voltage during testing to provide an output in parts per million.

6.5.8 Warm Up Routine

The frictional characteristics of gears and bearings vary greatly with operating temperature, and it is therefore necessary to ensure that these temperatures are consistent during any chassis dynamometer testing. The easiest way to achieve stable component temperatures is to spin the rotating machinery at a high enough speed until the inherent friction produces approximately the same amount of heat as is radiated out or removed by the cooling system. A built-in timer can be implemented to stop the warm up after a certain time interval, or alternately the user may simply watch some of the temperature sensors and manually conclude the warm up when a certain level is reached. During a warm up, the screen display shows all the available sensors, including temperature measurements of the roller drum axle oil, the vehicle engine oil and cooling water (if these thermocouples are installed). Figure 6.10 shows a typical warm up window.

The warming up process may be carried out in one of three ways. ‘Constant Speed’ uses the electric motor to maintain a predefined set speed, while the ‘Road Load’ warm up option allows the user to accelerate and decelerate a vehicle against a road

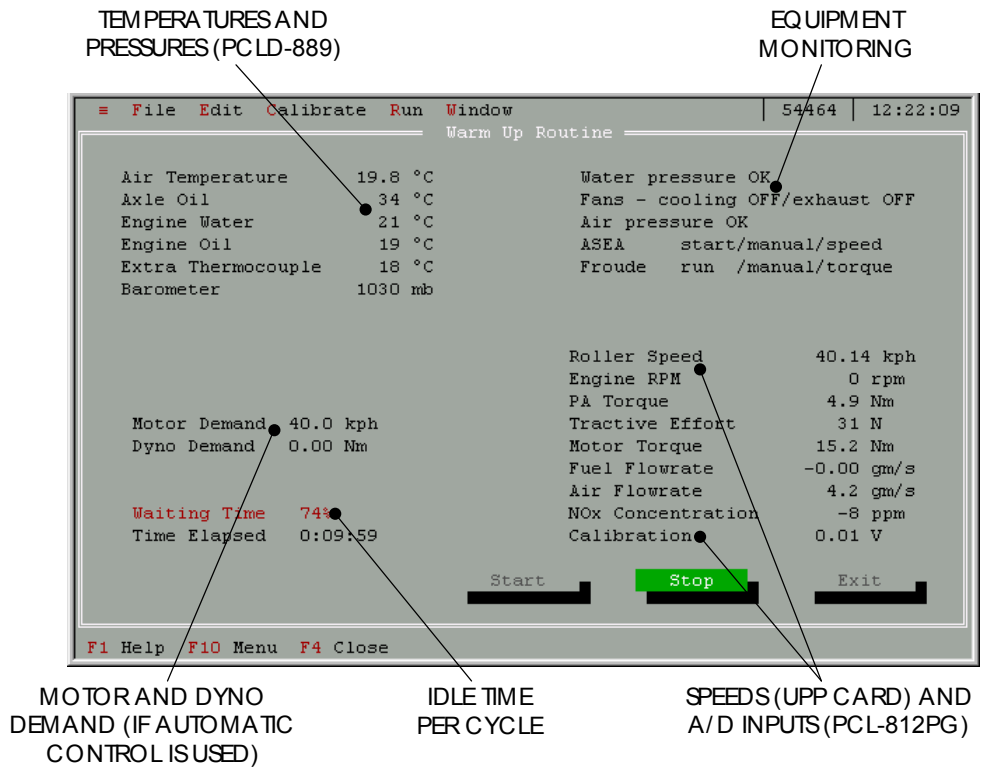

Figure 6.10 Warm up screen display

load model, which employs user-defined friction coefficients. 'Manual Warm Up' is an option in which the D/A capability is not employed and the user operates the electric motor and power absorber by physically manipulating the potentiometers and mode buttons on the respective equipment panels. The timer—and any automatic load demand—is set when the 'Start' button is activated and ceases if the allotted time has elapsed, or if the user stops the procedure.

The optimum format and duration of a warm up can be arrived at by experience, and depends on the type of testing and the vehicle. One way to determine whether the dynamometer has reached an ideal operating state is to carry out a series of friction calibration runs, observing changes in the frictional force at a certain velocity. A calculated friction which is consistent between runs indicates that the temperature is stable. Several trials were conducted to determine an appropriate speed and duration for the constant velocity warm up. The results of two of these trials are graphed in Appendix T. Initial running of 15 mins at approximately 50 kph, followed by a shorter period at 100 kph was expected to result in stable frictional characteristics for

the dynamometer with no vehicle in place. However, a short break of one or two minutes between warming up and testing may create variations in performance. It should be noted that even relatively large changes in bearing friction usually equated to less than 5 N force with respect to the drum surface, which was not serious in light of the other system inaccuracies.

6.5.9 Manual Control

'Warm Up', 'Road Load Driving', and 'Manual Control' are all instances of the same `DisplayDialog` class. This dialog box displays all the available A/D data as well as several equipment states such as the electric motor and power absorber modes, and whether or not there is sufficient air pressure for the axle brake, or water pressure for the dynamometer. Each of these three operating modes follows the basic data acquisition sequence, with similar appearances on screen. The major differences are that the 'Warm Up' option does not include the buttons or capability for recording data, and that the 'Manual Control' (distinct from the 'Manual Warm Up') mode provides user input boxes to set the D/A demands for the eddy-current dynamometer and electric motor. Each of the `DisplayDialog` functions samples data and updates demands at the slower rate of 5 Hz to allow for all the data acquisition and screen display operations.

The 'Manual Control' screen allows the user to switch the demand modes and magnitudes for both the motor and the power absorber, which is useful for investigation of the dynamometer performance and for flexible vehicle testing, including maximum power runs (as recorded in Section 8.2.2). Either the mouse or keyboard can be used to navigate about, and new D/A demands (in the correct units) can be typed in the appropriate box and sent to the equipment by pressing the Enter key, or activating the 'Accept' button. At any point, the current A/D data may be recorded to a file, which is chosen by the user before entering the 'Manual Control' routine. 'Snapshot' (see Figure 6.11) saves all the data at a single instant, while '5 sec Record' records the data in the file at 0.2 second intervals for 5 seconds. Provision is made for the user to change the duration of recording to anything between 0 and 10 seconds. 'Record ON' simply starts saving data at each interval and

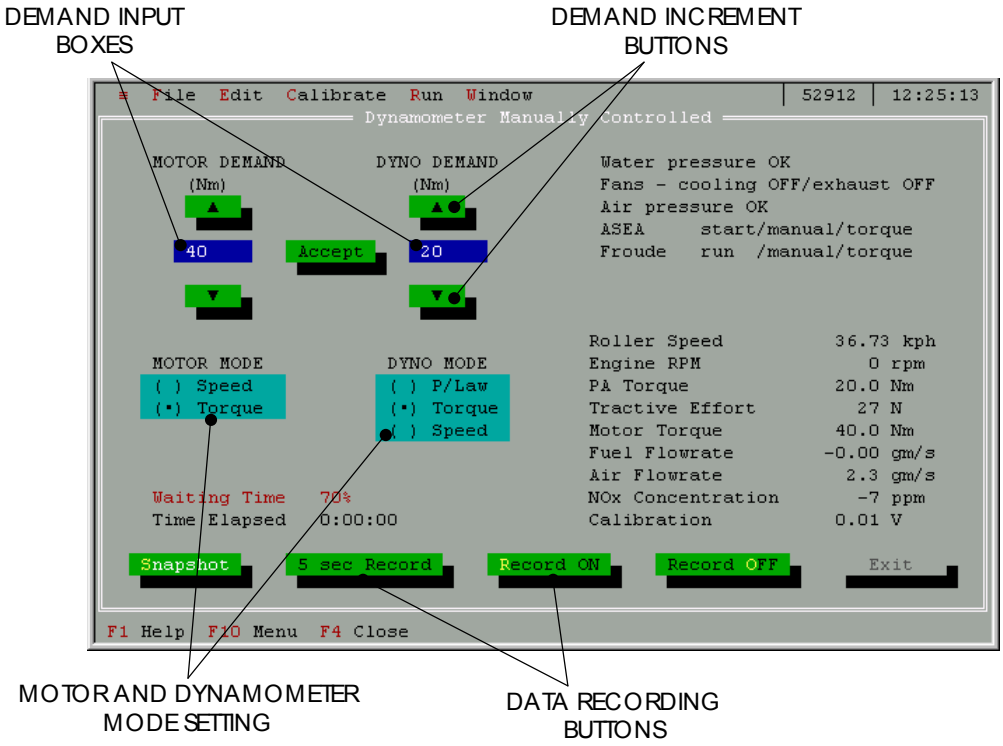

Figure 6.11 Screenshot of 'Manual Control' mode

does not stop until the 'Record OFF' button is pressed. The 'Exit' button is only made available when the dynamometer is running at a safe speed (e.g. less than 3 kph). As an additional safety feature, the software does not allow both the electric motor and dynamometer to be in speed mode at the same time. If both machines tried to achieve differing demand speeds, one or the other would be forced to increase its command signal indefinitely, potentially causing damage. Each time a new sequence of data saving is begun, a file header is written immediately before the first data set. This header contains useful information such as the whether the dynamometer was operating in 'Manual' or 'Road Load' mode, as well as the current time and date (see Appendix R).

As mentioned above, one use of the 'Manual Control' mode is in producing maximum power curves for vehicles on the chassis dynamometer. Beginning at low speed, and in the desired gear, maximum throttle is applied, and the 'Record ON' button is activated. The vehicle then accelerates against a fixed power absorber load (or the chassis dynamometer inertia alone) until a suitable maximum engine speed is reached, at which point the 'Record OFF' button is pressed and the throttle released.

On-the-fly calculations of power using the tractive effort load cell reading as per Section 6.5.3.3 can then be plotted against road or engine speed. The MATLAB routines detailed in Section 7.1.3.1 enable a superior plot to be produced by filtering the acceleration (and hence power) in a way which cannot be performed during the testing.

6.5.10 Road Load Driving

The 'Road Load Driving' function also uses the `DisplayDialog` class and screen display. The purpose of this routine is to run a vehicle under on-road conditions with respect to velocity-dependent friction, and inertial loads. The display is similar to that used for the 'Warm Up' procedure, except that it includes recording buttons, and does not require 'Start' or 'Stop' functions. For safety reasons, the user may exit this screen only when the roller speed is less than a predefined level (e.g. 3 kph).

The only readily adjustable parameter in 'Road Load' mode is the duration of the preset recording interval (shown as 5 seconds in Figure 6.11). The selection of the flywheel configuration and correct vehicle file are important for achieving realistic road load simulation. The combined inertia and frictional characteristics required to implement Equation 3-10 are retrieved from files before running. At all times while the display screen is visible, the basic loop of Section 6.5.3 is carried out at each 0.2 second interval and a new power absorber torque demand is calculated and sent via the PCL-812PG. The electric motor is generally switched off to avoid any unwanted torque blips or interference with the load cell signals.

Because the 'Road Load Driving' function applies a dynamometer load in the same way as the 'Driving Cycle' mode, it is useful for familiarising a human driver with the feel and response of the chassis dynamometer and vehicle before undertaking thorough testing. Also, investigations may be made into the appropriateness of certain velocity demand sequences that are not yet available as driving cycle files. Perhaps the most useful application of the 'Road Load Driving' routine is in recording the fuel consumption at constant speed under simulation conditions. These constant speed consumption values are usually quoted in km/litre and provide a standardised comparison between vehicles.

6.5.11 Mapping Test

The mapping test is a steady state examination of a vehicle's performance over a wide range of speeds and engine loads. It is useful for comparing one vehicle with another, or to determine the results of any tuning or alterations made to a single vehicle. The vehicle under test is driven on the dynamometer at a series of speeds, and at each speed undertakes a series of tractive effort loads, resisted by the power absorber. Some of the most useful measurements to be made are those of fuel consumption, exhaust emissions, and efficiency at each set point.

The University of Canterbury chassis dynamometer conducts mapping tests under speed control from the dynamometer, with the driver of the vehicle being required to match the desired tractive effort load by application of the accelerator pedal. All mapping tests are carried out in a single gear, which depends on the range of engine speeds to be investigated. After thoroughly warming up the vehicle and chassis dynamometer, and with the power absorber in speed control mode, the driver accelerates to the predetermined maximum speed, at which point the dynamometer holds the velocity constant. The driver then attempts to match the desired tractive effort load (indicated on screen, and measured at the drum axle load cell) with the accelerator. The minimum tractive effort load is largely determined by the stability of the power absorber controller at the lower end of its range. Once the minimum load has been achieved in a stable fashion, the user allows all the measured data inputs to be saved, and the next (increased) load is shown on screen. The driver continues to match the increased demands, while the dynamometer holds the rollers at a constant rotational velocity. When the maximum force output at that speed is reached (i.e. constant tractive effort at full throttle) this data is again saved and the next speed demand is sent to the power absorber. The intervals with which desired tractive effort is incremented and speed control is decremented are determined beforehand in the mapping test configuration window. The mapping test ends when the user decides that the vehicle can no longer maintain a constant speed in the current gear without excessive instability or possibility of engine stall. The 'Mapping Test' sequence is represented in flow diagram form in Figure 6.12. Note: Tractive Effort is abbreviated as T.E.

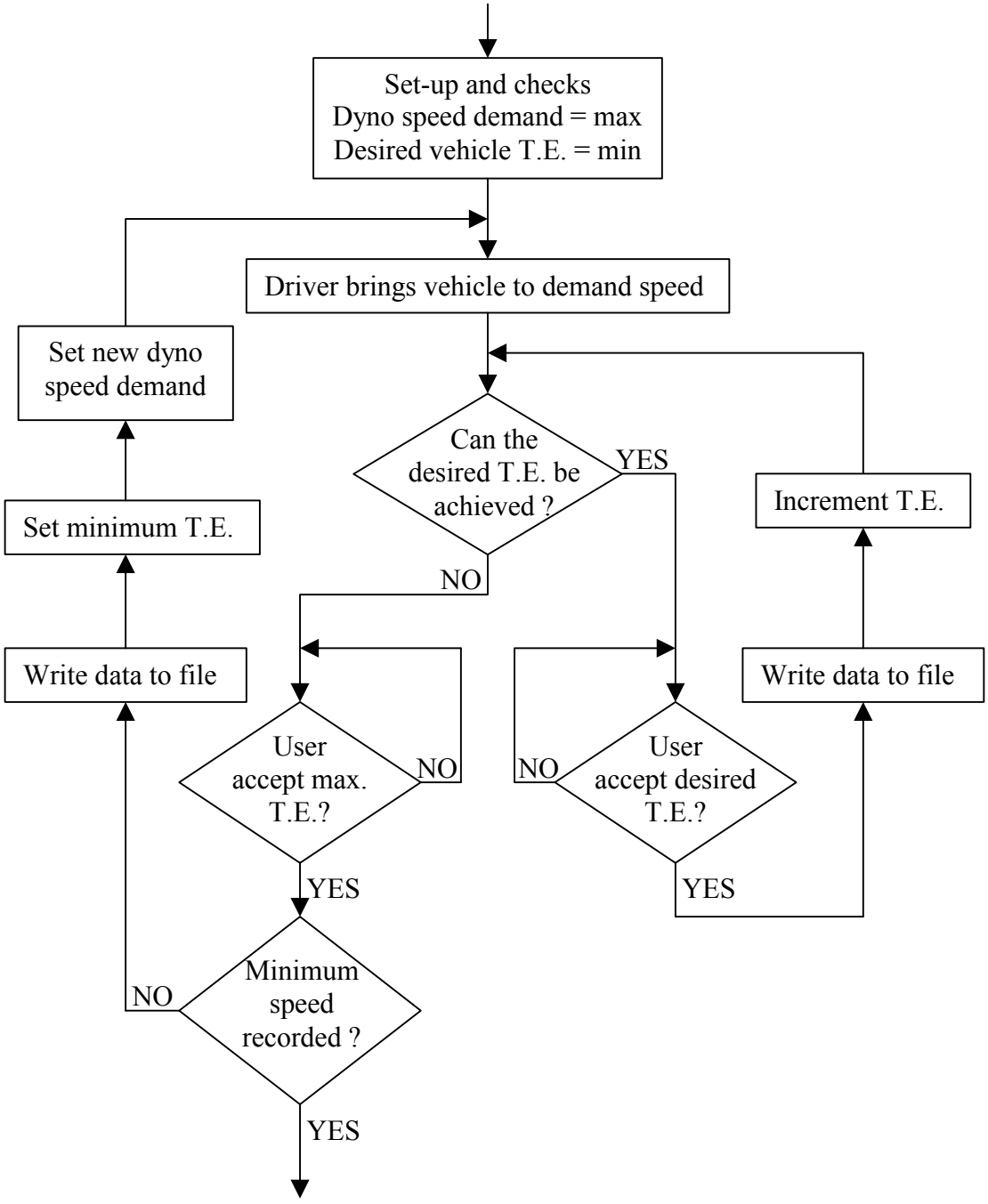

Figure 6.12 Flow diagram of mapping test procedure

The driver is presented with on-screen feedback about the current speed and tractive effort, with information on the average values, and fluctuations away from these averages. It is important that the load and speed are both stable and constant at each set point before the data is saved, and the display can be set up to indicate this stability by changing the colour of the text. Green text indicates that the measured

parameter has remained within preset fluctuation limits for a predetermined length of time. For example, the user might set in the configuration window that the tractive effort should not vary by more than 10 N from each set point and should remain within this ±10 N for a period of 1 second. Once the desired stability is achieved, the control program can be set to automatically record the data and move on to the next set point. However, to allow for the idiosyncrasies of driver and power absorber controls, and to accommodate some of the sensors which took longer to stabilise (see Section 8.2.3.3) the 'Accept' button was manually applied when sufficient steadiness had been achieved. An example of the on-screen display is shown in Figure 6.13, including the green fluctuation indicator.

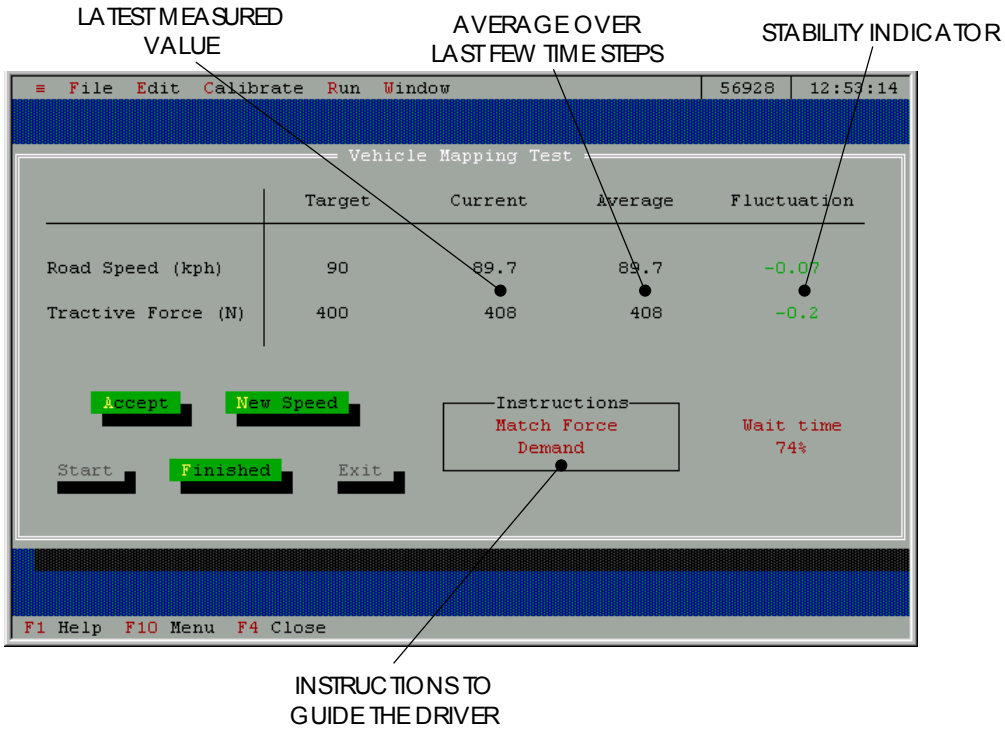

Figure 6.13 Screenshot of 'Mapping Test' display

This reduced display ensures greater clarity for the important parameters, and enables the data loop to proceed at the increased rate of 10 Hz. Despite not being displayed, all A/D channels are still sampled, averaged and saved to file when required. Because of the requirement for constant speed and load, and the fact that data saving is not required at each 0.1s interval, all measured data is saved as an average. The mapping test configuration allows the user to set the interval over which these averages are

carried out (e.g. 0.5 secs = 5 readings averaged), and a record is kept of all the necessary previous data points so that an average can be calculated and displayed on screen, or saved to the file.

As well as all the A/D channels, the desired tractive effort and speed demand are saved to the file, which is chosen by the user before commencement of the test. The maximum load achieved by the test vehicle for each speed is unlikely to lie exactly on one of the desired load steps. When the maximum vehicle tractive effort is between intervals, the stability indicator will not activate (turn green), and a '-1' is added to the file in place of the desired tractive effort as a reminder. Calculations of power (corrected for atmospheric conditions) and corrected tractive effort are both made with the assumption of zero acceleration, and are stored in the file at each set point. The format of the save file is similar to that of the other functions, and includes a date and time header at the start of each test data set. Commas between each number, and a new row for each set point makes for simple reading using the MATLAB routines detailed in Chapter 7.

It should be noted that there are other ways of reaching all the load and speed points of the vehicle map. One possibility is to make use of the dynamometer torque mode, meaning that the driver would control the constant speed requirement using the accelerator. This is a more natural throttle function for most drivers and may prove to be a superior technique. This method creates other difficulties and is discussed further in Section 9.2.

6.5.12 Driving Cycle

The most realistic and repeatable way to assess a vehicle's on-road performance is by conducting a 'Driving Cycle' test on the chassis dynamometer. A driving cycle consists of a series of desired velocities (and sometimes, vehicle gears), usually at one second intervals, which—as a whole—attempt to approximate the on-road accelerations and speeds undertaken by a vehicle under certain conditions. When carried out on a dynamometer, is it important that all the inertial and friction loads present on the road are simulated on the machine. A vast array of driving cycles exists to model the traffic and road conditions in various countries in urban driving conditions and on the open road. Research into the suitability of several of these

driving cycles has been carried out by Castro [1989] among others, and at the University of Canterbury by Hindin [1984]. Several standard cycles are listed in SAE Information Report J1506 [1993] and several of these are included in Appendix U, and on the CD accompanying this thesis.

While running a driving cycle, the chassis dynamometer control program retrieves the cycle speed demands from a text file and displays the desired speed sequence graphically, as a trace that scrolls across the computer monitor. The driver uses the vehicle accelerator, brake, and gears to follow the required speeds as closely as possible, while the actual measured speed is also shown on screen as a horizontal bar. New Zealand Standard NZS-5420 [1980](withdrawn) and Australian Standard AS 2877 [1986] detail the various conditions under which driving cycle testing on a chassis dynamometer should be carried out. In particular, the allowable departure from the required speed is explained with reference to time and speed tolerances. A graphical representation of these limits is included in Appendix V. Allowable speed and time variations may be set in the driving cycle configuration, and a record is kept of the amount of time the measured vehicle speed is not within the allowable tolerance (referred to below as *excursion time*).

After the initial checks are carried out, and the appropriate vehicle and driving cycle data files have been selected, the ‘Driving Cycle’ routine displays the scrolling screen shown in Figure 6.14. Data is saved to a file at each 0.1 second interval during the cycle, and each of the functions of the basic data acquisition sequence are included. As well as storing each of the A/D channels, the ‘Driving Cycle’ routine saves to file the time, timing loop delay (see Section 6.5.3.1), desired gear and speed, acceleration, raw and corrected tractive effort, power absorber demand, excursion time, and output power. The on-screen display includes the current and desired speeds, the loop delay, percentage of the cycle complete, the excursion time, and the vehicle gear to be engaged (if stated by the driving cycle). The updating sequence includes a road load calculation based on roller speed and acceleration, which is used to control the power absorber in torque mode. As with other data recording processes at non-constant speed, correct selection of the flywheel combination is important, so that the actual mass of the vehicle is closely approximated, and the correct inertia

simulation can be added by the dynamometer to make up the difference (as per Equation 3-10).

6.5.12.1 Scrolling Display

The quality and form of the driving cycle display greatly affects the human driver's ability to follow it, and it was important that the system showed timely and correct information in an intuitive way. For ideal driving cycle testing on a dynamometer, the vehicle transmission and throttle are electronically controlled so that reaction time and driver error are no longer factors. This type of system is readily available and marketed by companies such as Schenck and Froude Consine. However, satisfactory results may be obtained with experienced drivers, and computer control of vehicles on the University of Canterbury chassis dynamometer is not planned in the near future.

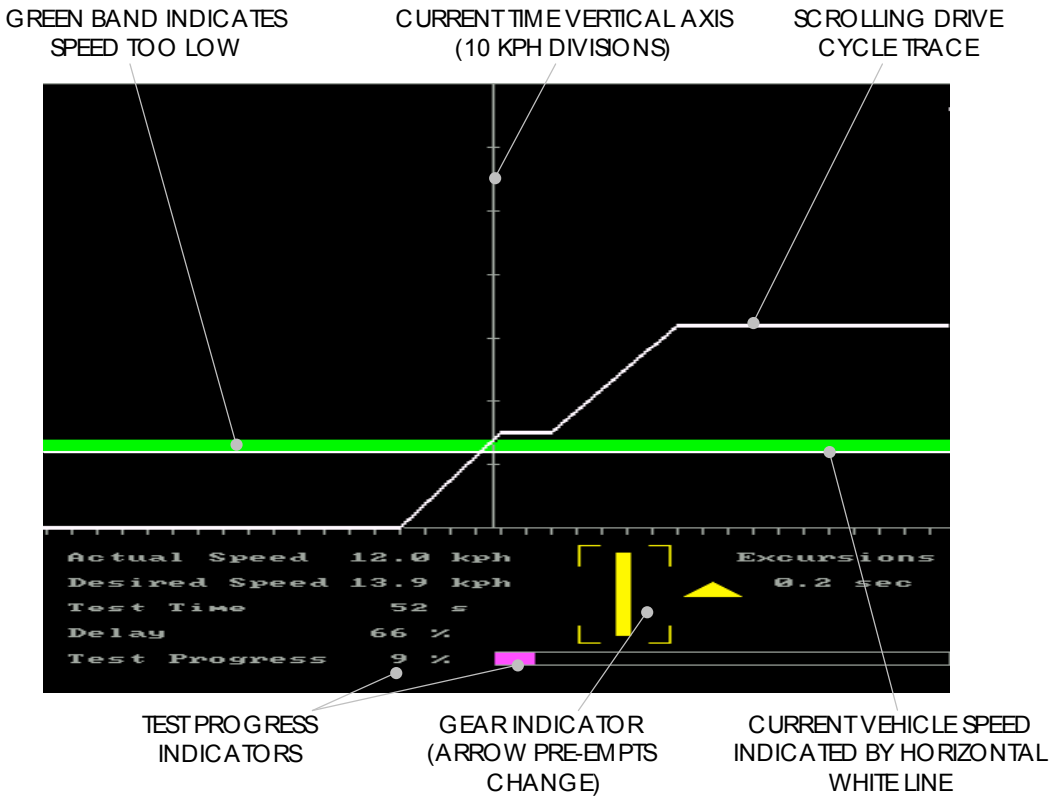

Figure 6.14 Screenshot of scrolling drive cycle display (white cycle trace scrolls from left to right)

Figure 6.14 shows a driving cycle in mid-action, with error band and gear indicator visible. The tick marks on the vertical axis are set at 10 kph intervals, while the horizontal axis markings show one second gaps. The demand speed (white) and the

horizontal axis tick marks move from right to left at the rate of 10 pixels per second (one pixel per update loop). The screen resolution enables 360 pixels in the horizontal direction, and 480 vertically—including 350 within the graph boundaries. The vertical axis in the centre of the screen indicates the current time, while the narrow, white horizontal line is the current vehicle speed. The green band above the current speed shows the difference between the desired and achieved velocities, and indicates that the driver needs to increase the vehicle's speed. A red band of the appropriate thickness appears if deceleration is required to reach the present demand speed. Each of these moving display units is placed using the `draw_line` or `fill_block` commands (contained in MODEX.H) with the required colour. The old pixels that no longer need to be displayed are then removed by substituting black lines and blocks, so that the illusion of the line vacating one position and moving to the next is maintained. The desired speed line is interpolated linearly to fill in the vacant data points between each second of cycle data.

The purple block and 'Test Progress' percentage show the amount of time elapsed as a proportion of the total cycle length. The gear indicator (showing [1]) uses a specific routine to output large numbers according to the gears defined in the driving cycle file, if these are provided. The gear selection routine (in TESTING.CPP) also reads two seconds ahead in the cycle, so the driver can be warned of upcoming gear changes. When a new gear demand is encountered in the file, the gear number is alternately blacked out and made visible (i.e. flashes) while an arrow (shown to the right of the number) indicates the direction of the gear change to be made (up, in the case of Figure 6.14).

The current speed and gear are to be matched by the driver at the vertical centre axis. However, several seconds of data must be recovered from the file in advance so that the upcoming trace can be displayed to right of the vertical cursor. This lead-in time enables the driver to anticipate the approaching speeds, and its duration may be altered in the source code (TESTING.CPP). This advance data is stored in an updating array and is also used to calculate whether the current speed is within the predefined tolerances. Because the allowable deviations also include a time component, the actual speed may anticipate or lag the desired speed changes and still

remain within the limits. For example, if the tolerances on speed were ±1 kph and ±0.5 sec an enlarged view taken from Figure 6.14 shows that although the desired speed at the current instant is 13.9 kph (i.e. range = 12.9–14.9 kph), the desired speed range 0.5 seconds ago was more like 11.6–13.6 kph, thus including the present achieved velocity (see Figure 6.15). A more in-depth description of the tolerance calculation is included in Section 7.1.4.

Excursion time (time spent outside the allowable limits) is calculated at each instant by the C++ control program according to the user-defined tolerances. However, the MATLAB post-processing software detailed in Chapter 7 can also be used to calculate these deviations, and to substitute other tolerance limits after the driving cycle test has been carried out.

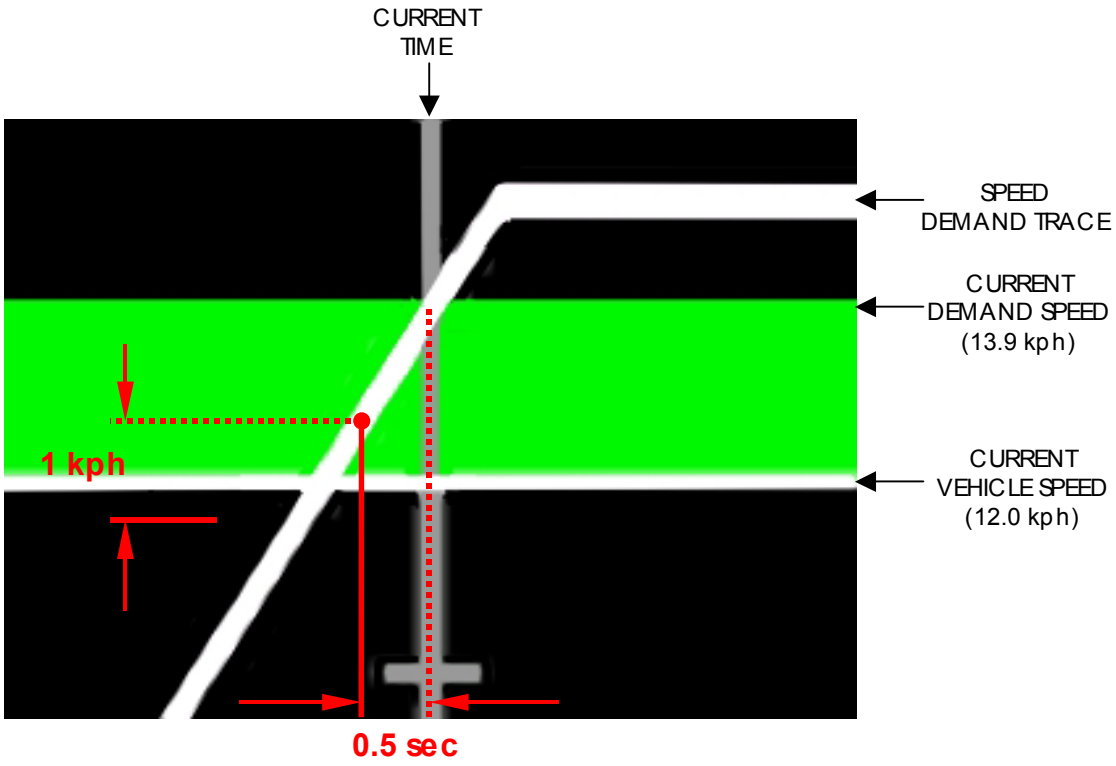

Figure 6.15 Enhanced driving cycle plot showing allowable time tolerance

6.5.12.2 Dynamometer Tracking and Response During Driving Cycles

The power absorber torque is applied according to Equation 3-10, which makes use of the current acceleration and speed, vehicle and dynamometer mass, and frictional coefficients. The constant component of this friction force results in a non-zero

torque demand even when the rollers are stationary. However, the design of the eddy-current dynamometer is such that it cannot apply a torque at zero, or near-zero speeds. Thus, the controller causes large current build-ups as the demand torque is not achieved. Once motion begins again, a large overshoot occurs, resulting in an inaccurate tractive force on the vehicle under test. Figure 6.16 shows the effect of a non-zero torque demand on the stationary dynamometer, which is then accelerated by a vehicle on the rollers.

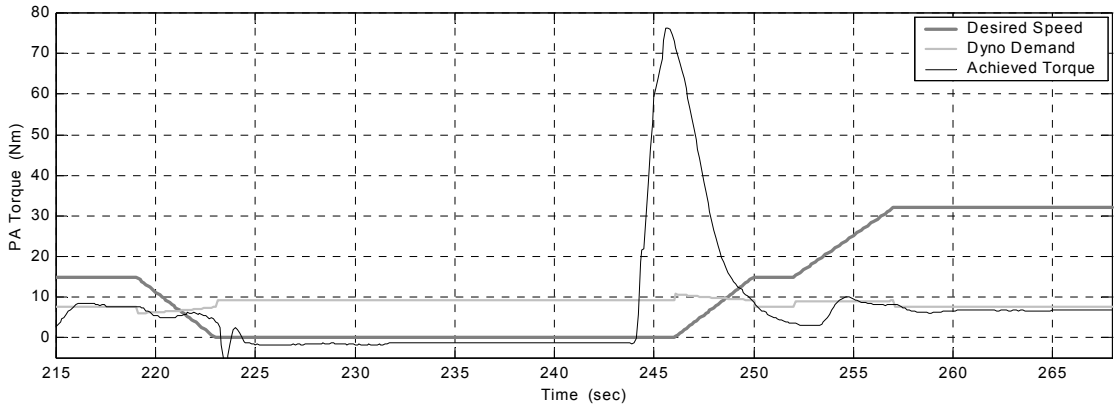

Figure 6.16 Power absorber torque overshoot

A software adjustment was made to ensure that this current build-up did not adversely affect driving cycle results. After the calculation of the required power absorber load, an additional programming check is carried out to determine whether the dynamometer is capable of delivering this demand torque. If the actual shaft velocity is less than a preset limit, and the driving cycle is in a deceleration or stationary mode, the power absorber demand is set to zero. By cutting out the demand *before* zero speed is reached, the eddy current—which takes a finite time to decrease—falls to zero just as the rollers are stopped. Figure 6.17 below shows a deceleration, stationary period, and acceleration under the software-adjusted power absorber demand.

The large overshoot shown in Figure 6.16 has been reduced by approximately 90%, at the expense of an increase in lag. Delays when the dynamometer load was reapplied were again due to the eddy-current response at low speed. This time-lag and overshoot is less evident at higher speeds, and the accompanying error was thought to be tolerable for driving cycle testing.

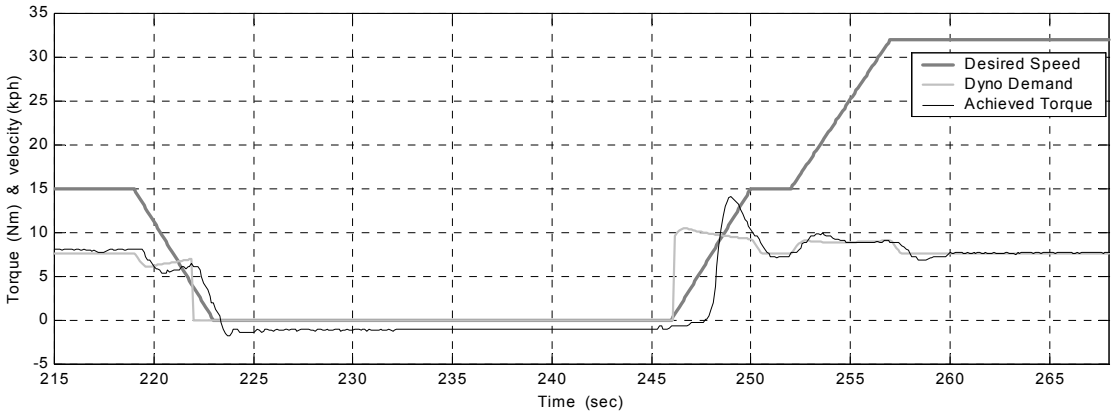

Figure 6.17 Power absorber torque with improved demand function

The current vehicle deceleration rate for determining the dynamometer cut-out is ascertained from the ideal cycle speed demands, to ensure stable and repeatable application and removal of power absorber load. For further dynamometer load stability, the ideal acceleration (i.e. difference between adjacent driving cycle demand speeds, divided by the time interval) may be substituted for the actual calculated acceleration in the road load equation. Power absorber cut-out, tractive effort correction, and road load calculation may each be carried out using this ideal acceleration or the calculated acceleration, as discussed in Chapter 4. Satisfactory results were achieved over several driving cycle tests (see Section 8.2.4) with the use of ideal accelerations. Obviously, in 'Road Load Driving' mode there is no ideal cycle to follow and the acceleration must still be calculated at each point in time.

CHAPTER 7:

Data Analysis and Presentation Software

7.1 Plotting and Analysis Software

A data analysis software package has been created using MATLAB for the purpose of viewing and editing previously recorded chassis dynamometer data in a Windows environment. A series of program files were written using MATLAB version 5.3, making use of the matrix-based data storage structures and built-in graphical display functions. These program files interact with each other and can be run by typing `viewdata` at the MATLAB command prompt while in the correct directory. All these so-called m-files (MATLAB files have the file extension *.m) are included on CD and may be viewed with any text editor. The MATLAB analysis package is menu-driven, providing the user with numbered options as shown in Figure 7.1.

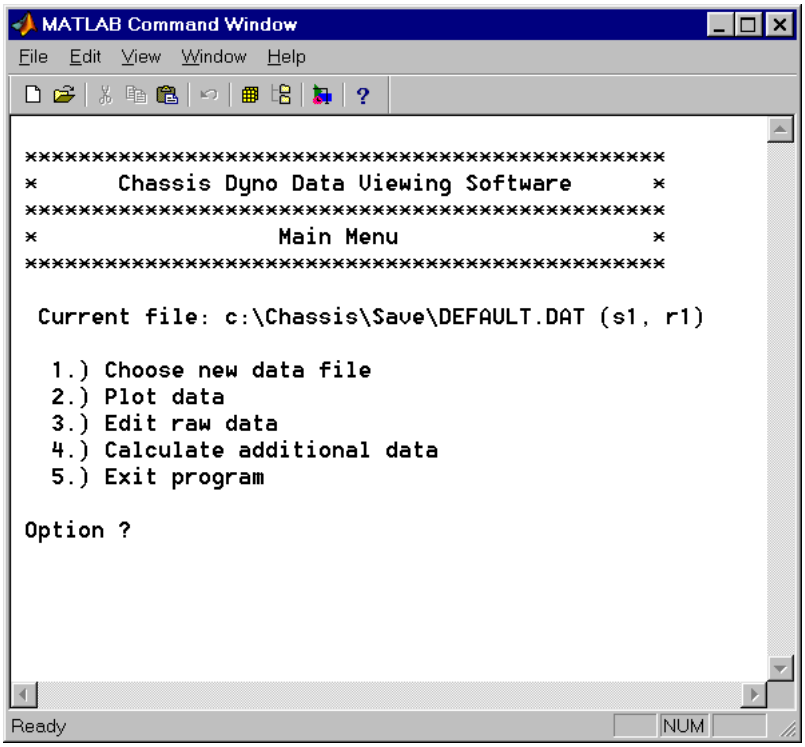

Figure 7.1 Example of MATLAB screen display showing the available options and a user prompt

7.1.1 Overview of MATLAB Functionality

The main menu allows the user to enter the submenus that control file selection, graphing, editing raw data, and calculating additional data. Each of these (with the exception of the data editing) has one or more m-files of its own. The overall menu structure is summarised in tabular form in Appendix W. The file selection menu allows the user to choose from any of the previously saved chassis dynamometer data sets, and then loads all the information into matrices for use by the plotting and calculating routines. The graphing routines enable plotting of the current data in a variety of ways, and are discussed further in Section 7.1.3. Raw data editing simply invokes a standard MATLAB function (`keyboard`) that enables all the current variables to be viewed individually and edited using MATLAB command-line entries. Additional data not saved by the C++ program—such as fuel consumption (km/l), energy consumption (J) and efficiency (%)—may be found using the 'Calculate Additional Data' function. Also included in this section is the driving cycle excursion calculation routine, which is discussed in full in Section 7.1.4. All the options used to carry out the various plotting and calculation activities may be altered by the user at will, and are stored in text files. Each time a particular menu is arrived at, the previous settings are recovered from the predefined file for immediate use or editing.

7.1.2 File Input/Output and Data Storage

The file structure produced by the C++ control program is such that it is easily read using MATLAB file I/O functions. An example file is included in Appendix R, which shows the divisions between the header and the data, and between each new data run. Commas are used to separate consecutive text or numerical data. Each time a new recording mode is entered in the control program (e.g. 'Manual Control', 'Vehicle Mapping' etc) a new *session* is begun. Within each session, the user may start and stop the recording of data several times, and each of these is referred to as a *run*. Each session must have at least one run before it is saved to the file. Each saved session contains a header with background information (e.g. current dynamometer frictional coefficients) and title information (the name and units of each recorded data channel). Each run is preceded by a date/time header, which includes the control program mode, and driving cycle information if applicable. During the file selection

routine, the entire file is first scanned to count the number of asterisk dividers (sessions) and equals-sign dividers (runs). Then the user enters the desired session and run, and the file is again traversed, this time only until the desired run is reached. At this point, consecutive data values are read (up to the end of the run) into a large matrix, which contains all the numerical data, with each row containing all the input channels at a single moment in time. The channel titles (e.g. 'Roller Speed') and units (e.g. 'kph') are also stored in separate matrices. The same process is performed when the MATLAB program is initially started up. The most recently used file, session, and run are recovered and the appropriate data is stored in matrices ready for use. These matrices are then passed between the m-files as required, so that the latest data is available to all parts of the software. Checking and reading from data files can be a relatively time consuming process. For example, a 390-second driving cycle file, with 27 data columns recorded every 0.1 seconds takes approximately 17 seconds to download into the appropriate matrices. However, once in matrix format, this information can be transferred between m-files or set up for graphical display in less than 1 second.

7.1.3 Plotting Functions

The primary function of the post-processing MATLAB programs is to display test data in a flexible and easy-to-use format. The standard MATLAB `plot` function can be used to plot any column in the data matrix against any other to observe trends within a test run, or to compare two or more separate runs. The user chooses the x and y data sets, as well as the colour of the line and whether the plot is to overlap or replace the previous plot, or produce a new plot window. The titles and units matrices are also accessed so that the axes are automatically labelled and the graph is provided with a title. The MATLAB graphing environment also allows the appearance of the plot area and text to be altered after plotting.

7.1.3.1 Plotting Power Curves

One indication of a vehicle's performance is the maximum power produced at the road wheels. Remaining in a single gear and accelerating under maximum throttle, the peak force and power can be found and related to the corresponding engine or road speed. Power curves are best performed under the 'Manual Control' mode (see

Section 6.5.9) with a constant—or zero—dynamometer torque. By using the raw tractive effort signal, the corrected tractive effort and power can be recalculated as per Equations 5-15 and 6-5 using a smoother acceleration with zero lag. Because the entire speed sequence is available (as opposed to on-the-fly calculations) and the speed changes are relatively steady, the acceleration is calculated using a simple central difference approximation.

$$\dot{v}_1 = \frac{v_2 - v_0}{2T} \tag{7-1}$$

Where: $\dot{v}_1$ = approximate acceleration at present point in time (m/s^2)

v_2 = velocity at next point in time (m/s)

v_0 = velocity at previous point in time (m/s)

T = time interval between velocity measurements (s)

In addition, the resulting corrected tractive effort and power sequences are filtered using the MATLAB function `filtfilt`. The `filtfilt` function uses predefined filter coefficients (in this case, from a 2nd-order Butterworth filter) to filter the given data first in one direction, then in the other. The result is a filtered data set with zero lag. A power curve produced using the test car (see Chapter 8) is shown below (Figure 7.2) with and without the MATLAB filter.

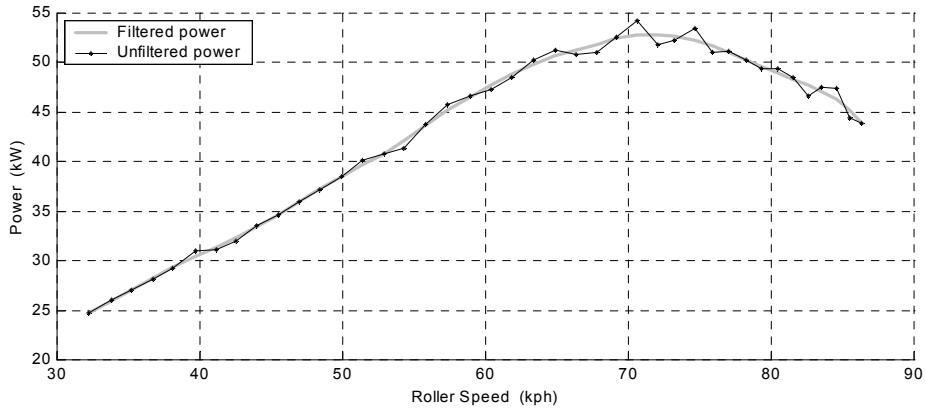

Figure 7.2 Test car power vs. speed with and without zero-lag Butterworth filter

Note also that the power is corrected for the atmospheric conditions during testing as per Equation 6-5 using the air temperature and pressure data from the save file.

Corrected tractive effort may also be plotted and is filtered in the same way as the calculated power.

Power and torque outputs are most often quoted in terms of engine speed, to negate the effects of gearing and wheel diameter. However, the engine speed signal measured by the chassis dynamometer data acquisition system was significantly less stable than the velocity readings, and an alternative was sought. If the vehicle gear ratios and tyre diameter are known, the ratio of road speed to engine speed in a given gear may be used to calculate the engine rpm at each measured velocity. However, if such information is not available, the instantaneous engine speed may be calculated using the *average* ratio of road speed to engine speed (as measured from the spark plug pulses).

$$Engine\ RPM \quad \approx \quad Road\ Speed \times \left(\frac{\Sigma Engine\ RPM}{\Sigma Road\ Speed} \right) \tag{7-2}$$

Figure 7.3 below shows a power curve plotted using the raw engine speed (measured by counting spark plug pulses) and one plotted using the engine speed as a function of road speed. Plots of this type may be configured using the options (such as line colour) mentioned in Section 7.1.3, but the horizontal axis may only contain road speed or engine speed, while the vertical axis represents either tractive effort or power.

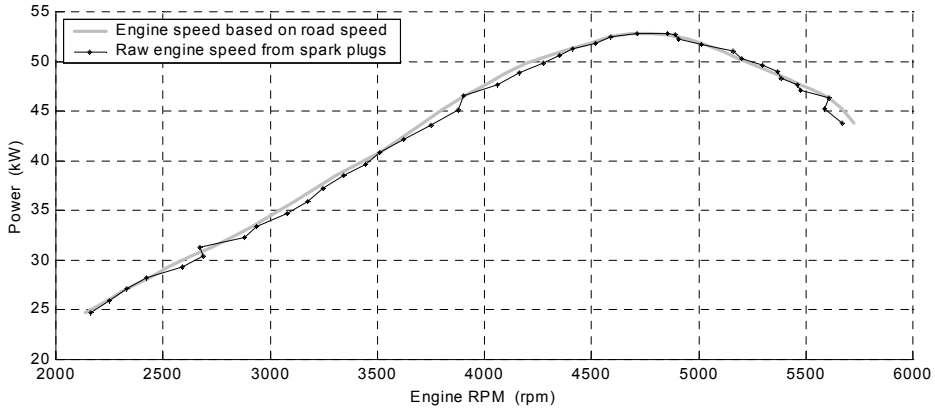

Figure 7.3 Test car power vs. engine speed using raw engine speed and using road speed to calculate approximate engine speed

7.1.3.2 Plotting Vehicle Mapping Tests

Vehicle mapping tests record data at the intersection of several loads and speeds. The physical procedure is detailed in Section 6.5.11 and results in all the data channels being recorded at each preset tractive force (load) and each speed. Any visual representation of this data must therefore consist of three dimensions, which requires a method of plotting a surface, as opposed to the lines that were sufficient for the plotting routines discussed in Section 7.1.3. Two-dimensional plotting is carried out in MATLAB by linearly approximating between data points (i.e. connecting known points with a straight line). However, a graphical representation of the mapping test data must be viewed as a smooth surface either shown from above, with colour designating magnitude, or in a three-dimensional form, with height on the third axis. It is also useful to view the actual numerical data in tabular form, which has been accomplished using Microsoft Excel (see Section 7.1.3.3).

MATLAB enables the plotting of surface graphs with its built-in function `surf`, which linearly interpolates in three dimensions to render the surface as a series of interconnected flat plates. The major difficulty in using this function is that it requires each of the *x*-axis columns and each of the *y*-axis rows to contain the same number of data points. Vehicle mapping data invariably contains columns (velocity) and rows (tractive force) of uneven length, and so cubic splines are used to produce a regular grid by interpolation and extrapolation of the original data. The process used to produce a vehicle map is shown in simplified form in Figure 7.4. The small graphs shown to the left indicate the number of data points; beginning with the raw data, and ending with the interpolated data set, which has a consistent number of row and columns (although some are zeroed before plotting). Velocity is shown on the *x*-axis with tractive effort on the *y*-axis. The dots represent single data points of a third variable (e.g. fuel consumption) whose magnitude would project out of the page.

After the required information is retrieved from the appropriate place in the data matrix (A in Figure 7.4), the Excel file-save is carried out, which is further discussed in Section 7.1.3.3. The mapping function (found in VIEWDATA_MAPPER.M) then sets up and zeros two matrices. The first intermediate matrix has the same number of

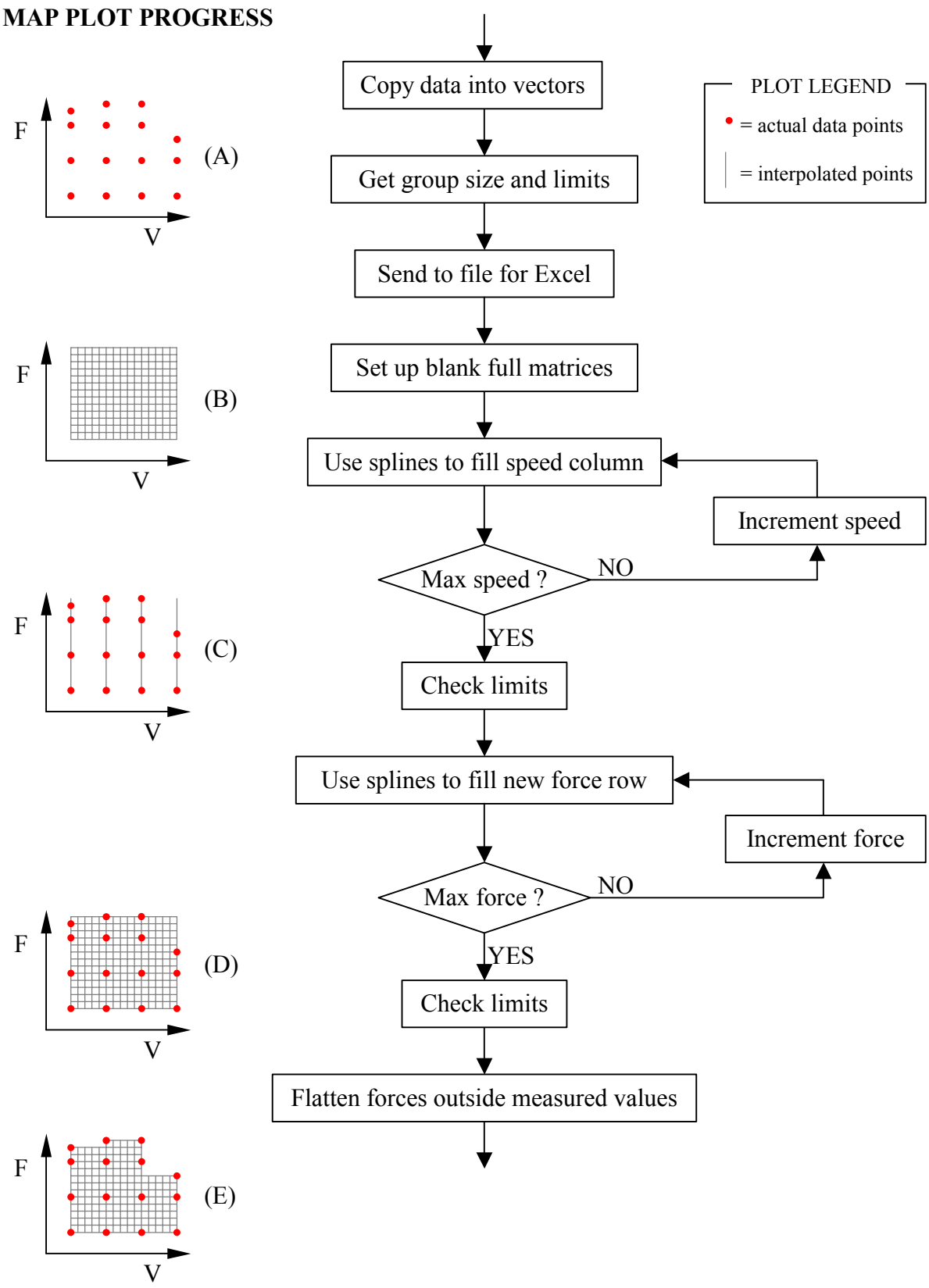

Figure 7.4 Flow chart of vehicle map plotting

speed columns but the maximal number of rows. The user can adjust the level of interpolation to achieve a smoother plot, and does so by setting the maximum number of data points to be interpolated on the *x*- and *y*-axes. A greater number of points takes more time to calculate, but provides a better looking and more accurate representation. The second matrix has the full number of rows and columns (B), and it is this matrix that is plotted using the MATLAB command `surf`. Each column of the intermediate matrix is filled out using columns from the original data and the MATLAB `spline` command. This function uses cubic splines to replicate the data at each original point, and interpolate for the points in between. Figure 7.5 shows a cubic spline interpolation, which extends a seven point series to a 101 point series, with a greater upper limit. This process places the full number of load rows into each speed column of the first intermediate matrix (C).

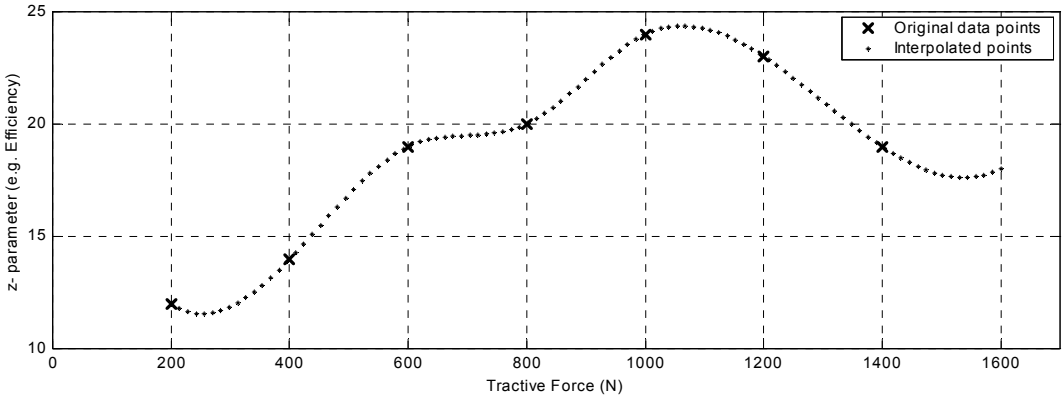

Figure 7.5 Example of cubic spline interpolation

When each of the original speeds has been traversed in this way, each *z*-value (i.e. the 'heights' of the graph) is checked against user-defined limits. Usually, a minimum of zero ensures that the spline function does not dip too low between data points, and a maximum can also be set for specialised plotting applications. If any of the spline values lie outside the allowable range, they are made equal to the limit. For example, if the lower limit was set at 10 and one of the interpolated *z*-values became 9.7, the checking routine would simply substitute a 10 in place of the 9.7.

Next, the intermediate matrix is used to fill the full plotting matrix by implementing spline functions along each of the new rows. In this case, each of the rows will be the same length—as each set of loads was conducted at similar speeds—and each is

interpolated to pad it out to the maximal number of points. At this stage, the second matrix (containing all the interpolated *z*-values) could be plotted using the `surf` function with appropriate *x* and *y* vectors (D). However, the filled out matrix includes full speed columns containing tractive effort points exceeding those that the test vehicle was able to produce. After the limits are again checked, all the matrix values that lie outside the original data range are set to zero—or some other user-defined value (E). Thus, an abrupt change in 'height' is encountered in the final plot to indicate the end of the measured data. When viewing in three-dimensional mode, this flattened area appears as such and can be misleading to the uninitiated observer. The option to whiteout the zeroed area is also made available to the user, and is particularly effective when viewing data solely as a colour contour plot from above. 2-D and 3-D plots are shown in Figures 7.6 and 7.7 for the same fuel flowrate data from the test vehicle.

7.1.3.3 Microsoft Excel Display

As well as providing a graphical display, it is useful to be able to view vehicle mapping data in its raw form. The recorded data may be viewed directly in the text file to which it was saved, or in a pseudo-graphical layout that sets out the information in tabular form. Microsoft Excel has been used to develop a format that displays the measured parameters in a grid that lines up with the speed and load at which each point was recorded. An example is shown in Figure 7.8, which represents the same mapping run as that shown in Figures 7.6 and 7.7.

Because the Excel grid is discrete, approximations must be made to assign the measured data points to one cell only. At each set-speed, the tractive force points will each be recorded at a slightly different velocity—despite the power absorber controlling in speed mode. To avoid the need for infinite horizontal variation within the columns, the average measured velocity at each set-speed has been substituted as an approximation for all the speeds in that column (e.g. all the data points recorded at a nominal velocity of 100 kph). On the vertical axis, the tractive force recorded at each data point has been rounded to the nearest 25 N step. For example, the data points in cells level with the 800 N label are known to lie in the range 787.5–812.5 (i.e. 800±12.5 N). Figure 7.8 shows a point just above the 800 N line at a velocity of

39 kph. This point was recorded with the measured tractive effort between 812.5 and 837.5 (or 825±12.5 N).

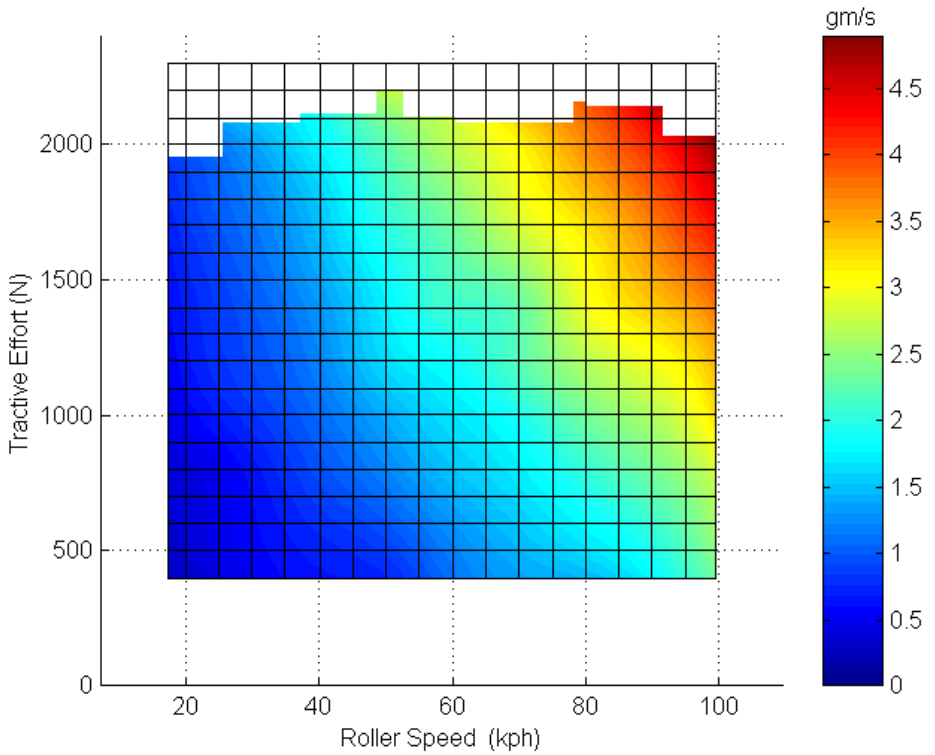

Figure 7.6 Two dimensional contour mapping plot for Toyota Celica fuel flowrate

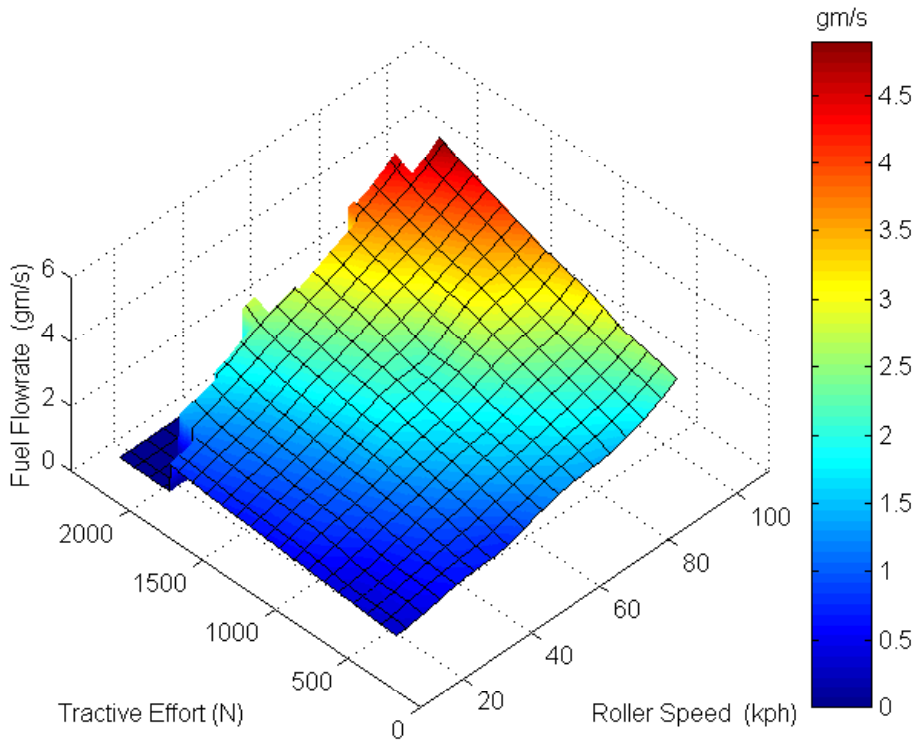

Figure 7.7 Three dimensional contour mapping plot for Toyota Celica fuel flowrate

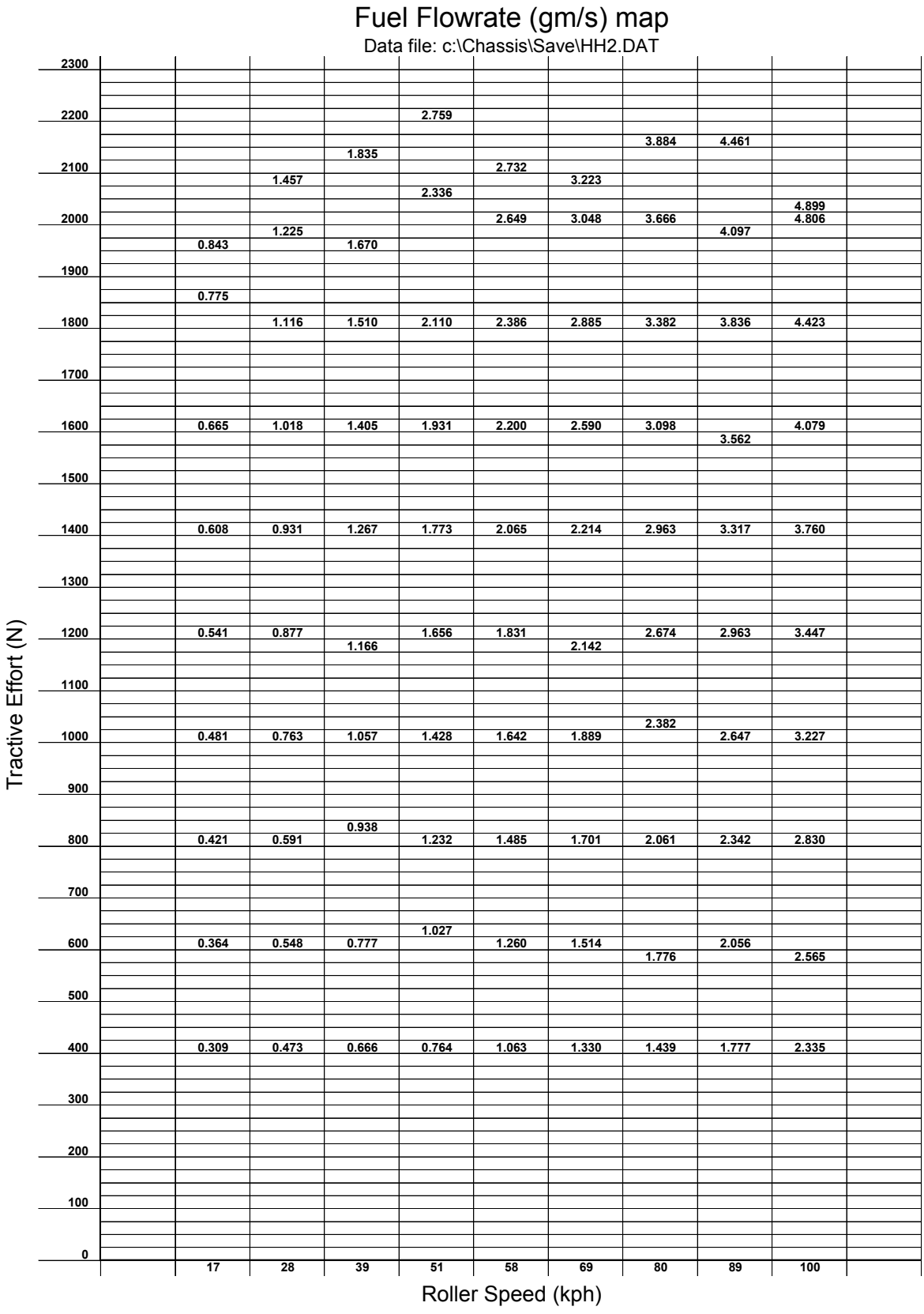

Figure 7.8 Text mapping plot for Toyota Celica fuel flowrate

In practice, these text plots are produced using an Excel macro (included in the template spreadsheet on CD), which performs the function of copying the data from a predefined file and transferring it into the plot area. To produce a plot such as Figure 7.8, the user must first generate a mapping plot in the MATLAB post-processing program, then the standard plot sheet is opened in Excel and the macro can be run. As part of the MATLAB plotting routine, a new text file is set up, which lays out the mapping data in a form that is easily copied into Microsoft Excel. This file consists of a regular grid, with zeros taking the place of load/speed combinations for which there is no recorded data. Another text file is also generated, which consists solely of a list of the three parameters for that map (speed, tractive force, and fuel flowrate, for example). This file is useful for comparisons between runs where the variations (e.g. in maximum tractive effort) may only be very small, and would not be visible on either the Excel text plot or the contour plots. Examples of the text file and the standard Excel plot sheet are included in Appendix X. The spreadsheet file also contains the average speeds for labelling the columns, and information such as the name and units of the variable to be displayed.

7.1.4 Driving Cycle Error Analysis

During driving cycle tests, adherence to the prescribed speed demand is measured in terms of a speed and time tolerance. Limits of ±1 kph in speed and ±0.5 seconds in time were chosen for the testing detailed in Chapter 8. This driving cycle tolerance is shown graphically in Appendix V. Although the C++ data acquisition routine calculates the excursions during the driving cycle run (see Section 6.5.12.1) it is useful to be able to apply different tolerances (to comply with different testing standards) after the test has been carried out.

The calculation of driving cycle excursions is included as an option in the ‘Calculate Additional Data’ menu of the MATLAB program and is conducted in a similar way to that used in the C++ testing control routine. The user is first prompted for the desired velocity (kph) and time (sec) tolerances, the latter of which is converted to a number of time steps (e.g. 0.8 seconds = 8 time steps at 10 Hz). The driving cycle sequence is then traversed one data point at a time, comparing the measured velocity at the present time to the cycle target speed within the limits. Figure 7.9 shows two

separate points being investigated and compared against the velocity range of all the demand speeds within the time envelope. In the example, the time and speed tolerances are 0.5 sec and 1 kph respectively. At each point, the time envelope consists of desired speeds 0.5 sec (five points) either side of the present time. To remain within the limits, the current measured speed must be less than the maximum cycle speed in the time envelope plus the speed allowance (1 kph), and greater than the minimum cycle speed in the envelope minus the speed allowance.

Example A

Time	-0.5s					Current time					+0.5s
Cycle (kph)	**0**	0	0	0	0	0.1	0.2	0.3	0.4	0.5	**0.6**
Measured (kph)	0	0	0	0	0	**0**	0	0	0.4	1.0	1.1

Cycle velocities included in time envelope = 0, 0, 0, 0, 0, 0.1, 0.2, 0.3, 0.4, 0.5, 0.6

Maximum cycle velocity in time envelope = 0.6 kph
Maximum allowable vehicle speed = 0.6 + tolerance = 0.6 +1.0 = **1.6** kph

Minimum cycle velocity in time envelope = 0.0 kph
Minimum allowable vehicle speed = 0.0 - tolerance = 0.0 – 1.0 = **–1.0** kph

Current speed = **0.0** kph

∴ Since **–1.0 ≤ 0.0 ≤ 1.6** the current speed is within the allowable limits

Example B

Time	-0.5s					Current time					+0.5s
Cycle (kph)	**5**	5	5	4.5	4	3.5	3	2.5	2	1.5	**1**
Measured (kph)	5	5.5	6.5	6.4	6.4	**6.4**	6	5	3.5	2.0	1

Cycle velocities included in time envelope = 5, 5, 5, 4.5, 4, 3.5, 5, 2.5, 2, 1.5, 1

Maximum cycle velocity in time envelope = 5.0 kph
Maximum allowable vehicle speed = 5.0 + tolerance = 5.0 +1.0 = **6.0** kph

Minimum cycle velocity in time envelope = 1.0 kph
Minimum allowable vehicle speed = 1.0 - tolerance = 1.0 – 1.0 = **0.0** kph

Current speed = **6.4** kph

∴ Since **0.0 ≤ 6.4 ≮ 6.0** the current speed is **not** within the allowable limits

Figure 7.9 Examples of velocity and time compliance calculation

The total excursion time (time spent outside the allowable limits) is displayed after this process is completed, and the cumulative excursion time is also stored as part of

the large data matrix so that it may be plotted against time, or any other driving cycle parameter.

7.2 Vehicle Energy Consumption Modelling

During a driving cycle, the vehicle under test consumes energy from its fuel source (be it electrical or chemical) and puts out power at the road wheels. It is important to be able to model the amount of energy used during a period of driving, so that the relative effects of friction, gravitational, and inertial forces can be investigated. The vehicle energy consumption modelling program is a simple, stand alone MATLAB routine than can be used to calculate either the total energy output of a vehicle under test, or the total energy that *should* be required by a vehicle undergoing a certain driving cycle. The ideal energy consumption for a given vehicle can be compared with the actual measured result to determine the effectiveness of the driving cycle routine and dynamometer road load demand functions.

Both the ideal-cycle and the measured-output functions make use of text files with a single column of numerical data. For calculating the predicted cycle output, the input file must contain a sequence of desired cycle speeds. The user must also provide vehicle details such as the mass and frictional coefficients so that the tractive force (and hence power) required to achieve a given acceleration and velocity can be calculated using Equation 7-3. The optional gravitational term, $m_V g \sin\theta$ may be included if the effect of road gradient is to be modelled. For calculating the actual vehicle energy output during a test, power measurements—corrected for atmospheric conditions—are required. Also necessary for both processes is the *idle power* consumption of the vehicle. Idle power represents the minimum amount of power that an engine will put out, and is discussed in more detail in Section 7.2.1.

$$F_V = m_{Veq}\frac{dv}{dt} + m_V g \sin\theta + f_{0V} + f_{1V}v + f_{2V}v^2 \tag{7-3}$$

$$Power\ Output\left(uncorrected\right) = F_V . v \tag{7-4}$$

For the purpose of modelling the vehicle forces in Equation 7-3, the acceleration is calculated from the desired driving cycle speeds using a central difference

approximation (see Equation 7-1). The power at each given velocity point is corrected for the atmospheric temperature and pressure (as per Equation 6-5), then multiplied by the time interval over which it is assumed to have been maintained, giving the energy consumed. The sum of each of these energy steps yields the total energy consumed over the entire driving cycle.

$$Energy\ Consumed\ (J) \quad = \quad \Sigma P_{corr} \Delta t \tag{7-5}$$

Where: Δt = length of each time interval between readings (sec)

The calculation of the measured power uses the corrected power values as returned by the C++ control program. Equation 7-5 is again used to generate the total energy consumed over the entire run.

7.2.1 Vehicle Idle Power

Equation 7-5 may be used to calculate the total energy consumed over a driving cycle in the ideal and real-world cases. However, there are times when the output power used in this equation becomes less than is practical for the engine to deliver, particularly when testing with internal combustion engines. When the vehicle engine is idling (i.e. velocity = 0), and especially during decelerations ($m_{Veq}\, dv/dt < 0$) the power output may be zero or negative. Unless the test vehicle employs regenerative braking, this zero or negative energy output value is not possible, and some assumption must be made. Thus, we employ what is known as an idle power, and assume for the purposes of energy consumption calculations that the power output cannot drop below this value. From the point of view of the fuel energy, there is a certain level of consumption that the internal combustion engine requires to overcome its internal friction and continue running when no throttle is applied. Since no throttle is applied during stationary or braking periods, it is logical to substitute the idle power under these circumstances.

If $Power < Idle\ Power$

Assume $Power = Idle\ Power$

As for the actual idle power magnitude, there are several approaches that may be applied. Vehicle energy consumption modelling previously carried out at the University of Canterbury [Epps, 1987] approximated the idle power as the power generated under slow driving conditions. Specifically, the idle power was calculated as the road load force at 10 kph multiplied by this velocity. An experimental method was desired to verify the suitability of this approximation, using measured power output and fuel consumption. Because power output can only be measured by the chassis dynamometer in terms of force and speed at the drums, a relationship was sought between idle power and the output power when a vehicle is driving on the dynamometer. Assuming that the engine efficiencies are similar during idle and low speed driving, the following equation will be true:

$$\frac{\textit{Fuel consumption during idle}}{\textit{Fuel consumption during running}} = \frac{\textit{Power during idle}}{\textit{Power during running}} \qquad (7\text{-}6)$$

To ensure that the driving conditions were as similar as possible to idle, the vehicle was driven in low gear with the engine running at the idle speed. With modern vehicles employing automatic choke, a state is easily achieved wherein the vehicle is propelled at a constant speed with no application of the accelerator pedal. For the test vehicle discussed in Chapter 8, idle speed and no-throttle motion were both achieved at an engine speed of approximately 650 rpm. At this point, the engine is supplying enough power to continue running (idle power) plus an additional power output to overcome rolling resistances and the chassis dynamometer friction. We assume that vehicle resistances are small and that the dynamometer friction (measured as tractive effort at the drums) represents the majority of the power consumption over and above the idle. Since fuel consumption during idle and driving can both be measured—along with the tractive effort and speed—idle power remains the only unknown in Equation 7-6. The test vehicle is used as an example in the calculation of idle power:

Fuel consumption at idle (650 rpm) = 0.167 gm/s
Fuel consumption while running (650 rpm) = 0.183 gm/s
Power generated at drums during idling = 0 W
Power generated at drums while running = 110 W

$$\frac{\textit{Fuel consumption during idle}}{\textit{Fuel consumption during running}} = \frac{0.167}{0.183} = 0.913$$

Idling takes up 91.3% of the fuel (i.e. turning the dynamometer takes up 8.7%)

Power consumed by the dynamometer during running = 110W = 8.7% of total

Total power consumed = $\frac{100}{8.7} \times 110$ = 1264W

Idle Power = 1264 – 110 = **1154 W**

This is significantly greater than the 600 W calculated using the vehicle road load at 10 kph. If the fuel consumption that is applied to the unmeasured transmission and rolling friction components could be measured and accounted for, the resulting experimental value would be closer to the approximation used by Epps. Considering that the idle power magnitudes in question were not great in comparison to the overall vehicle outputs, the experimental value was rounded down, and an idle power of 1000 W was implemented for the results quoted in Chapter 8.

CHAPTER 8:

Vehicle Testing Procedure and Sample Results

8.1 The Test Vehicle

The vehicle tests discussed in this chapter were carried out on a 1982 Toyota Celica owned by the University of Canterbury. This rear-wheel drive car was powered by a 6 cylinder, fuel injected, 2 litre engine and had completed approximately 206 000 km before testing commenced. Further details are included in the Vehicle Data Sheet (see Appendix Y), which is to be filled out for all vehicles tested on the chassis dynamometer. This section contains information regarding the on-road friction determination, and specific details of the dynamometer set up for the Toyota Celica, hereafter referred to as the test vehicle.

Plate 8.1 The test vehicle

8.1.1 Vehicle Friction Determination

In order to carry out realistic road load modelling on the chassis dynamometer, the frictional forces acting on the test vehicle during on-road driving must be determined or estimated. Deceleration tests have been used with considerable success in the past ([White & Korst, 1972], [Hindin, 1985]) and a method for conducting these coastdowns is described in detail in SAE J1263 [1999]. With knowledge of the vehicle mass, the frictional forces can be calculated from acceleration and velocity measurements between two given speeds. In practice, several on-road decelerations were performed and the results averaged.

The vehicle speed was measured and recorded electronically during each run by a purpose-built optical pickup mounted on the underside of the vehicle. A white strip was painted on the driveshaft, allowing each revolution to be detected and timed. Before the coastdowns were carried out, the number of driveshaft revolutions per wheel rotation was calculated by rolling the vehicle forward a set number of rotations, and measuring the distance. Although this method does not take into account possible changes in tyre diameter at high speed, it was thought to be sufficiently accurate when the vehicle tyres were inflated to recommended pressures. By keeping a record of the number of 2 μs time intervals between consecutive driveshaft rotations, the instantaneous velocity could be calculated (see Equations 8-1 and 8-2). An example resulting velocity coastdown curve is given in Figure 8.1.

$$\begin{aligned} \textit{Time per driveshaft rotation} \;=\; & \left(\textit{Time per clock pulse}\right)\times \\ & \left(\textit{Number of clock pulses per rotation}\right) \end{aligned} \tag{8-1}$$

$$\textit{Velocity} \;=\; \frac{\textit{Distance per driveshaft rotation}}{\textit{Time per driveshaft rotation}} \tag{8-2}$$

As well as vehicle mass, the calculation of friction constants requires information regarding air temperature and pressure during coastdowns, and the frontal area of the vehicle. The latter can be determined using an elevational photograph as shown in Appendix Z. The SAE procedure allows for wind conditions and small road gradients, among other factors, and the full calculation of vehicle friction is also included in Appendix Z.

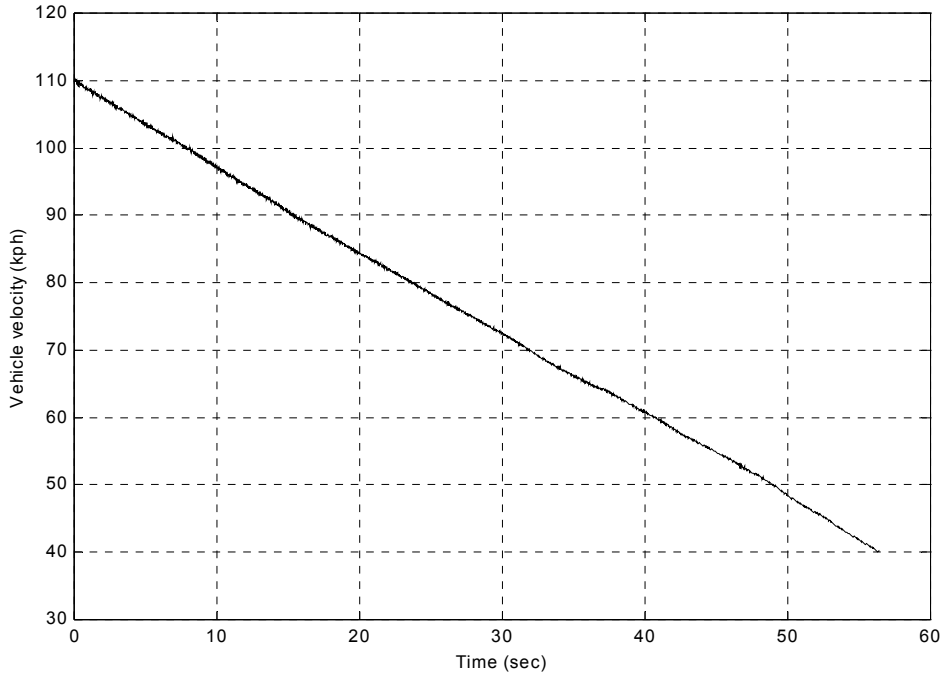

Figure 8.1 Coastdown velocity vs. time curve

The total on-road vehicle friction was found to be:

$$F_V = 214.9 - 0.439v + 0.413v^2 \quad (8\text{-}3)$$

With: v = velocity in m/s

These coefficients were used to calculate the net power absorber force required for road load simulation of the test vehicle on the dynamometer according to Equation 3-10. Theoretically, each of these constants should be positive, so that the friction always increases with velocity. However, the linear velocity coefficient (f_{1V}) shown above was calculated as a negative value, which was most likely a result of the least squares approximation. Vehicle coastdown data may be prone to this type of error, as the least squares curve fit is required to extrapolate beyond the minimum measured speed of 40 kph.

The f_{0Vd}, f_{1Vd}, and f_{2Vd} coefficients in Equation 3-10 were determined in a series of coastdowns with the test vehicle on the chassis dynamometer. The curb weight of the test vehicle was given as 1150 kg [Coomber, 1988], to which 100 kg was added to account for driver and fuel weight. In general, each vehicle should be accurately

weighed before testing. The standard approximation for the vehicle's inertial mass (see Section 3.1) resulted in an equivalent vehicle mass of 1290 kg. An equivalent flywheel mass of 1234 kg was employed for all subsequent tests, requiring that the eddy-current dynamometer output be as follows for the appropriate road load simulation:

$$F_{pa} = (1290 - 1234)\frac{dv}{dt} + (f_{0V} - f_{0Vd}) + (f_{1V} - f_{1Vd})v + (f_{2V} - f_{2Vd})v^2 \quad (8\text{-}4)$$

With: f_{0V} etc. from latest friction calibration

8.1.2 Specifics of Test Vehicle Set Up

Before testing, any vehicle must be tied down on the dynamometer rollers and have the appropriate instrumentation attached. For the Toyota Celica, the rear wheels were kept in contact with the roller drums using steel cables and turnbuckles provided for this purpose in the chassis dynamometer laboratory. The front wheels could be chocked, but it was found that the cabling alone was sufficient for lateral and longitudinal stability.

The test vehicle oil level indicator was removed, and the engine oil temperature was monitored by means of a thermocouple mounted in a substitute dipstick. Vehicle cooling water temperature was measured using a thermocouple inserted in the cooling circuit at the entrance to the radiator.

To measure the air-flow into the engine, the factory air filter intake was removed, and the Annubar drum output taped in its place. The seals and drain-holes in the filter were then plugged with RTV rubber compound so that all air entering the engine was required to pass through the flow measurement device. Air flowrates for the test vehicle were in the range 0–70 gm/s, requiring the larger of the two Annubar tubes to be used throughout the testing detailed in this chapter (see Appendix C.7 for Annubar description and calibration).

Measuring the fuel flowrate through the test vehicle's fuel injection system with a single flowmeter required some additional fuel line equipment. In most fuel injection systems, fuel is supplied to the injector rail at high pressure, and any excess that is

not used in the cylinders is returned to the tank via a separate line. By blocking the return line and re-routing the fuel as shown in Appendix C.6, all the fuel was made to pass through the Fluidyne flowmeter, enabling a single consumption value to be recorded. Plate 8.2 below shows the test set up viewed from the front of the vehicle.

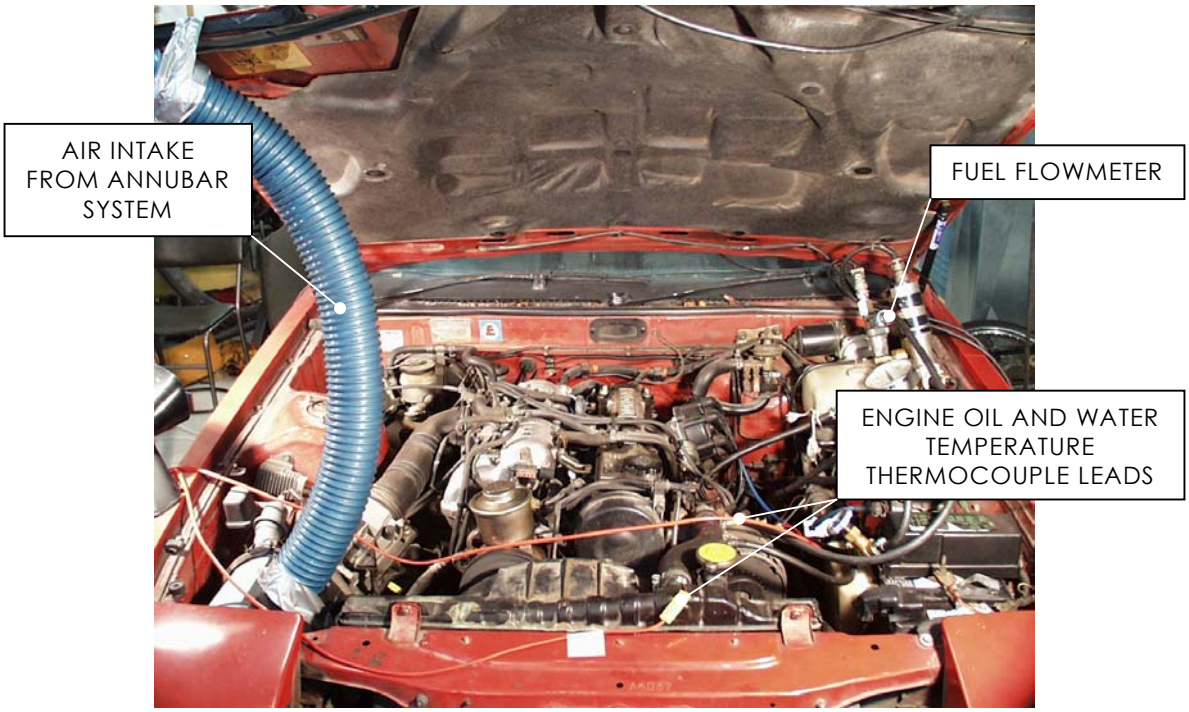

Plate 8.2 Test vehicle engine instrumentation

8.2 Sample Test Results

The test results discussed in this section were gathered in a series of trials conducted during November and December 2001, and January 2002. Several initial tests (not included here) were conducted to enable debugging and familiarisation with the equipment and vehicle driving techniques. All test data relates to the Toyota Celica test vehicle running on 96 octane petrol.

8.2.1 Test Vehicle Warm Up

Before each test session, both the chassis dynamometer and test vehicle were thoroughly warmed up. This generally began with of a period of time running under power from the electric motor with the vehicle engine idling and gearbox in neutral. Progressively faster roller speeds were introduced, while monitoring the drum axle oil temperature. After approximately 15 minutes of running, and with an axle oil

temperature of at least 47º (assisted by the oil heater) a brief period of high speed running (>100 kph for approximately 2 minutes) was conducted before the vehicle transmission was engaged. Switching off the electric motor and driving the dynamometer under power from the vehicle, the engine, tyres, and transmission were then warmed up. Speeds were varied and a moderate rate of engine revving (2000–3000 rpm) employed until the engine oil and cooling water both approached operating temperatures (>80º). Part of this vehicle warm up was often accomplished by following a driving cycle, particularly as practice for the driver before a recorded driving cycle test.

8.2.2 Maximum Throttle Acceleration Curves

Maximum throttle accelerations were carried out on the test vehicle mostly in 2nd gear and with no power absorber load. Slower accelerations brought about by the addition of dynamometer load or the use of higher gears did not significantly affect the underlying trends. As detailed in Section 6.5.9, the 'Manual Control' mode was used to facilitate these accelerations, during which recording generally began at about 35 kph and ceased at 5500–6000 rpm. Figure 8.2 shows three separate maximum throttle accelerations, one of which includes a power absorber load of 100 Nm. These graphs were plotted using the MATLAB filtering and power calculation routine discussed in Section 7.1.3.1.

The average maximum power for these three runs was 53.2 kW at 4800 rpm, with a standard deviation of 0.5 kW (1.0%). The highest peak reading was achieved during the run involving significant dynamometer load. This added load has the effect of slowing the acceleration and allowing the engine more time to stabilise the power output, resulting in a greater power. Although exact model information for the test vehicle could not be found, other Toyotas manufactured in 1982 and with comparable engines were listed by Autodata [1990] with a peak output power of around 90 kW. Manufacturers' power ratings are most often quoted in terms of engine output, so the driveline and peripheral equipment (e.g. fan-belt) losses are not included. An estimate of engine power at the flywheel may be arrived at by adding the transmission and rolling resistances (measured by coastdown on the dynamometer) to

the measured tractive effort. Peak power at the flywheel calculated in this way was slightly higher, at 54.7 kW.

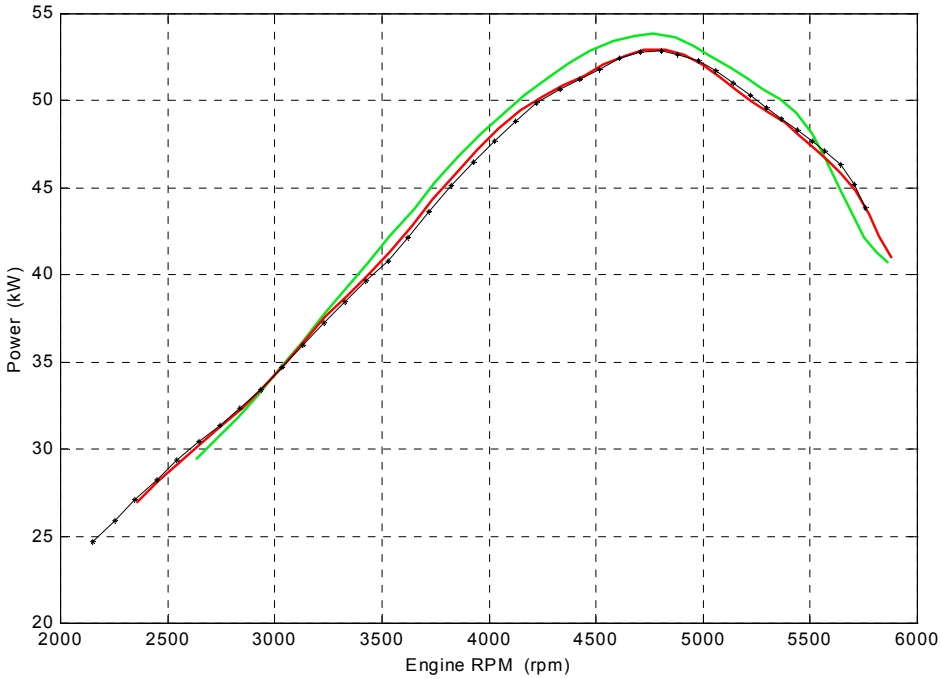

Figure 8.2 Power curves for test vehicle (green curve includes 100 Nm dynamometer load)

The average output power of 53 kW at the road surface was lower than expected, but was thought to be realistic in light of the inevitable decrease in peak power brought about by general wear and tear on the test vehicle.

The relationship between maximum engine torque (directly related to tractive force) and speed can also be investigated using full throttle accelerations. With the corrected tractive effort measurements used to calculate power in the previous paragraph, similar graphs can be plotted using the chassis dynamometer MATLAB routines.

It can be seen that the torque is more evenly distributed throughout the engine speed range than power, and has a less predictable form. Peak tractive effort (measured at the roller drums) from the same three acceleration runs as above was found to be 2880 N on average, with a standard deviation of 40 N (1.4%). The maximum tractive force was recorded at an engine speed of 4000 rpm (to the nearest 50 rpm).

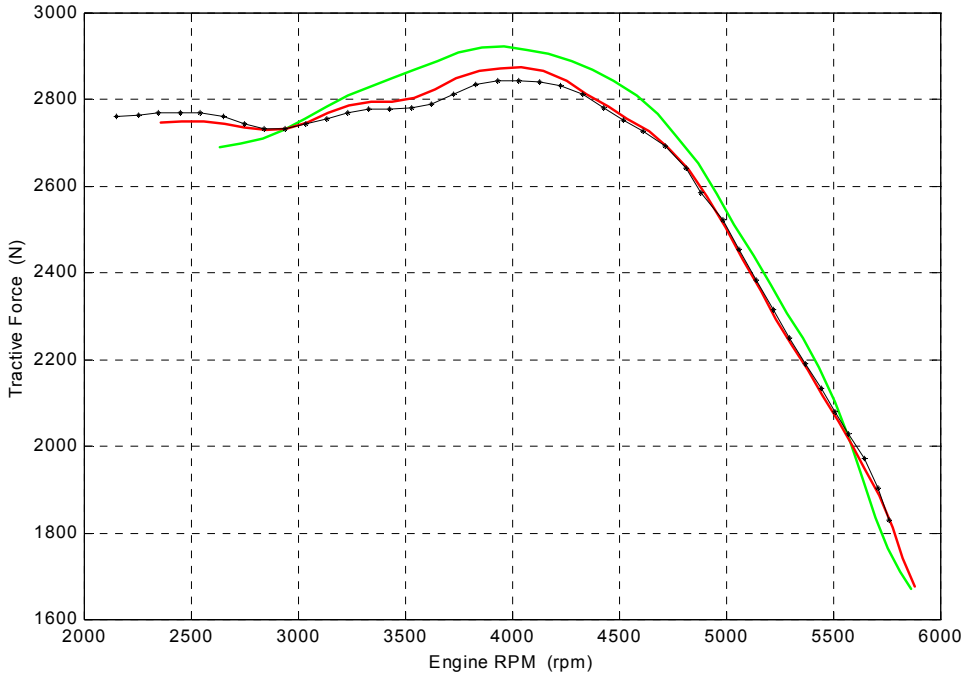

Figure 8.3 Tractive force curves for test vehicle (green curve includes 100 Nm dynamometer load)

8.2.3 Vehicle Mapping Tests

Several vehicle mapping tests were carried out in 3rd gear according to the method described in Section 6.5.11. With the driver setting the throttle for tractive effort, and the power absorber in speed-control mode, each tractive force up to the vehicle's limit was recorded at each set speed. Each complete mapping test run took 30–45 minutes to complete, depending on how rapidly the desired loads were achieved and whether or not the emissions equipment was in use.

8.2.3.1 Mapping Plot Form

Figure 8.4 shows two separate mapping tests, displaying the results in graphical form using the MATLAB plotting package described in Chapter 7. For all the vehicle maps shown in this chapter, vehicle speed is plotted on the *x*-axis, with tractive force on the *y*-axis. The map parameter of interest is displayed in the *z*-direction as colour contours, height and colour (see Figure 7.7) or plain text (see Figure 8.5).

The uneven shape observed at the top of each graph in Figure 8.4 is a result of the maximum force output at each given speed, which occurs when full throttle is

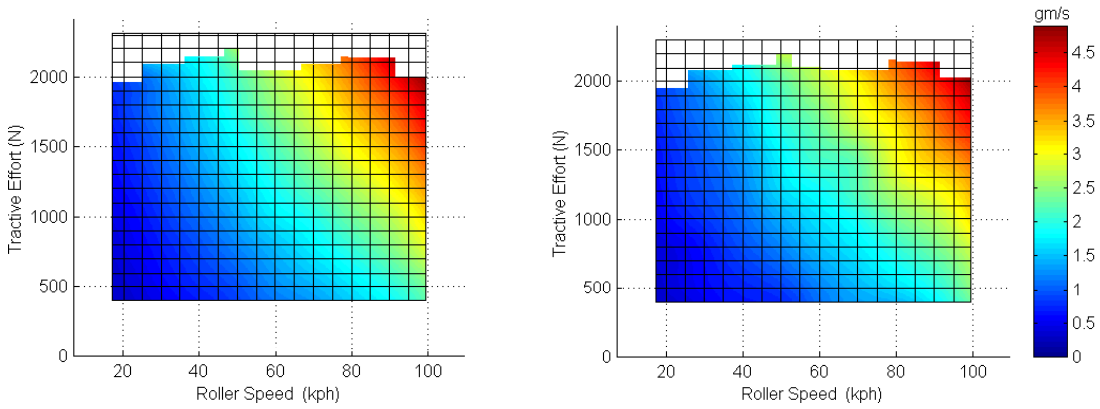

Figure 8.4 Fuel flowrate maps for two separate mapping test runs.

applied. Small differences in magnitude of these maximal forces between plots (seen especially at 60 kph) were a common testing irregularity, and may have been the result of atmospheric conditions, or the engine temperature.

The test vehicle maximum tractive effort is similar to that observed during the full throttle accelerations discussed in Section 8.2.2, with 100 kph equating to approximately 4500 rpm. The maximum power output during these mapping tests was encountered at the maximum recorded speed and load points and was measured for the test vehicle at 56 kW, which is slightly greater than that measured during the maximum throttle accelerations. Slower accelerations (i.e. under a greater dynamometer load) may be required to allow engine settling and development of full power.

8.2.3.2 Set Point Inaccuracies

Figure 8.5 shows the same information as Figure 8.4b in a text plot, produced using the MATLAB routines and Excel macro. Note that this plot is identical to Figure 7.8, but is included again for convenience, so reference may be made to it from this section. Similar Excel plots of all useful vehicle mapping test data are included in Appendix AA. Of interest are the exact (to the nearest kilometre per hour) speed column labels and the non-uniformity of the tractive effort points recorded, particularly approaching 2000 N. Ideally, each set of load readings would be registered at an exact speed interval. However, incorrect calibration of the eddy-

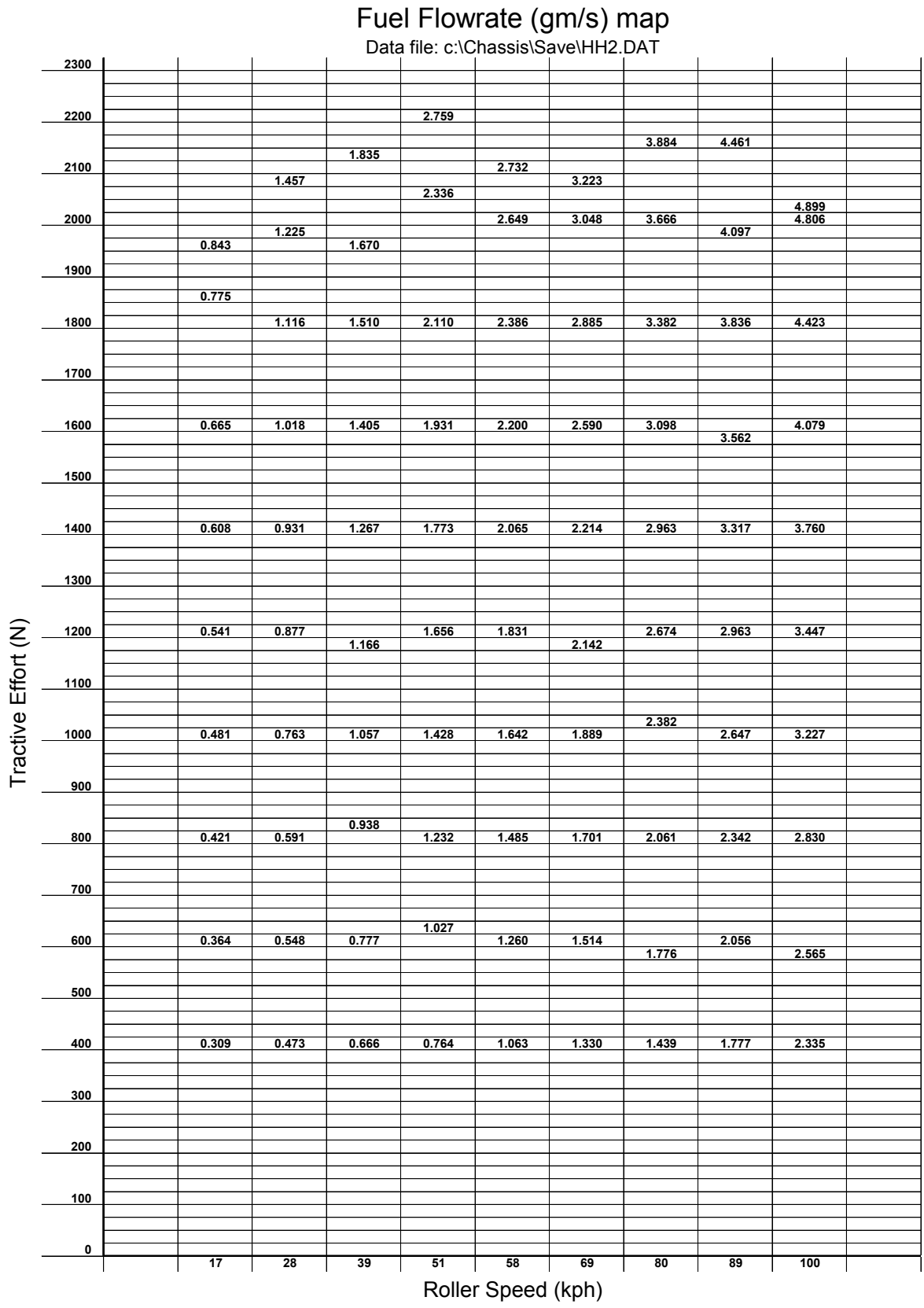

Figure 8.5 Fuel flowrate text map for test vehicle (duplicates Figure 7.8)

current dynamometer speed controller has resulted in average set speeds that are not at the desired 10 kph intervals. This effect was particularly apparent at low speeds, where the dynamometer may not act in a linear fashion. Although this makes comparison with other vehicle data (which may be recorded at the correct intervals) more difficult, useful information is still available, particularly with the use of interpolated plots such as Figures 8.6, 8.7 etc.

Most of the required tractive effort steps below 2000 N were achieved relatively easily with the test vehicle during the mapping test shown in Figure 8.5. However, only four out of eight speed columns include a tractive force at 2000±12.5 N. Note this does not include the data at 17 kph, for which the test vehicle has reached its maximum output below 2000 N. At this position on the throttle, relatively large accelerator depressions with little increase in power were followed by rapid jumps in tractive force. It was thought that this effect was due to static friction in either the vehicle throttle system, or the load cell linkage. Delicate throttle application and approaching the desired tractive effort from above often aided in the fulfilment of these difficult load demands. However, investigation into the tractive effort load cell and linkage friction is recommended to ensure repeatable results in the future.

8.2.3.3 Emissions Equipment

As mentioned previously, the time required to complete a vehicle mapping test was significantly increased when the emissions equipment was functioning. The University of Canterbury Mechanical Engineering Department emissions suite enables measurement of CO, CO_2, unburnt hydrocarbons, and oxides of nitrogen in engine exhausts. For the purposes of this initial chassis dynamometer work, only the Beckman NO_X meter (measuring the concentration of NO and NO_2) was employed. This device was used because it consisted of a stand-alone portable unit that enabled it to be transported to the automotive laboratory and set up for immediate use. The remainder of the emissions equipment is housed in a single cabinet (to which the NO_X meter can be added) containing all the necessary calibration and test gases, and serviced by a single, refrigerated sample line. It is anticipated that the CO, CO_2, and HC units will be added to the chassis dynamometer system in future as required. Sufficient A/D channels and external wiring have been set aside for this purpose. For

the vehicle testing discussed in this chapter, the NO_X meter was supplied by a 4 m section of Teflon tubing with two condensate traps. During changes in engine output, delays of approximately 10 seconds were encountered as the sample exhaust gas travelled down the supply line, through the NO_X meter sample refrigerator, and into the reaction chamber. It was decided that mapping test points should be held by the driver for at least 12 seconds each to ensure sample stability whenever NO_X emissions were to be tested.

As well as the necessary delays at each map point, additional difficulties were encountered during testing with the Beckman NO_X meter. The results from several mapping tests showed that the NO_X concentration measurements gathered in this way were highly variable and perhaps affected by the sample temperature and state of the system pump. For three such mapping tests, the average standard deviation between comparable values from each run was 165 ppm, or 5.9% of the maximum value. That is, if a large number of mapping tests were conducted, 95% of values would be expected to lie within 165 parts per million of the average for that set point. Later tests showed progressively worse repeatability as the pump began to overheat. It was expected that the sample pressure became insufficient under these conditions, and the condition of the NO_X meter pump should be investigated before any further emissions testing is carried out. To ensure a dry exhaust sample, one moisture trap was positioned close to the tailpipe, and a second was included in the NO_X meter flow circuit prior to entry into the reaction chamber. These devices incorporated containers of ice to facilitate condensation, which needed to be refilled during the course of a mapping test. Fresh ice was added—and any condensate removed—at two separate instances, usually between the speeds of 80 and 70 kph, as well as between the 50 and 40 kph data groups (note that the speeds were recorded in descending order). This process will not be necessary once when the entire emissions suite is in use with the accompanying refrigerated sample line. Figure 8.6 shows an example map plot with NO_X concentrations represented by colour contours.

The concentration of nitrogen oxides in the exhaust gas was greatest when the vehicle was under maximum power conditions, and peaks of approximately 2700 ppm can be

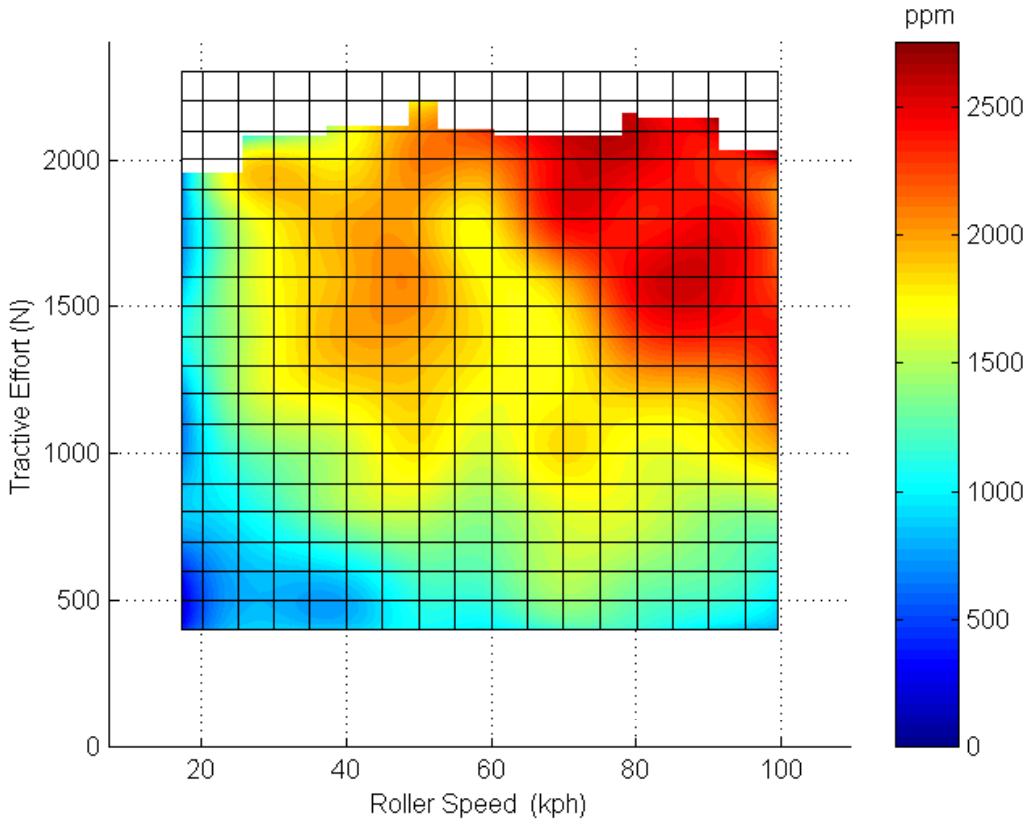

Figure 8.6 NO_X concentration map for test vehicle

seen in the upper right hand corner of Figure 8.6. There is also a secondary area of higher NO_X concentration at speeds near 50 kph with tractive forces above 1200 N.

8.2.3.4 Selected Results

As well as the exhaust emissions, several other useful parameters were measured or calculated from mapping runs on the test vehicle. Fuel consumption is particularly important, and may be expressed in terms of miles per gallon, litres per 100 km, or kilometres per litre (the latter of which is shown in Figure 8.8). Energy consumption, efficiency, and air-fuel ratio also depend on the measured fuel flowrate. Table 8.1 contains a summary of the variation in data at each measured point, combining three separate vehicle mapping tests. Standard deviations are given in their respective units, and as a percentage of the maximum measured value. That is, where an identical load (±12.5 N) and speed point (±1 kph) were present in each of the three runs, the three *z*-values were combined to record a standard deviation (which was then averaged with all the other matching points). Where the load and speed points

did not match, that piece of data was excluded from the averaging. These standard deviations provide a relative measure of the repeatability of each parameter, and several of these results are discussed in the following paragraphs.

	Fuel consumption (km/l)	**Air-fuel ratio (kg/kg)**	**Thermal efficiency (%)**	**Energy consumption (MJ/km)**	**NO_X concentration (ppm)**
Minimum	3.75	12.64	10.16	2.47	382
Maximum	13.54	29.97	30.60	8.90	2790
Average Std. Dev. (units)	0.16	1.03	0.52	0.10	165
Average Std. Dev. (%)	1.2	3.4	1.7	1.1	5.9

Table 8.1 Summary of mapping test data

With the exception of NO_X concentration, the least repeatable of these figures was the air-fuel ratio, in which 95% of the measured points would be expected to match other mapping runs within 1.03 kg/kg (3.4%). This degree of variation was due to unusually large air flowrate readings at low speeds and loads during one of the mapping tests. The maximum calculated air-to-fuel ratio of 29.97 was thought to be unrealistic, but is included here to demonstrate the variable nature of the air-flow measurements. It should be noted that the use of standard deviations to describe the variation between three separate tests is clearly questionable. A larger data set would be required to return useful standard deviation figures, and further work may be necessary to accurately determine the chassis dynamometer data variation.

Air-fuel ratios (and to a large degree, the other parameters) are dependent upon the electronic engine control system (if one is installed) of the vehicle under test. The set up of these systems may be for low emissions during cruising, maximum power, peak efficiency, or a combination of all these. The thermal efficiency, calculated on the basis of fuel energy in and power output at the road wheels, displayed acceptable repeatability during the mapping tests, and an example is shown in Figure 8.7. Peak efficiency was observed at approximately 40 kph and 1800 N tractive force. This load and speed configuration may be encountered during rapid acceleration around city streets. The broad efficiency distribution is evidence of the adjustments made throughout the output range by the engine controller.

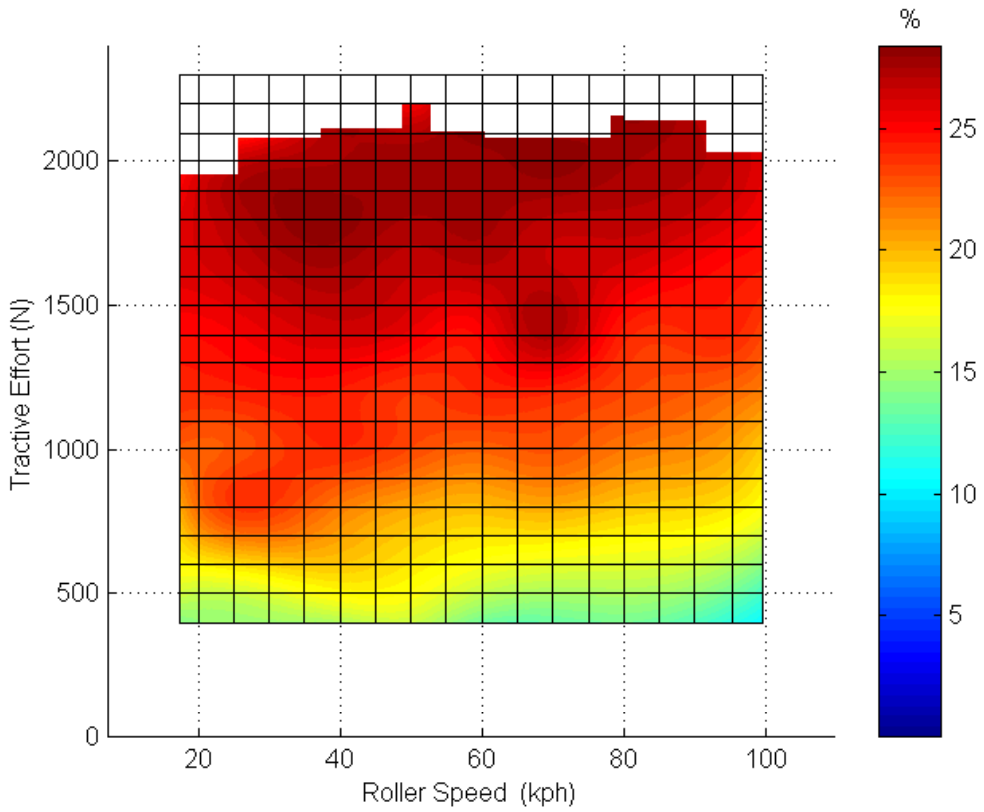

Figure 8.7 Thermal efficiency map for test vehicle

Energy consumption and fuel consumption are both shown in Table 8.1 in terms of distance covered, which is calculated using the velocity. As a result, both display similar trends, with the consumption remaining relatively constant across the entire speed range at each tractive effort set point. Figures 7.6 and 8.4 show the distribution of fuel flowrate (gm/s) over the vehicle mapping range, which takes the form of Figure 8.8 when stated as a function of velocity. Equations 8-5 and 8-6 demonstrate the calculation of fuel consumption (in distance per fuel volume) and energy consumption (in energy per distance) respectively.

$$Fuel\ Consumption = \frac{Velocity}{Fuel\ \ flowrate\left(volumetric\right)} \tag{8-5}$$

$$m/L = \frac{m}{s} \times \frac{s}{gm} \times \frac{gm}{L}$$

$$Energy\ Consumption = \frac{Fuel\ \ flowrate \times Fuel\ energy}{Velocity} \quad (8\text{-}6)$$

$$J/m = \frac{gm}{s} \times \frac{J}{gm} \times \frac{s}{m}$$

As shown in Figure 8.8, the fuel consumption ranged between 4 km/l and 13 km/l for the test vehicle. The average standard deviation for fuel and energy consumption map points recorded in this way was approximately 1%, which was thought to be acceptable.

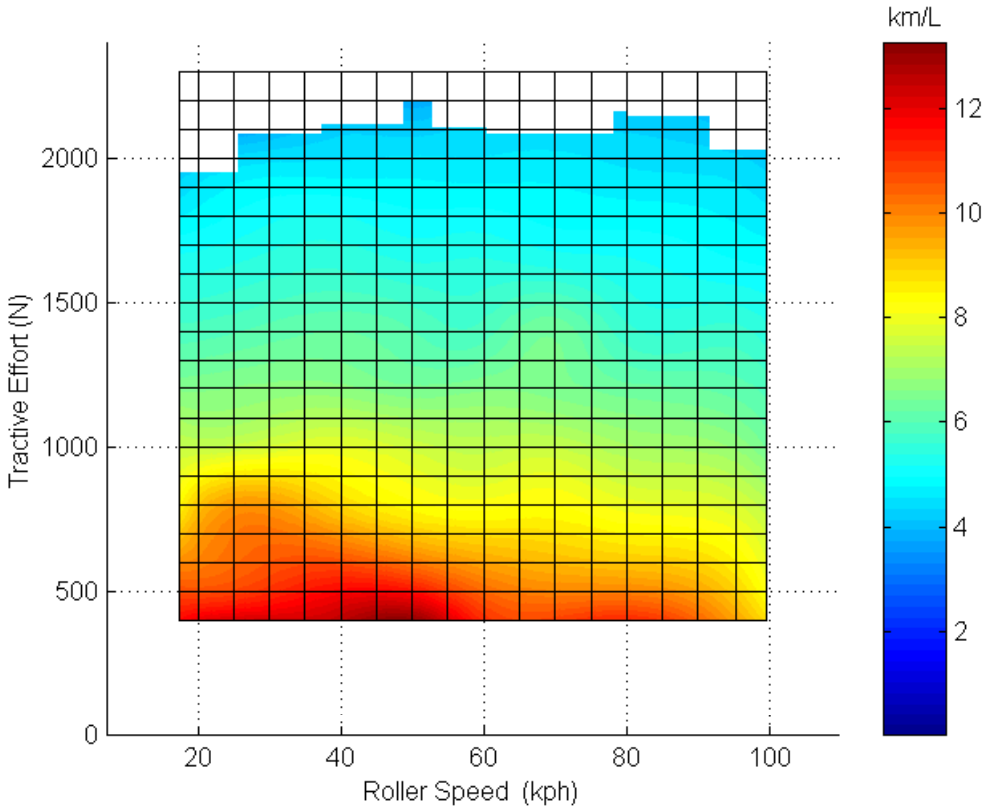

Figure 8.8 Fuel consumption map for test vehicle

8.2.4 Driving Cycle Testing

Proving tests for the driving cycle routine were conducted using the test vehicle and a cycle based on the Economic Commission for Europe (ECE) R15.04 Schedule. The chosen cycle simulates city driving in a similar way to the ECE R15.04, with a maximum speed of 50 kph, but the acceleration phases are generally more rapid. The test cycle was chosen because it was relatively brief (<7 mins) and simple, with

linear accelerations and decelerations between constant speed sections (as in the ECE R15.04). The straight-line nature of the various cycle phases (see Appendix U) enables an accurate diagnosis of chassis dynamometer faults and response characteristics, as shown in Figure 8.9.

Many driving cycle runs were completed during the testing and debugging of the system, enabling the driver to become more proficient at following the cycle while driving the test vehicle. During several early driving cycle runs, between 10 and 20 seconds were spent outside the allowable speed and time limits (referred to as excursion time in Sections 6.5.12 and 7.1.4). However, during the three driving cycle tests for which the results are analysed below, a minimum excursion time of 2.6s and an average of 4.6s was achieved for limits of ±1 kph on speed and ±0.5s on time. The SAE Recommended Practice, J1634 [1999] for electric vehicle testing, and Australian Standard AS 2877 [1986] both specify tolerances of ±3.2 kph and ±1s. However, none of the tests included in Table 8.2 recorded speeds outside these limits, and the tighter tolerances were imposed so some indication of the variation in cycle following might be observed.

Although each of the driving cycle tests discussed in this section contained departures from the prescribed speed sequence, the results were generally highly repeatable. Table 8.2 summarises three driving cycle runs over the test cycle. Standard deviations are provided in terms of the appropriate units and as a percentage of the average over three runs. The cycle distance was calculated by multiplying the average speed by the total cycle time (390 sec).

	Distance (m)	**Average Speed (kph)**	**Total Fuel (litres)**	**Energy Output (MJ)**	**Cycle Excursions (seconds)**
Run 1	1974.34	18.225	0.215	1.0233	2.6
Run 2	1980.28	18.279	0.221	0.9147	5.4
Run 3	1965.23	18.141	0.221	0.9323	5.9
Average	1973.28	18.215	0.219	0.9568	4.6
Ideal cycle	1978.60	18.264	-	1.0021	-
Std. dev. (units)	7.58	0.070	0.003	0.058	
Std. dev. (%)	0.4	0.4	1.6	6.1	

Table 8.2 Driving cycle results summary

The total distance travelled (numerically integrated from the velocity record) and average speed over the entire cycle were both within 0.3% of the actual driving cycle values, and exhibited excellent repeatability between runs. However, energy output totals were 4.5% lower on average than the value predicted by the vehicle energy consumption modelling routine discussed in Section 7.2 (using an idle power of 1000 W). In addition, significant variations about the mean energy were experienced. Initially, dynamometer lag (as shown in Figure 6.17) was thought to be the cause of these lower energy totals. However, the inertial load compensated for by the power absorber was relatively small, and the error introduced by this delay in the onset of dynamometer load was estimated at less than 5000 J (0.005 MJ). Selection of idle power may also affect this result, although it was thought that small changes in idle power magnitude would not have a major effect, since both the actual and modelled energy values take this into account in the same way. A more likely cause for the higher energy prediction was in the assumption of vehicle mass (including the rotational inertia approximation), which has consequences during the MATLAB modelling of the ideal energy output, as well as the flywheel settings and dynamometer driving cycle road load calculation. Trial and error adjustment of vehicle mass may lead to a closer estimate of the driving cycle energy output.

Figure 8.9 gives an example of a typical driving cycle sequence, showing the accuracy of the speed following, the engine speed, and fuel flowrate over a brief time period. All three plots show the same time interval for a single test, so response times can be observed by comparing vertically. The section of the cycle selected includes a constant acceleration from stationary in first gear, then a change into second gear followed by another acceleration and a constant speed period (in third gear). Figure 8.9a demonstrates several of the key issues in driving cycle demand following on the dynamometer. All points on this speed plot are within the allowable speed and time limits (±1 kph, and ±0.5s) although the departures at the 249 sec and 257 sec appear to be close to these limits. The oscillations observed between 257 sec and 260 sec were produced as a rapid decrease in acceleration (0.94–0 m/s^2) excited torsional vibrations in the chassis dynamometer shaft. In general, the most difficult portions of a driving cycle for the driver were accelerating from stationary, and changing gears before a constant speed section (as illustrated at 257 sec). Constant decelerations

under braking (not shown) and accelerations at higher speeds (252–256 sec) lead to less cycle excursions than the aforementioned speed demands.

Engine speed is presented in Figure 8.9b, which shows some of the electrical noise blips and variations that were typical of the inductive loop spark plug pickup. Engine revolutions per minute can be seen to rise and fall as the accelerator and clutch are applied to engage first gear (244–247 sec), second gear (251–252 sec), and third gear (257–258 sec). As expected, engine speeds vary according to road speed when the clutch is engaged during acceleration and constant speed sections.

Fuel flowrate as measured by the Fluidyne flowmeter (see Appendix C.6 for set up) is shown in Figure 8.9c. A predictable relationship between engine speed and fuel flowrate is observed with minimal lag during the rapid transients enforced by gear changes (compare engine rpm and fuel flowrate at 250–252 sec and 256–257 sec). The apparently slow decrease in flowrate following the shift to third gear (257 sec) was attributed to the increased power output (without significant change in engine speed) as the vehicle accelerated between 257 sec and 259 sec. The noise present in the Fluidyne flowmeter signal was typical of results during testing, but was not thought to be restrictive, as fuel flowrate values are usually averaged. Table 8.2 includes the average and standard deviation of the fuel consumption over the three sample driving cycle runs. The figure is expressed here in terms of total fuel consumed in litres, which is integrated from the average flowrate, and converted using the specific gravity of the fuel (0.743 kg/l). The standard deviation of 1.6% represents acceptable repeatability, and the 0.22 litres of fuel consumed equates to an average of 9.0 km/l. Fuel flowrate values over the course of the driving cycle testing reached a maximum of 1.60 gm/s at 49 kph in third gear. This flowrate and speed corresponds to a load of approximately 1200 N in the vehicle maps shown in Figures 8.4 and 8.5.

8.3 Dynamometer System Performance

This section gives an indication of the chassis dynamometer performance, in terms of equipment and software, based on the proving tests discussed in Section 8.2.

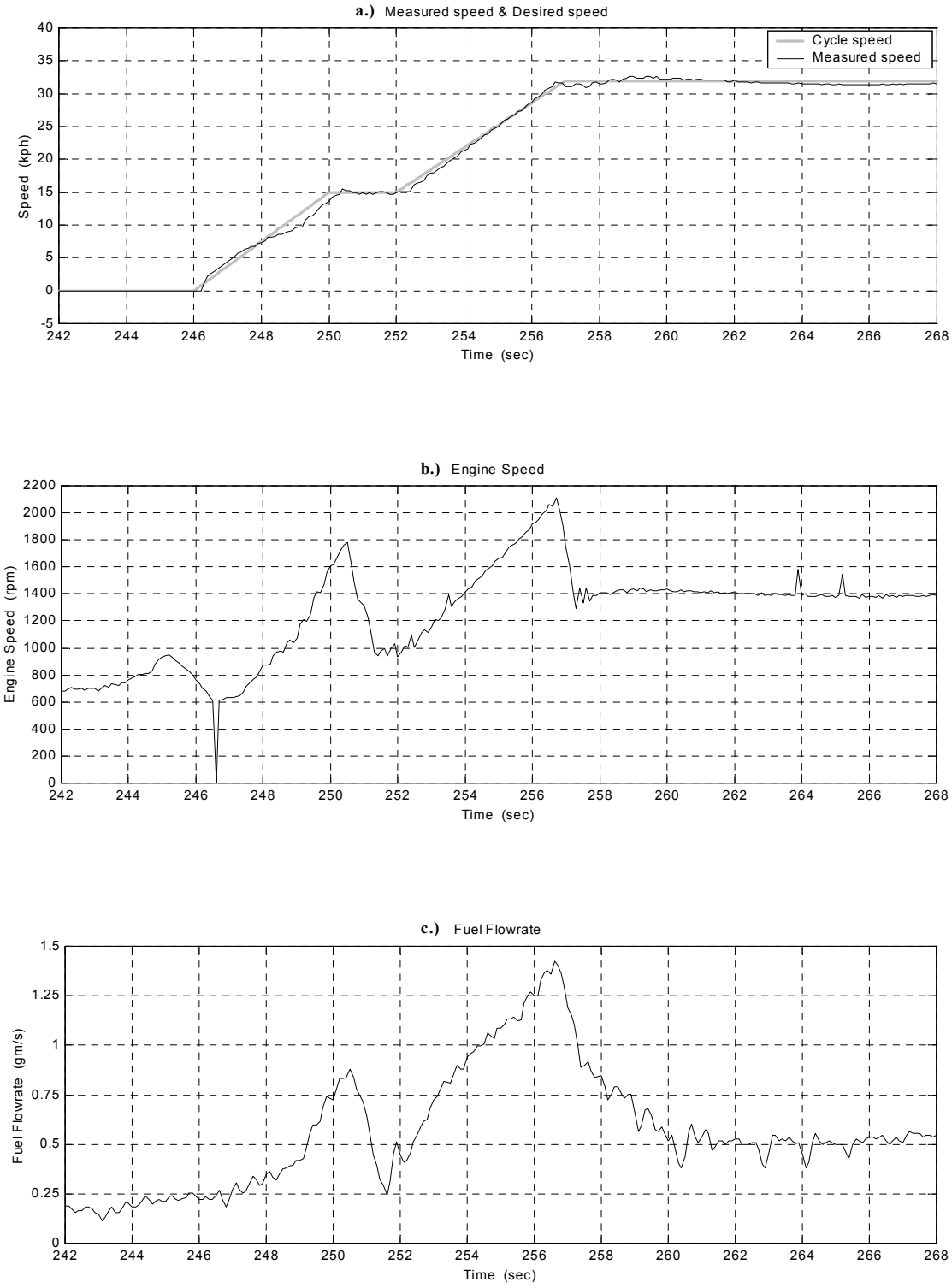

Figure 8.9 Sample driving cycle sections **a.)** Cycle speed and measured speed **b.)** Engine speed **c.)** Fuel flowrate

8.3.1 Chassis Dynamometer Capacity

The 1982 Toyota Celica used during testing was considerably older than the average passenger car in New Zealand at the time of writing. Newer vehicles, particularly high performance automobiles, were expected to significantly exceed the maximum power output of the test vehicle. Also, testing with larger vehicles such as light trucks may be desired in the future, which would require a greater equivalent mass from the flywheels.

In terms of speed, the maximum velocity attempted in the sample mapping tests was 100 kph. The dynamometer flywheels are rated to 120 kph, and lower gears may be engaged on the test vehicle to decrease the maximum speed requirement. Speeds up to 200 kph may be reached with no flywheels attached. It was expected that no driving cycles representing New Zealand conditions would contain speed demands in excess of 120 kph, and a maximum road load simulation speed of 120 kph was thought to be sufficient.

The chassis dynamometer was originally designed for a maximum power absorption of 300 kW, which is determined by the capacity of the Froude eddy-current dynamometer. The test vehicle produced less than 60 kW (20% of capacity), and it is again expected that most non-specialist applications will fall within the rated maximum power. Similarly, the maximum tractive effort recorded during testing was approximately 2200 N, representing less than 25% of the 10 000 N for which the drum axle load cell may be calibrated. To enhance A/D resolution and calibration accuracy, the signal was amplified such that a maximum of 5000 N tractive effort could be read in, although this setting may be changed if future applications demand greater tractive forces.

The mass of the test vehicle was assumed to be 1150 kg, which was increased to 1290 kg with the addition of driver and fuel weight, as well as a rotational inertia approximation. A flywheel configuration used during driving cycle testing lead to an equivalent mass of 1234 kg for the chassis dynamometer as a whole, which is 69% of the maximum 1794 kg. A range of simulated masses between 664 kg and 1794 kg can be achieved on the chassis dynamometer, which should be sufficient for most passenger cars and some light trucks.

A maximum fuel consumption of less than 5 gm/s was recorded on the test vehicle, whereas the Fluidyne flowmeter is rated up to 20 gm/s. Two Annubar tubes are available to be combined with one of two pressure transducers for the measurement of air flowrates to the vehicle engine. The smaller of the two pressure transducers measures pressures up to 152 mmH_2O, which equates at standard atmospheric conditions to 52 gm/s using the small Annubar tube and 134 gm/s using the larger tube. The larger pressure transducer measures up to 762 mmH_2O, which allows 117 gm/s or 467 gm/s depending on which Annubar tube is utilised. The maximum test vehicle air intake flowrate was approximately 70 gm/s, and was measured using the larger Annubar tube, with the lower capacity pressure transducer, allowing plenty of scope for greater flows.

8.3.2 Software Performance

Most of the major software processes are conducted in the MATLAB post-processing suite, for the analysis of driving cycles and the plotting of vehicle mapping tests. The calculations of total distance travelled and total fuel consumed consist of numerical integrations using a two-point Newton-Cotes (Trapezium) scheme. The average rate over each time interval is calculated and multiplied by the length of the interval. The result is a step-by-step linear approximation of the area beneath the rate curve, which may be prone to error in the presence of rapid changes in rate. However, the repeatability of the fuel consumption and total distance figures quoted in Table 8.2 confirms that—given the cycle-following excursions—the numerical integration technique is satisfactory.

The computer processing time is also of interest, since calculated data is usually required as soon as possible. Programs that were required to traverse the 3901 data points of the test driving cycle file tended to create the greatest delays. For example, opening a driving cycle file and loading all the measured parameters into the appropriate arrays (as per Section 7.1.2) took 17 seconds with the test driving cycle. The vehicle energy consumption routine required 18 seconds to calculate the power at each driving cycle point, compare it to the idle power, and add the energy output to the cumulative total.

The quality of vehicle mapping graphs is dependent upon the number of interpolated points the program must calculate between each of the measured points. The total number of points in each direction on the *x*- and *y*-axis is chosen by the user, and the time taken by the plotting routine (see Section 7.1.3.2) to produce the 2-D contour plot is shown is Table 8.3 below. For example, a 50-point plot consists of 50×50 interpolated points.

Points per axis	50	100	200	400
Computation time (sec)	4	8	20	62

Table 8.3 Vehicle mapping contour plot processing times

Most of the contour plots shown throughout Chapters 7 and 8 have been produced using 350 interpolation points on each axis. Figure 8.10 shows the effect of plotting with only 50 points. The resolution is not as sharp at the top of the plot (where the plotted value falls to zero in the space between two points). Also, the gridlines are drawn to the nearest point, and so appear uneven when insufficient interpolation points are plotted.

The other key factor that relies on computer processor speed is the time intervals used during the C++ data acquisition routines. As stated in Section 6.5.3.1, the program loop must have enough time to complete all its data acquisition, D/A, and screen display functions before the next 0.1 sec (or 0.2 sec, depending on the mode of operation) interval is reached. Although the 'Mapping Test' and 'Driving Cycle' routines operate at 10 Hz, it may be desirable to increase this sampling rate, or to run the 'Manual Control', 'Road Load Driving', and 'Warm Up' functions at greater than 5 Hz. A faster processor than the current AMD-K6/200 chip may be required to facilitate faster loop rates. Other alternatives include more economical screen displays, or running the data acquisition functions on an interrupt basis so that it can receive data at the same time as the control program is carrying out its other functions. These possibilities are further addressed in Section 9.2.

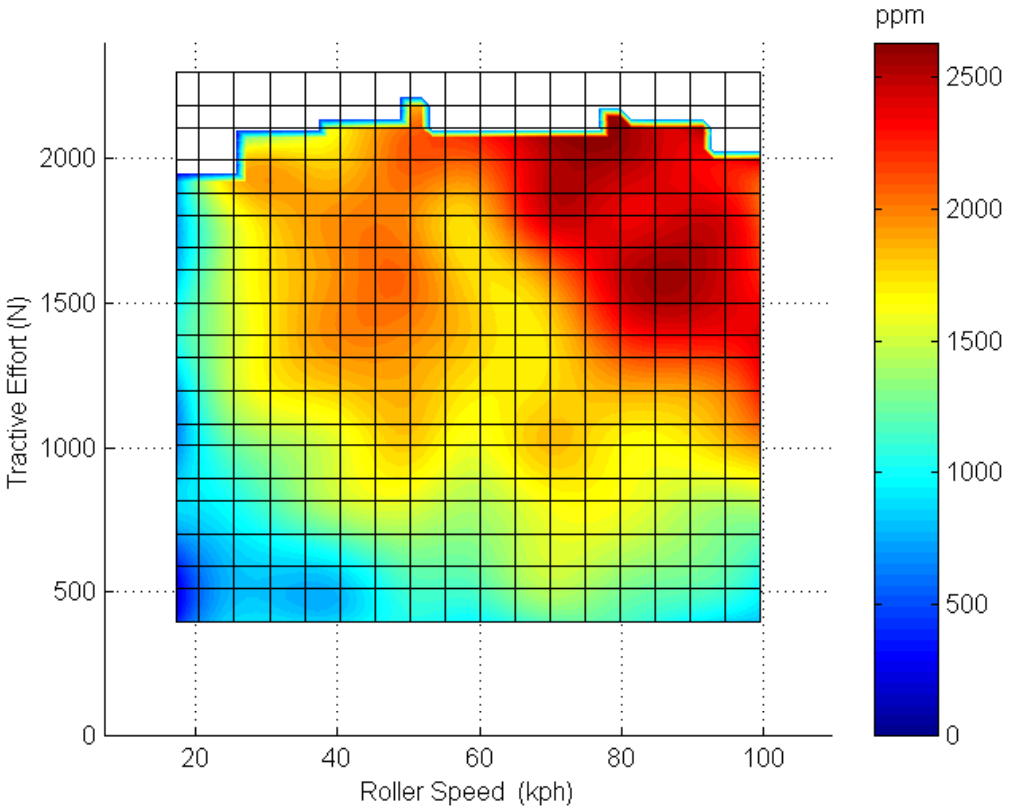

Figure 8.10 50-point interpolation plot of NO_X concentration (c.f. Figure 8.6)

CHAPTER 9:

Future Work and Potential Improvements

9.1 Hardware Improvements

Electrical noise is always a consideration in data acquisition systems. In the chassis dynamometer laboratory, there are two main causes of noise for the data acquisition system: the physical path of the current wiring, and the ineffective earthing of several devices. The display pendant arm that houses the driver's monitor and keyboard also carries potentiometers for manual control of the electric motor and dynamometer, as well and load cell and speed feedback gauges. In addition, the data signal wires for the engine spark pulses, vehicle thermocouples, and fuel flowrate (among others) are connected to the data acquisition system via the pendant arm, which necessitates a significant length of wiring from the end of the arm to wall, across the roof and into the control room.

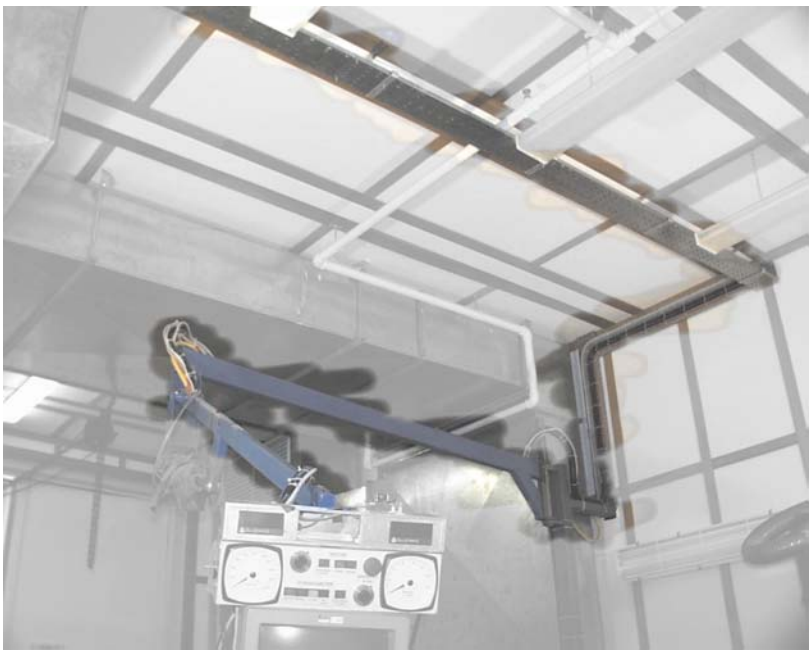

Plate 9.1 Electrical wiring path from driver's pendant arm across laboratory roof

This length acts as an aerial of sorts, picking up interference from outside sources as well. In addition, several floating ground loops exist within the various devices, including the electric motor and power absorber. A common earth should be established between each of the chassis dynamometer instruments, so that ground noise is less of a factor. Alternately, isolation amplifiers could be installed to avoid signal interference.

As mentioned in Section 8.2.3.3, the only exhaust emissions parameter measured during the proving tests was the concentration of oxides of nitrogen. Also, the pump servicing the Beckman NO_X meter appeared to be overheating, and may require some repair work. In future it is expected that all the original exhaust emissions equipment owned by the University of Canterbury Mechanical Engineering Department will be used for chassis dynamometer testing. The cabinet has recently been placed in an appropriate location in the automotive lab, and requires connection of the necessary A/D signal wires, and recalibrating of the CO, CO_2, and HC meters individually.

Section 4.3.1 details the unsatisfactory response of the dynamometer load cell to changes in temperature. Commercial load cells should be equipped with some form of temperature compensation. However, susceptibility of both the eddy-current dynamometer and roller drum load cells to temperature change suggests that these devices are faulty and in need of replacement. The age of these load cells—each over 20 years—may also be contributing to the hysteresis that has been observed in the measurement of dynamometer torque and tractive effort. In addition, problems achieving certain loads during vehicle mapping (see Section 8.2.3.2) were thought to be related to static friction in the tractive effort load cell linkage. Replacement of the load cell may reduce these difficulties, and further investigation into the linkage friction is recommended.

9.2 Data Acquisition Program

The most obvious improvement to the user interface and data acquisition program would be to operate in a Windows environment, as opposed to the current DOS format, which uses the Turbo Vision graphical user interface. The advantages of such a system would include: a user-friendly and familiar appearance, superior memory

management capability, and the capacity to provide data graphing immediately, without the use of additional post-processing applications such as MATLAB. However, switching to a Windows application would require a complete revision of the current source code, and also introduces timing difficulties as discussed in Section 6.2. In either case, the addition of a 'help' function would greatly enhance the usability of the system, especially for untrained operators. The memory constraints imposed by the 20-bit addressing of DOS applications meant that a comprehensive context-specific help—although achievable using Turbo Vision—was not possible for the current chassis dynamometer C++ programs.

Section 6.5.11 includes a description of the vehicle mapping procedure, in which the speed is held constant by the power absorber while each desired tractive effort demand is met in turn. This method requires the driver to control for tractive effort using the accelerator, which is not as natural a function as the speed holding accomplished by a driver on the road. In addition, control of the power absorber in torque mode was found to slightly be more stable than speed control, which was unexpected, and most likely a result of the tuning of their respective analogue controller potentiometers. An alternate mapping configuration calls on the driver to maintain the set speed with each descending load applied by the dynamometer. This method is more difficult at the maximum tractive effort points, as the power absorber torque must be set on a trial and error basis. Using the current system the speed control demand is maintained while the driver increases the load, until maximum throttle is applied, at which point the achieved tractive effort is recorded. With the dynamometer in torque control mode, the maximum tractive effort would be found by applying full throttle and adjusting the power absorber load until the speed began to drop away. It was thought that this adjustment could not easily be carried out under computer control, although future investigation may produce a stable routine.

Another important factor is the speed at which the computer operations are carried out. A faster processor may facilitate an increase in sampling rate, particularly during Manual Control and Road Load Driving modes, which are currently updated at the rate of 5 Hz. More efficient—or perhaps lower level—code may also enable faster sampling of A/D data, and user feedback on screen. Without introducing a faster

processor, the current routines may be improved by decreasing the amount of data displayed on-screen, or operating the data acquisition functions independently of the main program loop. With the use of hardware timing and interrupts, the PCL-812PG can perform data sampling functions at the same time as the computer processor is operating on the other program code. This would provide a significant improvement on the current scheme, which starts the data acquisition function, then waits until it is complete before continuing. However, there may be some difficulties implementing separate interrupt-based data sampling of the PCLD-889 daughter board, which requires a different digital output from the computer (via the PCL-812PG) to switch between each of the multiplexed channels.

Writing of the sampled data to a file also limits the operating speed of the control program. During each data acquisition loop, the new data is written to a predefined file, which is stored on the computer hard drive. A finite time period is required for the head to access any given location on the hard disk. This data-saving time period may be greatly reduced by saving to a temporary file in the computer's random access memory (RAM) during data recording processes. An imaginary drive may be created in RAM, which can be saved to in exactly the same way as the hard drive, or a floppy disk, but without the head-tracking time required for these operations. After the test run is complete, the data may be transferred from the temporary file to a file on the hard drive for permanent storage.

9.3 Post-Processing Software

The MATLAB calculation and plotting routines described in Chapter 7 have been used effectively to produce the results contained in Chapter 8, and may continue to be used without alteration. However, the stand-alone vehicle energy consumption modelling (VECM) program could be improved. At the present time, the VECM routine reads data from single-column files of cycle speeds or power measurements. These files must be manually 'cut-and-pasted' from the full test data files, which contain header information and recorded data from all the measured parameters. The addition of the VECM functionality to the existing suite of post-processing routines would enable menu-driven file selection and the reading of data from complete test data files.

CHAPTER 10:

Conclusion

The University of Canterbury chassis dynamometer has been described in this thesis, including the physical system configuration, inertia and friction calibration techniques, and control software. Although equipped to do so, the chassis dynamometer had not been used under computer control since being shifted to its present location in the Mechanical Engineering Department automotive laboratory. The work detailed in this thesis involved the preparation of the equipment for vehicle testing, and the accompanying software required to record and analyse test results.

With reference to the system equations of motion, various methods of determining the chassis dynamometer inertia and frictional characteristics have been described. Simultaneous solving of several coastdown runs was selected as the most appropriate method of inertia and friction determination in light of the performance of the ASEA electric motor, especially at low speeds. The inertia of the roller drum assembly has also been found by a similar method, enabling accurate representation of vehicle tractive force using the drum axle load cell.

Data acquisition and dynamometer user interface software has been written in C++, and has been described with reference to the memory constraints, and Turbo Vision visual display format that is a feature of this DOS application. The data sampling, digital-analogue demands, writing to file, and screen updates are timed using a Universal Pulse Processor card, and occur at 0.2 sec or 0.1 sec intervals depending on the mode of operation. Routines were created for warming up of the chassis dynamometer and vehicle, and for general testing, including a function which enables full throttle accelerations for determining maximum vehicle power output at the road wheels.

The ‘Mapping Test’ function allows the user to produce a map of vehicle performance over a wide range of tractive effort loads and speeds. The software program also includes a driving cycle routine, which allows a driver to execute speed patterns in a vehicle on the dynamometer by following a scrolling demand trace on the display monitor. Allowable speed and time errors may be specified, and sample tests using a driving sequence based on the ECE R15.04 urban cycle indicated that zero error speed following was possible, within certain limits.

Several data analysis and calculation programs have been written using MATLAB, and the program structure has been described, including the available menus and how the selected files are read into matrices from which they may be edited or graphed. Specialised routines are available for the plotting of the maximum power curves and vehicle mapping tests displayed throughout this thesis. Software has also been written for the purpose of comparing the ideal driving cycle power with measured outputs. The predicted total energy output was found to be 4.5% greater than the average energy consumption calculated from several test runs.

Vehicle power, mapping and driving cycle tests were conducted using a 1982 Toyota Celica, with a view to determining the accuracy and repeatability of the chassis dynamometer. Maximum power at the road wheels was determined in several full-throttle acceleration tests, which yielded peak power measurements with a standard deviation of 1.0%. Mapping tests were also carried out on the test vehicle to determine the instrumentation accuracy and suitability of the method in general. Satisfactory repeatability was observed for the measurement of velocity, fuel flowrate, dynamometer torque and tractive effort. Calculations of fuel consumption, thermal efficiency and energy consumption also yielded standard deviations of approximately 1%. However, the Annubar air flowrate equipment exhibited some unpredictability, and substandard results were obtained from the Beckman NO_X meter. The latter was thought to be the result of a blockage in the system, which may be remedied by overhauling the sample pump. Driving cycle data also proved to be sufficiently repeatable for meaningful testing to be conducted on the chassis dynamometer. For the three test cycle runs discussed in Chapter 8, the average

vehicle speed was within 0.05 kph of the prescribed cycle average, and the total fuel consumption figures exhibited a standard deviation of 0.003 litres (1.6%).

The inability of the Froude eddy-current power absorber to generate torque at zero velocity lead to the implementation of a software routine—included in the driving cycle dynamometer demand calculation—that disabled the demand output during deceleration or stationary periods. A 2 second lag in power absorber response was still evident, but overshoot was decreased by 90% in some cases and it was thought that the dynamometer provided satisfactory road load simulation for effective driving cycle testing.

Several key improvements to the system have been suggested in Chapter 9, including rewiring to decrease signal interference, and a number of ways in which the processing time required by the data acquisition routine could be minimised. However, the chassis dynamometer system has all the necessary hardware and software for a wide variety of focussed vehicle testing. In the future, it is expected that the chassis dynamometer will be used in the development of alternative fuels and new vehicle technologies, as well as tuning and performance tests on existing cars and light trucks.

References

AS 2877 (1986) *Methods of Test for Fuel Consumption of Motor Vehicles Designed to Comply With Australian Design Rules 37 and 40*. Standards Association of Australia

AutoData Ltd. (1990) *Technical Data: Tune Up and Specifications for Passenger Cars and Light Commercial Vehicles*. Maidenhead (England)

Burke, C.E., Nagler, L.H., Campbell, E.C., Zierer, W.E., Welch, H.L., Lundstrom, L.C., Kosier, T.D., McConnell, W.A. (1957) *Where Does All the Power Go?* S.A.E. Transactions, 65

Castro, F.A. (1989) *Automobile Fuel Consumption Estimates: ECE and EPA versus Real World*. Proceedings of a seminar organised by the commission of the European Communities, Directorate General for Energy, May 1988

Coomber, I.M. (1988) *Toyota Celica Owners Workshop Manual : (Feb 1982 to Sept 1985, all models, 1972cc)*. Sparkford, Nr. Yeovil, Somerset, England : Haynes

Elliot, D.R., Klamp, W.K., Kraemer, W.E. (1971) *Passenger Tire Power Consumption*. S.A.E. Transactions No. 710575

Epps, I.K. (1987) *Vehicle Energy Consumption Modelling*. University of Canterbury Department of Mechanical Engineering, Final Year Project 1987/63

Fraleigh, J.B., Beauregard, R.A. (1990) *Linear Algebra*. (2nd Edition) Addison-Wesley Publishing Company

Franklin, G.F., Powell, J.D., Emami-Naemi, A. (1994) *Feedback Control of Dynamic Systems*. (3rd Edition) Addison-Wesley Publishing Company

Froude Consine (2001) Website: *www.fki-eng.com/index.cfm?company=fc*

Hindin, P.J. (1984) *Comparison of Fuel Consumption Driving Patterns*. University of Canterbury Project 710/05/2

Hindin, P.J. (1985) *The Determination of Motor Vehicle Road Load*. Master of Engineering Thesis, Department of Mechanical Engineering, University of Canterbury

Hindin, P.J. (1986) *Vehicle Driveability Assessment using a Chassis Dynamometer.* IPENZ Transactions Vol.13 No.3/EMCh

NZS 5420 [withdrawn] (1980) *Methods of Test for Fuel Consumption of Cars.* Standards Association of New Zealand

Raine, J.K. (1981) *The Design of a Chassis Dynamometer for Programmable Vehicle Testing.* NZIE Transactions Vol.8 No.1/EMCh

Rototest (2001) Website: *www.chassisdynamometer.com*

SAE J1082 (1995) *Fuel Economy Measurement Road Test Procedure*. SAE Standard, Jun95. Society of Automotive Engineers, Inc.

SAE J1263 (1996) *Road Load Measurement and Dynamometer Simulation using Coastdown Techniques.* SAE Recommended Practice, Feb96. Society of Automotive Engineers, Inc.

SAE J1506 (1993) *Emission Test Driving Schedules.* SAE Information Report, Apr93. Society of Automotive Engineers, Inc.

SAE J1634 (1999) *Electric Vehicle Energy Consumption and Range Test Procedure.* SAE Recommended Practice, Apr99. Society of Automotive Engineers, Inc.

Schenck Pegasus GmbH (2001) Website: *www.schenck.net/PEGASUS/indexe.htm*

Taylor Dynamometer (2001) Website: *www.taylordyno.com*

Wheeler, D.J. (1963) *Principles of Vehicle Selection*. S.A.E. Transactions, 71.

White, R.A., Korst, H.H. (1972) *The Determination of Vehicle Drag Contributions from Coastdown Tests*. SAE Technical Paper Series 720099.

APPENDIX A:

Flywheel Equivalent Mass Combinations

The table below shows all the possible equivalent mass increments that may be achieved with the chassis dynamometer flywheel set. Asterisks indicate that the flywheel (or hollow shaft) is engaged. A description of the flywheel set is included in Section 2.2.

Hollow shaft	110 kg	220 kg	230 kg	450 kg	**Equivalent mass (kg)**
					664
*					784
*	*				894
*		*			1004
*	*	*			1114
*		*	*		1234
*	*	*	*		1344
*		*		*	1454
*	*		*	*	1574
*		*	*	*	1684
*	*	*	*	*	1794

Table A.1 Flywheel combinations and resultant equivalent masses

APPENDIX B:

Comparison of Chassis Dynamometer Specifications

See Table B.1 overleaf.

Brand Model	**Schenck[A]** **EMDY 48** (X-Drive)	**Froude[B]** **48 CM CD**	**Taylor[C]** **CM 90**	**Rototest (VPA)[D]** **620 F1 2WD**	**University of Canterbury**
Power capacity (kW)	150	150	373	628	300
Roller diameter (mm)	1219	1220	900	—	1200
Max speed	200 kph	200 kph	137 kph	3000 rpm	160 kph
Driven wheels	2	2	4	2	2
Max Tractive effort	5400 N	4500 N	10800 N	2000 Nm	9150 N
Max Axle Load	2000 kg	N/A	11340 kg/axle	N/A	8000 kg
Software	MS Excel & in-house display	MS Windows NT / modular C++	Windows-based ENGINE Vue ™	Windows display	DOS C++ (Turbo Vision)
Data Channels	150	N/A	24	N/A	16

Table B.1 Comparison of various commercial dynamometer systems with the University of Canterbury chassis dynamometer

N/A = information not available

Source: A Schenck website [2001] (see References)

B Froude Consine website [2001]

C Taylor Dynamometer website [2001]

D Rototest website [2001]

APPENDIX C:

Instrument Calibrations

C.1 Froude Eddy-Current Dynamometer Load Cell

Output: ±10 V

A/D configuration: PCL-812PG ±10 V

Estimated measurement uncertainty: ±1 Nm

Static calibration was first carried out with the dynamometer load cell in compression. That is, in the direction of positive rotation as defined in Chapter 3. The A/D signal was recorded as each known mass was added sequentially then removed from the dynamometer calibration arm. The linear fit was calculated using a least squares approximation.

Total Mass (kg)	Torque (Nm)	A/D signal (bits)
0.00	0.00	2050
22.68	113.35	1751
45.32	226.53	1451
68.00	339.91	1149
90.64	453.11	848
113.36	566.66	545
90.64	453.11	846
68.00	339.91	1147
45.32	226.53	1448
22.68	113.35	1749
0.00	0.00	2049

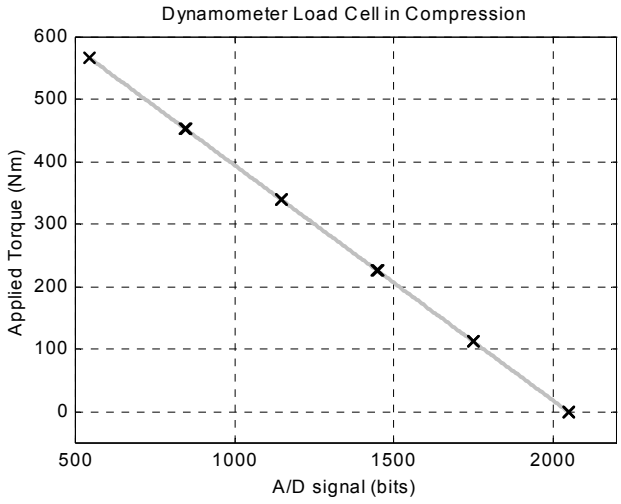

Table C.1 and **Figure C.1** Dynamometer load cell calibration in compression

$$\textit{Compression Torque}\,(Nm) \;=\; -0.3766 \times \textit{bits} + (\textit{Zero Constant}) \qquad \text{(C-1)}$$

Note: The *Zero Constant* (772.1 during calibration) is replaced when rezeroing the load cell to account for temperature differences (see Section 4.3.1).

The error in this A/D measurement was determined by calculating the difference between the load cell torque (as determined by Equation C-1) and the actual applied torque. The following graph shows the hysteresis evident during these static calibrations. Also, it was apparent that the calibration multiplier and constant (-0.3766 and 772.1 above) in compression were not appropriate for use when the load cell was in tension.

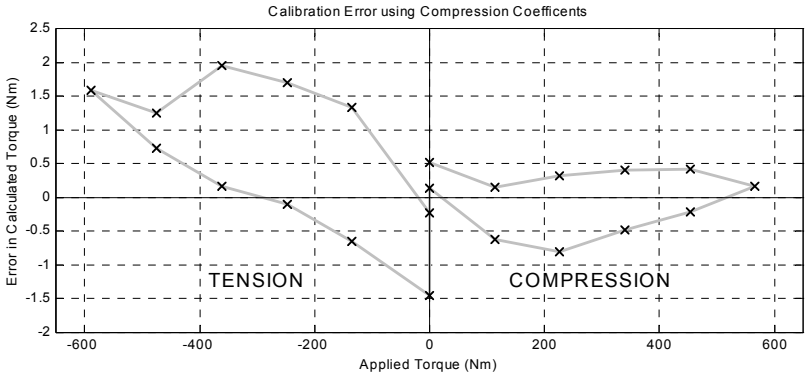

Figure C.2 Dynamometer load cell A/D error using compression calibration coefficients

A separate calibration equation was sought for the load cell in tension (by placing masses on the other side of the calibration arm). During everyday dynamometer operation, the user inputs the expected direction of roller motion during the rezeroing process. The new zero point is then used with the appropriate calibration multiplier in subsequent torque calculations.

Total Mass (kg)	Torque (Nm)	A/D signal (bits)
0.00	0.00	2051
-26.95	-134.72	2405
-49.66	-248.25	2705
-72.32	-361.51	3005
-95.04	-475.11	3309
-117.72	-588.49	3609
-95.04	-475.11	3310
-72.32	-361.51	3010
-49.66	-248.25	2710
-26.95	-134.72	2410
0.00	0.00	2054

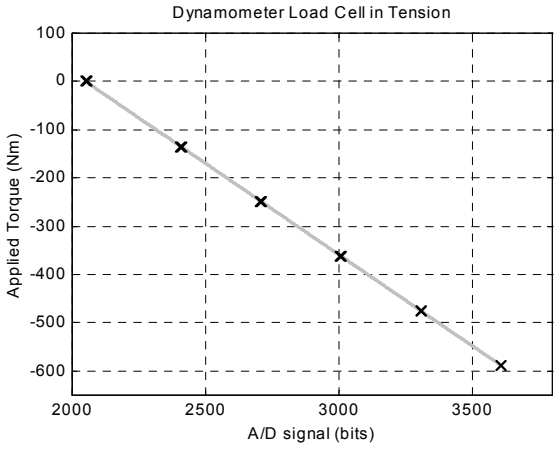

Table C.2 and **Figure C.3** Dynamometer load cell calibration in tension

$$\textbf{\textit{Tension Torque}}\left(\textbf{\textit{Nm}}\right) \;=\; -\mathbf{0.3799}\times\textbf{\textit{bits}} + \left(\textit{Zero Constant}\right) \qquad \text{(C-2)}$$

The difference between the torque calculated using this equation and the actual applied calibration torque is shown below, for loading in tension only.

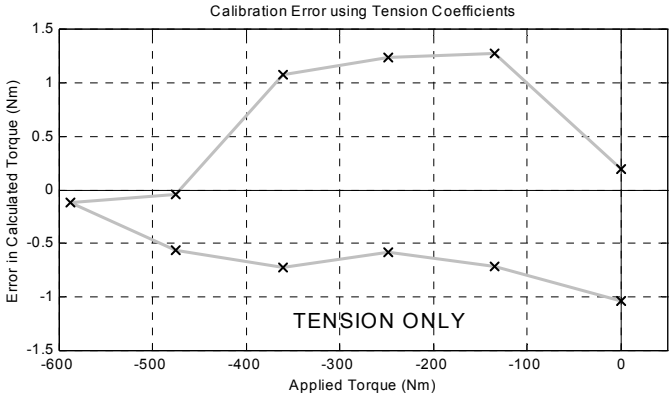

Figure C.4 Dynamometer load cell A/D error using tension calibration coefficients

C.2 Froude Eddy-Current Dynamometer Demand Signal Calibration

Input: -10–0 V

Estimated output uncertainty: ±0.5 Nm in Torque control mode
± 3 kph in Speed control mode

The dynamometer control functions were calibrated using the C++ software routines detailed in Chapter 6. A vehicle was driven on the chassis dynamometer to apply a force at the rollers, which was resisted by the power absorber in either constant speed or constant torque mode. Digital demand inputs were entered in 12-bit form (0–4095) and sent as a negative voltage (-10–0V) to the power absorber by the PCL-812PG.

Demand (bits)	Torque (Nm)
200	46.93
200	46.67
200	46.17
200	46.17
100	22.28
100	22.42
100	22.43
100	22.79
350	80.82
350	80.84
350	80.82
350	80.6
500	115.9
500	115.88
500	115.83
500	115.52

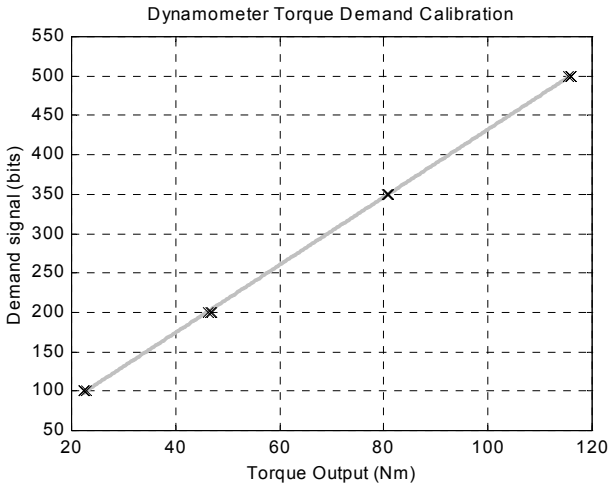

Table C.3 and **Figure C.5** Dynamometer torque control D/A calibration

$$\textit{Demand Bits} = 4.299 \times (\textit{Desired Torque}) + 2.1 \qquad \text{(C-3)}$$

Demand (bits)	Speed (kph)
3500	22.4
3500	24.5
3000	41.2
3000	41.2
2500	58.0
2500	58.0
2000	72.1
2000	72.0
1000	104.7
1000	104.7

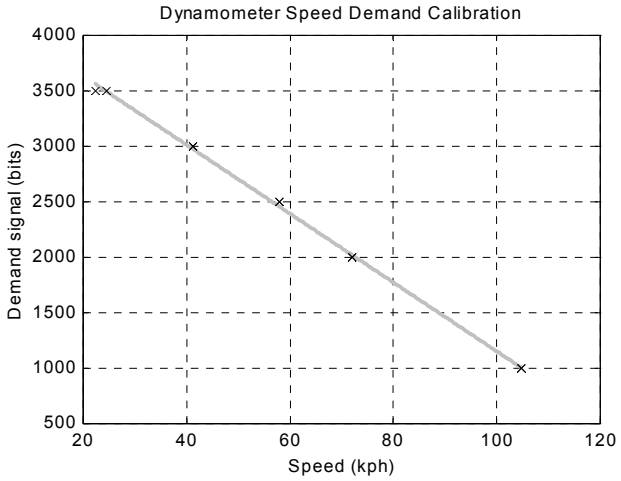

Table C.4 and **Figure C.6** Dynamometer speed control D/A calibration

$$\textit{Demand Bits} = -31.036 \times (\textit{Desired Speed}) + 4257.9 \qquad \text{(C-4)}$$

C.3 ASEA Electric Motor Load Cell

Output: ±5 V

A/D configuration: PCL-812PG ±5 V

Estimated measurement uncertainty: ±2.5 Nm

Static calibration was carried out on the electric motor load cell in both the positive and negative directions. Positive motor torque occurs when the motor is applying a force that will accelerate the chassis dynamometer when is it rotating in a positive direction as defined in Chapter 2. The A/D signal (0–4095) was recorded as each known mass was added sequentially then removed from the calibration arm. The calibration arm may be loaded on either side at any one time, enabling positive and negative torques to be measured.

Total Mass (kg)	Torque (Nm)	A/D signal (bits)
0.00	0.00	2048.6
5.00	24.53	2238.9
10.00	49.05	2435.5
15.00	73.58	2637.4
20.00	98.11	2834.3
25.00	122.64	3032.1
30.00	147.16	3233.5
35.00	171.69	3435.4
40.99	201.04	3681.5
44.97	220.60	3845.6
40.99	201.04	3686.3
35.00	171.69	3443.3
30.00	147.16	3241.4
25.00	122.64	3041.0
20.00	98.11	2842.9
15.00	73.58	2642.5
10.00	49.05	2440.6
5.00	24.53	2243.7
0.00	0.00	2051.9
0.00	0.00	2046.2
-10.00	-49.05	1662.2
-20.00	-98.11	1260.7
-30.00	-147.16	851.9
-35.00	-171.69	645.0
-40.99	-201.04	397.5
-44.97	-220.60	234.0
-40.99	-201.04	393.7
-35.00	-171.69	639.6
-30.00	-147.16	845.6
-20.00	-98.11	1253.2
-10.00	-49.05	1655.2
0.00	0.00	2042.5

Table C.5 Electric motor load cell calibration

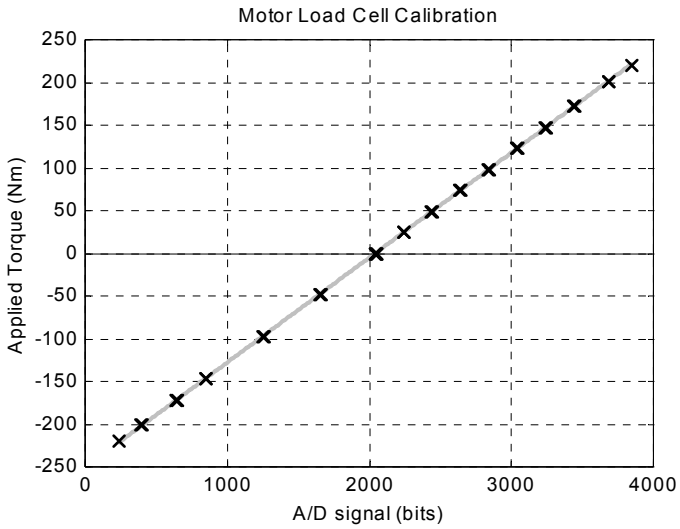

Figure C.7 Electric motor load cell calibration

$$Torque\,(Nm) = 0.1227 \times bits - 250.9 \qquad \text{(C-5)}$$

Errors during calibration were plotted as the difference between the applied torque, and the torque calculated using the previous A/D equation.

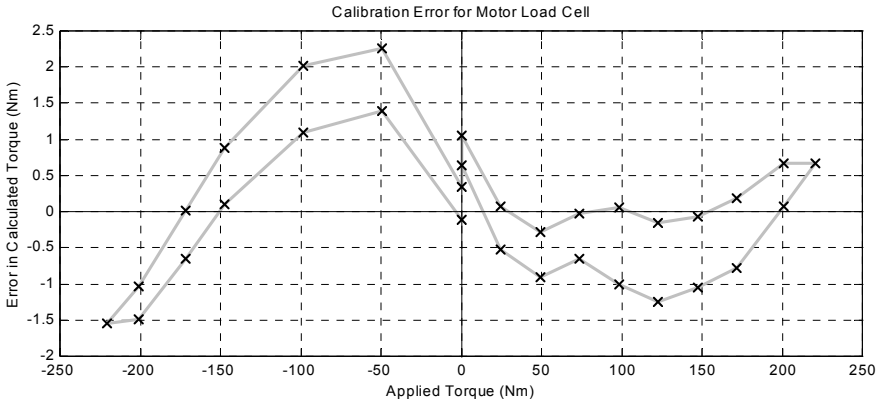

Figure C.8 Error in electric motor load cell A/D calibration in tension and compression

These errors may have been induced by a lack of concentricity in the system, and could have been reduced by applying a cubic fit to the calibration data. However, to simplify the data capture software, the linear approximation shown here was maintained. Because the response of the electric motor precluded its use during testing, a measurement uncertainty of ±2.5 Nm was thought to be acceptable.

C.4 ASEA Electric Motor Demand Signal Calibration

Input: ±10 V

Estimated output uncertainty: ± 2 Nm in Torque control mode
± 2 kph in Speed control mode

The ASEA electric motor was not used during testing (see Section 5.2.3), but required calibration so that approximate torque and velocity states could be achieved while warming up, or prior to dynamometer coastdown tests (see Chapter 6). Digital demand inputs were entered in 12-bit form (0–4095) and sent as a voltage (±10 V) to the electric motor by the PCL-812PG.

Demand (bits)	Torque (Nm)
0	-1.72
400	40.52
800	77.85
1200	114.64
1600	151.78
1600	151.66
1200	114.57
800	77.86
400	40.24
800	73.89
0	-1.43

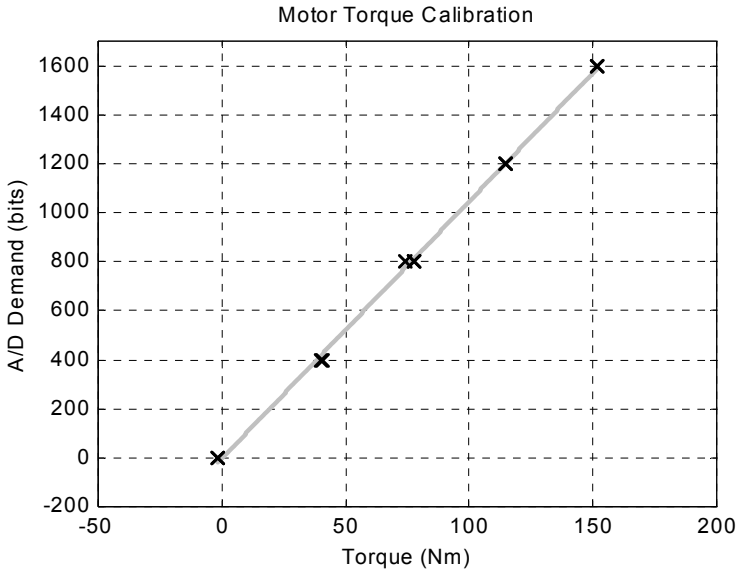

Table C.6 and **Figure C.9** Electric motor torque control D/A calibration

$$\textit{Demand bits} = 10.494 \times (\textit{Desired Torque}) - 1.2 \qquad \text{(C-6)}$$

With the exception of the zero demand points, motor torque was applied while under constant speed control (50 kph) from the power absorber. Torque at zero motor demand was measured at 50 kph while coasting down. The negative value at zero torque is representative of the motor friction, which will vary with velocity. At torque demands greater than zero, this friction is motored out and is indistinguishable from the electromagnetic motoring torque, since a single measurement is made at the motor load cell (see Chapter 5.1).

Demand (bits)	Speed (kph)
0	0.0
600	23.2
1200	47.7
1800	71.2
2400	95.6
3000	119.7
2400	95.5
1800	71.2
1200	47.7
600	23.0
0	0.0

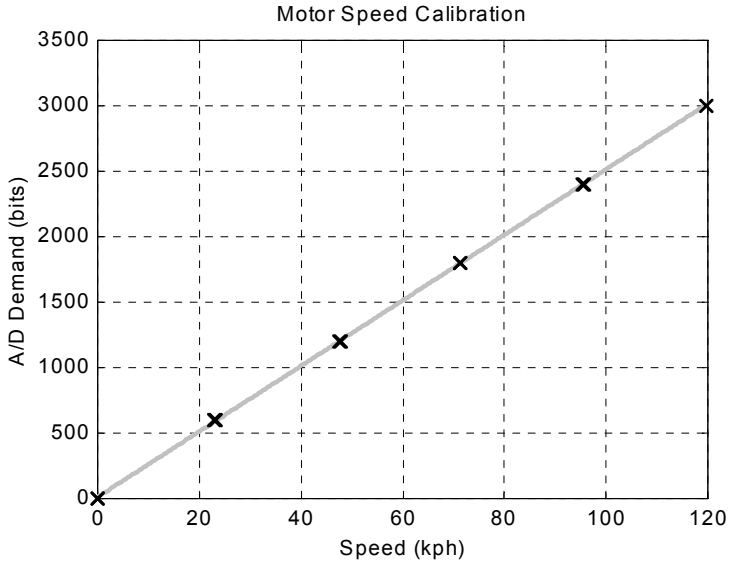

Table C.7 and **Figure C.10** Electric motor speed control D/A calibration

$$\textit{Demand bits} = 25.040 \times (\textit{Desired Speed}) + 9.9 \quad \text{(C-7)}$$

C.5 Tractive Effort Load Cell

Output: ±10 V
A/D configuration: PCL-812PG ±5 V
Estimated measurement uncertainty: ±9 N

As described in Section 4.3.2, the hysteresis of the tractive effort load cell and its associated linkage required a special calibration technique. Known masses were added to the load arm while the roller drums were rotated slowly by the electric motor. A vehicle was positioned on the rollers to prevent lifting of the drum axle from its trunnion bearings. As with the power absorber load cell, it was found that more accurate results could be obtained by calculating a different calibration multiplier for each of the compression and tension states of the load cell. Also, poor temperature compensation required that the load cell software be rezeroed to account for day-to-day temperature differences. Thus, the constant component of the calibration equations included here has been left as a variable. Equations are stated in terms of A/D bits (i.e. 0–4095) with the PCL-812PG range set at ±5 V.

Total Mass (kg)	Force (N)	A/D signal (bits)
0.00	0.00	2044
22.64	1110.25	1746
45.32	2222.80	1446
68.04	3337.46	1146
90.70	4448.74	846
113.41	5562.66	546
90.70	4448.74	845
68.04	3337.46	1145
45.32	2222.80	1444
22.64	1110.25	1744
0.00	0.00	2042

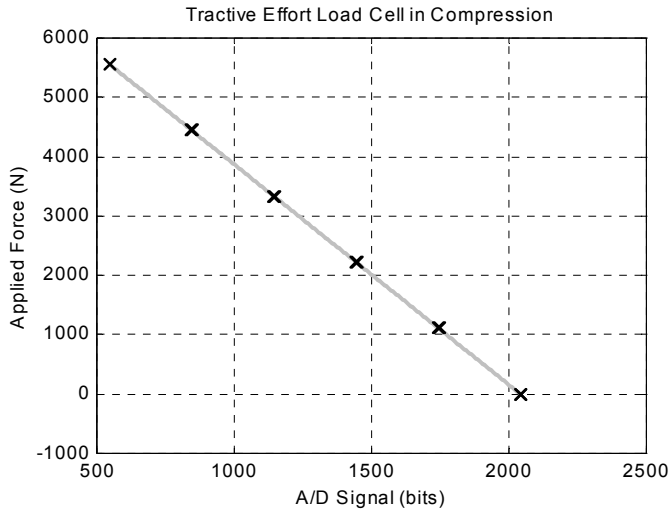

Table C.8 and **Figure C.11** Tractive effort load cell calibration in compression

$$\textit{Compression Force} = -3.715 \times \textit{bits} + \textit{Zero Constant} \qquad \text{(C-8)}$$

The error in this A/D measurement was determined by calculating the difference between the load cell force (as determined by Equation C-8) and the actual applied force.

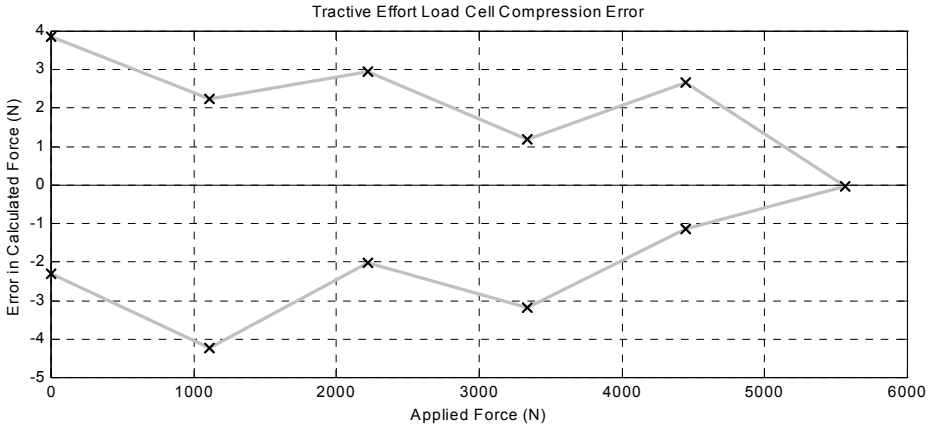

Figure C.12 Error in tractive effort load cell compression calibration

The load cell was loaded in tension in much the same way:

Total Mass (kg)	Force (N)	A/D signal (bits)
0.00	0.00	2044
-22.64	-1110.25	2338
-45.32	-2222.80	2635
-68.04	-3337.46	2933
-90.70	-4448.74	3229
-113.41	-5562.66	3526
-135.83	-6662.36	3821
-113.41	-5562.66	3528
-90.70	-4448.74	3231
-68.04	-3337.46	2936
-45.32	-2222.80	2637
-22.64	-1110.25	2338
0.00	0.00	2044

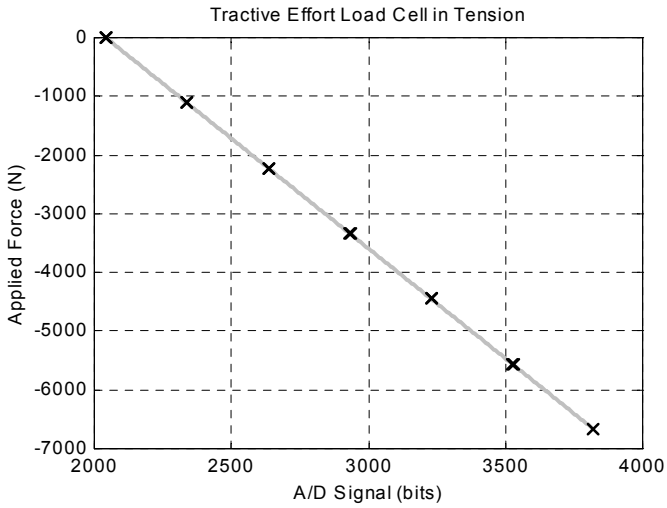

Table C.9 and **Figure C.13** Tractive effort load cell calibration in tension

$$\textit{Tension Force} \quad = \quad -3.747 \times \textit{bits} + \textit{Zero Constant} \qquad \text{(C-9)}$$

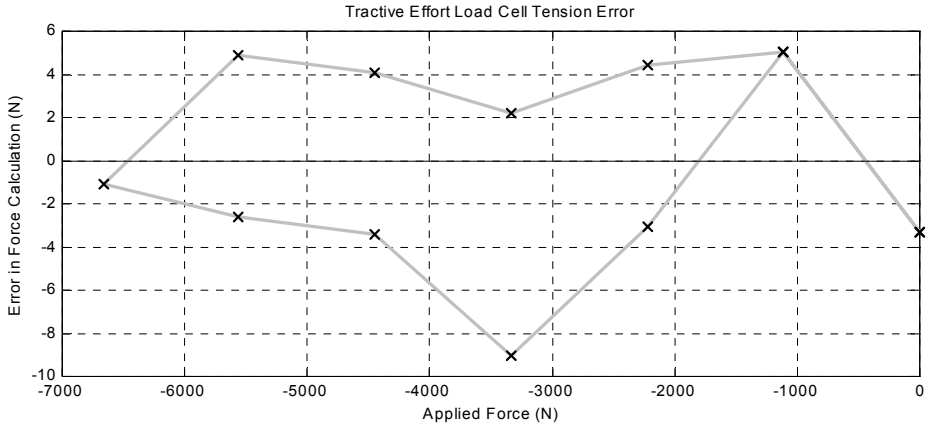

Figure C.14 Error for tractive effort A/D calibration in tension

Note: Both points at zero load, and both at –1110.25 N, overlap in Figure C.14 due to similar readings during adding and subtraction of calibration masses.

C.6 Fluidyne Fuel Flowmeter

Output: 0–5 V
A/D configuration: PCL-812PG ±5 V
Estimated measurement uncertainty: ±0.04 gm/s

Firstly, the flowrate and totaliser were tested against measured fuel quantities in order to test the repeatability, and to set the correct fuel density on the meter's potentiometers. A pump was used to pass fuel from a tank, through the flowmeter, through an adjustable valve, and into a container mounted on a set of electronic scales. The total mass of fuel was weighed and compared to the total indicated on the flowmeter digital display. Experiments were conducted over various time intervals and flowrates, and a density setting of 743 kg/m^3 was found to be appropriate. Human error in starting and stopping the totaliser, as well as the measurement uncertainty in the scales, led to an estimated error of ±0.2 gm at flowrates below 2 gm/s and ±1.0 gm at flowrates greater than 4 gm/s.

Nominal Flowrate (gm/s)	Mass of Fuel (gm)	Flowmeter Total (gm)	Error (gm)	Error (%)	Average Error (%)
1.2	200	200.4	0.4	0.20	
	200	200.2	0.2	0.10	
	240	239.9	-0.1	-0.04	**0.09**
3.5	200	200.5	0.5	0.25	
	200	200.3	0.3	0.15	
	200	200.3	0.3	0.15	**0.18**
5.7	450	449.9	-0.1	-0.02	
	450	448.1	-1.9	-0.42	
	400	398.9	-1.1	-0.28	
	400	398.6	-1.4	-0.35	**-0.27**

Table C.10 Flowmeter totaliser test results

The measurement accuracy for the total fuel reading was assumed to extend to the flowrate, and an uncertainty of ±0.5% was combined with the A/D uncertainty shown in Figure C.16. The A/D performance was assessed using a similar experimental set-up, and comparing the flowrate—as indicated on the flowmeter's digital display—with the A/D signal recorded in terms of bits (0–4095) with a PCL-812PG range of ±5 V.

Digital display (gm/s)	A/D signal (bits)†
0.00	2047.0
0.34	2082.5
0.79	2128.1
1.52	2203.5
2.12	2264.5
2.83	2337.0
3.61	2416.6
4.08	2464.9
4.49	2506.5
4.80	2537.7
5.20	2578.4
5.68	2627.5
6.12	2672.6
6.36	2697.1
6.55	2716.4
6.60	2721.5

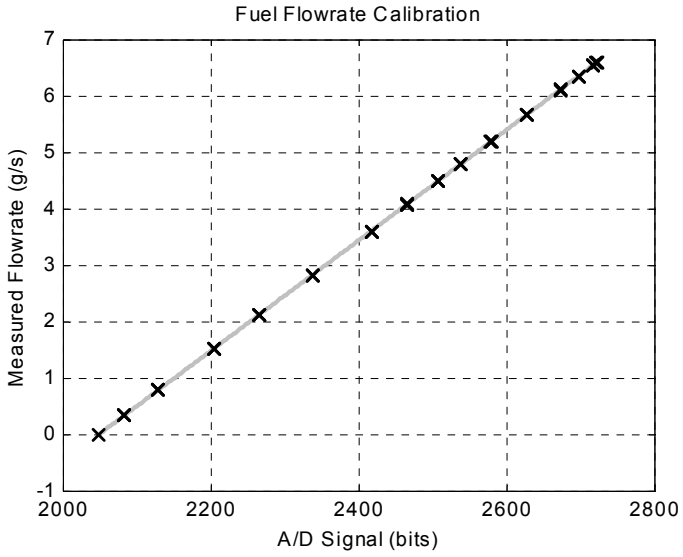

Table C.11 and **Figure C.15** Fuel flowmeter A/D calibration

$$\text{Flowrate}\left(\text{gm/s}\right) \;=\; \mathbf{0.009793} \times \text{bits} - \mathbf{20.05} \qquad \text{(C-10)}$$

† ***Note*****:** Each point included in the above table represents the average of three points recorded at the same flowrate.

The graph below shows the difference between the flowrate indicated by the meter, and the flowrate calculated using the A/D signal.

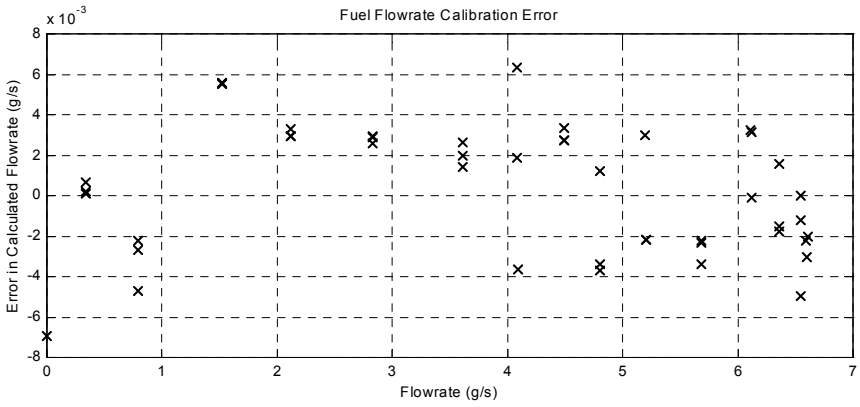

Figure C.16 Error in fuel flowmeter A/D calibration

The measurement uncertainty recorded previously (±0.5%) equates to ±0.025 gm/s at a fuel flowrate of 5 gm/s (the largest rate encountered during the testing detailed in

Chapter 8). Thus, the A/D uncertainty shown here (±0.007 gm/s) is the lesser of the two sources of error. An overall uncertainty of ±0.04 gm/s was thought to be sufficient to include meter accuracy and A/D conversion uncertainty for the measured flowrates.

The MATLAB software routines detailed in Chapter 7 include the facility to calculate the total fuel consumed during a test run. Because the digital outputs from the Fluidyne flowmeter do not include the total mass, the flowrate must be numerically integrated. A two-point Newton-Cotes (Trapezium) integration technique was used, which calculates the fuel mass over each time interval thus:

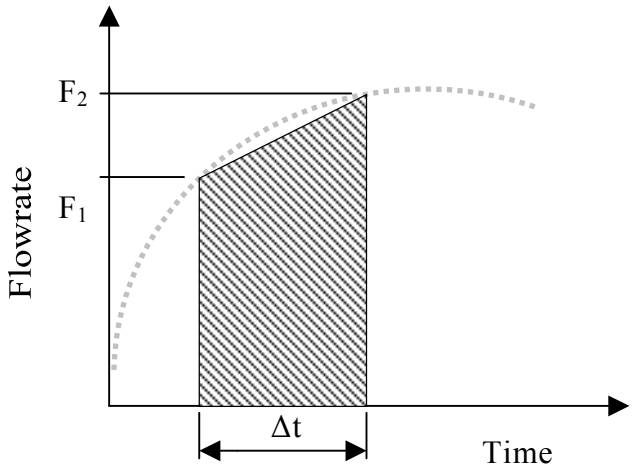

$$Mass = \frac{(F_1 + F_2) \times \Delta t}{2}$$

Figure C.17 Integration of flowrate using the 'Trapezium' rule

Several tests were conducted to determine the effectiveness of this approximation. The fuel was pumped, as per the calibration runs, with the flowrate being varied by a valve. A combination of non-uniform variations (as in Figure C.18) and step changes yielded an average error of 0.2% between the integrated total and the totaliser value recorded by the flowmeter.

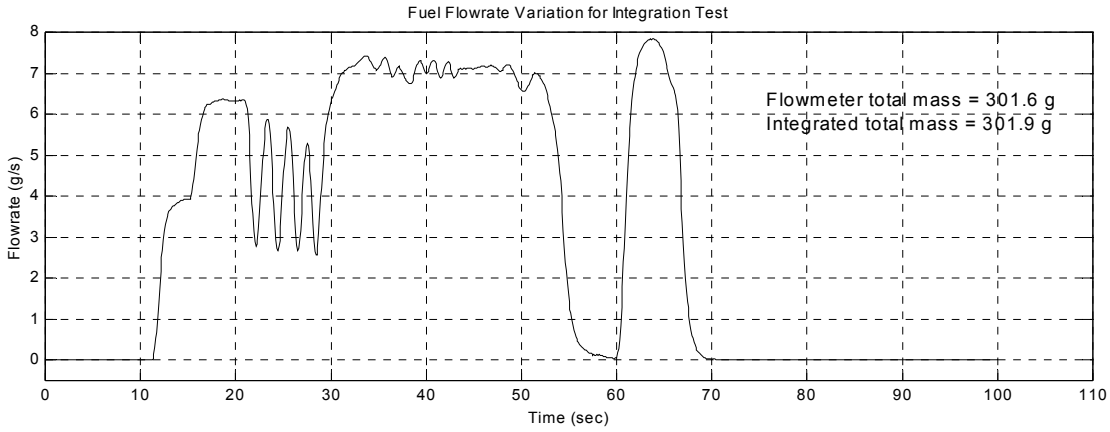

Figure C.18 Example of non-uniform rate test for fuel flow integration

Inserting the Fluidyne flowmeter into the fuel systems of carburetted vehicles involves making a break in the line, and connecting the device in series. Fuel-injected engines often require a different approach. For example, in the case of the test vehicle, the supply line provides fuel to the injector rail at a constant pressure, with a flowrate greater than or equal to the maximum consumption of the engine. Fuel that is not injected into the cylinders is returned to the tank via the return line. Unless both the supply and the return flowrates can be measured simultaneously (by two separate devices), the fuel consumption of the engine cannot be determined by simply inserting a meter in series. A schematic arrangement of the Toyota Celica test vehicle fuel system in Figure C.19 below. Figure C.20 shows the modified fuel flow path, including the Fluidyne flowmeter and adjustable valve used to regulate the supply pressure.

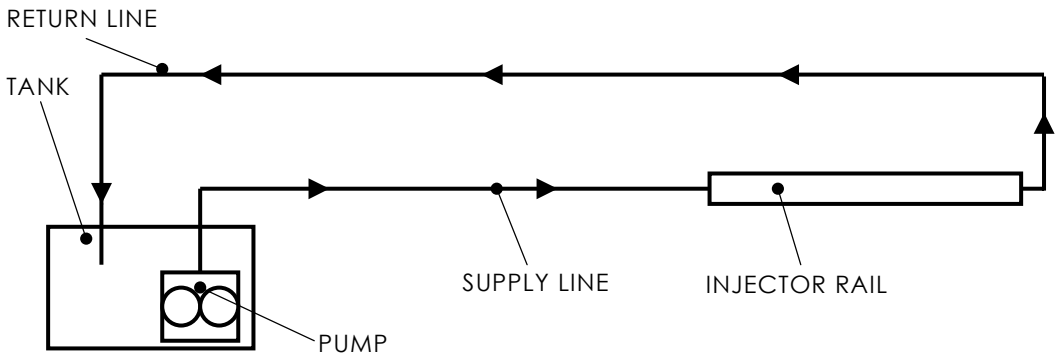

Figure C.19 Test vehicle original fuel system schematic

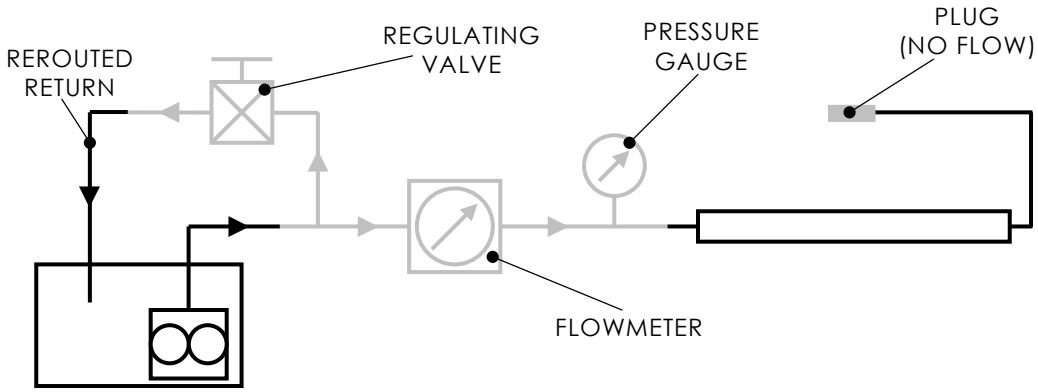

Figure C.20 Test vehicle fuel system reconfigured to include flowmeter

By plugging the return line and providing a path back to the tank *before* the fuel reaches the injectors, all the fuel passing into the injector rail (via the flowmeter) is consumed by the engine. Insufficient pressure at the new return valve will result in too much fuel flowing straight back into the tank. Pressure to the injectors is maintained by adjusting the valve, and monitoring a pressure gauge in the supply line.

C.7 Annubar Flow Sensors with Dieterich Standard Pressure Transducers

Output: 4–20 mA

A/D configuration: PCL-812PG ±5 V

Estimated measurement uncertainty: ±2 gm/s

The two Annubar devices indicate the flowrate by measuring pressure and applying a standard Annubar equation:

$$Flow\left(kg/hr\right) \;=\; \left(Annubar\ Constant\right)\sqrt{\frac{p_{amb}\times p_{Ann}}{\frac{9}{5}\times T_{amb}+492}} \qquad \text{(C-11)}$$

Where: p_{amb} = Ambient air pressure (mb)

p_{Ann} = Annubar pressure (mmH_2O)

T_{amb} = Ambient air temperature (ºC)

The Annubar Constant is 10.99 for the small inlet tube (1.610 in), and 43.998 for the large inlet tube (3.068 in). The validity of this relationship was confirmed by measuring the average flow velocity using a Pitot tube. For these initial experiments, the Annubar pressure was measured with a water manometer at relatively low flowrates.

RUN	Flow temp (°C)	Air Pressure (mb)	Pitot Average (mmH_2O)	Pitot velocity (m/s)	Annubar Pressure (mmH_2O)	Pitot Flowrate (kg/hr)	Annubar Flowrate (kg/hr)	Difference (%)
1	17	1014.0	0	0	0	0	0	0
2	20	1013.4	0.785	3.58	1.16	64.98	65.65	1.01
3	23	1012.7	1.587	5.12	2.36	91.89	93.12	1.34
4	25	1012.1	2.498	6.45	3.85	114.88	118.52	3.07

Table C.12 Flowrate measured using an Annubar compared to flowrate measured using a Pitot tube

The difference in flowrate between the two methods may have been brought about by misalignment of the Pitot tube. This error would tend to decrease the velocity—and hence flowrate—indicated by the Pitot tube arrangement. Thus, the error shown in the table was thought to be a maximum, and it was assumed that the Annubar pressure method was sufficiently accurate for chassis dynamometer work.

In order to read the Annubar pressure, electronic transducers with a variable current output were connected to the PCL-812PG A/D card. The air-flow measurement rig includes two Dieterich Standard pressure transducers, which provide an output of 4–20 mA over pressure ranges of 0–6 and 0–30 inH_2O respectively. A combination of the large Annubar tube and the smaller transducer enabled flowrates up to approximately 750 kg/hr (208 gm/s) under standard atmospheric conditions. The maximum air flowrate for the test vehicle described in Chapter 8 was approximately 70 gm/s. Measuring the potential across a 560 Ω resistor at the A/D card, the maximum voltage encountered during vehicle testing was 3.2 V.

With the PCL-812PG range set at ±5 V, the A/D output (0–4095) from the pressure transducers was compared with the Annubar pressure, as measured by a water manometer connected to the same pressure lines.

Pressure (mmH_2O)	0	0.1	0.8	7.1	12.6	15.9	25.0	34.0	42.4	46.0
A/D output (bits)	2939.0	2939.0	2958.9	3107.1	3242.5	3311.6	3528.7	3741.4	3927.1	4011.6

Table C.13 Annubar flowrate A/D calibration data

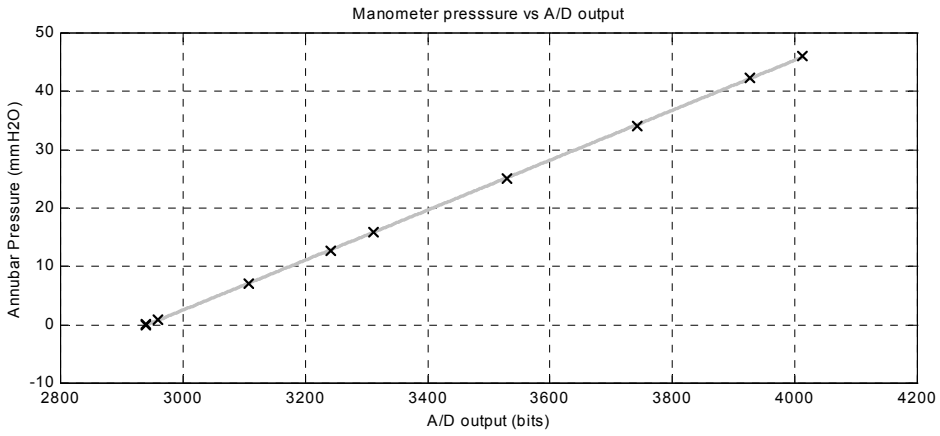

Figure C.21 Annubar flowrate A/D calibration data

$$\textbf{\textit{Pressure}}\left(mmH_2O\right) \;=\; \mathbf{0.04281} \times \textbf{\textit{bits}} - \mathbf{125.9} \qquad \text{(C-12)}$$

This pressure can be converted to a flowrate in kg/hr or gm/s using the Annubar equation on the previous page.

C.8 Airflow DB-1 Digital Barometer

Output: 0–1999 mV

A/D configuration: PCL-812PG ±1.25 V via PCLD-889

Estimated measurement uncertainty: ±4 mb

First, the digital display was related to the voltage output:

Digital Display (mb)	966	1005	996	1035	1020	1012
A/D bits	3632	3695	3680	3744	3719	3705

Table C.14 Barometer A/D signal calibration vs. display

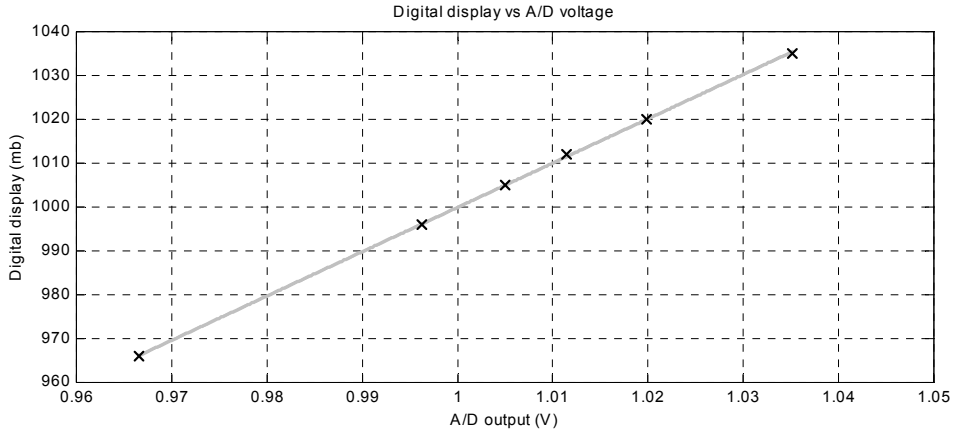

Figure C.22 Barometer A/D signal calibration vs. display

$$Display = 1010.1 \times volts - 10.2 \quad \text{(C-13)}$$

By relating the digital display to another—independently measured—set of pressures, the error in the digital barometer was determined.

Measured pressure (mb)	986.3	987.0	999.7	1033.6
Digital Display (mb)	1011.5	1015	1026	1061

Table C.15 Digital barometer reading vs. mercury barometer pressure

$$Pressure = 0.9784 \times Display - 4.4 \quad \text{(C-14)}$$

This allowed an overall corrected equation to be generated (using a least squares approximation) to calculate barometric pressure from the digital barometer voltage output.

$$\textbf{\textit{Pressure}}\left(\textbf{\textit{mb}}\right) \;=\; \mathbf{988.28} \times \textbf{\textit{volts}} - \mathbf{14.4} \qquad \text{(C-15)}$$

C.9 Thermocouple Temperature Sensors

Output: ±10 mV
A/D configuration: PCL-812PG ±2.5 V, ±5 V, ±10 V via PCLD-889
Estimated measurement uncertainty: ±0.4ºC for air temperature,
various for others

In the course of this project, thermocouples to measure air, vehicle engine coolant, and engine oil temperature were added to the existing drum axle oil sensor. Thermocouple voltages were recorded via the PCLD-889 daughter board with a gain of 1000. Once these voltages had been calculated from the A/D signal they were corrected using the cold-junction compensator included on the PCLD-889, with standard equations as shown below:

$$T = 0.0244 \times (CJC\ voltage) \tag{C-16}$$

Where T = Temperature (ºC) of cold junction

$$CJC\ Compensation = -(8.168 \times 10^{-7}) + (3.964 \times 10^{-5})T + (1.640 \times 10^{-8})T^2 \tag{C-17}$$

$$Compensated\ Thermocouple\ Voltage = (Measured\ Voltage) + (CJC\ Compensation) \tag{C-18}$$

Standard coefficients are also available to convert this compensated thermocouple voltage to a temperature in degrees. However, to account for small manufacturing and wiring differences, each thermocouple was calibrated individually and assigned a linear equation using a least squares approximation. Thermocouples were placed in a liquid bath, which was heated and cooled over the desired temperature range. Voltages were compared with an electronic platinum resistance thermometer (PRT), which was known to be accurate to ±0.1ºC.

It was decided that the drum axle thermocouple would not be removed from its position in the axle housing, and a combination of the other thermocouple calibration equations was implemented in lieu of a direct calibration. For the thermocouples measuring temperature of the axle oil, vehicle coolant, and vehicle engine oil, the

required accuracy is not great, since these serve only as an indicator to the user of the general thermal state of the drum axle or vehicle engine. It was more important to ensure that the ambient air thermocouple was accurate, because this temperature was used in the calculation of air flowrate (using the Annubar), as well as the correction of vehicle power for atmospheric conditions. Shown below is an example of the ambient air thermocouple calibration over the required temperatures, and a comparison of the temperature calculated using the A/D signal with that measured by the PRT reader.

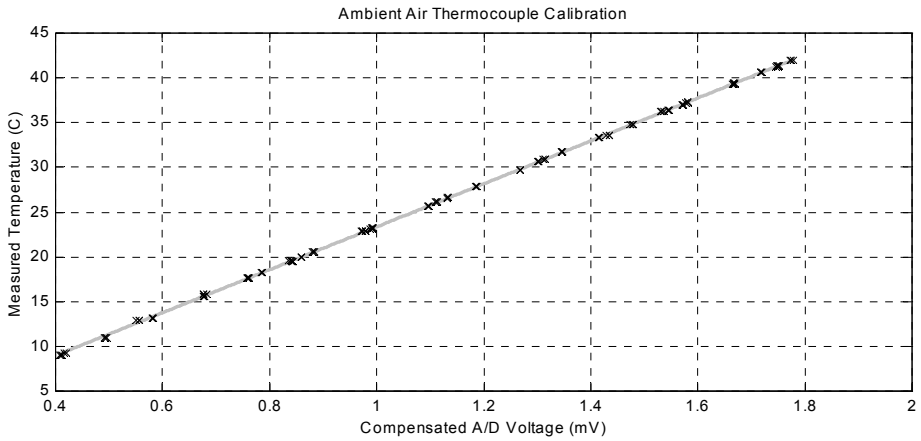

Figure C.23 Ambient air temperature thermocouple calibration

$$\textit{Temperature}\left(^{\circ}C\right) = 23.983 \times \left(\textit{millivolts}\right) - 0.83 \qquad \text{(C-19)}$$

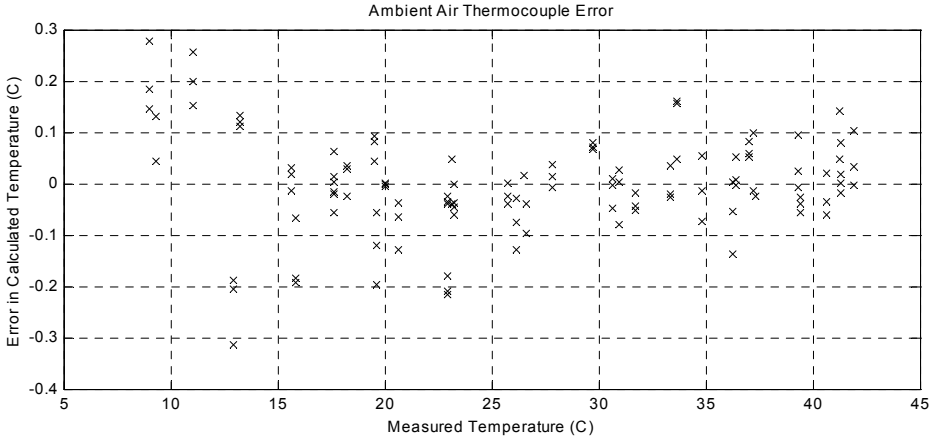

Figure C.24 Error in ambient air thermocouple A/D calibration

Table C.16 shows a summary of all the calibrated thermocouples, including the expected temperature and voltage ranges, as well as the estimated measurement uncertainty, including the uncertainty of PRT used during calibration. The air

temperature sensor appears to be more accurate than the other thermocouples because it was calibrated over a narrower temperature range. Thus, the linear approximation excludes potential non-linearities at higher temperatures in addition to the errors only being calculated over the anticipated temperature range. Greater uncertainties were assigned to the other thermocouples, due to the greater temperature range, or—in the case of the drum axle oil—the fact that the calibration coefficients were merely an estimate.

The thermocouple labelled 'Spare' in Table C.16 was calibrated for a future use, such as measuring exhaust temperature or inlet manifold temperature, but was not implemented during the testing discussed in Chapter 8. Future applications of this thermocouple may require greater accuracy than is required for engine and oil temperature monitoring. Therefore, this channel—which exhibited less variation during calibration—has been kept aside.

Thermocouple parameter	**Ambient air**	**Vehicle coolant**	**Vehicle engine oil**	**Spare**	**Drum axle oil**
Temperature range (°C)	0–45	0–150	0–150	0–150	0–100
Voltage range (±mV)	2	7	7	7	5
PCL-812PG range (±V)	2.5	10	10	10	5
Linear multiplier	23.983	23.410	24.263	24.076	23.600
Linear constant	-0.83	-0.15	-1.70	-1.95	-0.50
Uncertainty (±°C)	0.4	1.5	1.5	0.7	2.0

Table C.16 Thermocouple calibration summary

APPENDIX D:

Engine Speed Spark Pulse Pickup

A commercial inductive-loop pickup (pictured) was used to detect spark plug ignition pulses to the test vehicle engine. Additional circuitry was required to condition the output of this device for use with the UPP card. With knowledge of the number of spark plug pulses per engine revolution, the engine speed could be calculated:

$$Engine\ Speed\ (rpm) = \frac{Sparks\ per\ minute}{Sparks\ per\ rev} \quad \text{(D-1)}$$

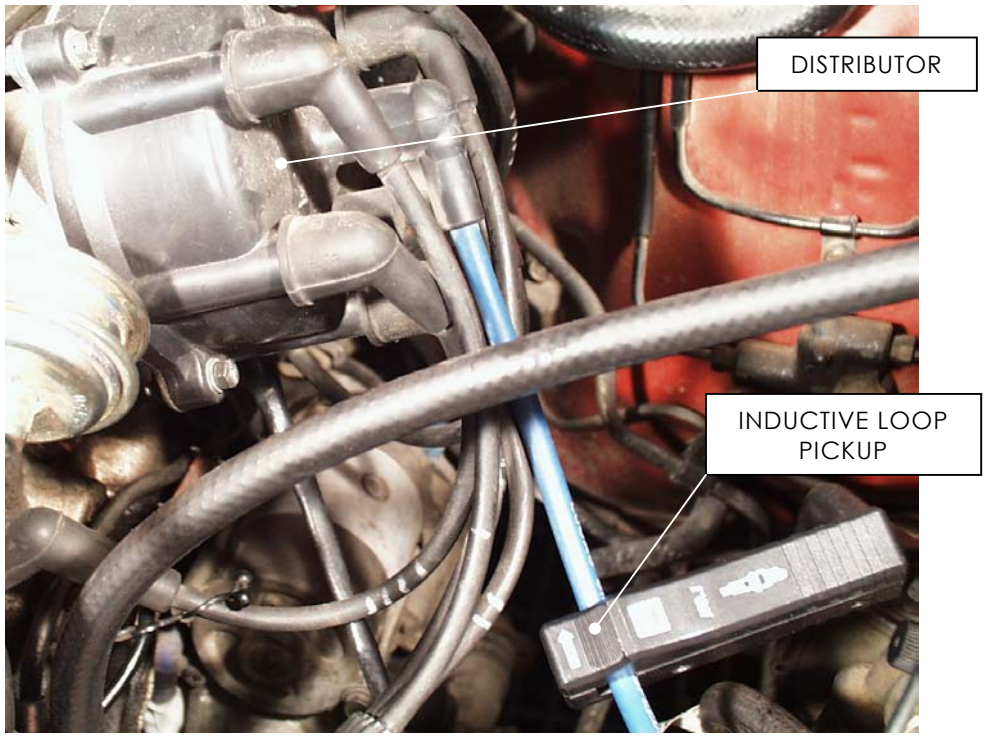

Plate D.1 Inductive loop spark plug pickup

APPENDIX E:

Step Response of Various Software Filters

The filters described in the Section 4.2 are plotted below in response to an instantaneous (i.e. between two discrete points in time) increase in velocity. In the case of the 'moving average' formulation, the speed series was filtered, and the acceleration calculated as the gradient between two adjacent filtered velocities ($\Delta v/\Delta t$). The least squares method allows analytic differentiation of the approximated curve, whereas the Butterworth filter calculates acceleration in one step as part of the filtering operation.

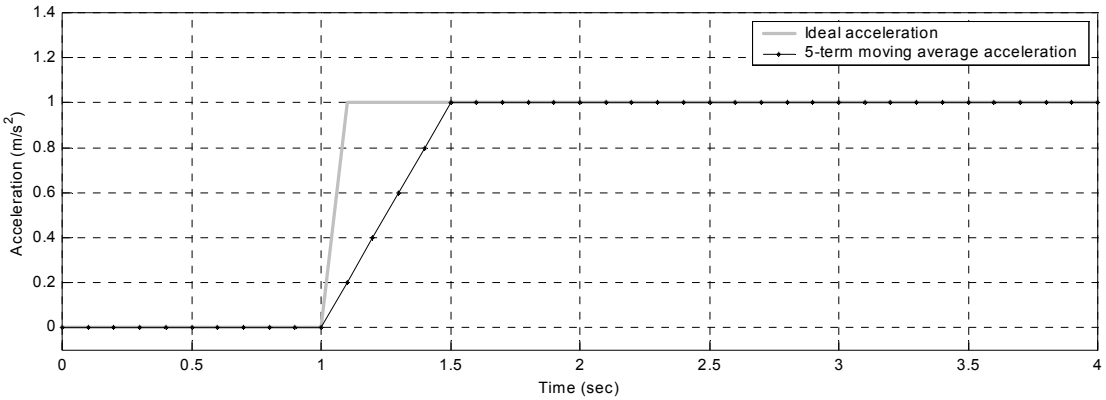

Figure E.1 Step response of 5-term moving-average software filter (10 Hz)

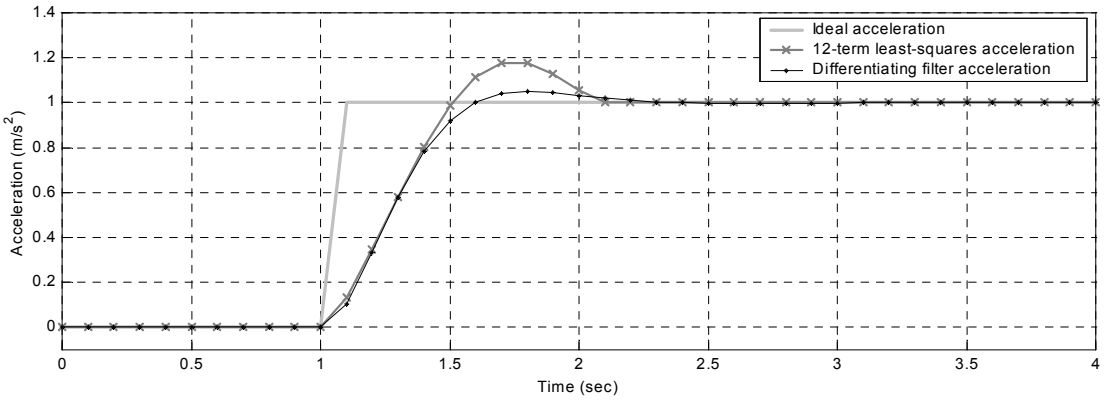

Figure E.2 Step response of 12-term least-squares filter and Butterworth differentiating filter (10 Hz)

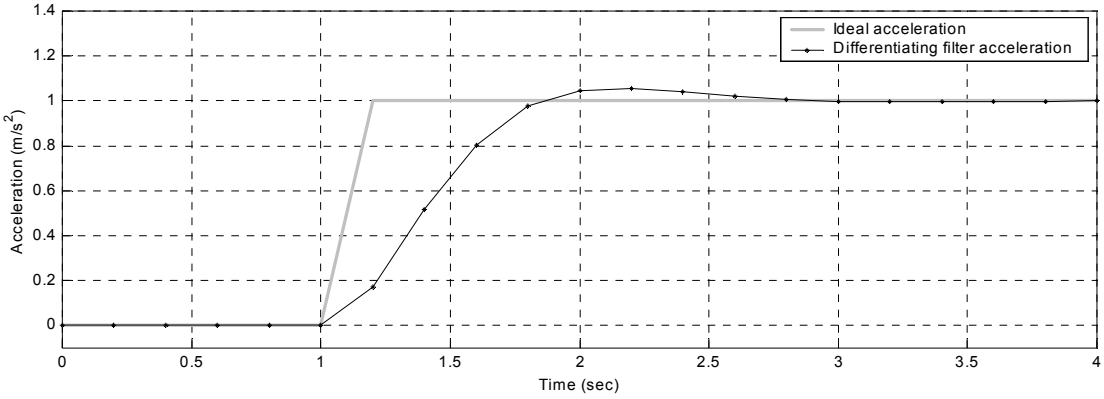

Figure E.3 Step response of Butterworth differentiating filter (5 Hz formulation)

APPENDIX F:

Least Squares Approximation

The example below demonstrates the general least squares approximation method in the specific case of a four-point series to be approximated by a quadratic curve.

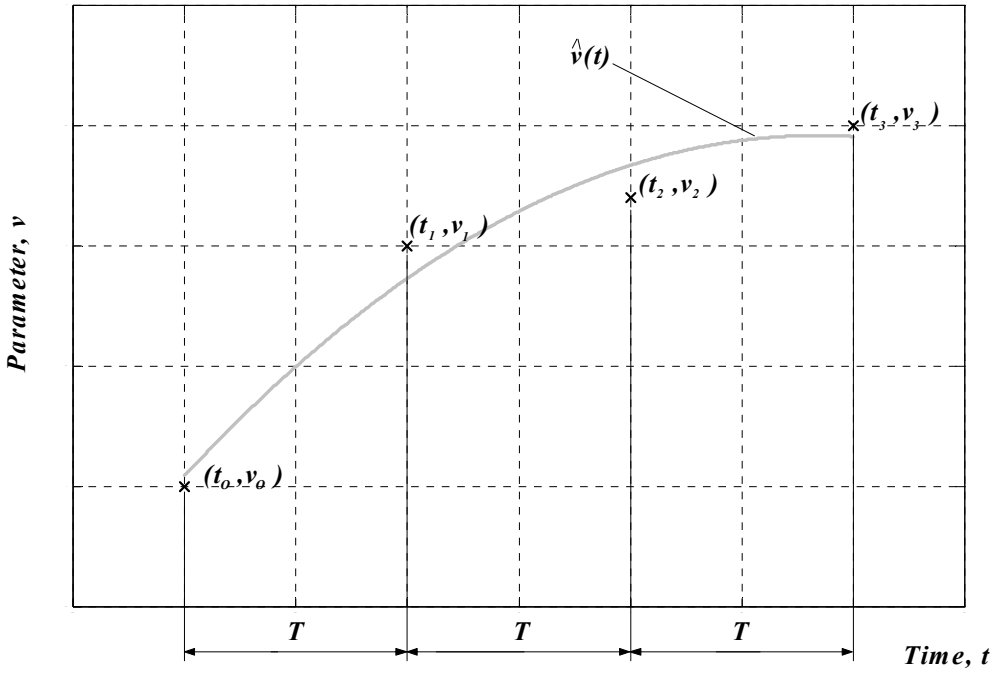

Figure F.1 Example least squares approximation

The approximation, $\hat{v}$ can be written:

$$\hat{v}_i = \alpha_0 + \alpha_1 t_i + \alpha_2 t_i^2 \qquad \text{(F-1)}$$

This approximation may also be represented vectorially to give four points on the approximated curve:

$$\begin{bmatrix} \hat{v}_0 \\ \hat{v}_1 \\ \hat{v}_2 \\ \hat{v}_3 \end{bmatrix} = \begin{bmatrix} 1 & 0 & 0 \\ 1 & T & T^2 \\ 1 & 2T & (2T)^2 \\ 1 & 3T & (3T)^2 \end{bmatrix} \begin{bmatrix} \alpha_0 \\ \alpha_1 \\ \alpha_2 \end{bmatrix} \tag{F-2}$$

Or:

$$\hat{\boldsymbol{v}} = \boldsymbol{X\alpha} \tag{F-3}$$

The error at each point is $\boldsymbol{X\alpha - v}$, which we wish to minimise by appropriate selection of the coefficients in $\boldsymbol{\alpha}$. This is achieved by using the standard least squares transformation [Fraleigh & Beauregard, 1990]:

$$\boldsymbol{\alpha} = \left(\boldsymbol{X}^T \boldsymbol{X}\right)^{-1} \boldsymbol{X}^T \boldsymbol{v} \tag{F-4}$$

Once α_0, α_1 and α_2 have been selected, Equation F-1 can be solved for $\hat{v}$, or differentiated to give the gradient, $\dot{\hat{v}}$ at any point in time, t_i.

$$\dot{\hat{v}}_i = \alpha_1 + 2\alpha_2 t_i \tag{F-5}$$

APPENDIX G:

Digital Filter Response

The following plots show the magnitude and phase response of the chosen acceleration filter as a function of frequency. The 2nd order filter (for use at 10 Hz sampling frequency) provided acceptable noise attenuation with a cutoff frequency of 17% of the Nyquist frequency (see Equation G-1, below). Note in Figure G.1 that the phase angle is zero at 5.3 rad/s, and that the magnitude drops away with increases or decreases in frequency from this point.

Zero phase angle at the cutoff frequency:

$$\begin{aligned} Cutoff\ \ frequency &= 0.17 \times Nyquist\ \ frequency \\ &= 0.17 \times \left(\frac{10\ Hz}{2} \right) = 0.85\ Hz = 5.34\ rad/s \end{aligned} \tag{G-1}$$

Similar plots could be produced for the 5 Hz digital filter, for which a cutoff frequency of 23% (3.61 rad/s) was employed. Note the use of logarithmic scales on the frequency axes in Figure G.1.

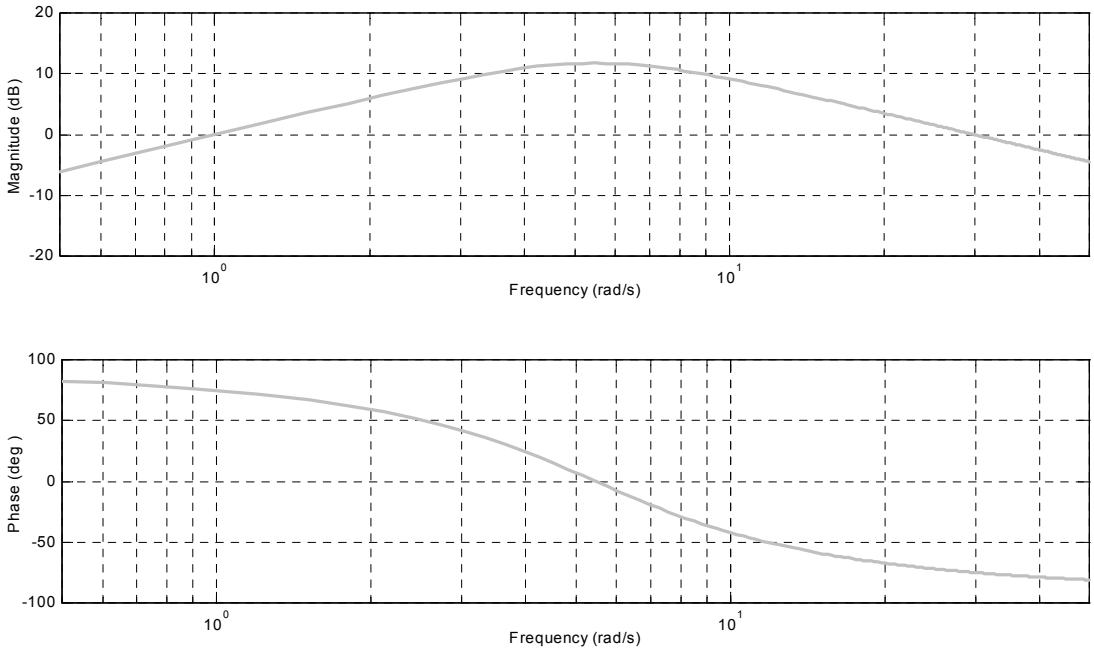

Figure G.1 Bode frequency-response plots for the chosen digital filter (for use at 10 Hz).

APPENDIX H:

Constant Speed Friction Determination

The chassis dynamometer was run at a series of constant velocities under power from the electric motor in speed control mode. A known dynamometer torque was applied during each run, so that the variable internal power absorber friction would not be included in the overall friction force (see Section 5.1). The motoring torque was then used to calculate the net frictional force (i.e. total motoring force – dyno force) referenced to the drum surface. Each graph below represents a combination of two sets of constant speed data.

Velocity (m/s)	Motoring Torque (Nm)	Net Force (N)
4.7	55.7	58.33
4.7	56.0	61.40
10.5	59.5	97.22
10.5	59.6	98.24
16.5	63.0	133.03
16.5	63.0	133.03
22.0	66.0	163.73
22.0	66.0	163.73
27.6	69.0	194.43
27.7	68.5	189.32
33.4	72.2	227.18
33.5	71.9	224.11

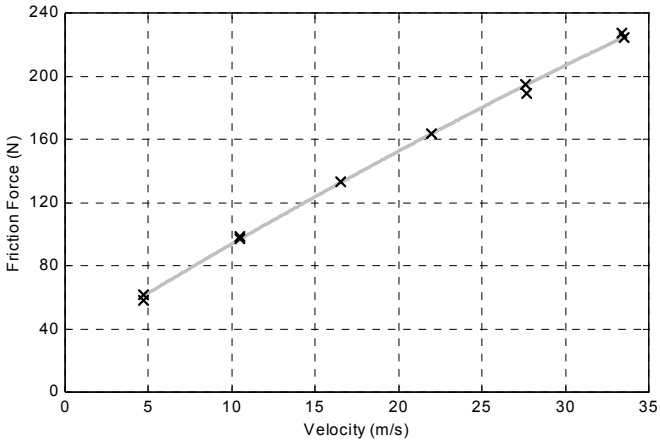

$$Friction\,(N) \;=\; 30.5 + 6.54v - 0.02v^2 \qquad \text{(H-1)}$$

Table H.1 and **Figure H.1** Constant speed friction calibration with 50 Nm dyno torque

Velocity (m/s)	Motoring Torque (Nm)	Net Force (N)
4.7	80.0	51.17
4.7	79.1	41.96
10.5	84.2	94.15
10.5	83.0	81.87
16.5	87.7	129.96
16.5	86.4	116.66
22.0	90.8	161.69
22.0	89.6	149.41
27.6	93.1	185.22
27.6	92.6	180.11
33.4	95.6	210.81
33.4	95.0	204.67

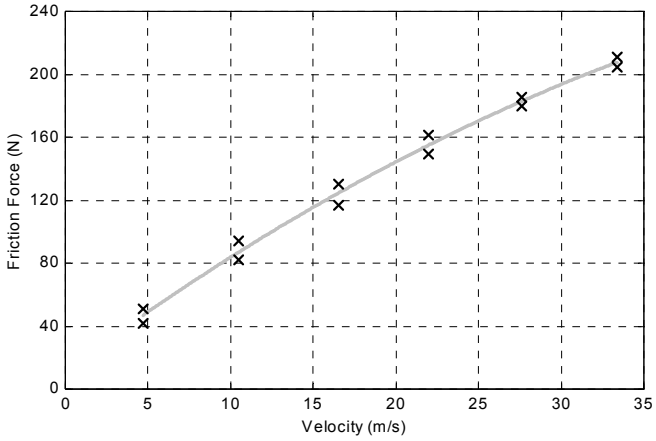

$$Friction\,(N) \;=\; 11.6 + 7.77v - 0.05v^2 \qquad \text{(H-2)}$$

Table H.2 and **Figure H.2** Constant speed friction calibration with 75 Nm dyno torque

Velocity (m/s)	Motoring Torque (Nm)	Net Force (N)
4.6	102.6	26.61
4.6	102.5	25.58
10.6	106.3	64.47
10.6	106	61.40
16.4	109.1	93.12
16.5	109.6	98.24
21.9	112.4	126.89
22.0	112.8	130.99
27.5	115.5	158.62
27.5	115.5	158.62
33.2	118.3	187.27
33.3	118.5	189.32

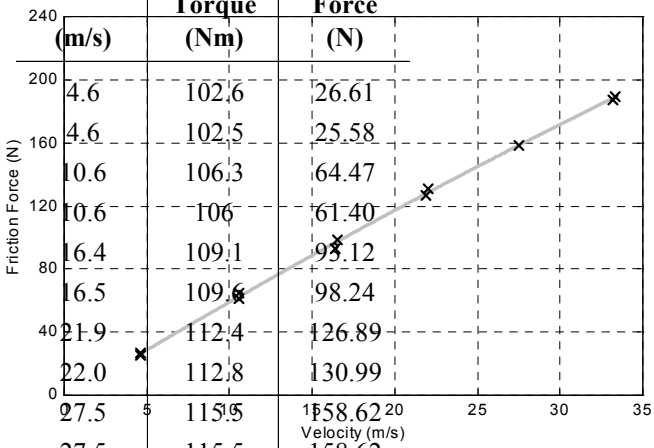

$$Friction\,(N) \;=\; -2.9 + 6.37v - 0.02v^2 \qquad \text{(H-3)}$$

Table H.3 and **Figure H.3** Constant speed friction calibration with 100 Nm dyno torque

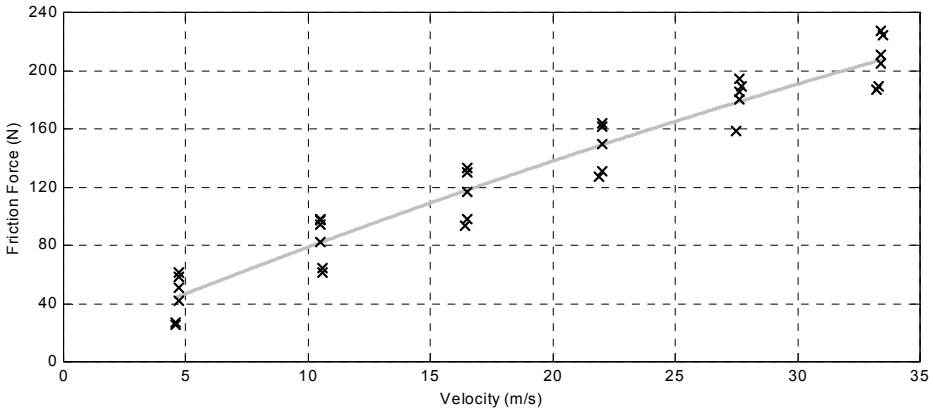

Figure H.4 Constant speed friction calibration combining all runs

$$Friction\,(N) \quad = \quad 13.28 + 6.86v - 0.03v^2 \tag{H-4}$$

APPENDIX I:

Inertia Coastdown Results with an Assumed Friction Force

The following data was gathered in a series of decelerations under constant torque from both the motor and the power absorber. The chassis dynamometer friction was assumed to be as follows:

$$F_f = 13.27 + 6.86v - 0.031v^2 \quad \text{(I-1)}$$

Where v is in m/s

So that the equivalent mass at any point in time during a coastdown can be found using Equation 5-1 (see Section 5.2.1).

Nominal dyno torque (Nm)	Average dyno torque (Nm)	Average motor torque (Nm)	Calculated equivalent mass (kg) Run 1 (kg)	Run 2 (kg)	Run 3 (kg)	Run 4 (kg)	Average equiv. Mass (kg)	Standard Deviation (kg)	(%)
50	51.02	25.32	726.5	730.1	734.3	731.5	730.6	3.2	0.44
75	77.17	25.93	713.7	716.2	717.1	718.7	716.4	2.1	0.29
100	102.53	26.32	709.3	711.7	711.7	715.6	712.1	2.6	0.37
125	128.29	25.76	707.7	707.3	707.2	707.6	707.5	0.2	0.03
Combined Data							**716.6**	**9.2**	**1.28**

Table I.1 Results summary table from inertia coastdowns incorporating motor torque and assumed friction coefficients.

APPENDIX J:

Inertia Determination Results using Acceleration/Deceleration Method

The tables below include the complete results of the inertia determination as detailed in Section 5.2.2. Results are summarised in Table 5.1.

v_A = Highest speed during run

v_A = Lowest speed during run

F_{motor} = Electric motor force, referenced to the drum surface

F_{dyno} = Power absorber force, referenced to the drum surface

Δt = Time interval for acceleration/deceleration

RESULTS SET A Equivalent Mass, m_{cd} = 696.2 kg

Deceleration	1	2	3	Average
v_A **(m/s)**	16.71	16.66	16.66	16.68
v_B **(m/s)**	22.18	22.18	22.13	22.16
F_{motor} **(N)**	256.98	258.00	258.00	257.66
F_{dyno} **(N)**	517.02	517.02	517.02	517.02
Δt **(s)**	9.90	9.90	9.90	9.90

Acceleration	1	2	3	Average
v_A **(m/s)**	16.66	16.66	16.57	16.63
v_B **(m/s)**	22.18	22.18	22.13	22.16
F_{motor} **(N)**	723.83	723.83	723.83	723.83
F_{dyno} **(N)**	208.86	207.83	207.83	208.17
Δt **(s)**	9.90	9.90	9.90	9.90

Table J.1 Acceleration/Deceleration results set A

RESULTS SET B Equivalent Mass, m_{cd} = 691.2 kg

Deceleration	1	2	3	Average
v_A **(m/s)**	12.63	12.68	12.63	12.65
v_B **(m/s)**	20.76	20.76	20.76	20.76
F_{motor} **(N)**	279.5	278.48	278.48	278.82
F_{dyno} **(N)**	718.71	718.71	720.76	719.39
Δt **(s)**	9.9	9.9	9.9	9.90

Acceleration	1	2	3	Average
v_A **(m/s)**	12.68	12.68	12.68	12.68
v_B **(m/s)**	20.76	20.76	20.8	20.77
F_{motor} **(N)**	901.46	901.98	901.98	901.81
F_{dyno} **(N)**	210.9	211.42	210.39	210.90
Δt **(s)**	9.9	9.9	9.9	9.90

Table J.2 Acceleration/Deceleration results set B

RESULTS SET C Equivalent Mass, m_{cd} = 723.1 kg

Deceleration	1	2	3	Average
v_A **(m/s)**	19.43	19.59	19.59	19.54
v_B **(m/s)**	24.91	24.96	24.96	24.94
F_{motor} **(N)**	165.96	165.04	165.24	165.41
F_{dyno} **(N)**	406.55	405.22	406.15	405.97
Δt **(s)**	9.9	9.9	9.9	9.90

Acceleration	1	2	3	Average
v_A **(m/s)**	19.49	19.49	19.49	19.49
v_B **(m/s)**	24.83	24.91	24.96	24.90
F_{motor} **(N)**	948.97	947.23	948.35	948.18
F_{dyno} **(N)**	398.77	398.67	398.57	398.67
Δt **(s)**	9.9	9.9	9.9	9.90

Table J.3 Acceleration/Deceleration results set C

RESULTS SET D Equivalent Mass, m_{cd} = 717.5 kg

Deceleration	1	2	3	Average
v_A **(m/s)**	14.37	14.42	14.42	14.40
v_B **(m/s)**	19.43	19.43	19.43	19.43
F_{motor} **(N)**	151.83	151.63	150.91	151.46
F_{dyno} **(N)**	382.7	381.47	381.51	381.89
Δt **(s)**	9.9	9.9	9.9	9.90

Acceleration	1	2	3	Average
v_A **(m/s)**	14.37	14.42	14.37	14.39
v_B **(m/s)**	19.43	19.49	19.49	19.47
F_{motor} **(N)**	898.5	898.8	898.39	898.56
F_{dyno} **(N)**	396.32	396.32	396.11	396.25
Δt **(s)**	9.9	9.9	9.9	9.90

Table J.4 Acceleration/Deceleration results set D

RESULTS SET E Equivalent Mass, m_{cd} = 719.0 kg

Deceleration	1	2	3	Average
v_A **(m/s)**	9.05	9.1	9.1	9.08
v_B **(m/s)**	13.86	13.86	13.86	13.86
F_{motor} **(N)**	144.54	144.69	143.7	144.31
F_{dyno} **(N)**	373.69	374.1	373.85	373.88
Δt **(s)**	9.9	9.9	9.9	9.90

Acceleration	1	2	3	Average
v_A **(m/s)**	9.1	9.1	9.1	9.10
v_B **(m/s)**	13.86	13.86	13.86	13.86
F_{motor} **(N)**	866.52	864.12	864.01	864.88
F_{dyno} **(N)**	402.26	401.92	401.2	401.79
Δt **(s)**	9.9	9.9	9.9	9.90

Table J.5 Acceleration/Deceleration results set E

APPENDIX K:

Electric Motor Response with Software Integrator

Figure K.1 below shows the electric motor step response under control from the existing analogue hardware and an additional software 'integrator'. The integrator term (dependent on the control error) was simply added to the D/A output as shown below:

$$D/A\ demand \quad = \quad Demand\ set\ point + u(k) \tag{K-1}$$

Where:

$$u(k) \quad = \quad (0.01)\,e(k) - u(k-1) \tag{K-2}$$

With: $e(k)$ = Error between set point and current measured torque (Nm)

$u(k)$ = Current integrator output (Nm)

$u(k\text{-}1)$ = Integrator output at previous time interval (Nm)

Note that while the 0.01 factor is small, the tiny fluctuations brought about by this additional control (which includes some lag between the error being read and the physical application of load) lead to instability in the motor torque. Note also that the integrator 'winds up' during the delay between the step input and the motor response. This wind-up leads the overshoot seen in Figure K.1.

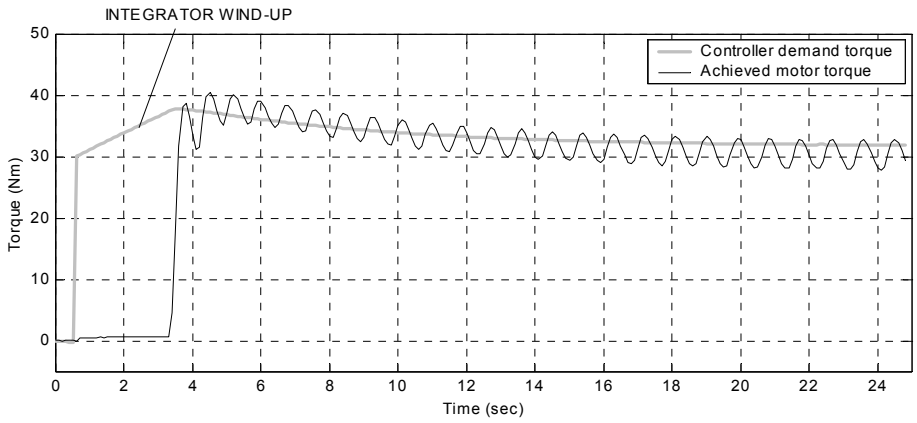

Figure K.1 Step response of electric motor with integrator control software

APPENDIX L:

Inertia Coastdown Combined Results

The results of 32 individual chassis dynamometer coastdowns were averaged and combined to arrive at a single base inertia for the system. Eight coastdowns were carried out at each of the power absorber torques shown below (see Table L.1) and the velocity and dynamometer load cell readings were averaged at each recorded point. Different power absorber torques were used to bring about different rates of deceleration.

Nominal dyno torque (Nm)	**40**	**60**	**80**	**100**
Coastdown run number	1	2	3	4
	5	6	7	8
	9	10	11	12
	13	14	15	16
	17	18	19	20
	21	22	23	24
	25	26	27	28
	29	30	31	32
Average grouping (see below)	40A	60A	80A	100A

Table L.1 Inertia coastdown runs combined to give four 'average coastdowns'

The 'average coastdowns' at each power absorber load were combined with the others in each of the possible ways, as shown in Table L.2. The resultant equivalent mass (in kg) for each pair was also calculated as an average. By simultaneously solving for equivalent mass (see Equation 5-6 in Section 5.3) at 20 different velocities in the range 35–105 kph, single mass was found for each combination of dynamometer torques. For example, the first row in Table L.2 contains the base masses calculated by simultaneously solving between 40A & 60A, 40A & 80A, and 40A & 100A.

	60A	**80A**	**100A**
40A	672.1	672.1	674.0
60A		672.1	674.9
80A			677.8

Table L.2 Equivalent masses (in kilograms) found by simultaneously solving for each averaged coastdown pair

The overall average equivalent mass was 673.8 kg, with a standard deviation from Table L.2 of 2.3 kg (0.34%).

APPENDIX M:

Friction Coastdown Repeatability Results

The total friction forces at two different speeds were calculated using the data from 32 separate coastdowns, under several different dynamometer loads. Equation 5-11 (see Section 5.4) may be solved with knowledge of the system inertia, dynamometer force, and instantaneous acceleration. The latter was differentiated from a quadratic least squares approximation of velocity throughout each coastdown run. In Table M.1 and Table M.2, the total friction is listed for each individual run, as well as the average friction found by combining all the coastdown runs at a particular dynamometer torque. An overall average (for each of the two speeds) was found by combining the data from all 32 coastdowns.

		Results Set A				**Results Set B**			
Nominal Dyno Torque (Nm)		**40**	**60**	**80**	**100**	**40**	**60**	**80**	**100**
Friction force (N) at 35 kph for individual coastdowns		71.26	72.38	73.71	71.36	74.53	73.92	74.84	73.82
		72.18	71.87	72.38	71.46	75.66	74.84	74.64	74.33
		71.97	72.59	73.10	71.05	73.71	74.02	75.86	74.74
		71.46	72.28	72.90	70.95	75.86	74.84	74.33	74.23
Average and variation for each dyno torque	mean (N)	71.72	72.28	73.02	71.21	74.94	74.41	74.92	74.28
	s.d. (N)	0.43	0.30	0.55	0.24	1.01	0.50	0.67	0.38
	s.d. (%)	0.60	0.42	0.75	0.34	1.34	0.68	0.89	0.51
Average and variation across all of Results Set	mean (N)	72.06				74.64			
	s.d. (N)	0.78				0.68			
	s.d. (%)	1.09				0.91			
Average and variation across all data	mean (N)	**73.35**							
	s.d. (N)	**1.50**							
	s.d. (%)	**2.04**							

Table M.1 Friction calibration results at 35 kph for 32 separate coastdowns

		Results Set A				Results Set B			
Nominal Dyno Torque (Nm)		**40**	**60**	**80**	**100**	**40**	**60**	**80**	**100**
Friction force (N) at 105 kph		135.3	135.1	136.3	136.7	136.4	138.0	138.6	136.2
for individual coastdowns		136.0	135.5	135.7	133.5	137.7	137.4	136.9	137.0
		136.3	134.8	136.3	136.4	136.8	138.5	138.4	135.8
		136.4	136.4	135.8	134.7	137.1	137.0	136.6	137.1
Average and variation	mean (N)	136.0	135.5	136.0	135.3	137.0	137.7	137.6	136.5
for each dyno torque	s.d. (N)	0.46	0.66	0.33	1.48	0.56	0.68	1.05	0.64
	s.d. (%)	0.34	0.49	0.24	1.10	0.41	0.49	0.76	0.47
Average and variation	mean (N)	135.7				137.2			
across all of Results Set	s.d. (N)	0.83				0.85			
	s.d. (%)	0.61				0.62			
Average and variation	mean (N)	**136.45**							
across all data	s.d. (N)	**1.13**							
	s.d. (%)	**0.83**							

Table M.2 Friction calibration results at 105 kph for 32 separate coastdowns

APPENDIX N:

Drum Inertia Coastdown Combined Results

The results of 32 individual chassis dynamometer coastdowns were averaged and combined to arrive at a single inertia for the roller drum assembly. Four coastdowns were carried out at each of the power absorber torques shown below (see Table N.1) and the velocity and tractive effort load cell readings were averaged at each recorded point.

Nominal dyno torque (Nm)	**40**	**60**	**80**	**100**
Coastdown run number	1	2	3	4
	5	6	7	8
	9	10	11	12
	13	14	15	16
	17	18	19	20
	21	22	23	24
	25	26	27	28
	29	30	31	32
Average grouping (see below)	40A	60A	80A	100A

Table N.1 Inertia coastdown runs combined to give four ‘average coastdowns’

The ‘average coastdowns’ at each power absorber load were combined with the others in each of the possible ways, as shown in Table N.2. The resultant equivalent mass (in kilograms) for each pair was also calculated as an average. Equation 5-14 was used (neglecting the trunnion friction) to determine the roller drum equivalent mass by simultaneously solving to eliminate the friction term, F_{dra}. The average inertia over 20 different velocities in the range 30–100 kph provided a single equivalent mass for each combination of dynamometer torques.

	60A	**80A**	**100A**
40A	601.8	602.1	599.0
60A		602.3	597.6
80A			593.0

Table N.2 Drum equivalent masses (kg) found by simultaneously solving for each averaged coastdown pair

The overall average equivalent mass was 599.3 kg, with a standard deviation from Table N.2 of 3.6 kg (0.60%).

APPENDIX O:

Drum Friction Coastdown Repeatability Results

The roller drum friction forces at two different speeds were calculated using the data from 32 separate coastdowns, under several different dynamometer loads (i.e. different rates of deceleration). Equation 5-14 (see Section 5.5.1) may be solved with knowledge of the drum inertia, tractive effort load cell force, and instantaneous acceleration (again, neglecting trunnion friction). The latter was differentiated from a quadratic least squares approximation of velocity throughout each coastdown run. In Tables O.1 and O.2, the friction is listed for each individual run, as well as the average friction found by combining all the coastdown runs at a particular dynamometer torque. An overall average (for each of the two speeds) was found by combining the data from all 32 coastdowns.

		Results Set A				**Results Set B**			
Nominal Dyno Torque (Nm)		**40**	**60**	**80**	**100**	**40**	**60**	**80**	**100**
Friction force (N) at 35 kph		6.87	6.58	5.45	7.21	4.05	3.86	2.30	3.46
for individual coastdowns		6.39	6.28	5.37	5.87	2.62	3.57	2.87	3.78
		5.49	7.02	4.95	5.86	2.97	3.56	1.84	3.41
		6.01	6.53	5.60	6.09	2.45	3.39	2.37	3.78
Average and variation	mean (N)	6.19	6.60	5.34	6.26	3.02	3.59	2.35	3.61
for each dyno torque	s.d. (N)	0.59	0.31	0.28	0.64	0.72	0.20	0.42	0.20
	s.d. (%)	9.5	4.7	5.2	10.3	23.8	5.5	18.0	5.6
Average and variation	mean (N)	6.10				3.14			
across all of Results Set	s.d. (N)	0.65				0.66			
	s.d. (%)	10.6				21.1			
Average and variation	mean (N)	**4.6**							
across all data	s.d. (N)	**1.6**							
	s.d. (%)	**35.4**							

Table O.1 Drum friction calibration results at 35 kph for 32 separate coastdowns

		Results Set A				Results Set B			
Nominal Dyno Torque (Nm)		**40**	**60**	**80**	**100**	**40**	**60**	**80**	**100**
Friction force (N) at 105 kph		23.8	23.2	24.2	24.4	20.8	20.5	21.0	21.8
for individual coastdowns		24.5	23.7	24.0	25.2	22.3	20.0	20.2	22.1
		26.0	22.3	23.7	25.2	21.5	20.5	20.9	22.6
		23.8	23.5	22.8	24.5	22.8	20.0	21.0	21.6
Average and variation	mean (N)	24.5	23.2	23.7	24.8	21.8	20.2	20.8	22.0
for each dyno torque	s.d. (N)	1.05	0.64	0.64	0.43	0.87	0.29	0.38	0.43
	s.d. (%)	4.3	2.8	2.7	1.7	4.0	1.4	1.8	2.0
Average and variation	mean (N)	24.0				21.2			
across all of Results Set	s.d. (N)	0.94				0.91			
	s.d. (%)	3.9				4.3			
Average and variation	mean (N)	**22.6**							
across all data	s.d. (N)	**1.7**							
	s.d. (%)	**7.5**							

Table O.2 Drum friction calibration results at 105 kph for 32 separate coastdowns

Note that the uncertainties represented by the large (as a percentage) standard deviations are with the estimated measurement uncertainty of the tractive effort load cell (±9 N, see Appendix C.5).

APPENDIX P:

C++ Program Menu Structure

Menu	Menu Options	Sub-Menu Options
Info	Program info	
	Video mode	
	Colours	
File	Open	
	View	
	New	
	Save	
	Save as	
	Set config file	
	Set vehicle file	
	Set cycle file	
	Edit vehicle specs	New vehicle file
		Edit existing file
	DOS shell	
	Exit	
Edit	Undo	
	Cut	
	Copy	
	Paste	
	Show clipboard	
	Clear	
Calibrate	PCL-812PG A/D card	A/D inputs
		D/A outputs
	Friction Constants	Dynamometer friction
		Vehicle + dyno friction
	Rezero load cells	Dyno load cell
		Tractive effort load cell
	Emissions equipment	NOx meter
	Test Program	
Run	Warm Up	
	Road load driving	
	Manual control	
	Mapping test	
	Driving cycle	
Window	Size/move	
	Zoom	
	Cascade	
	Tile	
	Next	
	Previous	
	Close	

Table P.1 Main chassis dynamometer program menu options

APPENDIX Q:

C++ Program A/D Configuration File

Figure Q.1 below shows the form of the *.cfg text files, which contain all the necessary configurations for A/D data sampling, inputs from external sources such as the UPP card, and D/A demand outputs. An explanation of each parameter is included in Table Q.1.

```
Roller Speed        #51,0,0,0,0,-1,1.0,0,0.1,160, %6.2f,kph#        External Input
Engine RPM          #52,0,0,0,0,-1,1.0,0,0.1,10000, %5.0f,rpm#      External Input
spare               #53,0,0,0,0,-1,1.0,0,0.1,1, %5.1f,V#           External Input
spare               #54,0,0,0,0,-1,1.0,0,0.1,1, %5.1f,V#           External Input
spare               #55,0,0,0,0,-1,1.0,0,0.1,1, %5.1f,V#           External Input
PA Torque           #1,0,1,0,0,-1,-0.3769,-0.3781,0.0,400, %5.1f,Nm#       812 channel
Tractive Effort     #2,0,1,1,0,-1,-3.7149,-3.7486,0,5000, %5.0f,N#         812 channel
Motor Torque        #3,0,1,2,0,-1,0.1228,-250.87,0.5,220, %5.1f,Nm#        812 channel
Fuel Flowrate       #4,0,1,1,0,-1,0.009793,-20.0588,0.1,20, %5.2f,gm/s#    812 channel
Air Flowrate        #5,0,1,1,0,-1,0.0429,-126.15,0.0,150, %5.1f,gm/s#      812 channel
NOx Concentration   #6,0,1,1,0,-1,1,1,0.0,10000, %5.0f,ppm#                812 channel
Calibration         #0,0,1,0,0,-1,0.004883,-10,0,3, %5.2f,V#               812 channel
spare               #7,0,1,0,1,-1,1.0,0.0,0.3,1, %4.1f,V#                  812 channel
spare               #10,0,1,0,1,-1,1.0,0.0,0.3,1, %4.1f,V#                 812 channel
spare               #11,0,1,0,1,-1,1.0,0.0,0.3,1, %4.1f,V#                 812 channel
spare               #12,0,1,0,1,-1,1.0,0.0,0.3,1, %4.1f,V#                 812 channel
spare               #13,0,1,0,1,-1,1.0,0.0,0.3,1, %4.1f,V#                 812 channel
spare               #14,0,1,0,1,-1,1.0,0.0,0.3,1, %4.1f,V#                 812 channel
spare               #15,0,1,0,1,-1,1.0,0.0,0.3,1, %4.1f,V#                 812 channel
Air Temperature     #9,0,1,2,7,7,23983,-0.6293,0,50, %4.1f,øC#      889 channel 0
Axle Oil            #9,1,1,1,7,7,23600,-0.30  ,0,60, %4.0f,øC#      889 channel 1
Engine Water        #9,2,5,0,7,7,23410,0.0461,0,110, %4.0f,øC#      889 channel 2
Engine Oil          #9,3,5,0,7,7,24263,-1.4979,0,200, %4.0f,øC#     889 channel 3
Extra Thermocouple  #9,4,5,0,7,7,24076,-1.7488,0,100, %4.0f,øC#     889 channel 3
Barometer           #9,10,2,3,1,-2,988.44,-14.55,500.0,1100, %4.0f,mb#  889 channel 10
test 1              #9,14,1,0,1,-1,1.0,0.0,0.3,10, %4.1f,øC#        889 channel 14
test 2              #9,15,1,0,1,-1,1.0,0.0,0.3,10, %4.1f,øC#        889 channel 15
spare               #9,5,1,1,7,-1,1.0,0.0,0,10, %4.1f,øC#           889 channel 5
spare               #9,6,1,2,7,-1,1.0,0.0,0,10, %4.1f,øC#           889 channel 6
spare               #9,7,1,0,7,-1,1.0,0.0,0,10, %4.1f,øC#           889 channel 7
spare               #9,8,1,0,7,-1,1.0,0.0,0,10, %4.1f,øC#           889 channel 8
spare               #9,9,1,0,7,-1,1.0,0.0,0.5,10, %4.1f,øC#         889 channel 9
spare               #9,11,1,0,1,-1,1.0,0.0,0.3,10, %4.1f,V#         889 channel 11
spare               #9,12,1,0,1,-1,1.0,0.0,0.3,10, %4.1f,V#         889 channel 12
spare               #9,13,1,0,1,-1,1.0,0.0,0.3,10, %4.1f,V#         889 channel 13
Motor Speed         #0,120,0,0,25.040,9.9,5, %4.1f,kph#             812 analog output
Motor Torque        #0,200,0,0,10.494,-1.2,9.91, %4.1f,Nm#          812 analog output
Dyno Speed          #1,120,0,0,-31.017,4256.3,10, %4.1f,kph#        812 analog output
Dyno Torque         #1,200,0,0,4.299,2.138,10, %5.2f,Nm#            812 analog output
Dyno Power Law      #1,3.0,0,0,1000,0,0, %2.1f,p#                   812 analog output
```

Figure Q.1 Example of the configuration file as read by the C++ control program

Parameter	Example	Notes
Channel title	Motor Torque	Text to be printed in data file and on-screen
Delimiter	#	Signals that title is finished
PCL-812PG channel	3	9 = multiplexer channel (column also used for D/A device)
PCLD-889 channel	0	Not used for direct PCL-812PG signals
Samples to average	1	If channel is to be read more than once per cycle (Not currently used)
PCL-812PG range code	2	0 = ±10 V, 1 = ±5 V, 2 = ±2.5 V etc
PCLD-889 gain code	0	7 = ×1000, 6 = ×500 (Not used for PCL-812PG signals)
Thermocouple type	-1	7 = K-type (Not used for PCL-812PG signals)
Linear multiplier	0.1228	To convert A/D bits (0-4096) to appropriate units
Linear offset†	-250.87	Output = Multiplier×bits + Offset
Zero tolerance	0.5	Minimum recorded value, below which 0 is substituted
Upper limit	220	A warning is issued if this maximum safe reading is reached
Text format string	%5.1f	C++ floating point display format (incl. decimal places)
Units	Nm	Shown on-screen and in data file
Delimiter	#	Signals end of data columns
Channel notes	812 channel	Note in file for user (not read by C++ program)

† Note: In the case of the tractive effort and dynamometer load cells, the multiplier and offset columns each store a multiplier for either positive or negative loading. The offset is stored in a separate file, which is updated when the load cell is rezeroed.

Table Q.1 Explanation of the configuration file parameters (using Motor Torque as an example)

APPENDIX R:

Example of C++ Program Data File Output

Figure R.1 on the following page shows part of a text file saved using the C++ data acquisition and control program.

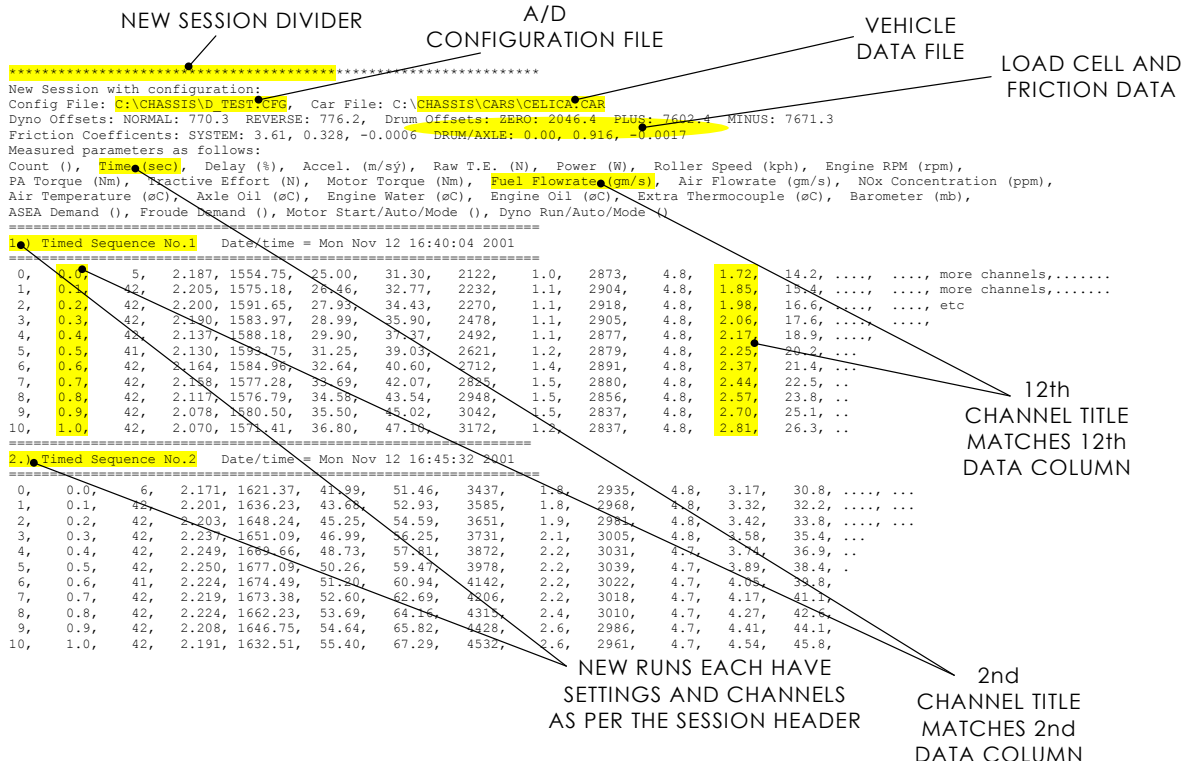

Figure R.1 Example data-file output from C++ data acquisition program

APPENDIX S:

Chassis Dynamometer Friction Coastdown Raw Data

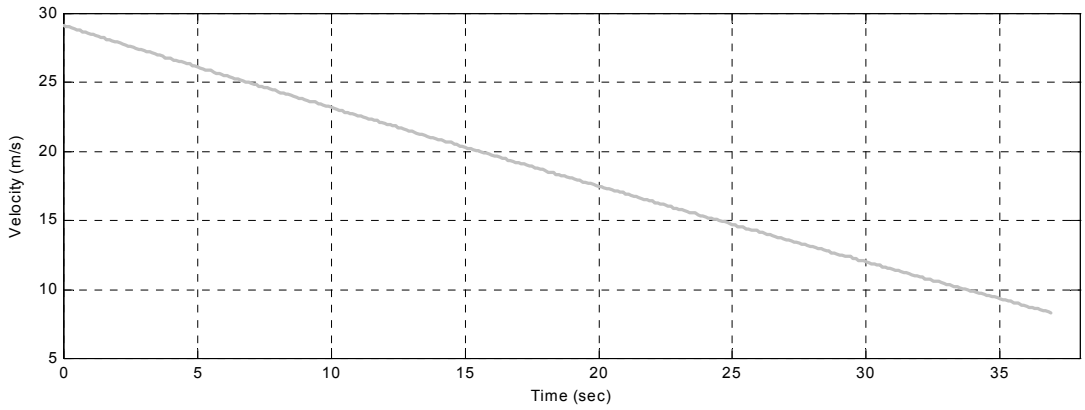

Figure S.1 Raw velocity measured during chassis dynamometer friction coastdown

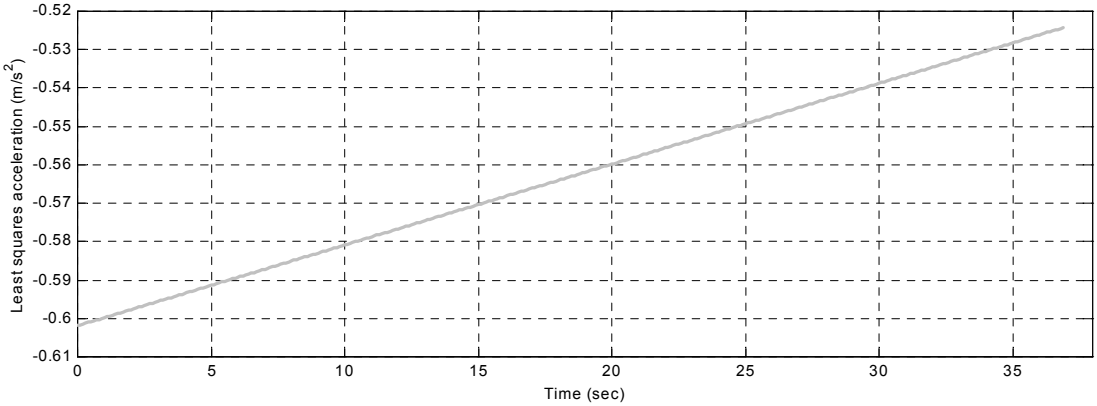

Figure S.2 Coastdown acceleration calculated from least squares approximation of velocity

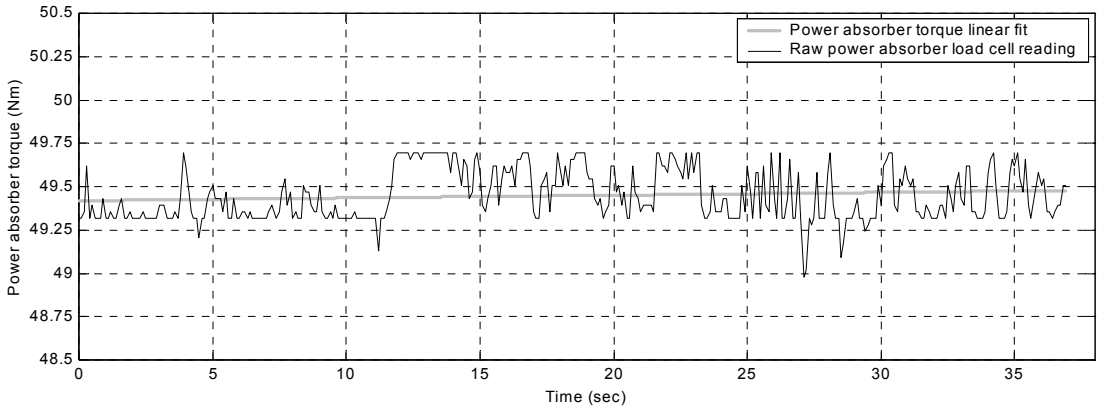

Figure S.3 Coastdown power absorber torque raw data and least squares linear approximation

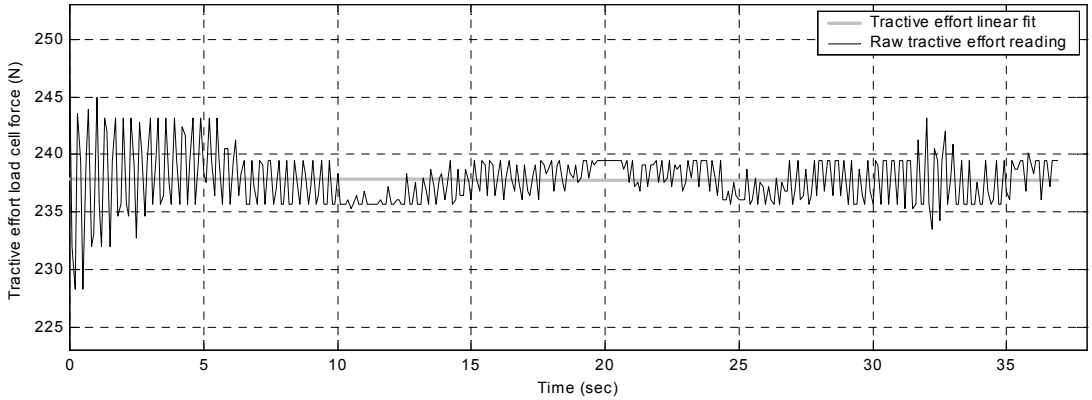

Figure S.4 Coastdown tractive force raw data and least squares linear approximation

APPENDIX T:

Dynamometer Warm Up Procedure

To stabilise the frictional characteristics of the shaft bearings and differential, the dynamometer was rotated under power from the electric motor. The necessary speed and duration of this warming up period was determined in several tests, using friction coastdowns (see Section 5.4) to calculate the overall system friction at a certain speed (35 kph for Figures T.1 and T.2 below). The time periods labelled with letters indicate intervals of constant speed running, while each data point is the result of a single coastdown.

Interval	Velocity (kph)	Duration (min)
A	60	15
B	60	15
C	120	3
	50	1

Table T.1 Warm up activities indicated in Figure T.1

Note that interval C includes more than one constant velocity phase.

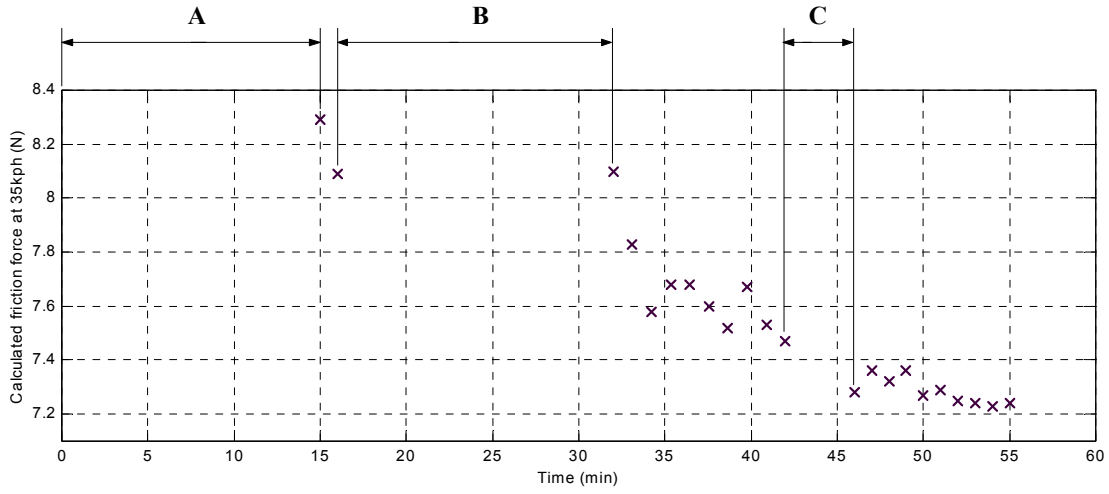

Figure T.1 First warm up test results showing frictional force referenced to the drum surface

Figure T.1 shows that 30 minutes at 60 kph (intervals A and B) was insufficient to reach a stable frictional state. As the coastdowns were performed between intervals B and C, the raising of the dynamometer speed to approximately 120 kph for the start of each run continued to raise the temperature—and hence, lower the friction—in the bearings and differential gears. A more stable state was achieved after brief running at 120 kph (interval C), as shown by the flattening trend in the calculated friction.

Interval	Velocity (kph)	Duration (min)
A	60	15
B	80	1
	100	1
	120	8

Table T.2 Warm up activities indicated in Figure T.2

Note that all warm up procedures were carried out before the series of friction coastdowns.

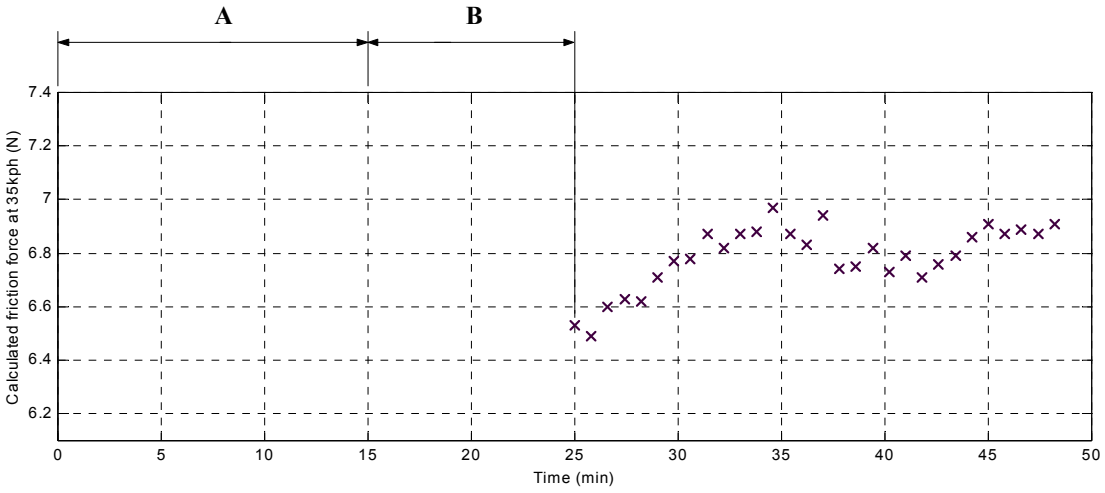

Figure T.2 Second warm-up test results showing frictional force referenced to the drum surface

After the initial warming up, the system friction *increased* with subsequent coastdowns, although less than the decrease shown in Figure T.1. This suggests that the contacting elements were cooling down, and that the frictional forces immediately after the warm up period were less than the equilibrium reached during consecutive friction coastdowns. In fact, once the drum axle oil reaches its desired temperature range (≈50ºC controlled by a heat exchanger), the equilibrium friction

(and rate of heat generation and dissipation) may be slightly different for each chassis dynamometer velocity. It was concluded that 15 minutes of running at 50 kph, followed by a shorter (≈5 min) period at 100 kph would be a satisfactory warm up to cover both driving cycle and mapping tests. The initial period is included to distribute and raise the temperature of the drum axle oil, as well as slowly raise the temperature of the other components before the higher velocity warm up period. Further rotation at a speed of 100 kph should lower the system friction to a level similar to the equilibrium conditions that might be reached during testing.

APPENDIX U:

Selected Driving Cycles

With the exception of Figure U.1, the following driving cycles are those specified in SAE J1506 [2001]. Driving cycle files are also included on the accompanying CD.

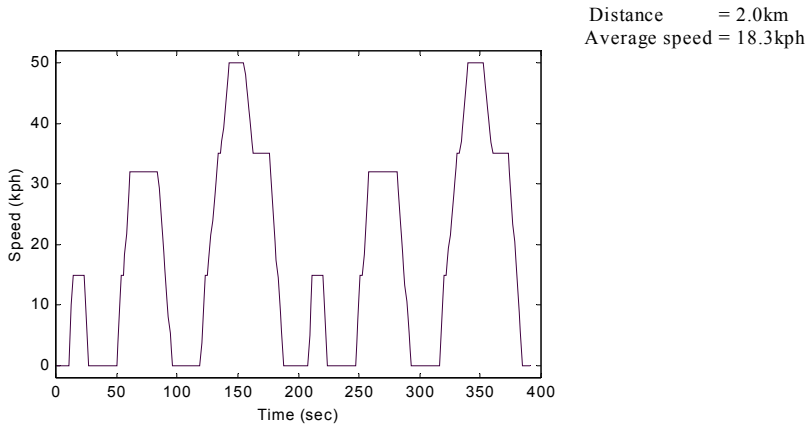

Figure U.1 Driving cycle used for testing at University of Canterbury

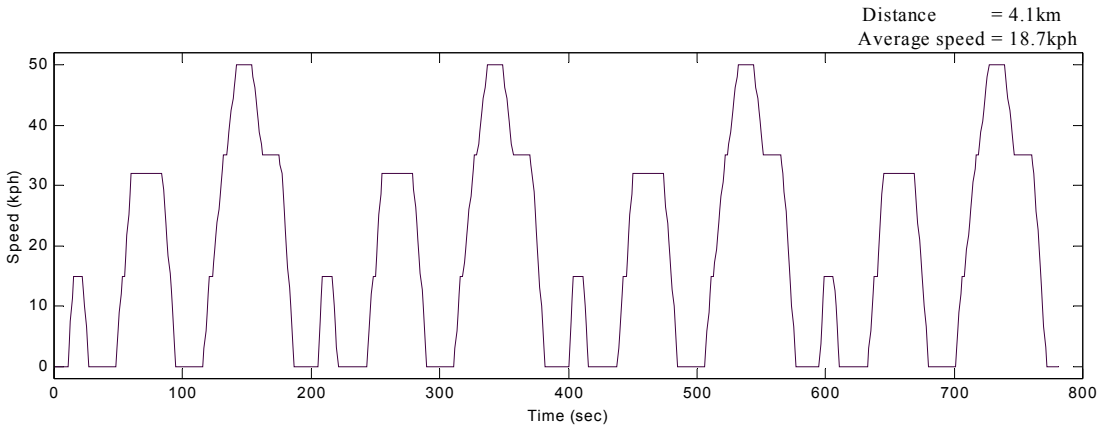

Figure U.2 Economic Commission for Europe (ECE) R15.04 Schedule

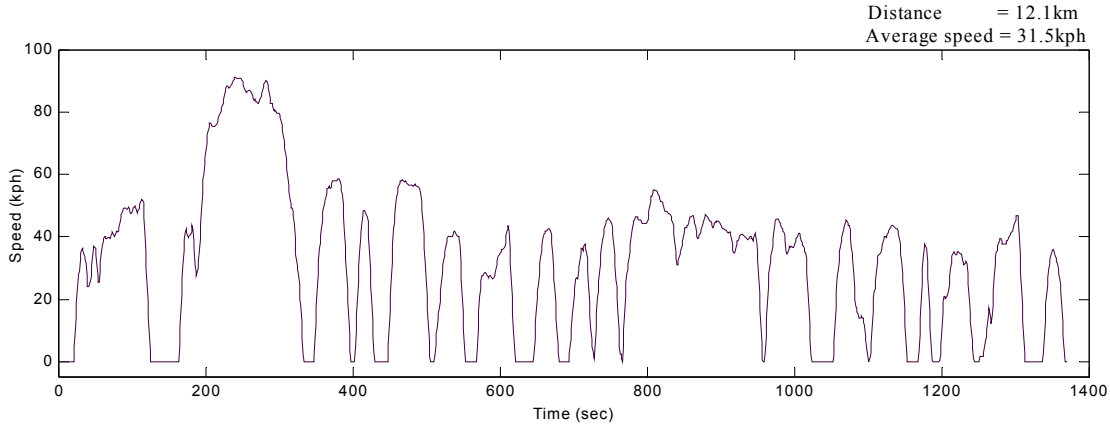

Figure U.3 EPA Urban Dynamometer Driving Schedule (UDDS)

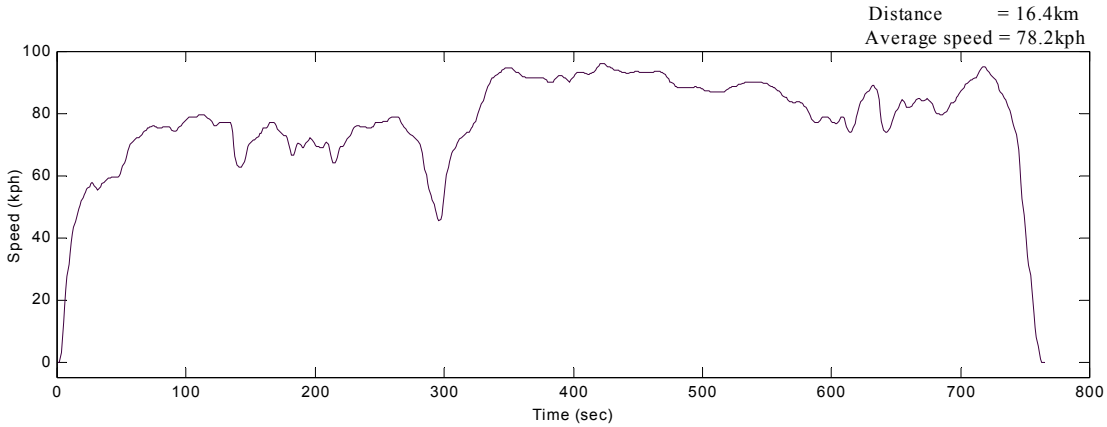

Figure U.4 Highway Fuel Economy Test Schedule (HWFET)

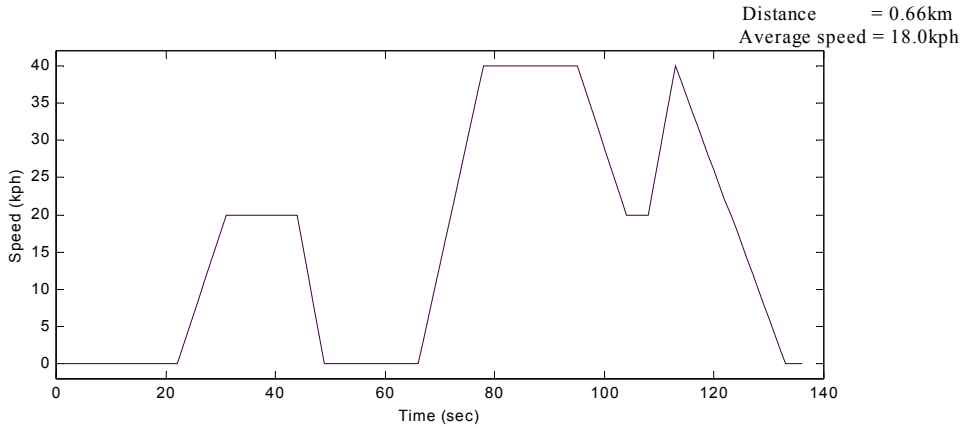

Figure U.5 Japanese 10-Mode Test Schedule

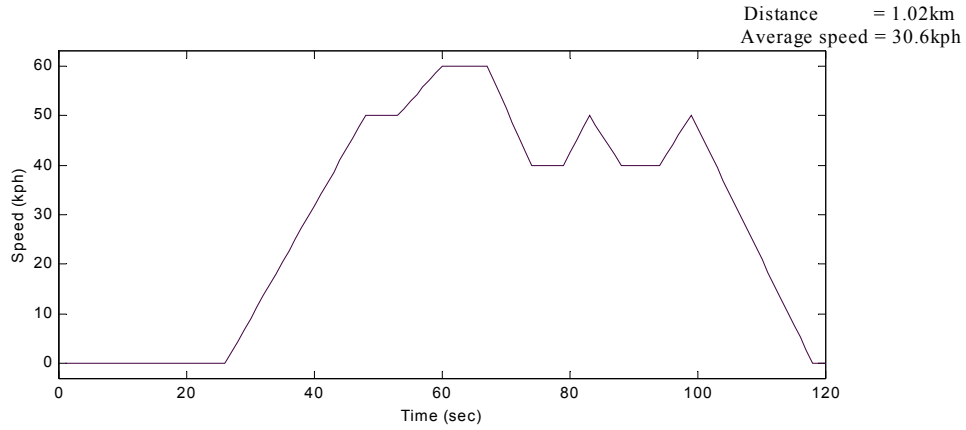

Figure U.6 Japanese 11-mode Test Schedule

APPENDIX V:

NZS 5420:1980 Dynamometer Driving Cycle Tolerance

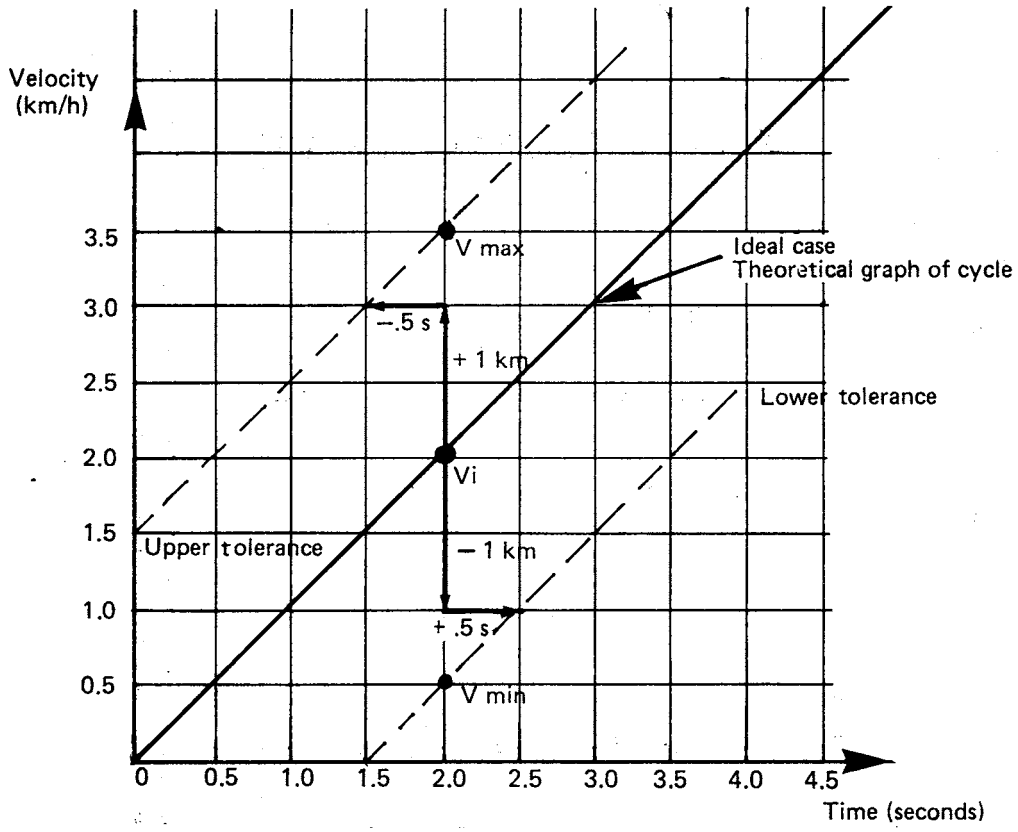

Figure V.1 Explanatory diagram for clarification of combined speed and time limits (Fig. 2 in New Zealand Standard NZS 5420 (withdrawn) [1980]

APPENDIX W:

MATLAB Program Menu Structure

Main Menu	Sub-Menu	Sub-Menu Options
Choose new data file	Select a file	
	Change extension	
	Change directory	
	Return to Main Menu	
Plot data	Change x and y variables	
	Change plot options	
	Customise legend	
	Execute plot	
	Plot power/torque curve	
	Vehicle mapping menu	Change z and x variables
		NEW or REFRESH
		Level of interpolation
		Default options
		Limit options
		Execute plot
		Exit mapping menu
	Exit plot menu	
Edit raw data		
Calculate additional data	Set fuel specifications	
	Calculate additional data	
	Calculate drive cycle excursions	
	Exit calculation menu	
Exit program		

Table W.1 Menu structure of MATLAB post-processing program

APPENDIX X:

Files for Excel Plotting of Vehicle Mapping Data

Each time a vehicle mapping test is plotted using the MATLAB routine detailed in Section 7.1.3.2, a raw data file (Figure X.1) and a zero-padded grid file are produced. The text plots (as per Figure 7.8) are generated using the spreadsheet shown in Figure X.2, with an Excel macro, which retrieves the latest data from the zero-padded grid file (similar to the grid shown on the left of Figure X.2) for plotting. A copy of this spreadsheet is also included on the accompanying compact disc.

Velocity (kph)	Tractive_Force (N)	Fuel_Flowrate (gm/s)
17.1776	1955.9740	0.8430
17.3249	1840.3660	0.7745
17.2329	1605.8215	0.6648
17.2513	1406.6702	0.6084
17.2513	1203.2051	0.5408
17.3065	1008.1865	0.4813
17.2513	795.9034	0.4205
17.3249	607.4649	0.3638
17.3802	400.8932	0.3087
27.4695	2085.3600	1.4567
27.2670	1971.2994	1.2247
27.2670	1811.6699	1.1160
27.2117	1597.7152	1.0184
27.1749	1406.3145	0.9313
28.4085	1197.7678	0.8770
28.2612	998.8357	0.7633
27.8377	807.1908	0.5913
27.8930	590.3657	0.5482
27.9298	406.2272	0.4728

Figure X.1 Partial copy of raw mapping data file

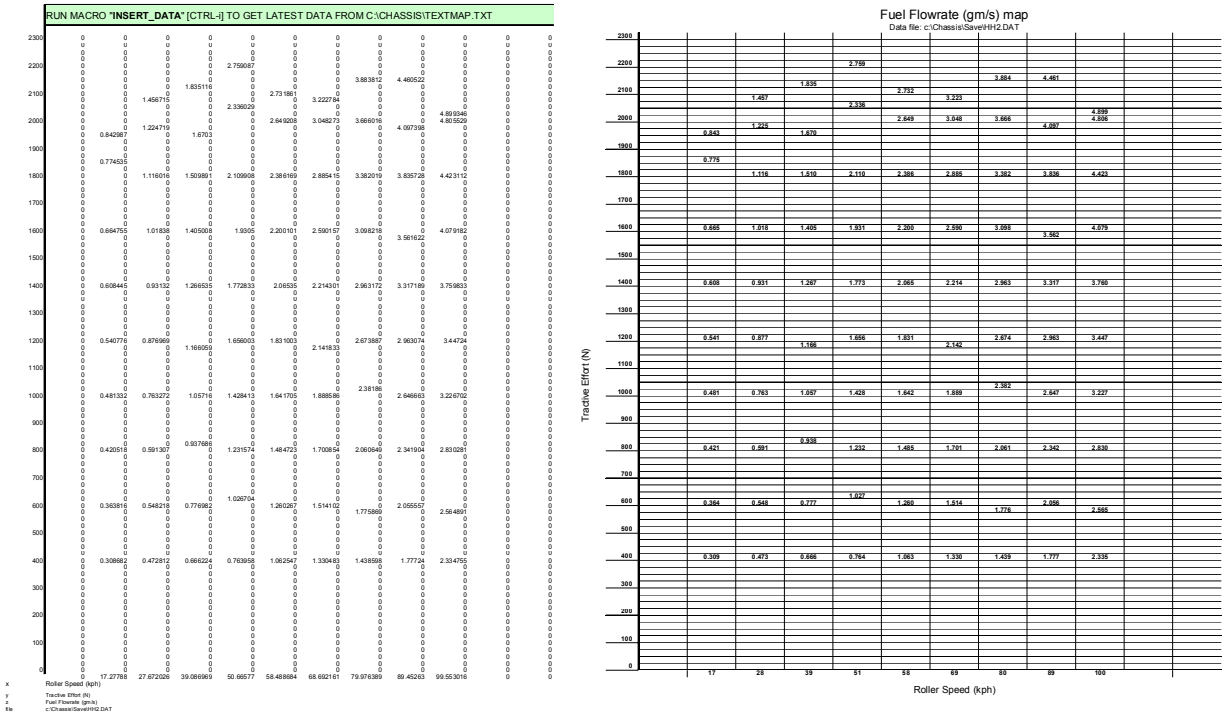

Figure X.2 Excel spreadsheet used to create vehicle map text plots

APPENDIX Y:

Example Vehicle Data Sheet

Vehicle Data Sheet	
Type of Vehicle (car/bus/truck)	Car
Make/Model	Toyota Celica
Year	1982
Owner	University of Canterbury
Registration	PL 3859
Engine Type/Size	1G-E 6cyl. 2000cc
Initial Odometer Reading (km)	206110
Accessories (if any)	-
Unladen mass (kg)	1150
Reference Mass (unladen+100kg)	1250
Dynamometer Equivalent Mass (kg)	1234
Transmission Type	5 spd manual
Axle Ratio	unknown
Tyre Make	Firestone
Tyre Model/Size	F-570 P195/70 R14
Tyre Pressures (kPa)	Front 190 Rear 190
Average Tyre Tread (mm)	RF:3 LF:4 RR:4 LR:5
Tyre Scrub (mm/metre)	Front 2 (inward) Rear 0
Fuel Pump	Standard
Carburettor/EFI	EFI
Ignition Make/Type	Nippondenso
NOTES:	

Table Y.1 Example vehicle data sheet

APPENDIX Z:

Vehicle Coastdown Friction Calculations

Z.1 On-Road Coastdown Tests

Friction coefficients for the test vehicle were determined experimentally based on the method prescribed by the SAE Recommended Practice, SAE J1263 [1999].

Several coastdowns between the speeds of 120 kph and 40 kph were carried out on a section of Tram Road, near Ohoka, Canterbury in both directions. The vehicle velocity was measured by timing driveshaft rotations using the optical device mentioned in Section 8.1.1. Initially, the relationship between driveshaft rotations and displacement of the vehicle was investigated by rolling the vehicle slowly forward a set number of driveshaft rotations, and measuring the distance travelled.

Driveshaft rotations	Distance (m)	Metres per rotation
25	12.20	0.488
60	29.21	0.487
60	29.23	0.487
		0.487

Table Z.1 Test vehicle distance per driveshaft rotation calibration

Raw velocity vs. time data was approximated by a least squares curve fit, so that the deceleration at each point could be calculated. With knowledge of the vehicle deceleration and mass, the frictional force resisting motion is given by:

$$m_{Veq}\frac{dv}{dt} = f_{0V} + f_{1V}v + f_{2V}v^2 \qquad \text{(Z-1)}$$

Where: m_{Veq} = Equivalent mass of vehicle including rotational masses

f_{0V}, f_{1V}, f_{2V} = Vehicle frictional coefficients

The equivalent mass of the rotating inertias is added to the vehicle mass, and is approximated as $0.035 \times$*(vehicle mass)*. The three unknowns (f_{0V}, f_{1V}, f_{2V}) may be solved for simultaneously by calculating $m_{Veq}(dv/dt)$ at several points on the same coastdown curve.

Of the eight coastdown runs measured, three were discarded, either because an insufficient maximum speed was achieved before beginning the deceleration, or because of excessive wind gusts. Ideal coastdown conditions include a perfectly flat road and zero wind. However, a measurable wind was present (this can be corrected for, as below), and the calculated coefficients indicated a significant road gradient. The resulting frictional coefficients do not necessarily comply with the acceptability criteria detailed in SAE J1263, but were deemed sufficiently accurate for the chassis dynamometer proving tests in Chapter 8.

Run	Temperature (K)	Wind (m/s)	f_{0V}	f_{1V}	f_{2V}
1	295.7	2.20	161.63	0.008	0.0331
2	296.2	-1.65	266.85	0.455	0.0274
3	296.8	1.10	-2.65	4.173	0.0057
4	297.4	-0.55	387.80	-2.355	0.0453
5	298.0	0.00	13.04	3.949	0.0058
6	298.3	-0.40	301.84	-0.465	0.0314
7	298.6	0.80	151.69	0.095	0.0302
8	299.0	-1.20	307.46	-0.875	0.0348

Highlight = discarded runs

Table Z.2 Vehicle friction coastdown data

Note that the coefficients are stated such that v in Equation Z-1 is in kilometres per hour, and friction force is in Newtons. Also, the air temperature and wind velocity were recorded only at the beginning of runs 1 and 5, and after run 8, with the remainder of the data linearly interpolated.

Z.2 Correction of Friction Coefficients

Corrections can be made to these coefficients to allow for wind, air temperature, and air pressure—all of which may affect the frictional resistance to the vehicle's motion. Firstly, the rolling resistance is separated from the wind effects to provide a wind correction to f_{0V}:

$$\mu_0 W = \frac{\left(f_{0V} - f_{2V} v_x^{\,2} - \frac{1}{2} \rho C_{DY} A v_y^{\,2} \right)}{1 - \mu' v_x^{\,2}} \qquad \text{(Z-2)}$$

Where: $\mu_0 W$ = is used in Equation Z-3, below

ρ = Mass density of ambient air (kg/m^3)

μ' = Velocity coefficient of rolling resistance

C_{DY} = Crosswind aerodynamic drag coefficient

v_x = Component of wind parallel to track (kph)

v_y = Component of wind perpendicular to track (kph)

When exact vehicle data is not available:

μ' = 19×10^{-6} (kph)$^{-2}$

C_{DY} = 0.8181 (m/s)^2/(kph)^2

The temperature dependence of the rolling resistance is corrected thus:

$$f'_{0V} = \mu_0 W \left[1 + k_t \left(T - T_0 \right) \right] \qquad \text{(Z-3)}$$

Where: T = Ambient air temperature (K)

T_0 = Standard temperature (293.15 K)

k_t = 8.6×10^{-3} /ºC unless specific vehicle data is available

The coefficient of the v^2 term is then adjusted to the standard atmospheric conditions:

$$f'_{2V} = \left(\frac{p_0 T}{p T_0}\right)\left[f_{2V} - \mu'(\mu_0 W)\right] + \mu' f'_{0V} \qquad \text{(Z-4)}$$

Where: p = Barometric pressure (mmHg)

p_0 = 736.6 mmHg

The linear multiplier, f_{1V} is small and the SAE recommended practice approximates this factor as zero. However, f_{1V} was maintained for the current work so that its effect could be investigated.

Z.3 Sample Friction Coefficient Calculations

Run 1 (see Table Z.2) has been included as an example of these correction calculations. Equation Z-2 becomes:

$$\mu_0 W = \frac{\left(161.6 - 0.033 \times (3.379)^2 - \frac{1}{2} 1.17 \times C_{DY} \times 1.65 \times (7.163)^2\right)}{1 - \mu'(3.379)^2} = 120.83$$

Where: $v_x = \cos(angle\ of\ wind) \times (2.2 \times 3.6) = 3.379\ kph$

$v_y = \sin(angle\ of\ wind) \times (2.2 \times 3.6) = 7.163\ kph$

$\rho = \frac{air\ pressure}{T \times 2.15159} = \frac{743}{295.7 \times 2.15159} = 1.168\ kg/m^3$

A = Frontal area of vehicle, determined using a planimeter on an elevational photograph (see Plate Z.1).

Plate Z.1 Elevational photograph of test vehicle for frontal area determination

The corrected f_{0V} is found using Equation Z-3:

$$f'_{0V} = 120.83 \times \left[1 + k_t\left(295.66 - 293.16\right)\right] = 123.43$$

And f_{2V} becomes:

$$f'_{2V} = \left(\frac{736.6 \times 295.66}{743.0 \times 293.15}\right)\left[0.033 - \mu'\left(120.83\right)\right] + \mu' \times 123.43$$

Table Z.2 contains all the corrected friction coefficients of the runs that were not discarded.

Run	f'_{0V}	f_{1V}	f'_{2V}
1	123.43	0.008	0.0333
2	250.46	0.455	0.0276
6	313.77	-0.465	0.0320
7	153.24	0.095	0.0307
8	310.20	-0.875	0.0355
Weighted Average	214.90	-0.122	0.0318

Table Z.3 Summary of corrected vehicle friction coefficients

Because there were an uneven number of acceptable uphill (runs 1 and 7) and downhill (runs 2, 6, and 8) results sets, the average friction coefficients were weighted. An even contribution from each direction was achieved in the final average with Equation Z-5, using the constant friction coefficient as an example.

$$f_{0Vaverage} = \frac{3\left(f_{0V1} + f_{0V7}\right) + 2\left(f_{0V2} + f_{0V6} + f_{0V8}\right)}{12} \quad \text{(Z-5)}$$

Where: f_{0V1} = Constant friction coefficient calculated from run 1

f_{0V2} = Constant friction coefficient calculated from run 2

etc…

The coefficients in Table Z.3 are scaled to calculate friction force (N) given a velocity in kilometres per hour. The overall vehicle friction equation with v in terms of metres per second was:

$$\textit{Vehicle Friction (N)} = \mathbf{214.9 - 0.439}\,v + \mathbf{0.413}\,v^2$$

APPENDIX AA:

Selected Vehicle Map Plots

The following Excel plots show data for the test vehicle collected during a single vehicle mapping test conducted on 29th November 2001.

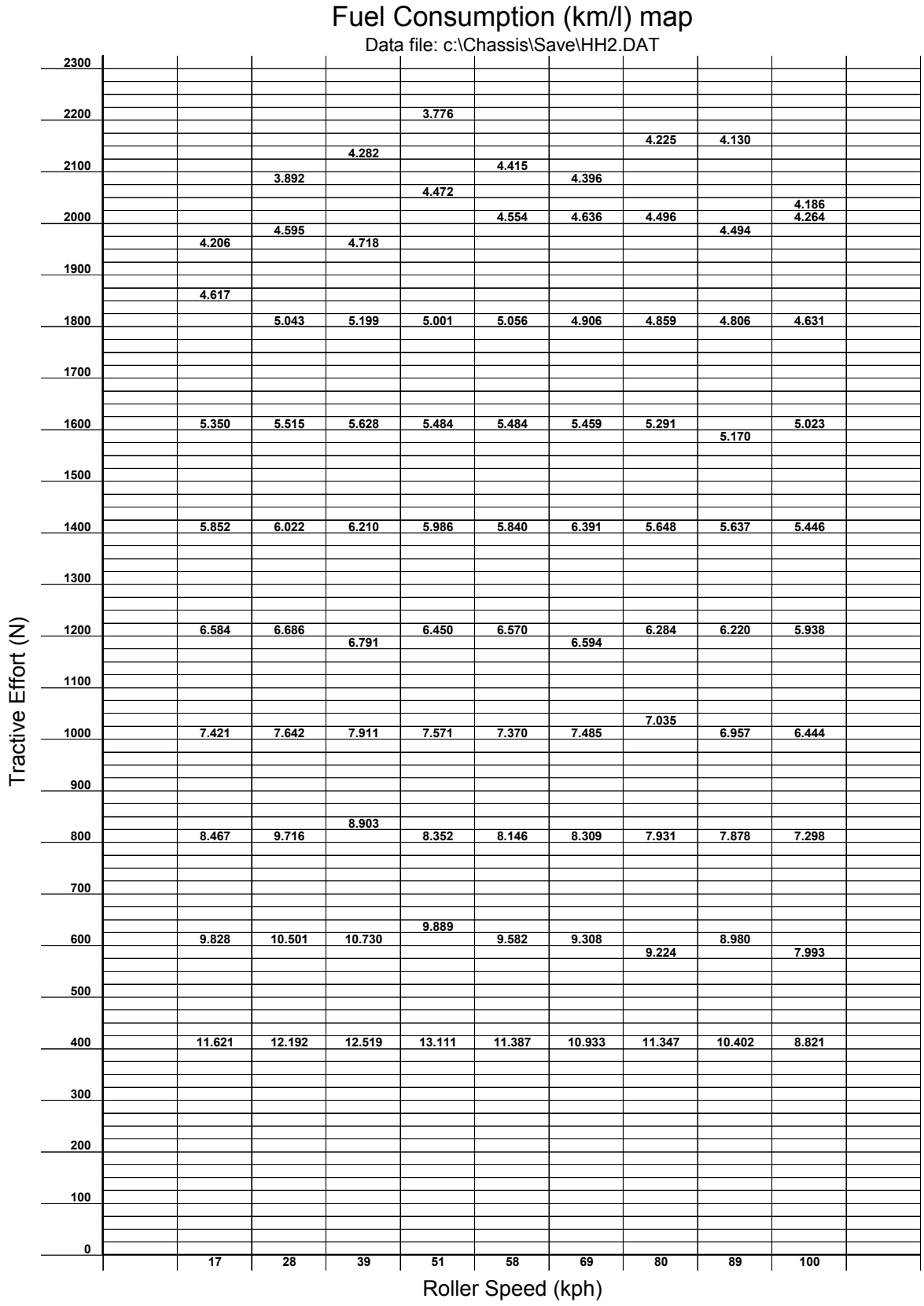

Figure AA.1 Fuel consumption (km/litre) map for the test vehicle

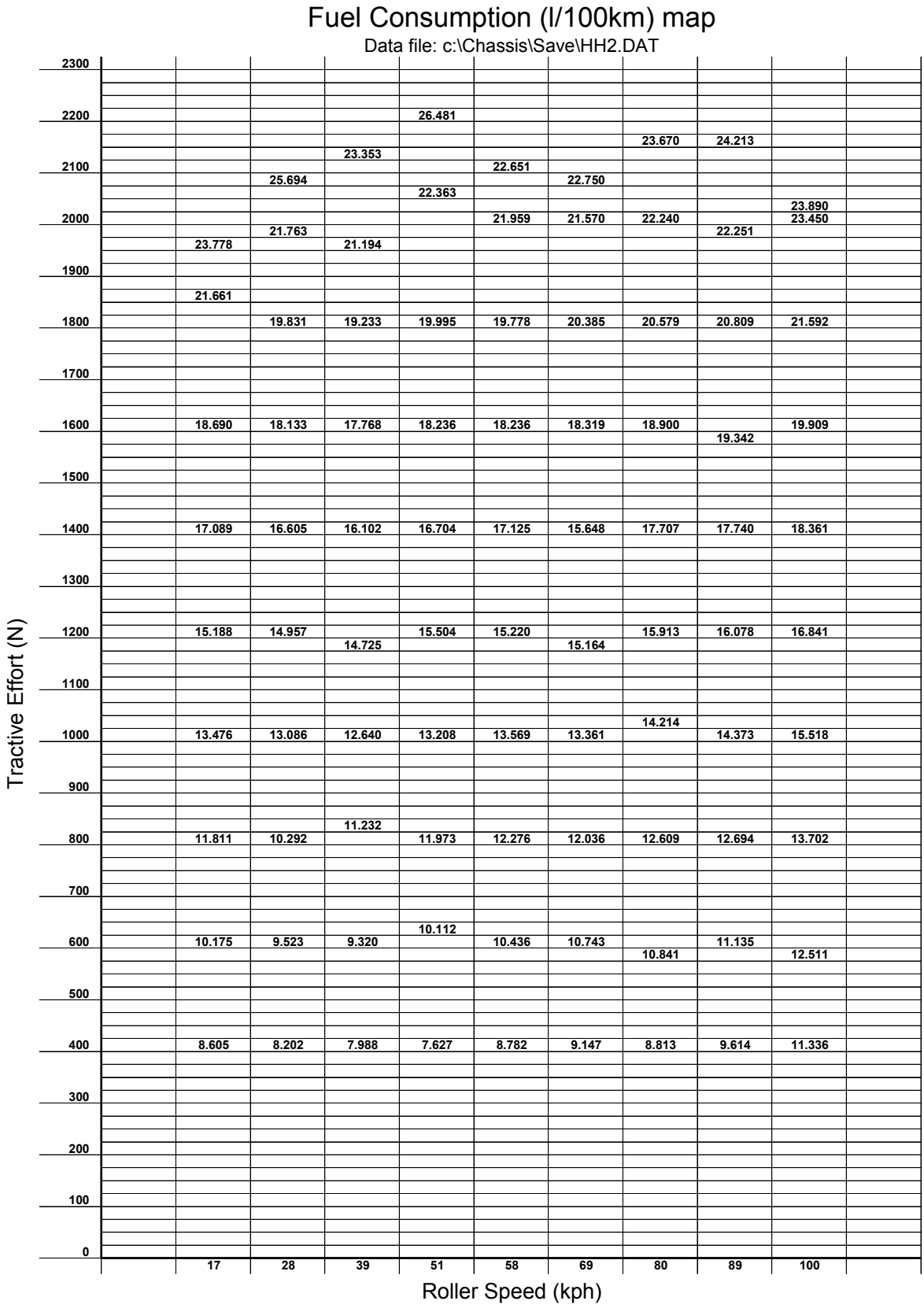

Figure AA.2 Fuel consumption (litres/100km) for the test vehicle

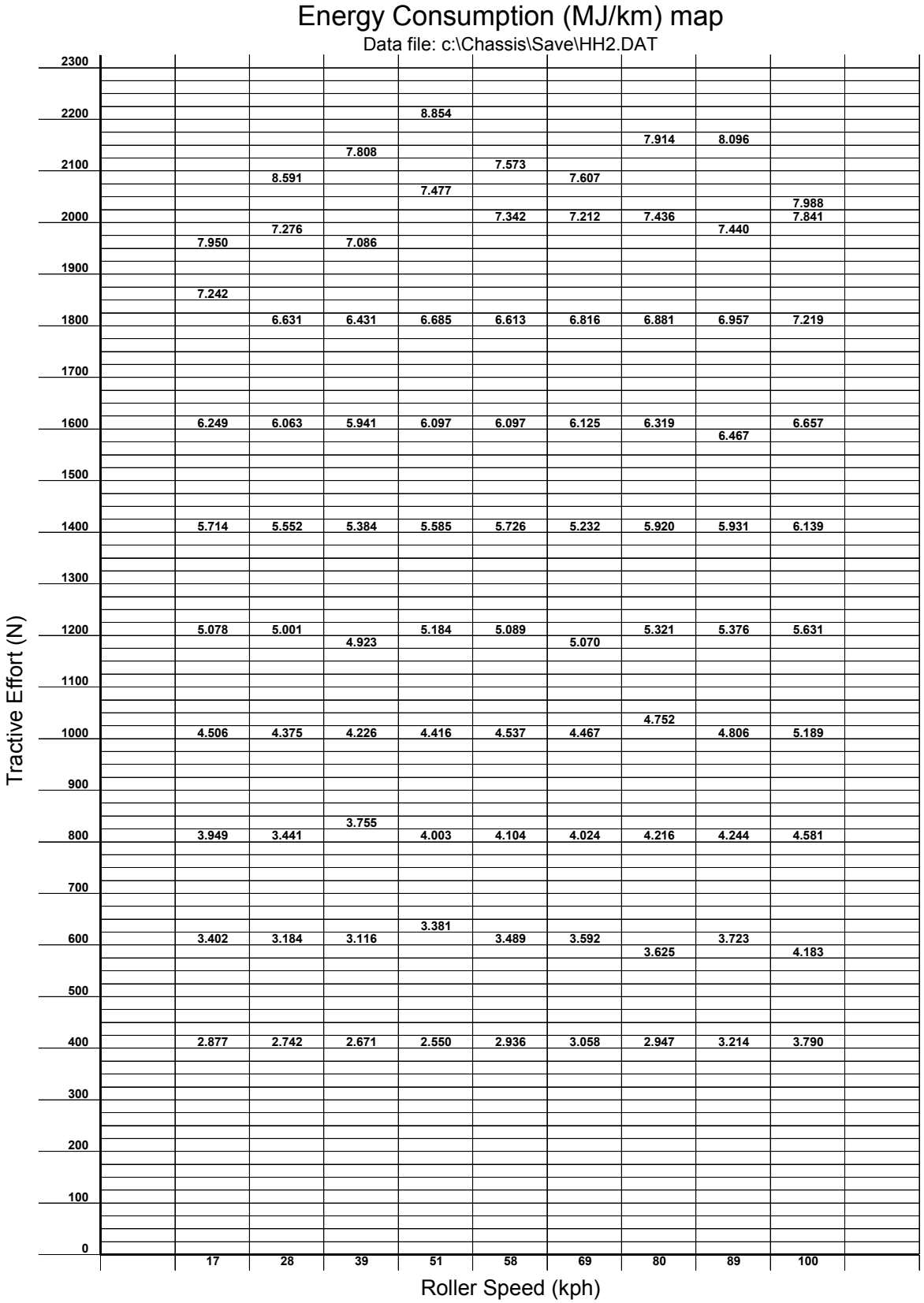

Figure AA.3 Energy consumption (MJ/km) for the test vehicle

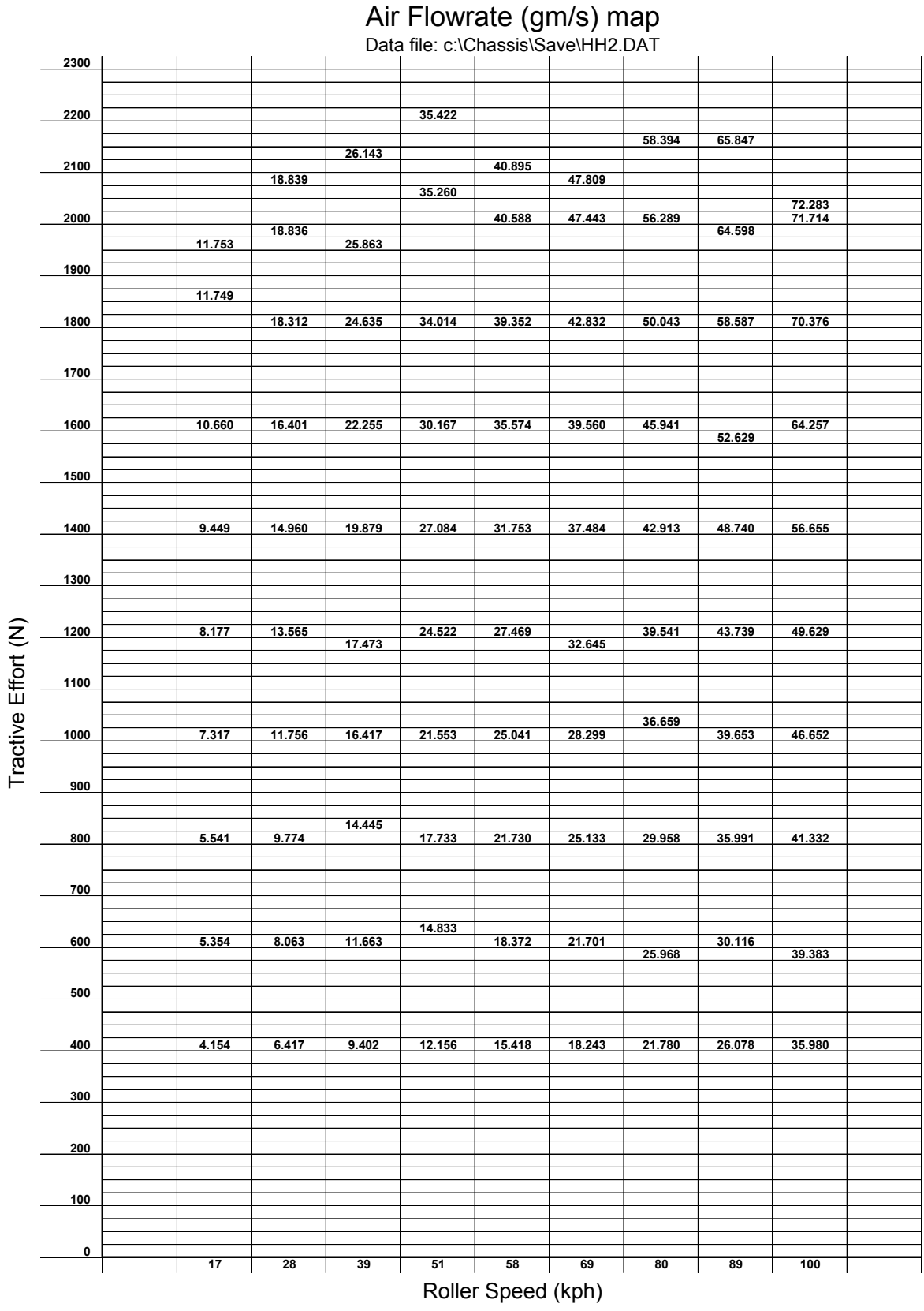

Figure AA.4 Air flowrate (gm/s) for the test vehicle

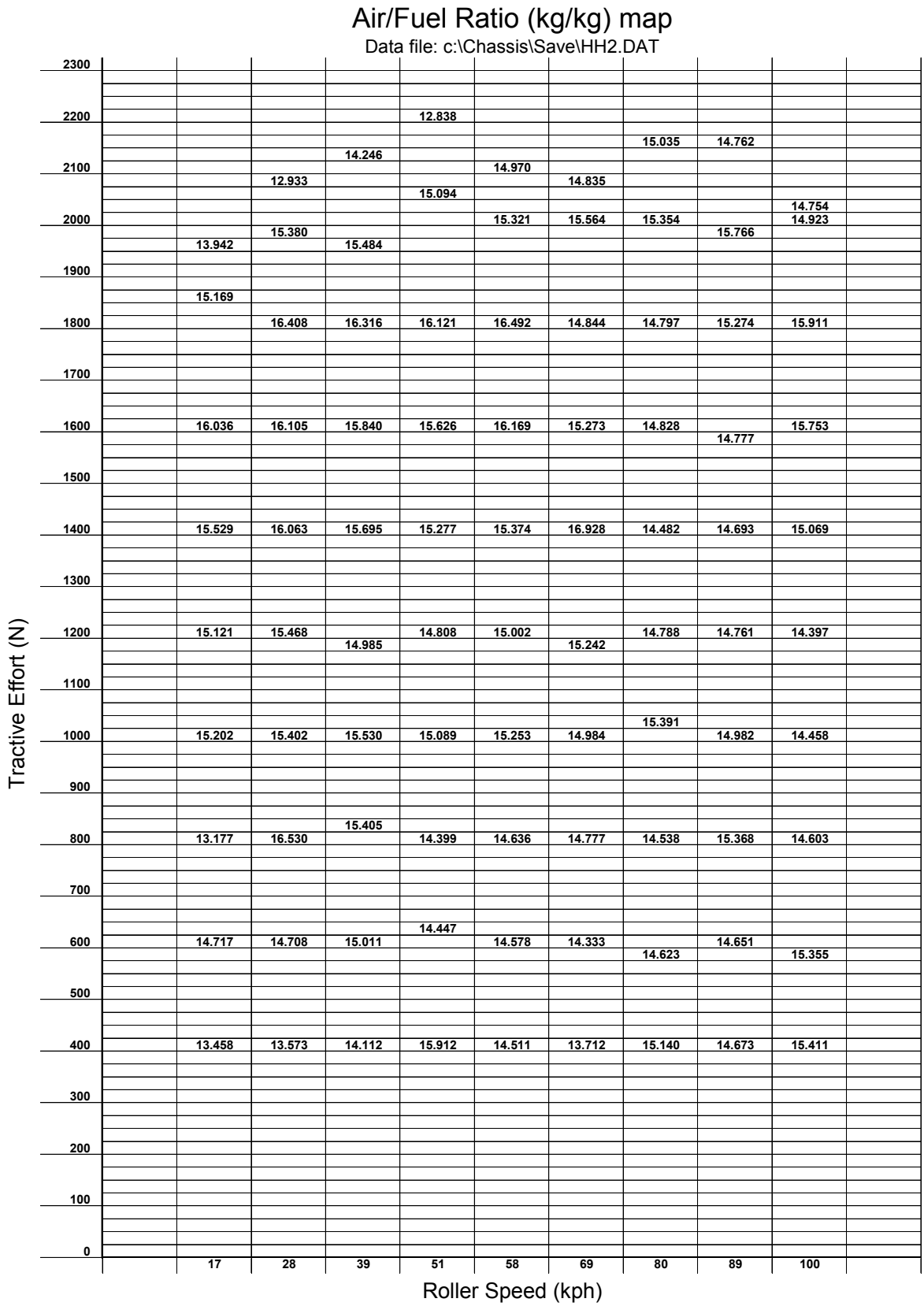

Figure AA.5 Air/Fuel ratio (weight basis) for the test vehicle

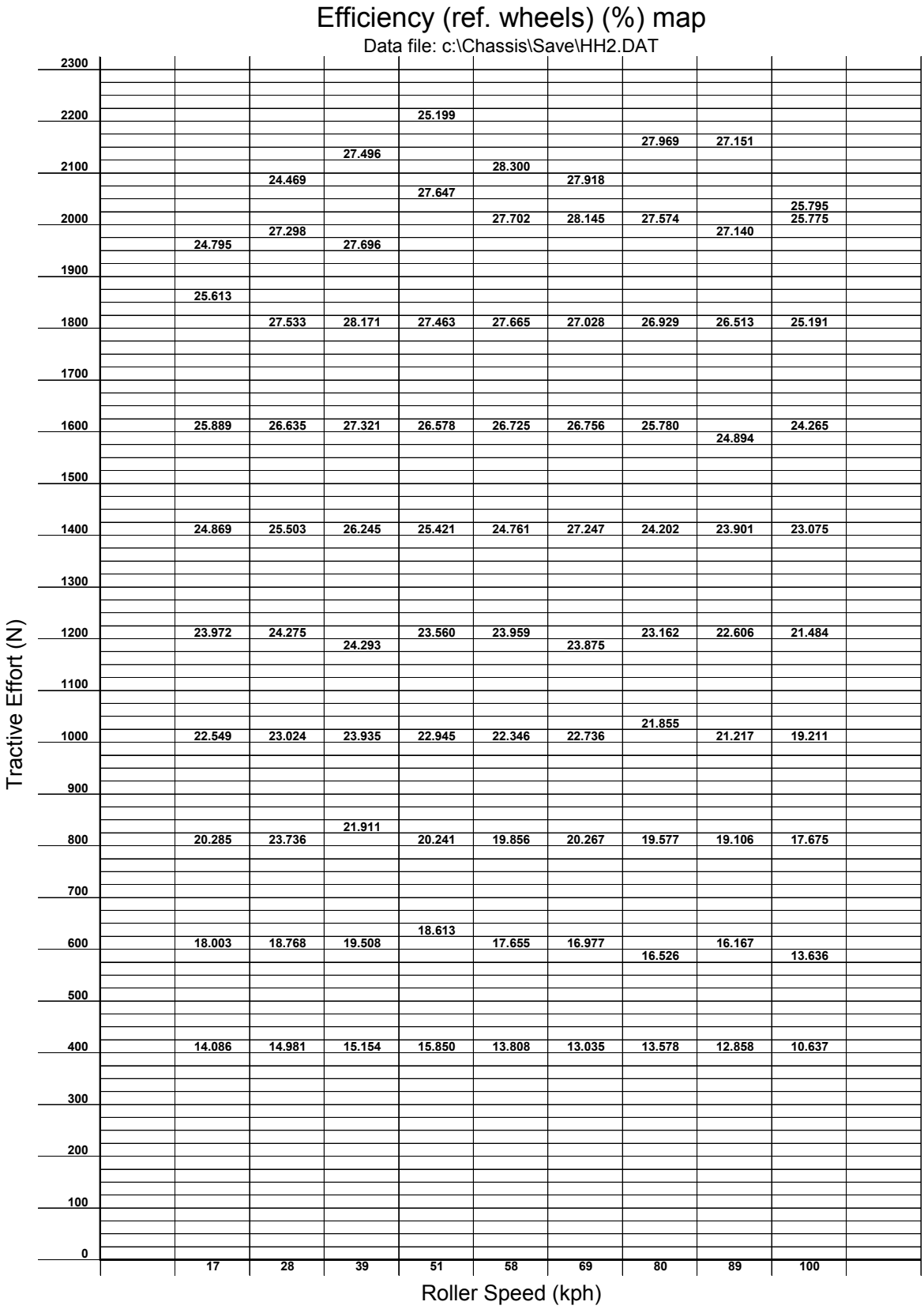

Figure AA.6 Efficiency referred to the road wheels for the test vehicle

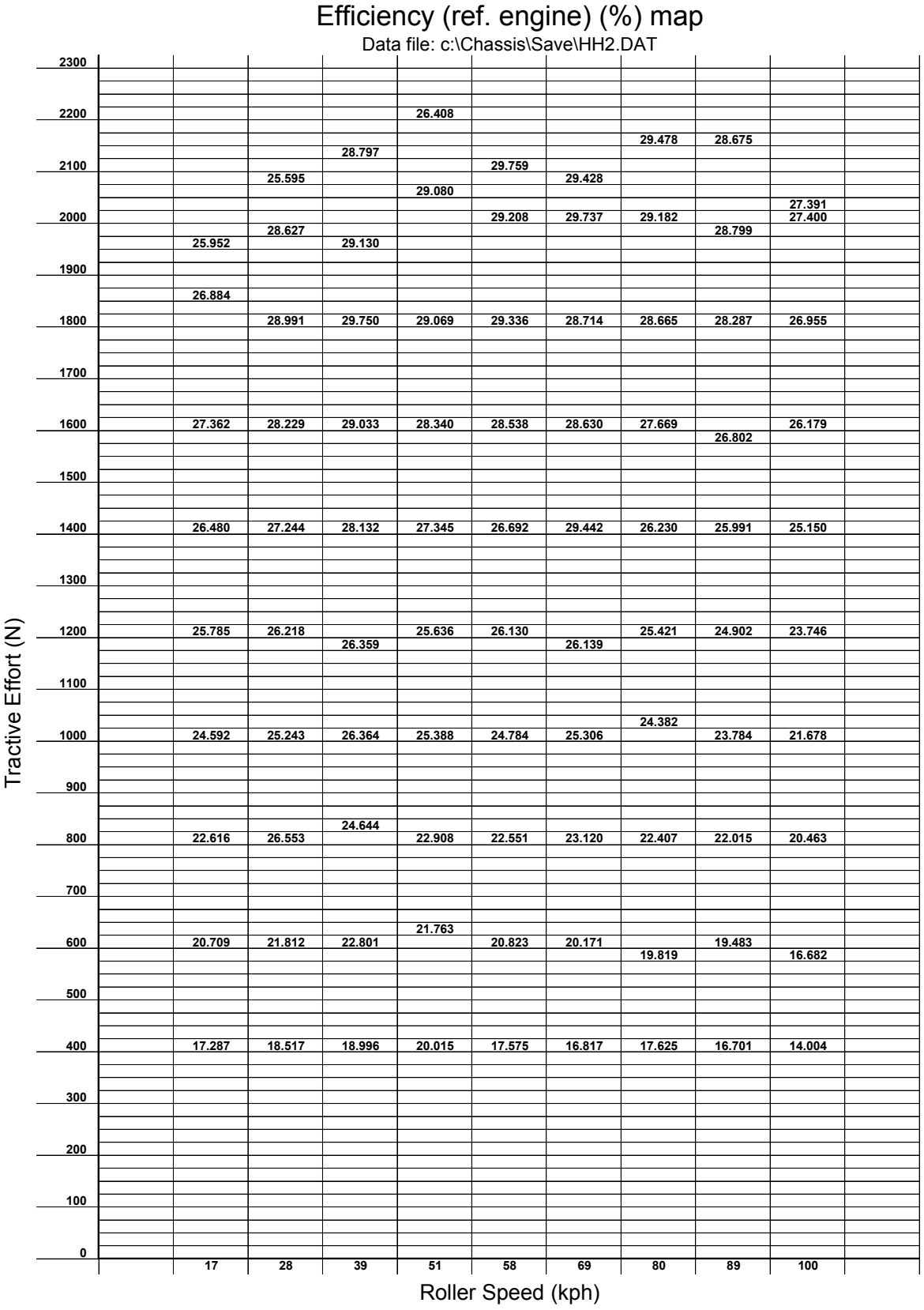

Figure AA.7 Efficiency referred to the engine flywheel for the test vehicle

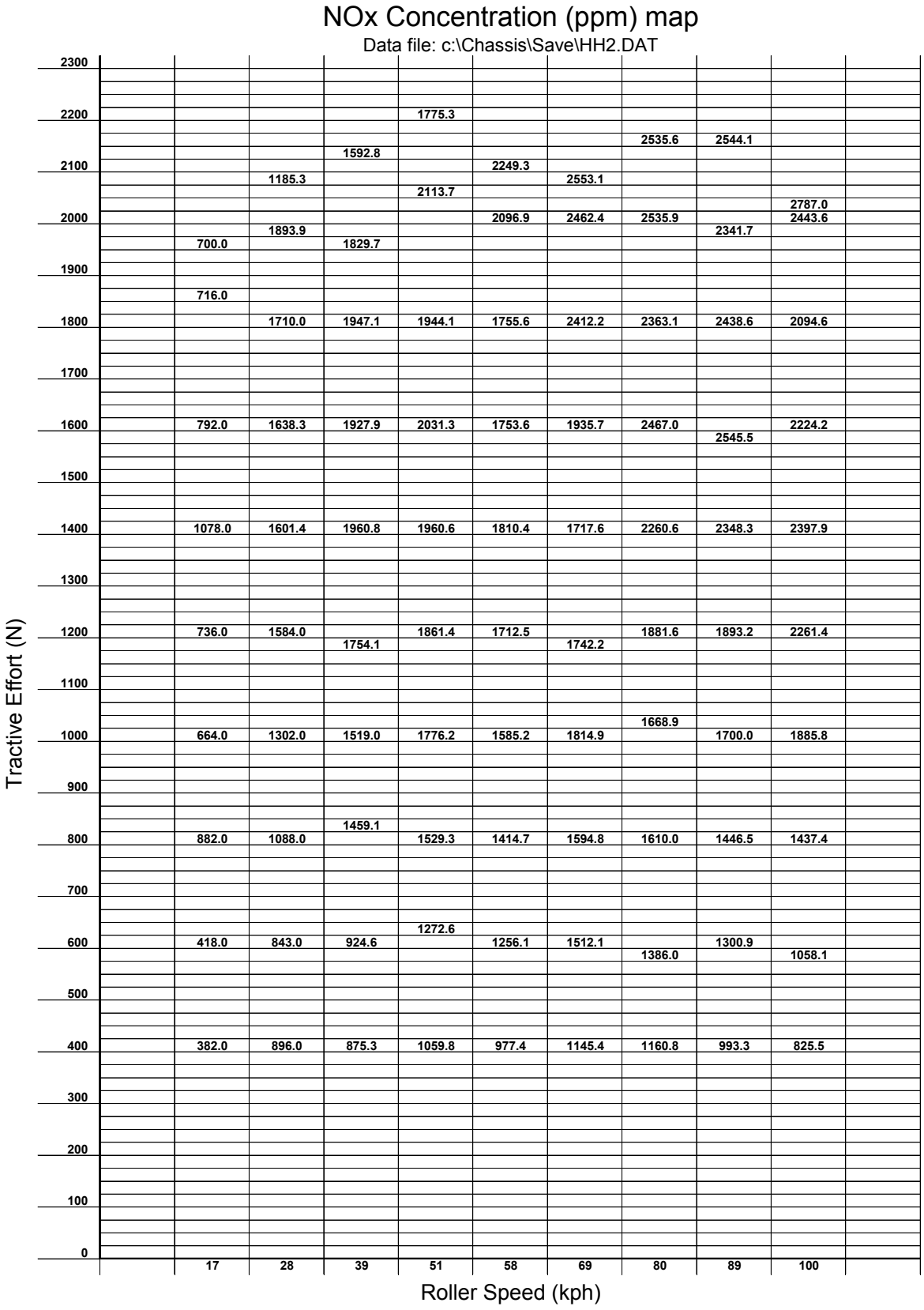

Figure AA.8 Exhaust NO_X concentration (ppm) for the test vehicle

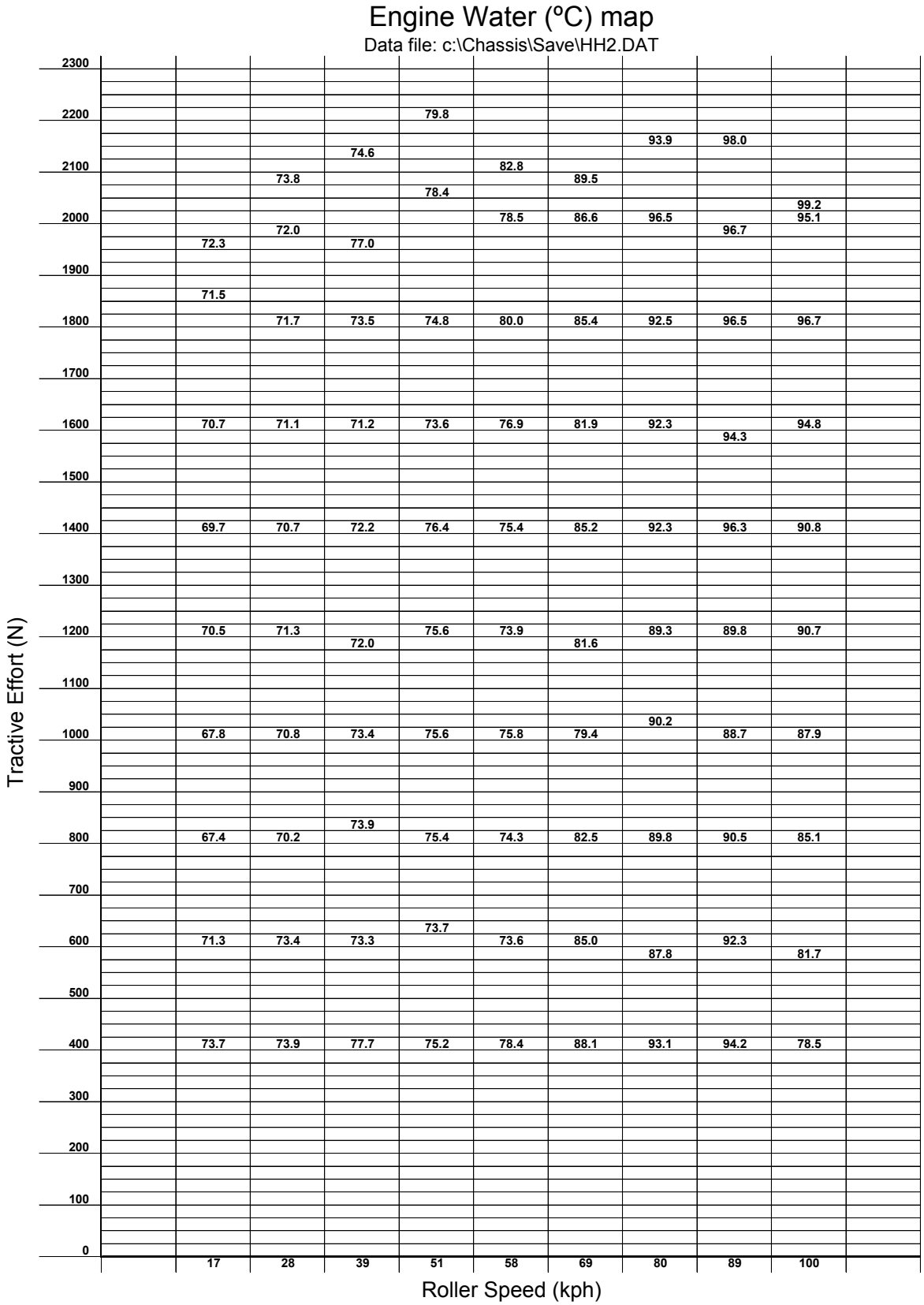

Figure AA.9 Engine water temperature (ºC) for the test vehicle

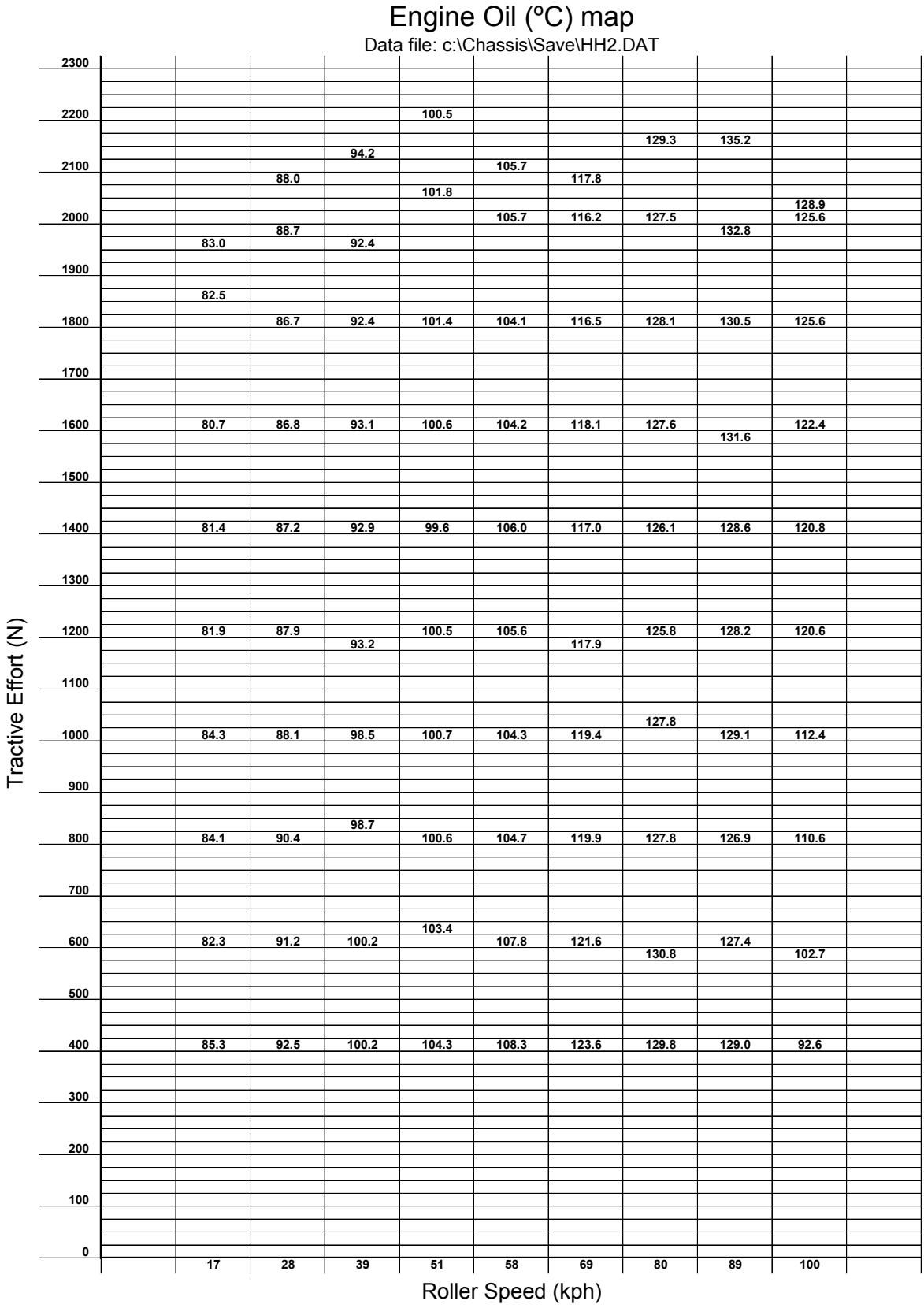

Figure AA.10 Engine oil temperature (ºC) for the test vehicle

APPENDIX BB:

Contents of Compact Disc

Item	Description
C++ Files	Directory containing source code for main chassis dynamometer control program
MATLAB files	Directory containing MATLAB m-files for inertia determination, VECM, and post-processing (calculation and plotting)
Sample Output Files	Examples of raw data output from a maximum throttle acceleration (bb3.dat), a mapping test (hh2.dat) and a driving cycle test (jj1.dri)
Selected Driving Cycles	Text files of driving schedules included in Appendix U
Text Plotting	Text map Excel spreadsheet, with example text file for running plot macro
Chassis.exe	Executable chassis dynamometer control program

Table BB.1 Table of compact disc contents